A multi-scale mathematical model for simulating and optimising the growth of Bambara groundnut

by

Josie Dodd

June 2017

School of Biosciences; University of Nottingham

Department of Mathematics and Statistics; University of Reading

Thesis submitted for the degree of Doctor of Philosophy

Declaration

I confirm that this is my own work and the use of all material from other sources has been properly and fully acknowledged.

Josie Rosanne Dodd
June 2017

Acknowledgements

I would like to thank my academic supervisors Dr Marcus Tindall, Dr Peter Sweby, Dr Sean Mayes, Dr Erik Murchie, Dr Asha S. Karunaratne, and Dr Festo Massawe for all of their support and guidance over the past four years; without which I would have been lost.

To my family and friends I would like to extend a special thanks for their constant love and support. In particular I would like to thank my immediate family Ellie, Janet and Paul Dodd for encouraging me to do a PhD, my partner Jack for being who he is and also Emily, Nicola and Jack (again) for proof-reading my thesis.

Finally, I would like to thank the Engineering and Physical Science Research Council (EPSRC) and Crops For the Future (CFF) for funding the research project.

Abstract

A principal objective in agriculture is to maximise food production; this is particularly relevant with the added demands of an ever increasing population, coupled with the unpredictability that climate change brings. Further improvements in productivity can only be achieved with an increased understanding of plant and crop processes. In this respect, mathematical modelling of plants and crops plays an important role.

In this thesis we present a two-scale mathematical model of crop yield, that accounts for plant growth and canopy interactions. A system of ordinary differential equations (ODEs) has been developed for each individual plant, where equations are coupled via a term that describes plant competition. Both analytical and numerical methods have been considered to describe this competition. This model has been formulated for an underutilised African legume called bambara groundnut, a drought tolerant crop, which is currently being investigated to be used more widely as a food source in light of climate change and food security. Like many plant species, bambara groundnut exhibits physiological diversity which may affect the overall growth dynamics and crop yield. Such plant diversity is not regularly accounted for in crop scale models. Our model not only allows us to account for plant diversity, but we can investigate the effect of individual plant traits (e.g. plant canopy size and growth rates, planting distance) on the crop scale yield.

The mathematical model has been formulated and validated using experimental data collected from the Tropical Crops Research Unit (TCRU) and Future Crops greenhouses at the University of Nottingham.

We find that the mathematical model developed in this thesis is able to predict the growth of a population of bambara groundnut well and we go on to optimise the arrangement of individual plants for a series of scenarios. The primary aim of this is to maximise crop yield.

Whilst formulated specifically for bambara groundnut, our model may also be extended to other crop species. In this thesis we demonstrate that the model is also able to simulate the growth of oil palm. We then apply the mathematical model to maximise crop yield in an intercropping environment; the planting of two or more species together in the same field area. We again investigate a series of scenarios that require optimisation and find that the optimisation techniques are able to provide plausible recommendations.

This work has been undertaken in a multidisciplinary environment involving interactions with Plant Scientists at the University of Nottingham (Nottingham and Malaysia) and the Crops for the Future Research Centre, Malaysia.

Contents

Definitions of terms and symbols

$A(t)$	Leaf area of a plant at time t
a, b, c	Species parameters that determine leaf area growth
α_c	Non-dimensional growth rate for plant canopy biomass
α_g	The growth rate for plant ground cover (non-dimensional and dimensional)
α_h	The growth rate for plant height (non-dimensional and dimensional)
α_L	Non-dimensional growth rate for plant leaf area
α_P	The growth rate of pod mass (non-dimensional and dimensional)
B	Species coefficient for canopy spread
b_g, c_g, d_g	Species parameters that determine change in ground cover
h_0, c_0, A_0, P_0, T_{D0}	Initial conditions for plant height, leaf area, canopy biomass, pod mass and thermal time
$c(t)$	The total biomass of a plant canopy at time t
c_k	The biomass gained per unit radiation
D	Distance between two plants
D_r	Distance between plants in a row
D_c	Distance between plants in a column
d_c	Canopy biomass decay rate (non-dimensional and dimensional)
d_h	Plant height decay rate (non-dimensional and dimensional)

d_L	Plant leaf area decay rate (non-dimensional and dimensional)
d_P	Plant pod mass decay rate (non-dimensional and dimensional)
$h(t)$	Pant height at time t
g	Grams
$G(t)$	Plant ground cover at time t
G_0	Initial ground cover
$\gamma(t)$	Leaf area index (leaf area per ground cover) at time t
κ	Extinction coefficient (non-dimensional and dimensional)
k_h	Plant height carrying capacity
K_h	Non-dimensional plant height carrying capacity
k_c	Canopy biomass carrying capacity
K_c	Non-dimensional canopy biomass carrying capacity
L_A	Leaf area per leaf
$LM(t)$	Leaf mass of a plant at time t
MAE	Mean absolute error
N-S	Nash-Sutcliffe model efficiency value
N	The number of plants in a plot
$O(t)$	Proportion of a plants canopy that is shadowed at time t
$P(t)$	Plant pod mass at time t
$\hat{P}$	The plot width/length
Plant Arrangement	The combination of plant layout, pattern and planting distance
Plant Layout	The positioning of plants in relation to each other
Plant Pattern	The positioning of different species of plants in relation to each other
ϕ	Specific leaf area (leaf area per leaf area)
ψ	Ratio of stem mass to leaf mass
R	Intercepted radiation
R_0	The photosynthetically active radiation
$\sigma,\ \lambda$	Overlap approximation parameters
$SM(t)$	Stem mass of a plant at time t
T	Temperature
$T_C(T,t)$	Cumulative thermal time at temperature T and time t
$T_D(T)$	Daily thermal time at temperature T
$T_{crit},\ T_{opt},\ T_{ceil}$	The minimum, optimum and maximum temperatures for plant growth, respectively
$T_{sc},\ T_{sl},\ T_{sp}$	The temperature stress for canopy biomass, leaf area and pod mass growth, respectively

Chapter 1

Introduction

The work undertaken in this thesis is part of a larger collaborative effort of the BamYIELD programme. BamYIELD is one of five international research programmes of Crops For the Future (CFF) and is dedicated to the research and development of underutilised legumes using the test species bambara groundnut. More details of CFF and it's projects can be found at www.cffresearch.org. The overall aim of BamYIELD is to optimise the contribution of bambara groundnut to world food security and poverty alleviation in developing countries. Although they use bambara groundnut as a focus, the approaches developed as part of their research are designed to be easily applied to other underutilised legumes.

In this thesis we focus our efforts on optimising the growth of bambara groundnut in regards to management practices, such as individual plant placement, in order to maximise crop yield. To do this we develop a multi-scale mathematical model (plant to crop scale) that describes the growth and yield of bambara groundnut over time.

A model can have many different meanings inside and outside of biology and in the loosest terms refers to a representation of a construct or organism. This can be a physical or theoretical representation designed to describe certain aspects of the particular entity. In Mathematical Biology and particularly in this work, the focus is on mathematical modelling defined as the use of mathematics to describe or simulate the behaviour of a physical system.

A dynamical mathematical model is designed and formulated using a combination of data found in the literature, experimental data collected from the Tropical Crops Research Unit (TCRU) at the University of Nottingham and also data collected specifically for this work from the Future Crops greenhouses at the University of Nottingham. The model consists of a system of ODEs for each individual plant, where equations are coupled via a term that describes plant competition. Both analytical and numerical methods are considered to describe this competition. In line with the principles of BamYIELD, although the mathematical model has been formulated for bambara groundnut, the design is such that it can be applied to other species of plants and we demonstrate its robustness in this respect later in this thesis.

By simulating plant growth at the individual scale, we can investigate the effect of between plant canopy-canopy interactions. As such, once the model is formulated we apply it to the investigation of planting arrangements that maximise crop yield. This is done for both homogeneous (single species) and heterogeneous (multi-species) planting.

In the remainder of this chapter, we define underutilised crops and discuss the important role they have in the world's future, we introduce in more detail the test species bambara groundnut and describe its growth habits and finally we outline the content of this thesis.

1.1 Underutilised Crops

There are many challenges that humanity will face in the twenty-first century, including the impact that climate change, increasing populations and urbanisation will have on the world's food security [4]. There are over 7000 species of plant that, at some point in time, have been cultivated to provide food [39]. Currently, only 30 species contribute 95% of the world's food supply [57] and it is not clear if this currently limited selection of crops will be robust enough to meet future challenges.

The term 'Underutilised crops' refers to the plant species that show considerable

promise in contributing to the world's food source but are currently grown at a much smaller scale than their potential warrants [39]. These crops are often indigenous and play an important role in the diets and livelihoods of the people that grow them. Further development and attention to these crops gives a great opportunity to diversify the world diet, reduce over reliance on the 30 core crops and aid in the reduction of poverty [39].

1.2 Bambara groundnut

Bambara groundnut is one such underutilised species that has been recognised by CFF for its considerable ability to produce high yields in drought conditions [4]. The cause of its underutilisation can largely be attributed to the perception that it has little economic potential internationally. As such, it is largely grown locally, by female farmers for subsistence only [7]. In this section we describe the growth behaviour of bambara groundnut. A picture of a typical plant can be found in Figure 1.1.

Figure 1.1: Bambara groundnut (*Vigna subterranea* (L.) Verdc) [13]

It is an indigenous African legume and it's main production area is semi-arid

Africa, where it is the third most important legume in regards to consumption and socio-economic impact. Other than semi-arid Africa, it has also become an increasingly important crop in Indonesia, Thailand and Malaysia [7]. It produces highly nutritious seeds, which are used for both human and animal consumption and is able to produce these seeds in nutrient poor soils where many crops would be unable to grow. It is considered to be a very robust crop that is not only drought tolerant, but also relatively disease free [36].

There is a wide range of genetic diversity within bambara groundnut species, largely due to its wide distribution of growth within Africa. This is one such feature that makes it an attractive candidate for further development as there is much scope for selection. This genetic diversity impacts upon a wide range of plant traits, such as leaf, flower and pod number, and also seed size, colour and pattern; all of these traits have been successfully manipulated using selection processes in previous crop improvement programmes [7].

Bambara groundnut is often grown in mixed cropping systems, where it is intercropped with cereals, tuber crops, vegetables and other legumes. Its importance in intercropping systems is attributed to its strong ability to improve soil fertility with enhanced levels of nitrogen fixation compared to other legumes [36].

Bambara groundnut is an annual herb, that grows to approximately 30cm high. It is similar to the groundnut (peanut) in morphology in that it grows leaves on lateral stems just above ground level. It can be categorised into three types; bunched, semi-bunched and spreading with the internode length determining which category it lies in. The plant produces pods, which are almost spherical in shape and usually develop underground. Each pod contains at least one seed, and can sometimes contain up to four. It is the seeds, both ripe and unripe, that are used for human and animal consumption in a range of dishes. Immature seeds can be eaten fresh or grilled, however, mature seeds are hard and are consumed by either pounding into a flour or boiled into a stiff porridge. Seeds are variable in their shape, colour and hardness and it is the appearance of the pods along with the plants spreading type

which determine which cultivar (plant variety) they belong to [36].

Germination occurs generally between seven and fifteen days depending on water availability, temperature and genetic variety [20]. Plants begin to produce flowers between 30-55 days after sowing and fertilised flowers produce pods underground approximately 30 days after fertilisation [36]. It has been found that the time from sowing to flowering is not always affected by the number of daylight hours in a day, however the time to podding is [7].

As an underutilised crop, there has been no rigorous breeding programmes that give academically established varieties [4]. Instead it is landraces, defined as a locally adapted variety of a species, that are grown by farmers [32]. In this work, two such landraces are investigated, Uniswa Red and S19-3. Of these, S19-3 is considered to have been evolved for hot, dry climates causing it to have a faster life cycle, which minimises the potential damage caused by droughts. Uniswa Red is more adapted to wetter, colder climates and has a longer life cycle.

1.3 Aims and objectives

The aim of this PhD is to develop a multi-scale mathematical model that simulates the growth and development of a single bambara groundnut plant, taking into consideration the interaction of the individual plant with its neighbours. This is done for multiple plants at one time, with data for each plant aggregated to the crop level.

The design of the model is such that variations in temperature and solar radiation can be accounted for. The mathematical model is compared to experimental data to determine the predictive power of the model. Once a reliable model has been developed, we apply this model to:

1. investigate the effect that individual plant positions have on crop yield;
2. investigate the effect that variation at the individual plant level has on the crop level;
3. optimise planting arrangement to maximise yield;

4. extend the model to investigate the planting of multiple species in one area; and

5. optimise the arrangement of two species in an area to maximise yield.

1.4 Thesis outline

– **Chapter 2** is a review of the existing literature on mathematical modelling of plants and crops paying particular attention to models that bridge the gap between individual plant modelling and crop modelling. Here we also describe previous simulations of bambara groundnut.

– **Chapter 3** introduces the initial mathematical model that describes the growth and development of bambara groundnut. The model is formulated using data from the literature and Tropical Crops Research Unit (TCRU) experiments. We then investigate the model analytically and compare the numerical solution to data.

– **Chapter 4** gives an overview of the model revisions that are made to the initial model. We again compare the numerical solution to experimental data sets and conduct further investigatory experiments on the mathematical model.

– **Chapter 5** gives an overview of the experiments conducted for this work in the Future Crops greenhouses. Further revisions to the model are then discussed.

– **Chapter 6** is a discussion of how to optimise the placement of individual plants of the same species in order to maximise the final yield of the total crop. A number of planting arrangements are investigated and an optimisation algorithm is formulated.

– **Chapter 7** is a discussion of how to optimise the placement of individual plants of two different species in order to maximise yield. Four fictional species are introduced for which optimisation investigations are conducted. Further to

this, an investigation of optimum sowing date is conducted. The mathematical model is then formulated for oil palm and an investigation on optimum planting arrangement of bambara groundnut and oil palm is undertaken.

– **Chapter 8** summarises the results of this PhD, discusses how this research has achieved the aims and objectives set out in this chapter and makes recommendations for future research.

Chapter 2

Review of Literature

2.1 Introduction

A principal objective in agriculture is to maximise food production; this is particularly relevant with the added demands of an ever increasing population, coupled with the unpredictability that climate change brings. Further improvements in productivity can only be achieved with an increased understanding of plant and crop processes. In this respect, mathematical modelling of plants and crops plays an important role. There has been a large amount of work undertaken in this area with two fundamental aims, firstly, to investigate and develop understanding of plant processes and secondly, to make predictions. The majority of this work, for either aim, focuses either on describing processes within a plant such as genetic regulatory networks [28], descriptions of an entire plant in isolation [60] or the growth of many plants simultaneously, i.e crop growth [35]. To describe these processes, it may be useful to utilise a crop or plant model. Crop models provide a quantitative means of predicting growth, development and yield of a crop [47]. They are useful in modelling the interactions between crop growth and environmental factors, making them useful for evaluating growth limitation caused by climate factors [3]. Even for one particular purpose there are many variations in the approaches used. Beyond crop models (those that deal with the aggregate scale), plant models (those that consider

the single scale) are tools that can be used to better understand the underlying processes of crop development. The process of plant growth can be studied at several levels of detail, ranging from sub-plant level to the multi-plant level.

At the crop scale, physiological processes at the plant scale are often taken for granted leaving biomass formation and food yield to be typically taken as a function of management factors, such as water irrigation and soil tillage [26]. It is a challenge in science to explain findings at the crop scale in terms of the physiological processes at the plant scale. As a community, mathematical modellers are beginning to bridge the gaps between these pieces of knowledge, however our understanding in these areas is often qualitative and does not explain the more subtle processes of plant morphology and biochemistry [26].

In this chapter, we aim to summarise the main approaches for mathematically modelling crops and plants at their different scales, paying particular attention to methods of incorporating a single plant model within a crop scale one.

2.2 Brief overview of model types

There are many types of approaches to modelling plant/crop growth that span a vast range of purposes and cover various levels of the growth process of the plant. Levels can range from biochemical pathways and substance transportation within a plant to scoping best management practice and yield forecasting [51]. The choice in approach depends on the purpose of the model and also the resources available, for example what experimental data are available to parameterise the model or how much computational power is at one's disposal to carry out the simulations. We now describe these model types, describing their limitations and advantages.

All models can be split into two categories; static and developmental. Static models are independent of time and designed to capture the physical state of the plant/crop at a particular point. In contrast, developmental models map growth and behaviour over time.

Within these two categories, modelling approaches can further be broken down

into a number of subsets with a lot of overlap between them, hence, a mathematical model describing plant growth is likely to contain a combination of model types.

Developmental models can be descriptive or mechanistic. Descriptive models integrate the results of measurements over time whilst mechanistic models attempt to describe the underlying processes of the plant system [52]. Descriptive models are useful for re-enacting plant development [51] but reflect little or none of the mechanisms behind crop growth [40]. Mechanistic models provide more insight into how a plant functions. These mechanistic (or explanatory) models contain sub-models for at least one hierarchical level deeper than the response that we are trying to describe [51]. For instance, we may wish to describe the crop level behaviour and to do this mechanistically we would describe the crop in terms of the individual plants within it. Despite including an extra layer of detail, even a very comprehensive mechanistic model cannot describe all of the underlying mechanisms as designing and running such a model would be impractical [40]. Mechanistic models may also be referred to as virtual plants or functional-structural models. Both mechanistic and descriptive models can be thought of as either scientific, designed to improve our understanding of crop growth, or engineering, designed to provide sound management practice for farmers.

Cornede *et al.* [19] describes functional-structural models as those that combine the architecture of a plant and also include the biological processes that describe plant growth. These types of models may also be referred to as individual based models [52]. At the individual plant scale, these models allow for a very detailed description of plant architecture allowing for more accurate insight into plant development. These detailed models allow for an enhanced awareness of a plant's micro-climate sensed by sub-parts of a single plant or even the micro-climate experienced by a single plant within a field of neighbouring plants. Attaining a model of this detail can only be achieved through the computationally intensive process of plant digitalisation. In addition, this detailed work is only a good representation of the plant in question and can not be easily generalised. Despite these complications

there is a real need to study the extension of individual functional-structural models to plant populations, such as multi-scale crop models. Further details of such models can also be found in the works of Prusinkiewicz and Yan *et al* [**?**, 60] in addition to many other sources.

Patricia *et al.* [51] characterises empirical, deterministic and stochastic plant/ crop models in the following way. Empirical models are directly informed by observed data and can be used for several scales of growth ranging from sub-plant to crop level. The correlation and regression analysis of these models do provide some qualitative understanding of variables, but they are often site and plant specific and not easily generalised. Thus using these models to aid decision making is severely limited. Deterministic models provide estimates of crop yield or biomass without any associated probability distribution and typically make no attempt to estimate an associated level of uncertainty in the parameter values or input data (e.g. environmental). Models such as these can be useful when these inputs are known, however in cases where there exists large amounts of uncertainty in parameters or input data, the models can become unreliable. In contrast stochastic models allow for more random variation in parameters, although these come at the cost of being much more complicated to formulate.

Mathematically speaking, there are three types of models, algebraic, which connects variables and parameters; differential, which connect rates of change with variables and parameters and finally, stochastic, which introduces an element of probability. In this thesis it is largely dynamical differential models that we consider.

2.3 The practical use of mathematical models

There has been much debate about the practical use of mathematical modelling in agriculture and there is no consensus as to the value of computational models. However, there are many who recognise the increasing importance of mathematical models in the area [52]. Over the past few decades, steps have been taken to improve

mathematical models [1] and there is an increasing demand to bridge the gap between mechanistic models of individual plants and the crop population scale. These can be used to not only estimate crop yield but also to investigate how to optimise management practices to maximise yield.

A mathematical model cannot include all of the processes for fear of becoming intractable. This means that a plant model will not cover the full spectrum of behaviour experienced in reality [26].

Aggarwal [1] outlines how uncertainties in data (e.g. solar radiation, temperature, water availability) affect mathematical models. Deterministic models in particular are heavily dependent on inputs. The outputs, such as yield, evapotranspiration and nitrogen uptake experience inaccuracy due to uncertainties in both model structure and input data. This data uncertainty is largely comprised of incomplete information on input variables, for example, weather variables often experience a lot of spatial and temporal variation. Generally, bias in outputs such as yield data, evapotranspiration and nitrogen uptake is low and within model error, however for a water or nitrogen limited environment, bias is considerably more. Progress in eliminating uncertainties in input data is limited by the availability of reliable instruments. Over the past 20 years there have been considerable improvements to instruments and many new tools have been developed. The driving force behind these developments in data collection and the instruments used is the insatiable demand from crop modellers for data [47].

2.4 Modelling individual plant growth

A more thorough understanding of plant growth and development is fundamental in improving crop yield. As such, there has been an increase in mathematical models that describe growth in terms of plant processes and abiotic factors in recent years [21]. We now discuss mathematical models that describe such growth at the individual plant level.

Many models that work on the individual plant scale examine the allocation of

assimilated nutrients for cell reproduction, hereby referred to as assimilates. Ma *et al.* [44] discusses the growth of an individual plant in regards to its source-sink relationships, paying specific attention to competition between assimilates within the plant and plant topology, but does not discuss competition between plants. In this work, a functional-structural model is developed to simulate fruit-set patterns among *Capsicum* cultivars. Plant biomass was described using a single ordinary differential equation (ODE) that was dependent on solar radiation and leaf area index. Plant biomass was then partitioned to the various sinks using empirically based equations. The topological structure of this model was incorporated by defining physiological ages to predetermined sections of the plant, for example the lower stem of the tomato plant had the oldest physiological age and secondary branches had the youngest. More examples of models of this nature can be found in Marcelis [40]. These types of models have been found to show good correlation with experimental data, but their use in predicting total crop yield is limited due to their complexity and the difficulties of parameter estimation.

There has been an ever increasing importance placed on including plant architecture within models [21]. Godin [24] provides us with several methods of representing plant architecture with a range of complexities to be used in functional-structural models. Many representations are explored, such as plant topology described in the context of graph theory. The complexity of the plant architecture ranges from course level representations such as modelling an entire plant structure as a single module, to much finer levels where the trees structure is split into many repeated components (e.g. branches, stems and leaves). At the most basic level, geometric representations of tree crowns can be used efficiently to model light interception. These geometric representations can take the form of a cylinder or sphere, but can also take more flexible and complex representations that come at 'intermediate' computational cost between simpler geometric shapes and more elaborate computational representations. More complex representations of a plant's topological structure can help to refine the knowledge of developmental processes within the plant, such as

the transportation of nutrients. It is important to stipulate however that Godin [24] focuses on the single plant scale with a lot of detail. Using such a model on the many plant scale would become very computationally intensive.

Cournede *et al.* [19] discusses a zone of influence model in the context of agriculture, where the zone of influence is the area a single plant impacts upon. This is a variety of the mechanistic approach that is functional-structural modelling, where individual plant biomass is described using a discrete system whereby the zone of influence is represented by a circle. Plant growth at the individual plant level is described by empirical mathematical functions, which are solved computationally. Competition between two plants is given by the geometric overlap between the two circles that represent their canopies. This is an extension of much earlier studies that investigate mathematical models concerning competition between individual trees [9]. The zone of influence can change over time as the plant grows, however it can also be set to a constant value equalling the plot area divided by the number of plants in that area, this would give the average area available for one plant. This concept is used in several other works with some success [8, 53]

In contrast to the generalised approach of Cournede *et al* [19], Godin [25] describes a more detailed topological method. In this case the plant is divided into its individual components and interactions between these are modelled using tree-graph structures. The components can be divided into spatial or mechanical ones. These models can be allowed to vary in time, however the process of doing this is somewhat arbitrary and consists of piecing together separate 'snap-shots' of the plants' topological structure.

Models that investigate the more precise aspects of canopy structure are useful in examining processes such as the optimisation of photosynthesis. This can be useful in designing breeding programs to increase a plant's yield ability [56]. The application of these detailed architectural models to predicting whole crop yield is less obvious. The complexity of individual plant models is such that they provide a computationally intensive model in their own right, thus including them as a

sub-module of a higher-level crop model can be impractical.

2.5 Modelling crop growth

The concept of modelling crop growth can have different meanings. To some, modelling growth can mean modelling the development of the crop through its phenonological phases. It can also mean simulating crop yield, biomass, nitrogen uptake or fixation. For all these cases, modelling may refer to simulating over time or singularly at maturation. In this work we focus on simulating growth in terms of yield and biomass in response to environmental factors such as temperature and solar radiation over time. As such, we restrict the review of the extensive amount of literature to this area.

Typically, above-ground biomass is predicted as a function of leaf area index (LAI), the extinction coefficient (which relates to the crop canopy geometry) and the radiation use efficiency [19, 20, 32]. Leaf growth is an important factor in this type of model, but despite this the processes behind it are not fully understood by crop modellers [40]. There are two main schools of thought for modelling the leaf area or leaf appearance rate. Marcelis [40] describes a method of predicting leaf area development as a function of canopy biomass. He also discusses the simulation of leaf area as a function of leaf appearance rate, to be calculated separately from the biomass equation. Both approaches are general and can be applied to many types and species of plant and we explore both later in this work.

It is common in crop level models to treat all plants within the crop as a single entity and simulate a uniform field of crops making predictions on an area basis [60]. In doing so intra-specific competition is included using density factors so that an empirical relationship between plant density and final yield is formulated.

In the cases where all plants within the crop are *not* treated as a single entity, an individual-based approach is used where the growth of each plant is described. Bauer *et al.* [8] discusses the importance of including spatial positioning and a zone of influence where interactions with neighbours occur in individual-based methods.

In this work, the growth rate of individual plant size is determined using non-linear mathematical functions. In addition to the growth of individual plants, Bauer models the change in population of a field of plants. Here, plant reproduction rate is determined by a linear relationship relating to individual plant size and the spatial positioning of newly introduced plants is determined using a two-dimensional exponential probability function. Plant mortality is determined by plant age and also the degree of competition so that once the combined affect of these two variables meets a certain threshold, the plant is assumed to die. The aim of this work was to investigate the cyclic dynamics in perennial plant populations.

The zone of influence model described by Cournede *et al.* [19] is another individual-based model that describes crop scale. Here, both the growth of individual plants and interactions between them is addressed and aggregated to the many plant level. The growth of a population of plants is simulated where individual plants are coupled together with the inclusion of neighbour-neighbour competition for light. Here, competition is calculated as being a function of spatial overlap between two plant canopies. Plant shadowing is calculated using a Poisson probability model that determines whether an infinitesimally small element of a plant's surface area is shadowed by a neighbouring plant. The model assumes strictly vertical irradiance and canopy foliage is uniformly distributed amongst the zone of influence. Despite these generalisations, the method gives a good general approach and applications of this methodology are far reaching.

The way in which competition is included in an individual-based model can vary. Schneider *et al.* [53] explores a number of methods of incorporating inter-plant competition, which are referred to as competition kernels. These kernels included, but were not limited to, spatial overlap between two circular canopies, where canopy area was taken to be a function of biomass. The inter-plant competition for all kernels is limited to pairs of plants and does not explore the case of multiple plants overlapping at the same point. The interactions that one plant has with others is summed over all neighbouring plants. It was found in this work that zone of

influence models were significantly more efficient at capturing crop behaviour and also that there existed a large amount of asymmetry in competition whereby if one of the two competing plants was significantly larger than the other, the smaller plant experiences the majority of competition.

Cournede *et al.* [19] and Scneider *et al.* [53] both explore the case of a zone of influence that varies over time, however Cournede *et al.* [19] also discusses the impact of forcing a constant zone of influence. It was shown that the constant zone of influence approach works well for high density crops, but fails for low density crops and does not give a good fit to data for the early stages of growth.

2.6 Modelling Bambara Groundnut

Although the literature surrounding crop modelling is extensive, that which relates directly to bambara groundnut is significantly sparser. There has been much work done in quantifying external (e.g. weather) and crop management effects on the yield of bambara groundnut [6, 45], however there is a limited amount of information on simulating the behaviour of the crop. Many of the current models are mechanistic in approach and largely consider crop maturation rates [11]. Fewer still have examined biomass and yield development. Those that do, do not examine in detail the effect of canopy interactions on biomass production. The total number of crops is treated as a single entity and competition is incorporated using a density factor [20, 31]. This works like a dampening factor so that growth is limited by a parameter ranging between 0 and 1, where a 1 would indicate no competition and 0 would indicate that competition has prevented further growth.

Current bambara groundnut models show reasonable similarities between simulations and experimental data, however these simulations are often site specific and underestimate above ground dry matter production in the greenhouse. It is theorised that this could be due to underestimating the photosynthetic potential of the plant [20]. It may also be that the dampening factor included for competition is too strong. This gives rise to further need for a mathematical model that includes

a more detailed description of plant architecture on the single plant scale, which is then scaled up to the many plant, or crop, scale.

Karunaratne *et al.* [31] discusses the importance of temperature in modelling bambara groundnut. Like many of the major crops such as wheat, cowpea and rice, bambara groundnut has been shown to be strongly affected by extremes in temperature. In the thesis of Karunaratne [32], the BAMGRO model was developed that uses a system of dynamical equations to simulate the leaf development, plant biomass and pod mass of the entire crop. This work pays particular attention to the effect that temperature and drought have on growth at the crop level.

The BAMGRO model [31] operates between two interconnected processes: the crop maturation rate and the rate of biomass acquisition. Crop maturation rate, or crop phenology, is the movement of the plant through the different developmental phases of crop growth. Movement through these phases is considered non-reversible and strongly dependant on temperature. The developmental stages can largely be described with respect to two major phases: vegetative and reproductive. Unlike many grains used for food, where the change between vegetative and reproductive acts like a switch, the phases overlap for the bambara groundnut. Thus the plant continues to develop new leaves in the reproductive stage.

The rate of leaf appearance is measured as a function of cumulative thermal time where the thermal time is the sum of the average daily temperature [20, 31]. This can be done in a number of ways, either the leaves per cumulative thermal time can be measured as a series of piecewise linear relationships [20] or a Gaussian relationship can be used to model the new leaf rate [31]. This approach has also been used in mathematical models of other plant species [16]. The advancement in developmental (phenological) age, i.e. the stages of growth, is also measured in terms of thermal time. This is one of the most widely used approaches in crop models [5, 18, 27, 31]. It has been shown that phenological stages such as emergence, leaf initiation and leaf appearance rate occur at a precise thermal time after germination [18].

In the BAMGRO model [31], the leaf appearance rate and hence the leaf number

and leaf area are calculated as a function of thermal time. This is then incorporated into the biomass acquisition equation to simulate the green biomass and crop yield. We explore this method, as well as the method of calculating leaf area as a function of canopy biomass, in Chapters 3 and 4.

Brink *et al.* [11] recognises the strong link between photo-period and temperature on the phenological development but applies it in a different way. Here a relatively simple method is applied to modelling bambara groundnut. The rate of progress towards a phenological stage is calculated using a combination of three linear equations that depend on temperature and photo-period. A benefit of this method is that the interaction of photoperiod and temperature on the influence on the crop disappears. This is beneficial as the study Brink also demonstrates that not all of the plants are affected by long photo-periods and has been applied to several types of annual crops such as soya bean, cowpea, chickpea, lentil and barley in the work of Summerfield *et al.* [55].

2.7 Intercropping

Intercropping is defined as a practice of growing two or more different species of plants together in the same area. The position of individual plants in an intercropped environment in addition to sowing time, time of emergence and time to maturation can have a significant impact on the competition between plants [22]. There are many ways in which plant species can be arranged in relation to each other, ranging from adjacent patches of species to cropping systems that replicate a more natural ecosystem. Malezieux *et al.* [46] describes in more detail the different forms of species mixtures with varying complexity and gives examples of where different arrangements are typically applied. Using physical experiments to investigate the effect different planting arrangements of two species has on yield is costly and time-consuming and can be greatly reduced with the application of mathematical models.

The practice of intercropping has several advantages, ranging from ensuring the

best use of available resources to promoting biodiversity. A key benefit of intercropped systems is the enhanced robustness to total crop failure in unpredictable environments [46]. As a nitrogen fixing crop with high drought tolerance, bambara groundnut is considered to be a particularly suitable crop for intercropping. It is most frequently mixed with crop species such as cowpea, maise and sorghum [6]. As such, being able to mathematically model bambara groundnut growth within an intercropping environment was an important part of this work. In this section we discuss some of the literature surrounding current intercropping models.

There are many models that simulate competition for various resources in intercropped environments [10, 23, 17]; in these models the inclusion of competition for light is a frequent feature [10]. Graf [17] discusses such an approach for simulating competition for light, which involves splitting the total crop canopy into a number of horizontal layers. This approach requires knowledge of respective plant heights of individual species and the vertical distribution of leaf area. The number of layers is determined by the plant heights of each species and competition for light is calculated at each horizontal layer of canopy for each species. In the top layer only the light intercepted by the tallest plants is calculated, at a lower level the light intercepted by some of the shorter plants and also the lower leaves of the taller plants is calculated and so on. All plants of the same species in this model are treated as one entity and the position of species in relation to each other are not taken into account. This approach is common with crop-weed models where the position of the competing plants is not user determined and thus cannot be assumed. A similar approach to this has however been applied to competing crops, such as in [10], although it is necessary to make the assumption that the arrangement of species is horizontally homogeneous i.e. that plant spacing is uniform. Gou *et al.* [23] describes an approach to simulating the competition between two species that are separated into rows in an arrangement referred to in the literature as relay strip planting. Some horizontal heterogeneity is included here as the distance between rows can change. In this work, plants are solely competing for light and the daily

intercepted light is calculated for each species individually. All plants belonging to the same species are treated identically here.

Zone of influence models, where architectural representations of individual plants are aggregated to the crop scale, are another method of simulating intercropped systems [46]. Garcia-Barrios *et al.* [22] describes an example of such a model where a system of ODEs is used to mathematically model the canopy biomass of a number of individual plants which are aggregated to the multi-plant level. The impact that one plant has on another is a function of the distance between them and empirically found values. Plant interactions are limited to two plants at a time, and so the case where three or more plants competing at one point is not considered. In this work the canopy biomass of Radish and Bushbean in an inter-cropped environment is investigated, it was found that this model was able to predict the canopy biomass of each species satisfactorily.

These spatially explicit methods allow for the heterogeneity of the system and include the architectural organisation of different species, however, they are more often applied to simulating tree growth and are rarely applied to annual crops [46].

2.8 Applications of crop growth models/ model validation

Even if a mathematical model demonstrates a robust ability to simulate crop behaviour it may come across problems concerning uptake and validation by farmers. Some of the issues facing crop modellers are summarised in this section.

Agronomic trials are often expensive and so validating a mathematical model can often be financially infeasible [37]. In contrast to traditional experiments, crop experiments are often testing several hypotheses at once [51]. In addition, field experiments, and even greenhouse experiments, are rarely precise, thus giving indefinite results to compare with the model [51].

It is a problem for crop modelling in general to attain rigorously designed and well documented long-term experiments to validate crop models [35].

Model performance is limited to the quality of the input data and so without accurate parameter values, it is unlikely that any model will give accurate results for a variety of scenarios. Furthermore, not all the processes of plant development are fully understood, meaning that crop modelling parameters are approximated based on empirical estimations rather than physiological understanding of the underlying processes. The problem with this is that the empirical values are often site specific and are not always transferable to other sites. In addition to this, many crop models rely on meteorological data, which is in itself difficult to model. Hence modelling future crop yield based on estimations of future weather data can be unreliable [51].

The pros and cons of highly detailed crop models are examined by Yan *et al* [60]. Complex models may be able to provide a dynamic representation of crop growth, however this has the cost of higher computational times. In addition, more complicated models have a larger number of parameters in need of calibrating. It is not always possible to measure these parameters directly and finding values for them requires model data optimisation. It is possible to attain a good fit of the experimental data with even a flawed model if using extensive optimisation on many unknown model parameters. In addition, the accuracy of the optimisation method needs to be taken into account in order to assess the accuracy of the parameter estimates.

One issue for increasing the uptake of mathematical models is that overly complex models with difficult input requirements, such as weather data, can make it difficult for researchers in developing countries to run the models [37]. This is particularly relevant when working with underutilised crops, as these are typically grown in developing countries.

2.9 Chapter summary

In this chapter a summary of the different approaches to mathematically modelling plants and crops was presented and, in particular, approaches that have been applied to bambara groundnut. A brief overview of the many categories was given, followed

by a more detailed discussion of approaches that consider individual plants within the crop scale.

The review of single plant modelling focused on work ascertaining to underlying plant processes and involved a level of detail that would be impractical when applied to a multi-plant model. In particular, plant architecture of varying levels of complexity was considered, ranging from the simplest form being a circular zone of influence that a plant impacts upon, to the most complex form where individual stems and leaf positions are considered. We found that the best approach depended on the aim of the work.

Within the discussion of population scale mathematical models, we found that there were two main approaches, one where all plants were treated as a single entity and another where an individual-based approach was applied. The former demonstrated a strong predictive ability, however the latter was able to provide more insight into how certain management practices could affect yield. It was found that for modelling bambara groundnut, only the first approach has been considered.

A discussion of intercropping was then undertaken and it was found that the spacing of individual plants in relation to each other was not always taken into account and the plant canopy was treated homogeneously. Individual-based zone of influence models provided a spatially explicit approach that are able to incorporate irregular plant spacing. In these models there is no consensus on how to incorporate competition and approaches range from linear empirical relationships to the consideration of geometric overlap.

In the remainder of this thesis we discuss an individual-based zone of influence approach to modelling bambara groundnut, paying specific attention to competition for light. A series of ordinary differential equations (ODEs) are used to simulate the growth of a single plant within a multi-plant environment. We begin with the minimal number of ODEs possible to describe the growth of one plant so as to keep the system as simple as possible. More ODEs are introduced over time so that enough detail is provided within the model to allow us to make recommendations

for best management practices. We assume a simplified plant architecture where the plant canopy is described by a cylindrical canopy raised on a core stem. The competition between plants is calculated as a function of the geometric overlap between plant canopies and we allow for more than two plants to compete for light at one point.

Chapter 3

A Mathematical Model of Bambara Groundnut

In this chapter, an individual-based mathematical model of bambara groundnut is formulated. We begin with a description of plant growth at the single plant scale. Following this, interactions between two competing plants are examined, which is later scaled to the multi-plant (crop) scale. The single and multi-plant scales are linked via canopy interactions that an individual plant has with its neighbours.

Model parameters are informed and the model tested using literature and greenhouse experimental data.

3.1 A single plant model

Consider a single plant growing without competition from neighbouring plants; there are countless processes occurring within this plant that all play a part in its growth and development. A mathematical model designed to simulate all of these processes is infeasible as it would be impractically complex. Instead, certain processes are selected depending on what one hopes to gain from mathematically modelling the growth of this plant. The motivation of this work is to investigate the effect that variation at the individual plant scale has on the crop scale. This is done using the primary output of crop yield. In particular, we are interested in understanding plant

canopy interactions and their impact on plant growth and overall crop yield.

In order to formulate the model, we first consider the plant structure. Leaves grow on multiple lateral stems that spread along the ground, as illustrated in Figure 3.1. The spread of the plant canopy ranges from bunched to spreading for different species. For the purposes of this model, the plant canopy is simplified to a disc representing the layers of leaves, raised above the ground by a core stem. This approximation accounts for all main aspects of the plant's geometry we wish to include, while simplifying the mathematical modelling process. In addition, this simplified plant geometry is transferable to many other plant physiologies such as other legumes and also oil palm, which is particularly relevant in Chapter 7 when we apply the model to other species.

(a) (b)

Figure 3.1: (a) is a schematic of the plant canopy of bambara groundnut; and (b) is a birds-eye view of a single bambara groundnut plant 51 days after sowing.

The growth of a plant in the absence of competition will depend on other environmental conditions external to the plant, such as solar radiation, nutrients in the soil, water and temperature. In this study, we limit our investigation to competition for light, as such water and soil nutrients are assumed to be non-limiting, leaving

temperature and solar radiation to be the primary influencers of plant growth.

It is acknowledged that the gain in biomass of a plant is directly dependent on the absorbed radiation, which is absorbed through sunlight [40]. In this work, sunlight is assumed to be constant and does not vary in space or time. It is known that radiation is absorbed through the leaves and so to calculate the energy gained from sunlight, leaf area needs to be calculated. Marcelis [40] discusses the advantages and disadvantages of simulating leaf area independently or as a function of canopy biomass. He stipulates that calculating leaf area as a function of canopy biomass is appropriate when simulating a greenhouse environment, however shifts the problem from simulating leaf area to simulating specific leaf area (the leaf area per unit ground cover) over time [40]. In this model we adopt this approach and assume that leaf area and canopy biomass have a uniform relationship; this method eliminates the need for a further equation describing leaf area.

We now introduce a method of determining leaf area from canopy biomass. A relationship between leaf mass $LM(t)$ and total leaf area $A(t)$ known as the specific leaf area ϕ, gives an associated ratio between leaf area and canopy biomass

$$\phi = \frac{A(t)}{LM(t)}, \tag{3.1}$$

which is assumed to be constant over time for simplification. In addition, the relationship between leaf mass and stem mass $SM(t)$ can be described by a constant of proportionality ψ given by

$$SM(t) = \psi \times LM(t). \tag{3.2}$$

Evidence of this can be found in Figure 3.6 in Section 3.4.1 where parameterisation is discussed more thoroughly. The total canopy biomass $c(t)$ is equal to the sum of the leaf and stem mass so that

$$c(t) = SM(t) + LM(t) = (1 + \psi)\, LM(t). \tag{3.3}$$

Substituting equation (3.1) and (3.2) into (3.3) and rearranging for $A(t)$ gives

$$A(t) = \frac{\phi c(t)}{1 + \psi}. \tag{3.4}$$

Leaf area, leaf, stem and canopy biomass vary over time, however ψ and ϕ are assumed constant.

Now that leaf area can be described as a function of canopy biomass, the intercepted radiation a plant canopy is able to absorb per unit surface area R can be calculated. The light transmitting through the canopy decreases exponentially with canopy thickness, given by leaf area index. A well established approximation for a plant's radiation absorption is given by the Beer-Lambert law [15]

$$R = R_0(1 - exp(-\kappa\gamma(t))). \tag{3.5}$$

Here R_0 is the available photosynthetically active radiation above the canopy, κ is the extinction coefficient, which relates to the geometry of the leaf position (e.g. for flat leaves this will be equal to one) and $\gamma(t)$ denotes the leaf area index, which is the leaf area per unit ground surface area. This method of calculating the absorbed radiation is common in plant models and typically $\gamma(t)$ is calculated so that the total leaf area of all plants is divided by the total plot area. In our case, where plants are considered on an individual basis, an adaptation of this is used. Here, a local leaf area index is defined, which is the ratio of plant leaf area and ground area per plant such that

$$\gamma(t) = \frac{A(t)}{G(t)}, \tag{3.6}$$

where $G(t)$ is the ground cover of the plant's canopy. Here, $\gamma(t)$ can be thought of as the thickness of the disc that represents a plant canopy; a large $\gamma(t)$ value would mean a high ratio of leaf area to plant ground cover and so more layers of leaves and thus a thicker disc. Conversely, a small $\gamma(t)$ would indicate a lower leaf area to plant ground cover value and so fewer layers of leaves.

Ground cover can be determined in terms of the leaf area using an established

empirical relationship [19] given by

$$G(t) = G_0^{(1-B)} A(t)^B, \tag{3.7}$$

where G_0 is the initial ground cover, $A(t)$ is the leaf area and B is an empirical value that relates to the spread of the plant and ranges between zero and one.

To find the total radiation that has been absorbed by a plant, the total radiation per area R, given in equation (3.5), needs to be multiplied by the surface area of the plant's canopy which intercepts radiation i.e. the ground cover $G(t)$. After absorbing the photosynthetically active radiation, the plant must then convert that energy to biomass. This is incorporated into the model by including an efficiency coefficient c_k, which describes the mass gained per unit radiation. In addition, no matter how much radiation the plant is exposed to, there is a maximum size the plant can reach. This limiting factor is incorporated via the inclusion of a carrying capacity k_c, so that as biomass approaches k_c, growth rate decreases.

Combining the total incoming radiation with the plant's ability to convert radiation into mass gives the canopy biomass growth rate as

$$\text{Canopy growth rate} = Rc_k G(t) \left(1 - \frac{c(t)}{k_c}\right). \tag{3.8}$$

There is also some amount of canopy decay due to leaf senescence and pests. This is assumed proportional to the size of the canopy and is given by

$$\text{Canopy decay rate} = d_c c(t), \tag{3.9}$$

where d_c is the biomass decay rate and is assumed constant. By combining the relationships described in equations (3.8) and (3.9) the change in canopy biomass over time can be written as

$$\frac{dc(t)}{dt} = R_0 c_k G(t)(1 - e^{-\kappa\gamma(t)}) \left(1 - \frac{c(t)}{k_c}\right) - d_c c(t). \tag{3.10}$$

This newly devised equation is similar to previous mathematical models [32, 19], however with the addition of a carrying capacity.

Substituting equation (3.4) into (3.6) and (3.7) and then substituting equations (3.6) and (3.7) into (3.10) leads to a non-linear ODE describing the growth of a single plant in terms of $c(t)$,

$$\begin{aligned}\frac{dc(t)}{dt} &= R_0 c_k G_0^{(1-B)} \left(\frac{\phi c(t)}{1+\psi}\right)^B \left(1 - e^{-\kappa\left(\frac{\phi c(t)}{G_0(1+\psi)}\right)^{1-B}}\right)\left(1 - \frac{c(t)}{k_c}\right) \\ &\quad -d_c c(t). \end{aligned} \tag{3.11}$$

The initial condition for this equation is the mass of one single leaf and its associated stem such that $c(0) = c_0$.

3.2 Quantifying competition between plants

In order to scale the single plant to the many plant scale, competition between plants must be included. To do this, we first consider interactions between two plant canopies and a means of quantifying canopy-canopy competition between them is introduced here. Before doing so we discuss necessary assumptions that have been made regarding the plant canopies.

It has been previously stated that plant canopies are assumed to be circular discs raised above the ground by a central stem. The disc represents the layers of leaves within the canopy. A schematic diagram of two such interacting plants is shown in Figure 3.2. Similarly, it has been stated that light and temperature are the only limiting growth factors. Since temperature is not a competitive resource, the only form of competition we are interested in is the competition for light as a result of canopy-canopy shadowing. A plant that shadows another plant blocks sunlight from reaching the shorter plant's canopy so that competition for sunlight between plants will depend on which plant is taller. There are thus three scenarios which may occur for two adjacent plants:

1. The two plants grow at the same height for all time until they reach their

maximum size; or

2. Plant 1 grows higher than Plant 2 and its canopy overshadows that of Plant 2; or

3. Plant 2 grows higher than Plant 1 and its canopy overshadows that of Plant 1.

Scenario 3 is illustrated in Figure 3.2(a), a birds-eye view of two interacting plants is illustrated in Figure 3.2(b), where the distance between the centre of each plant is denoted by D.

The inter-plant competition can then be described by the proportion of the lower canopy that is shadowed by the taller one.

3.2.1 Calculating canopy-canopy shadowing/overlap

Here we calculate the overlap of two intersecting plant canopies where overlap O is defined as the fraction of area that the shorter plant's canopy has shadowed by the taller plant.

The two plant canopies are represented by Circle 1 (c_1) and Circle 2 (c_2) with radii r_1 and r_2, respectively, as shown in Figure 3.3. Since we assume that sunlight comes from directly above the plants, the area of Plant 1's canopy that is shadowed by Plant 2 is given by the area of intersection of these two circles, denoted by I. To calculate I in terms of r_1, r_2 and D we need to determine how these are related. To do this we subtend lines from the centre of each circle to points on their circumference where they intersect. This leads to the shaded rhombus in Figure 3.3. We will now demonstrate how we calculate I for several varying states of intersection.

Figure 3.3 shows two segments s_1 and s_2 of c_1 and c_2 divided into three regions A, I, and B, where $A + I$ is a segment of c_1, $B + I$ is a segment of c_2 and I is the area of intersection that we wish to determine. The sum of segments s_1 and s_2 is given such that

$$s_1 + s_2 = A + 2I + B, \tag{3.12}$$

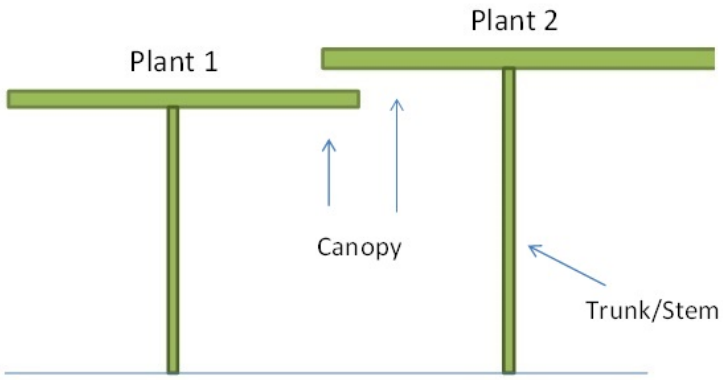

(a)

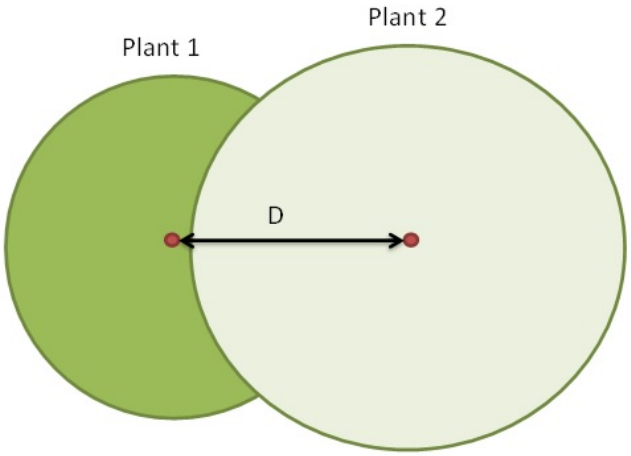

(b)

Figure 3.2: Two competing plants, where D is the distance between the centre of the two circles that represent the interacting plant canopies. (a) is a side view of two competing plants, where Plant 2 has grown higher than Plant 1 thus overshadowing part of its canopy. (b) is a birds-eye view of two competing plants, where Plant 2 has grown higher than Plant 1 thus overshadowing part of its canopy. The intersection of the two circles gives the spatial overlap between the plants and thus the proportion by which Plant 2 shadows the canopy of Plant 1.

Rearranging (3.12) for I gives

$$I = s_1 + s_2 - (A + B + I). \tag{3.13}$$

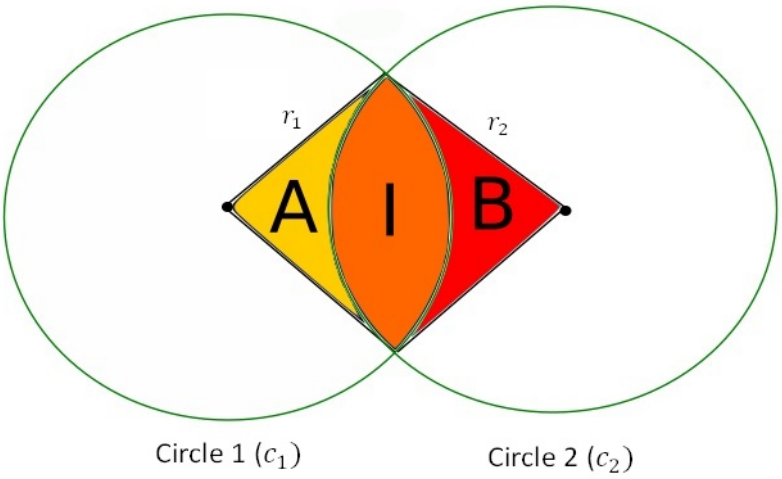

Figure 3.3: Two circles representing the canopies of two competing plants. A segment of each circle is highlighted so that $s_1 = A + I$ is the segment s_1 of Circle 1 and $s_2 = B + I$ is a segment s_2 of Circle 2. The area of intersection of the two circles is given by I.

The area of $A + B + I$ can now be found in terms of the distance between plant centres D and the vertical distance between the two intersecting points (See Figure 3.4).

To determine I it is necessary to find the area of segments s_1 and s_2 and the distance between the two points of intersection of the two circles. We now find the points of intersection. Let the centre points of c_1 and c_2 be $(0, 0)$ and $(D, 0)$ respectively, with radii r_1 and r_2 so that the two circles can be described by

$$x^2 + y^2 = r_1^2, \tag{3.14}$$

$$(D - x)^2 + y^2 = r_2^2. \tag{3.15}$$

Combining equations (3.14) and (3.15) and rearranging for x we obtain

$$x = \frac{D^2 - r_1^2 + r_2^2}{2D}, \tag{3.16}$$

which gives the perpendicular distance between the two intersection points and the centre point of Circle 1. Similarly the perpendicular distance between the points of intersection of the two circles and the centre of Circle 2 is given by $D - x$, as illustrated in Figure 3.4.

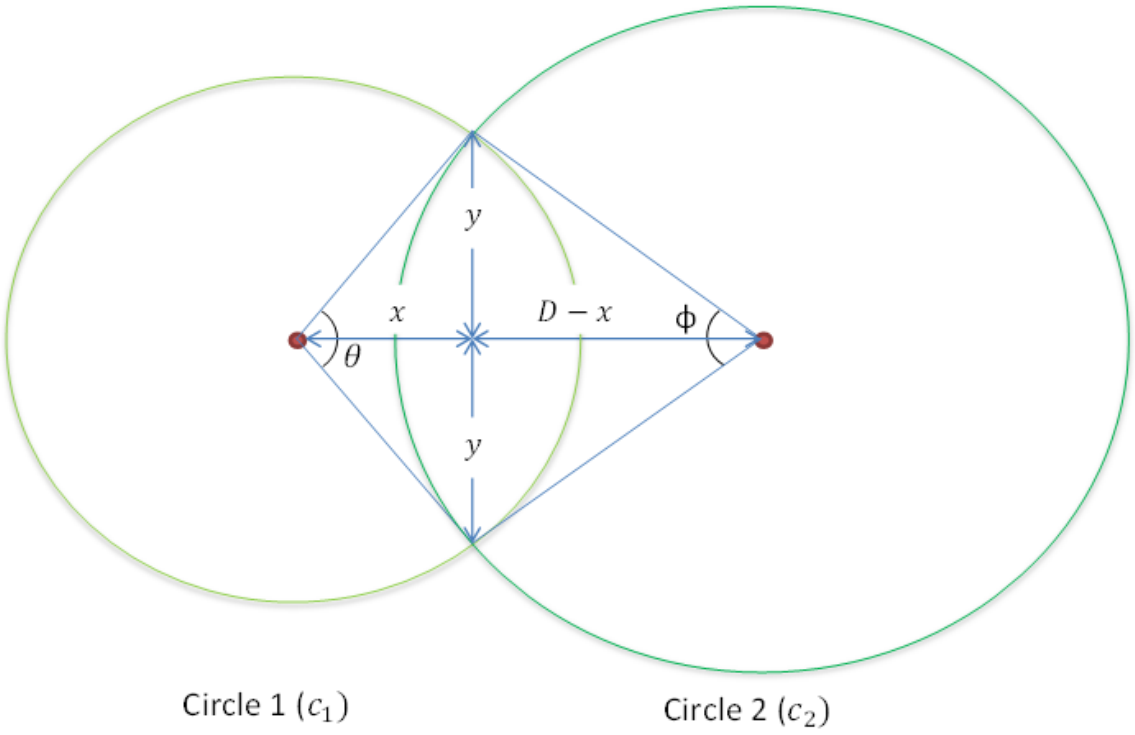

Figure 3.4: Two circles representing the canopies of two competing plants. The angles made by subtended lines from the points of intersections and the centre points of Circles 1 and 2 are given by θ and ϕ, respectively.

It follows that for $x > 0$ then

$$\theta = \cos^{-1}\left(\frac{x}{r_1}\right) \tag{3.17}$$

where θ, is the angle shown in Figure 3.4. The area of $A + I$ is then given by

$$s_1 = \frac{r_1^2}{2}\theta. \tag{3.18}$$

Bringing equations (3.16), (3.17) and (3.18) together gives

$$s_1 = A + I = r_1^2 \cos^{-1}\left(\frac{D^2 - r_2^2 + r_1^2}{2Dr_1}\right).$$

Similarly,

$$s_2 = B + I = r_2^2 \cos^{-1}\left(\frac{D^2 + r_2^2 - r_1^2}{2Dr_2}\right).$$

All that is left is to find the area of $A + B + I$. The area of a rhombus is given by $\frac{1}{2}pq$ where p is the length of the longest diagonal, given here by D and q is the length of the shortest diagonal, given here by $2y$, which is the distance between the two points of intersection. This can be found by rearranging for y in equation (3.14) such that

$$y = \frac{1}{2D}\sqrt{6D^2r_1^2 - D^4 - 2D^2r_2^2 + 2r_1^2r_2^2 - r_1^4 - r_2^4},$$

which leads to

$$\begin{aligned} A + B + I &= \frac{1}{2}pq = Dy \\ &= \frac{1}{2}\sqrt{6D^2r_1^2 - D^4 - 2D^2r_2^2 + 2r_1^2r_2^2 - r_1^4 - r_2^4}. \end{aligned} \tag{3.19}$$

Finally, substituting equation (3.19) into equation (3.13) leads to

$$\begin{aligned} I &= r_1^2 \cos^{-1}\left(\frac{D^2 + r_1^2 - r_2^2}{2Dr_1}\right) + r_2^2 \cos^{-1}\left(\frac{D^2 + r_2^2 - r_1^2}{2Dr_2}\right) \\ &\quad -\frac{1}{2}\sqrt{6D^2r_1^2 - D^4 - 2D^2r_2^2 + 2r_1^2r_2^2 - r_1^4 - r_2^4}. \end{aligned} \tag{3.20}$$

We now consider various scenarios regarding this interaction. If:

- $r_1 + r_2 < D$ then the canopies of the two plants do not interact;
- $D + r_1 < r_2$ then c_2 completely covers c_1 and so the overlap area is equal to the area of c_1; and
- $D + r_2 < r_1$ then c_1 completely covers c_2 and so the overlap area is equal to the area of c_2.

The area of overlap between the two circles given in equation (3.20) works for the case $x > 0$; however, if the points of intersection of the two circles are not between the centre points of the two circles, a different formula must be obtained.

In a case such as this, one of the circles would be much larger than the other. We now consider the case where Circle 2 is much larger than Circle 1. Therefore $x < 0$, which causes the points of intersection to be placed to the left of Circle 1's centre point, as illustrated in Figure 3.5.

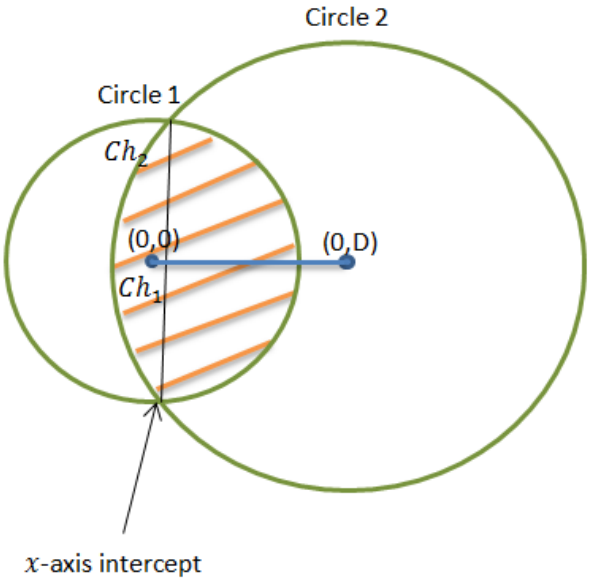

Figure 3.5: Two circles representing the canopies of two competing plants. Here Circle 2 is considerably larger than Circle 1. In this case, the points of intersection of the two circles occurs to the left of the centre point of Circle 1. The chords of the two circles are denoted by ch_1 and ch_2 respectively. The area I is marked with hashed lines.

In this case I is a large proportion of Circle 1's canopy. We define ch_1 and ch_2 as areas limited by a chord of Circle 1 and Circle 2 respectively, as illustrated in Figure 3.5. To find I, ch_2 needs to be subtracted from the ch_1 and the sum of this

needs to be subtracted from the area of Circle 1 A_1 such that

$$I = A_1 - (ch_1 - ch_2). \tag{3.21}$$

The area of ch_1 and ch_2 are given such that

$$\begin{aligned} ch_1 &= r_1^2 cos^{-1}\left(\frac{-D^2 + r_1^2 - r_2^2}{2Dr_1}\right) - \\ &\quad \frac{r_1^2 - D^2 - r_2^2}{4D^2}\sqrt{6D^2r_1^2 - D^4 - 2D^2r_2^2 + 2r_1^2r_2^2 - r_1^4 - r_2^4}, \end{aligned} \tag{3.22}$$

and

$$\begin{aligned} ch_2 &= r_1^2 cos^{-1}\left(\frac{D^2 + r_1^2 - r_2^2}{2Dr_2}\right) - \\ &\quad \frac{D^2 + r_1^2 - r_2^2}{4D^2}\sqrt{6D^2r_1^2 - D^4 - 2D^2r_2^2 + 2r_1^2r_2^2 - r_1^4 - r_2^4}. \end{aligned} \tag{3.23}$$

Substituting ch_1 and ch_2 into equation (3.21) gives

$$\begin{aligned} I &= c_1 - r_1^2 cos^{-1}\left(\frac{D^2 + r_1^2 - r_2^2}{2Dr_1}\right) + r_2^2 cos^{-1}\left(\frac{D^2 + r_1^2 - r_2^2}{2Dr_2}\right) \\ &\quad -D\sqrt{6D^2r_1^2 - D^4 - 2D^2r_2^2 + 2r_1^2r_2^2 - r_1^4 - r_2^4}. \end{aligned} \tag{3.24}$$

Similarly if Circle 1 was much larger than Circle 2 so that $x > D$ then the chord area of Circle 1 needs to be subtracted from the chord area of Circle 2 giving

$$\begin{aligned} I &= c_2 - r_1^2 cos^{-1}\left(\frac{D^2 - r_1^2 + r_2^2}{2Dr_1}\right) + r_2^2 cos^{-1}\left(\frac{-D^2 - r_1^2 + r_2^2}{2Dr_2}\right) \\ &\quad -D\sqrt{6D^2r_1^2 - D^4 - 2D^2r_2^2 + 2r_1^2r_2^2 - r_1^4 - r_2^4}. \end{aligned} \tag{3.25}$$

The circles that symbolise plant canopies are designed to represent the area that the canopy biomass described in equation (3.11) occupies, or in other words, the zone of influence. As the circle size changes over time with canopy biomass, then I also changes over time. We therefore apply a time dependency to equations (3.20),

(3.24), and (3.25) which gives

$$I(t) = \begin{cases} r_1^2(t)\cos^{-1}\left(\frac{D^2+r_1^2(t)-r_2^2(t)}{2Dr_1(t)}\right) + r_2^2(t)\cos^{-1}\left(\frac{D^2+r_2^2(t)-r_1^2(t)}{2Dr_2(t)}\right) \\ \quad -\frac{1}{2}\sqrt{6D^2r_1^2 - D^4 - 2D^2r_2^2 + 2r_1^2r_2^2 - r_1^4 - r_2^4}, & 0 < x < D \\ c_1(t) - r_2^2(t)cos^{-1}\left(\frac{D^2+r_1^2(t)-r_2^2(t)}{2Dr_2(t)}\right) + r_2^2(t)cos^{-1}\left(\frac{D^2-r_1^2(t)-r_2^2(t)}{2Dr_2(t)}\right) \\ \quad +D\sqrt{6D^2r_1^2 - D^4 - 2D^2r_2^2 + 2r_1^2r_2^2 - r_1^4 - r_2^4}, & x < 0 \\ c_2(t) - r_1^2(t)cos^{-1}\left(\frac{D^2-r_1^2(t)+r_2^2(t)}{2Dr_1(t)}\right) + r_2^2(t)cos^{-1}\left(\frac{-D^2-r_1^2+r_2^2}{2Dr_2}\right) \\ \quad -D\sqrt{6D^2r_1^2 - D^4 - 2D^2r_2^2 + 2r_1^2r_2^2 - r_1^4 - r_2^4} & x > D. \end{cases} \tag{3.26}$$

This concludes the formulation of I and we now wish to apply this to our mathematical model. In order to find the proportion of a plant's canopy that is shadowed by a taller plant (O), the shadowed plant needs to be identified and therefore plant height need to be determined. Thus, a new equation that describes the plant height over time is introduced. We assume that plant height is unaffected by canopy biomass and is assumed to grow logistically and decay exponentially so that the heights of Plant 1 and Plant 2 are given by

$$\frac{dh_1(t)}{dt} = \alpha_h h_1(t)\left(1 - \frac{h_1(t)}{k_{h1}}\right) - d_h h_1(t), \tag{3.27}$$

$$\frac{dh_2(t)}{dt} = \alpha_h h_2(t)\left(1 - \frac{h_2(t)}{k_{h2}}\right) - d_h h_2(t), \tag{3.28}$$

where $h_i(t), \quad i \in [1, 2]$ is the plant height of Plant 1 and Plant 2, respectively at time t, α_h is the height growth rate (assumed the same for each plant), k_{h1} and k_{h2} are the maximum plant heights for Plant 1 and Plant 2, respectively. We allow this parameter to be different between the two plants so that we can impose a difference in heights between Plants 1 and 2. Finally, d_h is the degradation rate for the height of the plant (also assumed the same for each plant). The initial condition for height is the same for both plants and equivalent to that of one fully emerged leaf and

stem, given by h_0. This decoupled empirical approach to modelling plant height is adopted as the level of detail required is to compare heights across a population. As such, determining height in a mechanistic way would add an unnecessary level of complexity.

Over time, the height of two neighbouring plants is compared, so that the taller and shorter plant can be established as illustrated in Figure 3.2. Once the heights of the plants has been calculated, the overlap of Plant 1 O_1 can be calculated such that

$$O_1(t) = \begin{cases} \frac{I(t)}{G_1(t)}, & h_1(t) < h_2(t) \\ 0, & h_1(t) > h_2(t). \end{cases} \tag{3.29}$$

Similarly, the overlap of Plant 2 can be calculated such that

$$O_2(t) = \begin{cases} \frac{I(t)}{G_2(t)}, & h_2(t) < h_1(t) \\ 0, & h_2(t) > h_1(t). \end{cases} \tag{3.30}$$

This concludes the discussion of the method of mathematically quantifying competition between two plants. The manner in which it is included into the individual plant model to make the two plant model is now considered.

3.3 Two-plant competition model

Before moving onto the many plant scale we consider our model in the context of two interacting plants. The biomass growth rate, as described in equation (3.8), relates to the total amount of radiation that the exposed plant canopy can absorb and how efficient the plant is at converting energy into mass. If a plant is shadowed by another the amount of exposed plant canopy decreases and so too does the biomass growth rate. The amount that the growth rate decreases is equal to the proportion of canopy that is shadowed. Then the two non-linear ODE model that describes the

growth of the two competing plant canopies is given by

$$\frac{dc_1(t)}{dt} = R_0 c_k G_0^{(1-B)} \left(\frac{\phi c_1(t)}{1+\psi}\right)^B (1 - e^{-\kappa\left(\frac{\phi c_1(t)}{G_0(1+\psi)}\right)^{1-B}}) (1 - O_1(t)) \left(1 - \frac{c_1(t)}{k_c}\right) - d_c c_1(t), \tag{3.31}$$

$$\frac{dc_2(t)}{dt} = R_0 c_k G_0^{(1-B)} \left(\frac{\phi c_2(t)}{1+\psi}\right)^B (1 - e^{-\kappa\left(\frac{\phi c_2(t)}{G_0(1+\psi)}\right)^{1-B}}) (1 - O_2(t)) \left(1 - \frac{c_2(t)}{k_c}\right) - d_c c_2(t), \tag{3.32}$$

with

$$c_1(0) = c_0 \quad \text{and} \quad c_2(0) = c_0.$$

Here parameters for both plants are identical with the only difference between the $c_1(t)$ and $c_2(t)$ equations being that incurred by competition. The heights of Plant 1 and Plant 2 are described by equations (3.27) and (3.28), respectively, where $k_{h1} \neq k_{h2}$.

3.3.1 Non-dimensionalisation

Non-dimensionalisation is the process of rescaling a dimensional system into non-dimensional variables using a suitable variable scaling. It is accomplished by dividing each variable by a constant scaling parameter. By non-dimensionalising, parameters are grouped giving a simplified view of the model equations. This causes the analysis of the model equations to be simpler, including but not limited to a sensitivity analysis and parameterisation.

For the model described in this section, let the dimensional variables h_1, h_2, c_1, c_2 and t be rescaled such that

$$h_i(\tau) = h_0 \hat{h}_i(\tau), \quad c_i(t) = c_0 \hat{c}_i(\tau) \quad \text{with} \quad i \in [1,2] \quad \text{and} \quad t = \frac{\tau}{\alpha_h}$$

where a hat signifies a non-dimensional physical variable and τ denotes non-dimensional time. Then equations (3.27), (3.28), (3.31) and (3.32) can be non-dimensionalised

to

$$\frac{d\hat{h}_1(\tau)}{d\tau} = \hat{h}_1(\tau)\left(1-\bar{K}_{h1}\hat{h}_1(\tau)\right) - d_h\hat{h}_1(\tau), \tag{3.33}$$

$$\frac{d\hat{c}_1(\tau)}{d\tau} = \alpha_c\hat{c}_1(\tau)\left(1-exp\left(-\bar{\kappa}\hat{c}_1^{(1-B)}(\tau)\right)\right)\left(1-O_1(\hat{h}_1,\hat{h}_2,\tau)\right)\times \left(1-\bar{K}_c\hat{c}_1(\tau)\right) - \bar{d}_c\hat{c}_1(\tau), \tag{3.34}$$

$$\frac{d\hat{h}_2(\tau)}{d\tau} = \hat{h}_2(\tau)\left(1-\bar{K}_{h2}\hat{h}_2(\tau)\right) - d_h\hat{h}_2(\tau), \tag{3.35}$$

$$\frac{d\hat{c}_2(\tau)}{d\tau} = \alpha_c\hat{c}_2(\tau)\left(1-exp\left(-\bar{\kappa}\hat{c}_2^{(1-B)}(\tau)\right)\right)\left(1-O_2(\hat{h}_1,\hat{h}_2,\tau)\right)\times \left(1-\bar{K}_c\hat{c}_2(\tau)\right) - \bar{d}_c\hat{c}_2(\tau), \tag{3.36}$$

where

$$\bar{K}_h = \frac{h_0}{k_h}, \qquad \bar{d}_h = \frac{d_h}{\alpha_h}, \qquad \alpha_c = \frac{R_0c_kG_0^{(1-B)}}{\alpha_h}\left(\frac{\phi}{1+\psi}\right)^B c_0^{(B-1)},$$

$$\bar{\kappa} = e\left(\frac{\phi c_0}{1+\psi}\right)^{(1-B)} G_0^{(B-1)}, \qquad \bar{K}_c = \frac{c_0}{k_c} \qquad \text{and} \qquad \bar{d}_c = \frac{d_c}{\alpha_h}.$$

The initial conditions are

$$\hat{h}_1(0) = \hat{c}_1(0) = \hat{h}_2(0) = \hat{c}_2(0) = 1.$$

Equations (3.34) and (3.36) describe the non-dimensional system of equations devised to simulate the growth of two plants. Henceforth this will be the system of equations that we will consider, however, hereafter the hats and bars will be dropped for notational convenience.

3.3.2 Two-plant model analysis

This section details the steady-state analysis of the two-plant model and the necessary simplifications that have been made in order to perform the analysis. The two plants are arranged with distance D between canopy centres, where D has been chosen so that the two canopies will interact.

The change in plant height over time is assumed to be unaffected by canopy

biomass and as such equations (3.33) and (3.35) de-couple from equations (3.34) and (3.36) and can be solved analytically to give

$$h_1(\tau) = \frac{h_0(1-d_h)exp((1-d_h)\tau)}{1-d_h-k_{h1}h_0+k_{h1}exp((1-d_h)\tau)h_0}, \tag{3.37}$$

$$h_2(\tau) = \frac{h_0(1-d_h)exp((1-d_h)\tau)}{1-d_h-k_{h2}h_0+k_{h2}exp((1-d_h)\tau)h_0}. \tag{3.38}$$

We assume the following simplifications so that the system becomes more amenable to mathematical analysis. Firstly, it is assumed that there is a constant leaf area index given by $\gamma_1 = 1 = \gamma_2$, which means that the ground cover is equal to the leaf area, i.e. single layer of leaves. As γ is no longer a variable then $(1 - exp(-\kappa\gamma))$ can be absorbed into the constant α_c. In addition, since the ground cover is equal to the leaf area then $B = 1$. Finally we assume that Plant 1 is taller than Plant 2, (i.e. $k_{h1} > k_{h2}$) and the plants are positioned close enough so that their canopies interact. We therefore no longer consider equations (3.37)-(3.38) and instead focus on the equations for canopy biomass. Since Plant 2 is being shadowed, its biomass growth will be affected whereas Plant 1 will be unaffected by the presence of Plant 2. With these assumptions we reduce the system given by equations (3.34) and (3.36) to

$$\frac{dc_1(\tau)}{d\tau} = \alpha_c c_1(\tau)\left(1 - K_c c_1(\tau)\right) - d_c c_1(\tau). \tag{3.39}$$

$$\frac{dc_2(\tau)}{d\tau} = \alpha_c c_2(\tau)\left(1 - \frac{O(h_1,h_2,\tau)}{\beta c_2}\right)\left(1 - K_c c_2(\tau)\right) - d_c c_2(\tau). \tag{3.40}$$

Given the complexity of the overlap expression of equation (3.26), it is necessary to approximate the overlap with an appropriate simplification. By observing that $I \propto r^2$, where r is the radius of the area of ground that the plant covers and also that leaf area is equal to the ground cover, it can be seen that $I \propto A$, where A denotes leaf area. Thus overlap is approximated using a linear function of c_1, namely

$$O(t) = \frac{\sigma(c_1(t) - \lambda)}{G_2(t)}, \tag{3.41}$$

where σ is the overlap growth rate and λ is the canopy biomass for which plant-plant overlap begins. The values for both parameters are yet to be determined. We later show, when numerical simulations of the system are conducted, that this is an appropriate approximation by comparing the approximation with the exact solution in Figure 3.11 of Section 3.4.

The linear approximation for O is only applicable when overlap exists, therefore it is necessary for

$$\sigma = \begin{cases} 0, & \text{if } c_2 = 0, \\ 0, & \text{if } c_1 \leq \lambda, \\ \sigma_1, & c_1 > \lambda, \end{cases}$$

where $\lambda > 0$.

The approximate canopy biomass of Plants 1 and 2 are thus given by

$$\begin{aligned} \frac{dc_1(\tau)}{d\tau} &= \alpha_c c_1(\tau)\left(1 - K_c c_1(\tau)\right) - d_c c_1(\tau) = f(c_1, c_2), \qquad (3.42) \\ \frac{dc_2(\tau)}{d\tau} &= \alpha_c c_2(\tau)\left(1 - \frac{\sigma(c_1(\tau) - \lambda)}{\beta c_2(\tau)}\right)\left(1 - K_c c_2(\tau)\right) - d_c c_2(\tau) \\ &= g(c_1, c_2), \qquad (3.43) \end{aligned}$$

where

$$\beta = G_0\left(\frac{\phi c_0}{1+\psi}\right),$$

is constant. The initial conditions are given by

$$c_1(0) = 1 = c_2(0).$$

Since equation (3.43) cannot both be solved in closed form analytically, we instead determine the steady states of the model equations and their stability in order to determine the system behaviour. The system steady-states are found by setting $\frac{dc_1}{d\tau} = \frac{dc_2}{d\tau} = 0$ so that

$$f: \qquad \alpha_c c_1^* \left(1 - K_c c_1^*\right) - d_c c_1^* = 0, \tag{3.44}$$

$$g: \qquad \alpha_c c_2^* \left(1 - \frac{\sigma(c_1^* - \lambda)}{\beta c_2^*}\right)\left(1 - K_c c_2^*\right) - d_c c_2^* = 0, \tag{3.45}$$

and solving for the steady-state canopy biomass c_1^* and c_2^*, respectively. By solving equation (3.44) for c_1^* it can be seen that

$$c_1^* = 0 \qquad \text{or} \qquad c_1^* = \frac{\alpha_c - d_c}{\alpha_c K_c}.$$

Substituting $c_1^* = 0$ into equation (3.45) and solving for c_2^* yields

$$c_2^* = 0 \qquad \text{or} \qquad c_2^* = \frac{\alpha_c - d_c}{\alpha_c K_c}.$$

Substituting $c_1^* = \frac{\alpha_c - d_c}{\alpha_c K_c}$ into equation (3.45) and solving for c_2^* yields

$$c_2^* = 0, \qquad c_2^* = \frac{-\beta_1 + \sqrt{\beta_1^2 - 4\beta_2}}{2} \qquad \text{or,} \qquad c_2^* = \frac{-\beta_1 - \sqrt{\beta_1^2 - 4\beta_2}}{2},$$

where

$$\beta_1 = \frac{d_c - \alpha_c}{\alpha_c K_c} - \beta\left(\frac{\sigma(\alpha_c - d_c)}{\alpha_c K_c} - \sigma\lambda\right), \tag{3.46}$$

$$\beta_2 = \frac{\beta}{K_c}\left(\frac{\sigma(\alpha_c - d_c)}{\alpha_c K_c} - \sigma\lambda\right). \tag{3.47}$$

To summarise, equations (3.44) and (3.45) have the following five steady-states

$$(c_1^*, c_2^*)_1 = (0, 0), \tag{3.48}$$

$$(c_1^*, c_2^*)_2 = \left(0, \frac{\alpha_c - d_c}{\alpha_c K_c}\right), \tag{3.49}$$

$$(c_1^*, c_2^*)_3 = \left(\frac{\alpha_c - d_c}{\alpha_c K_c}, 0\right), \tag{3.50}$$

$$(c_1^*, c_2^*)_4 = \left(\frac{\alpha_c - d_c}{\alpha_c K_c}, \frac{-\beta_1 + \sqrt{\beta_1^2 - 4\beta_2}}{2}\right), \tag{3.51}$$

$$(c_1^*, c_2^*)_5 = \left(\frac{\alpha_c - d_c}{\alpha_c K_c}, \frac{-\beta_1 - \sqrt{\beta_1^2 - 4\beta_2}}{2}\right). \tag{3.52}$$

We now consider parameter bounds for these steady-states to be real and positive. For steady-states (3.49)-(3.52) to be positive, which is a necessary condition for the plants to be physical, we require the growth rate α_c to be larger than the decay rate d_c. For steady states $(c_1^*, c_2^*)_4$ and $(c_1^*, c_2^*)_5$ we can see that since $\frac{\sigma(\alpha_c - d_c)}{\alpha_c K_c} - \sigma\lambda$ refers to the overlap, which by definition is greater than or equal to 0, $\beta_2 \geq 0$, therefore we require $\beta_1 < 0$ for $(c_1^*, c_2^*)_4$ and $(c_1^*, c_2^*)_5$ to be positive. We also require $\beta_1^2 - 4\beta_2 > 0$ for both steady-states to be real.

It is of interest to determine the linear stability of the system when a perturbation is applied to the steady-states [43]. In order to determine the stability of each steady-state we must solve

$$\left|\hat{A} - \Lambda I\right|_{(c_1^*, c_2^*)} = 0, \tag{3.53}$$

for the eigenvalue Λ, where $\hat{A}$ is the community matrix calculated such that

$$\hat{A} = \begin{pmatrix} \frac{\partial f}{\partial \hat{c}_1} & \frac{\partial f}{\partial \hat{c}_2} \\ \frac{\partial g}{\partial \hat{c}_1} & \frac{\partial g}{\partial \hat{c}_2} \end{pmatrix}. \tag{3.54}$$

Note that for stability, we require $Re(\Lambda) \leq 0$ [43].

The community matrix for the system of equations described by equations (3.44)

and (3.45) is constructed such that:

$$\frac{\partial f}{\partial \hat{c}_1} = \alpha_c - 2\alpha_c K_c c_1 - d_c, \tag{3.55}$$
$$\frac{\partial f}{\partial \hat{c}_2} = 0, \tag{3.56}$$
$$\frac{\partial g}{\partial \hat{c}_1} = -\alpha_c \beta \sigma (1 - K_c c_2), \tag{3.57}$$
$$\frac{\partial g}{\partial \hat{c}_2} = \alpha_c - 2\alpha_c K_c c_2 + \alpha_c K_c \beta \sigma (c_1 - \lambda) - d_c. \tag{3.58}$$

We can now solve equation (3.53) for Λ giving two solutions

$$\Lambda_1 = \alpha_c - 2\alpha_c K_c c_1 - d_c \quad \text{and} \quad \Lambda_2 = \alpha_c - 2\alpha_c K_c c_2 + \alpha_c K_c \beta \sigma (c_1 - \lambda) - d_c. \tag{3.59}$$

We now use this result to determine the linear stability of each of the five steady-states by substituting solutions (3.48) to (3.52) into equations (3.59).

For steady-state 1, $c_1^* = 0 = c_2^*$ and $\sigma = 0$ (as there is no plant shadowing). Thus

$$\Lambda_1 = \alpha_c - d_c, \tag{3.60}$$

and

$$\Lambda_2 = \alpha_c - d_c. \tag{3.61}$$

For this steady-state to be stable we require $\Lambda_1 < 0$ and $\Lambda_2 < 0$ and hence $\alpha_c - d_c < 0$. If this is the case then the remaining steady-states do not exist in the positive quadrant as they are not real, positive values. Hence $(\hat{c}_1^*, \hat{c}_2^*)_1$ is only a stable steady-state if no other steady-states exist and the canopy growth rate of each plant is less than the decay rate.

For $(c_1^*, c_2^*)_2$ we again have $\sigma = 0$ since there is still no plant shadowing. Substituting yields

$$\Lambda_1 = \alpha_c - d_c \quad \text{and} \quad \Lambda_2 = -(\alpha_c - d_c). \tag{3.62}$$

If $\Lambda_1 < 0$ and $\Lambda_2 < 0$, then $\alpha_c - d_c < 0$ and $-(\alpha_c - d_c) < 0$, which is clearly a contradiction and so steady-state 2 is unstable for all values of α_c and d_c.

Likewise for $(c_1^*, c_2^*)_3$ and $\sigma = 0$ as again there is no plant shadowing. Substituting $(\hat{c}_1^*, \hat{c}_2^*)_3$ into equations Λ_1 and Λ_2 yields

$$\Lambda_1 = -(\alpha_c - d_c) \quad \text{and} \quad \Lambda_2 = \alpha_c - d_c. \tag{3.63}$$

To be stable we require $\Lambda_1 < 0$ and $\Lambda_2 < 0$, hence $-(\alpha_c - d_c) < 0$ and $\alpha_c - d_c < 0$, which again is clearly a contradiction and so steady-state three is also unstable for all values of α_c and d_c. Therefore for our system of equations it is not possible to have one single plant as a stable steady-state since all parameter values, barring those ascertaining to height, are equal and so if one plant grows so will the other. Note that this may not be the case if variation was applied to individual plant parameters.

Substituting $(\hat{c}_4^*, \hat{c}_2^*)_4$ yields the eigenvalues

$$\Lambda_1 = -(\alpha_c - d_c), \tag{3.64}$$

and

$$\Lambda_2 = \alpha_c - d_c - \alpha_c K_c \left(-\beta_1 + \sqrt{\beta_1^2 - 4\beta_2}\right) + \alpha_c K_c \frac{\sigma}{\beta}\left(\frac{\alpha_c - d_c}{\alpha_c K_c} - \lambda\right). \tag{3.65}$$

For $\Lambda_1 < 0$ we require $-(\alpha_c - d_c) < 0$, which is a requirement for steady-state four to exist. To establish the sign of Λ_2 we must substitute β_1 from equation (3.46) into equation (3.65) such that

$$\begin{aligned} \Lambda_2 &= \alpha_c K_c \left(\frac{d_c - \alpha_c}{\alpha_c K_c} - \frac{\sigma}{\beta}\left(\frac{\alpha_c - d_c}{\alpha_c K_c} - \lambda\right) - \sqrt{\beta_1^2 - 4\beta_2} + \frac{\sigma}{\beta}\left(\frac{\alpha_c - d_c}{\alpha_c K_c} - \lambda\right)\right) \\ &\quad + \alpha_c - d_c, \\ &= -\alpha_c K_c \sqrt{\beta_1^2 - 4\beta_2}. \end{aligned} \tag{3.66}$$

Since we require $\sqrt{\beta_1^2 - 4\beta_2}$ to be real for $(\hat{c}_4^*, \hat{c}_2^*)_4$ to be real, then if $(\hat{c}_4^*, \hat{c}_2^*)_4$ exists $\Lambda_2 < 0$ and it is stable.

Substituting the fifth steady-state, $(\hat{c}_1^*, \hat{c}_2^*)_5 = \left(\frac{\alpha_c - d_c}{\alpha_c K_c}, \frac{-\beta_1 - \sqrt{\beta_1^2 - 4\beta_2}}{2}\right)$, into equa-

tions Λ_1 and Λ_2 yield the following eigenvalues:

$$\Lambda_1 = -(\alpha_c - d_c), \tag{3.67}$$

and

$$\Lambda_2 = \alpha_c - d_c - \alpha_c K_c \left(-\beta_1 - \sqrt{\beta_1^2 - 4\beta_2}\right) + \alpha_c K_c \frac{\sigma}{\beta}\left(\frac{\alpha_c - d_c}{\alpha_c K_c} - \lambda\right). \tag{3.68}$$

For $\Lambda_1 < 0$ we require $-(\alpha_c - d_c) < 0$, which is a requirement for steady-state four and five to exist. To establish the sign of Λ_2 we must again substitute β_1 from equation (3.46) into equation (3.68) such that

$$\begin{aligned} \Lambda_2 &= \alpha_c K_c \left(\frac{d_c - \alpha_c}{\alpha_c K_c} + \frac{\sigma}{\beta}\left(\frac{\alpha_c - d_c}{\alpha_c K_c} - \lambda\right) + \sqrt{\beta_1^2 - 4\beta_2} + \frac{\sigma}{\beta}\left(\frac{\alpha_c - d_c}{\alpha_c K_c} - \lambda\right)\right) \\ &\quad + \alpha_c - d_c, \\ &= \alpha_c K_c \sqrt{\beta_1^2 - 4\beta_2}). \end{aligned} \tag{3.69}$$

From equation (3.69) it is clear that $\Lambda_2 > 0$ since $\sqrt{\beta_1^2 - 4\beta_2}$ being real and positive is a condition for steady-state five to exist. Hence, steady-state five is unstable.

To summarise, there is only one real positive stable steady-state, which is either $(c_1^*, c_2^*)_1$ or $(c_1^*, c_2^*)_4$ depending on the relationship between α_c and d_c. Hence, there is only one pair of values the system will tend towards. The pair of values is non-zero if and only if the canopy decay rate is smaller than the growth rate. Clearly $(c_1^*, c_2^*)_1$ is the case where both plants do not grow and is not of interest to us when investigating the interaction of two competing plants. Thus we will only consider $(c_1^*, c_2^*)_4$ as it is the only non-trivial stable steady-state.

3.4 Numerical simulations

In this section a numerical investigation of two interacting plants described by equations (3.34) and (3.36) is conducted. The parameterisation of the model equations is described in Section 3.4.1. We compare the steady-state solution for two interacting plants to the numerical simulation to confirm that the numerical solver applied to

our model equations is appropriate.

In our model $t = 0$ corresponds to fourteen days of total plant growth, which is approximately the time of emergence of bambara groundnut, to 150 days, which is approximately the time that the plant matures. The two plants are arranged side by side with a distance that allows their canopies to interact. The system of equations is solved numerically using the inbuilt MATLAB ODE solver ode15s, which is specifically designed for stiff systems. This solver allows for relative and absolute tolerances to be predetermined, by the user, and adjusts the time step so that the tolerances are met; in this case, both tolerances have been set to 1×10^{-6}. These simulations use the test species Uniswa Red and S19-3, the parameters of which can be found in Table 3.1. This validity of this numerical method is checked in Section 3.4.2.

3.4.1 Parameterisation

The model described by equations (3.33) to (3.36) have been parametrised using a range of techniques including values sourced from the literature, informed estimates of unknown parameters and model data fitting. We began parametrisation by using those values directly available from the literature. Where such values were not available, estimates were made to parameters based upon their role in the growth and development of the plant. This approach was then refined by comparing the model with data, however data on individual plant growth were not available. The experimental data available to us for parameterisation are from the Tropical Crops Research Unit (TCRU) greenhouse experiments conducted in 2003 and 2006. A detailed description of the experimental methodology can be found in [32]. The data consist of two species: Uniswa Red and S19-3, undergoing temperature treatments of 23°C, 28°C, and 33°C. Leaf number, leaf area, leaf mass, stem mass, root mass, pod mass and total biomass have been monitored over sixteen day intervals starting at thirty three days. The distance between plants is constant with 35cm between columns and 20cm between rows and the supply of water is non-limiting. The

Parameter	Value	Description	Source
α_h	0.75	The height growth rate (day^{-1})	This study
k_h	20^*, $30^\dagger$	The carrying capacity for the height of plant j (m)	This study
d_h	0.02	The decay rate of the plant height (day^{-1})	This study
R_0	8	The total photosynthetically incoming radiation that penetrates the greenhouse ($MJm^{-2}day^{-1}$)	Met Office [41]
c_k	3.02^*, $2.02^\dagger$	Radiation use efficiency (gMj^{-1})	This study
κ	0.6	The light extinction coefficient	Cornelissen [20]
k_c	188.31^*, $184.92^\dagger$	The maximum carrying capacity for the canopy biomass of a plant (g)	This study
d_c	$1.2 \times 10^{-3*}$, $5 \times 10^{-4\dagger}$	The decay rate of the canopy biomass (day^{-1})	This study
ϕ	$1.65 \times 10^{-2*}$, $1.62 \times 10^{-2\dagger}$	Specific Leaf Area, the leaf area per gram of leaf mass (m^2g^{-1})	This study
ψ	0.55^*, $0.56^\dagger$	Partitioning coefficient, the fraction of above ground biomass appropriated to the stem.	This study
B	0.7^*, $0.71^\dagger$	Canopy spreading parameter	This study
h_0	0.05	The initial conditions for plant height (m)	This study
c_0	0.24^*, $0.19^\dagger$	The initial conditions for plant canopy (g)	This study

Table 3.1: Table of parameter values and descriptions for informing equations (3.37) to (3.40). For parameters that are species specific, * denotes the species S19-3 and † denotes Uniswa Red.

distance between plants is such that they experience competition from multiple plants at one point, data are collected using a destructive process and so the growth of one plant in isolation can not be attained. As such, the parameters c_k, k_c and d_c have been found by taking a model-data least squared fit using the scaled up multi-plant model described in Section 3.7. A summary of all parameters used in this model for species' Uniswa Red and S19-3 can be found in Table 3.1.

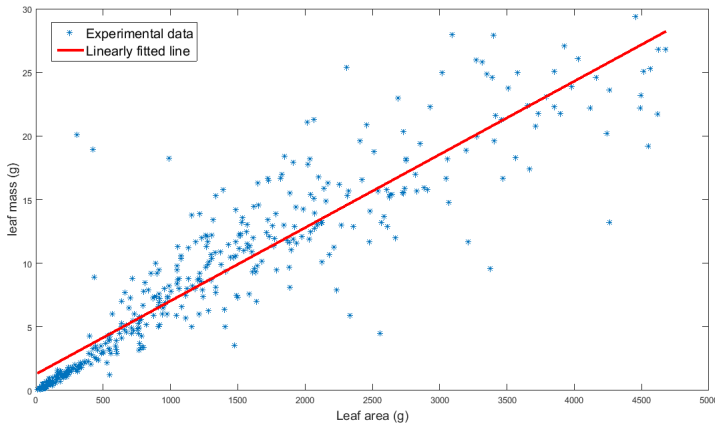

(a) The relationship between leaf area and leaf mass.

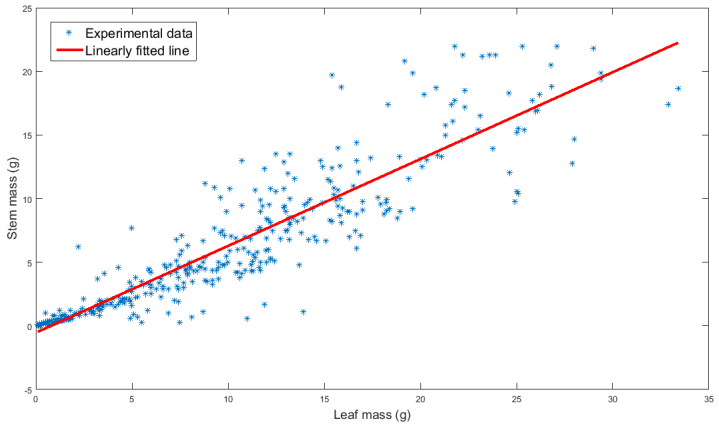

(b) The relationship between leaf mass and stem mass.

Figure 3.6: The experimental data that provided the parameter values ϕ and ψ for the species Uniswa Red. The data provided are from plants arranged in three rows of five with a distance of 0.2m between rows and 0.35m between columns, for three temperature regimes of 23°C, 28°C, and 33°C.

The parameters R_0, and κ have been taken directly from the literature, the values and sources of which can be found in Table 3.1.

The parameters ϕ and ψ have been approximated directly from TCRU experimental greenhouse data, which are given in Figures 3.6 and 3.7 for species Uniswa Red and S19-3, respectively. The specific leaf area ϕ is assumed constant over time and is given by the ratio between leaf area and leaf mass. From Figures 3.6(a) and 3.7(a) we can see that there is a linear relationship between leaf area and leaf mass, which is consistent with our assumption made in equation (3.1) and so for each plant

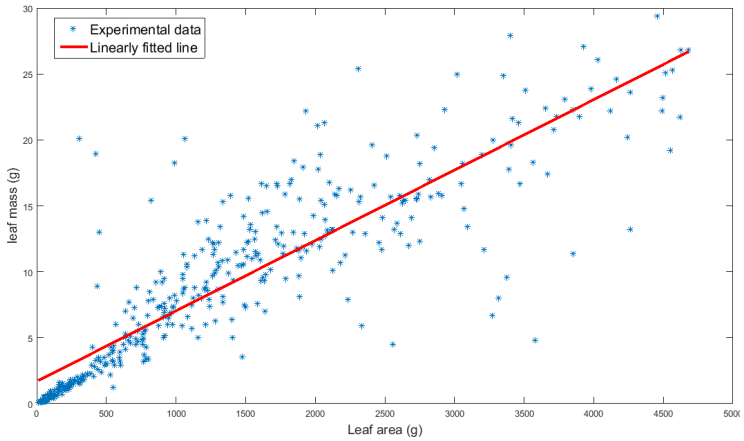

(a) The relationship between leaf area and leaf mass for each plant of the experimental data.

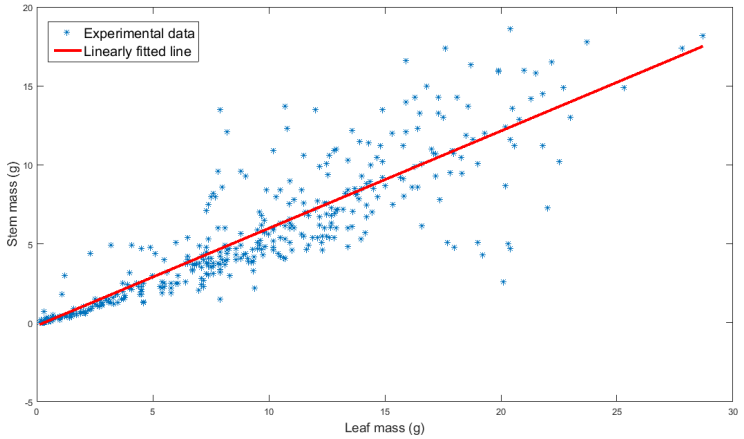

(b) The relationship between leaf mass and stem mass for each plant of the experimental data.

Figure 3.7: The experimental data that provided the parameter values ϕ and ψ for the species S19-3. The data provided are from plants arranged in three rows of five with a distance of 0.2m between rows and 0.35m between columns, for three temperature regimes of 23°C, 28°C, and 33°C.

in the experiment, labelled with a subscript i, we find

$$\phi_i = \frac{A_i}{LM_i}.$$

Then ϕ_i is averaged over all plants in the experiments to give ϕ. Similarly the stem mass partitioning coefficient ψ is assumed constant over time and is given by the

ratio between leaf mass and stem mass. From Figures 3.6(b) and 3.7(b) we can see that there is a linear relationship between leaf mass and stem mass, which is consistent with the assumption made in equation (3.2) and so for each plant in the experiment, labelled with a subscript i, we find

$$\psi_i = \frac{SM_i}{LM_i}.$$

Then ψ_i is averaged over all plants of each species to give ψ. To find ϕ and ψ, the outliers, defined as being more than 1.5 times the interquartile range above the upper quartile or below the lower, have been removed.

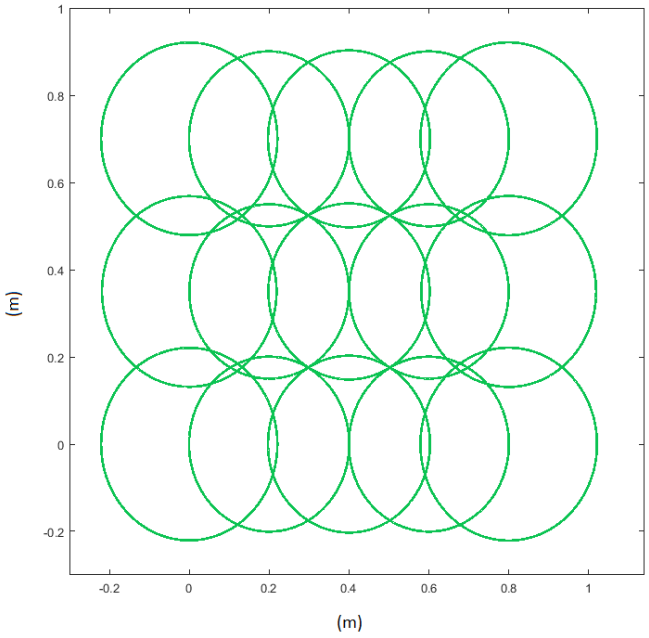

Figure 3.8: A birds-eye view of plants simulated to demonstrate the plant layout of the experiments. Distance between plants in a row is 20cm; the distance between rows is 35cm.

The values for the parameters k_c, c_k, B and d_c are not readily available from the literature or the experimental data. In order to determine them we took a least-squares fit of the TCRU experimental greenhouse data against a model simulation

of the growth of fifteen plants given by

$$\begin{aligned}\frac{dc_i(\tau)}{d\tau} &= \alpha_c c_i(\tau)\left(1-exp\left(-\kappa c_i^{(1-B)}(\tau)\right)\right)(1-O_i(h_1,h_2,...h_N,\tau))\,(1-K_c c_i(\tau)) \\ &\quad -d_c c_i(\tau)\end{aligned}$$

for $i \in [1, 15]$.

For both the experiments and simulations, plants are arranged with a distance between columns of 0.35m and a distance between rows of 0.2m, the temperature is 28°C as this is the closest to the optimum temperature for both species Uniswa Red and S19-3.

In the experimental dataset the canopy biomass of 15-20 plants had been collected and averaged for eight time points, where the plants were randomly selected from a larger set of experimental plants. For the simulations, we average the canopy biomass of 15 plants the arrangement of which is given in Figure 3.8. The inbuilt MATLAB function lsqcurvefit which is a nonlinear least-squares solver is then used to conduct the least-squared fit.

There is no experimental data for the heights of the plants and so the model parameter values have been approximated using biological knowledge from the literature [20]. We assume that all plant heights are the same so that competition is shared over two interacting plants as described in Section 3.5.3. We choose this approach since observations of plants in the field showed that although plants are not exactly the same height, all plants experience competition in the form of shadowing from neighbours to a similar degree. This is because the leaves of adjacent plants mingle with the multi-layered canopy. We assume each plant takes 50% of the total competition.

In this section it is assumed that parameters for all plants are the same, however it is possible to add random variation to each parameter and we explore this case in the following chapter.

The non-dimensional parameters are found using the relationships described in Section 3.3.1 and can be found in Table 3.2.

Non-dimensional parameters	Value
K_h	0.0025^*, $0.0016^\dagger$
d_h	1.3×10^{-2}
α_c	0.30^*, $0.22^\dagger$
κ	0.6
K_c	$1.95 \times 10^{-3*}$,$1.58 \times 10^{-3\dagger}$
d_c	$1.6 \times 10^{-3*}$, $6.67 \times 10^{-2\dagger}$

Table 3.2: Table of non-dimensional parameter values. For parameters that are species specific, * denotes the species S19-3 and † denotes Uniswa Red.

3.4.2 Simulation of two interacting plants

A simulation is conducted of the two plants that are described by equations (3.33) to (3.36) separated by a distance of 0.3m. All parameter values except K_h are the same for these two plants. Figure 3.9 shows a birds-eye view of the two plant canopies over six time points of the simulation and Figure 3.10 shows the evolution of canopy biomass and plant height over time for the two plants.

As can be seen from Figures 3.9 and 3.10 the two plants grow side by side with their canopies growing large enough to interact. Plant 1 is taller than Plant 2 and when the plant canopies begin to interact, the canopy growth rate of Plant 2 slows.

In this case the overlap is calculated analytically as in equation (3.26), which we will now refer to as O_{Exact}. We now wish to compare this case with that when overlap is approximated as in the steady-state analysis given in equation (3.41); we will refer to this as O_{Approx}. This will allow us to confirm the validity of the findings of the steady-state analysis. To use the approximate formula for overlap, parameters σ and λ must be found. To do this a data fit has been applied to equation (3.41). A numerical simulation of two plants with planting distance of $D = 0.3$m and parameter values found in Table 3.2 for Uniswa Red is conducted. The canopy-canopy overlap O is calculated as described in equation (3.26) and recorded over time. Then σ and λ are found so that equation (3.41) best fits O_{Exact} calculated within the simulation. The non-linear least-squares MATLAB solver, lsqcurvefit, is used to fit the data. The advantage of lsqcurvefit is that it is simple

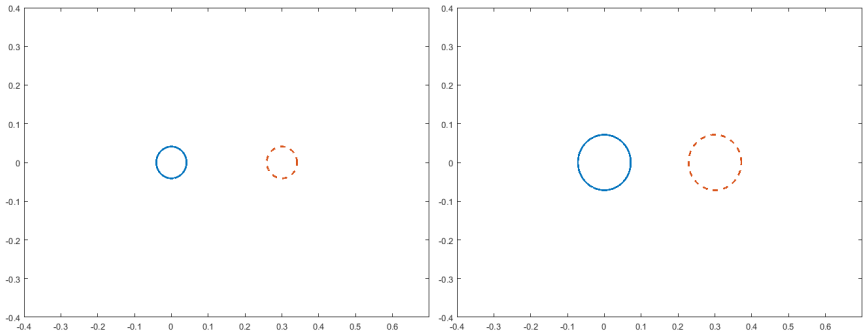

(a) 25 days

(b) 50 days

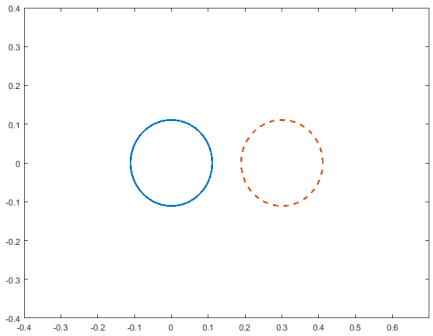

(c) 75 days

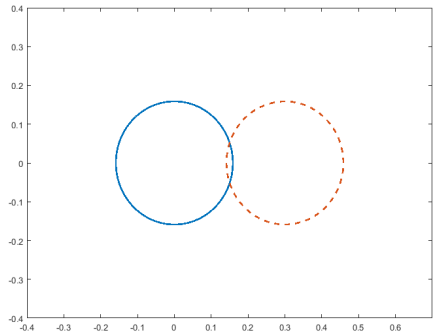

(d) 100 days

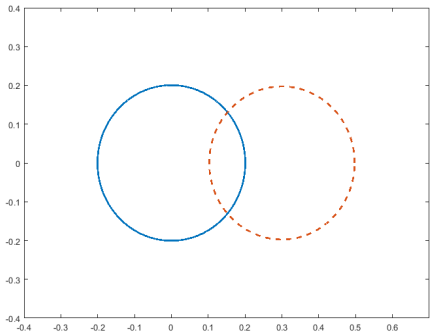

(e) 125 days

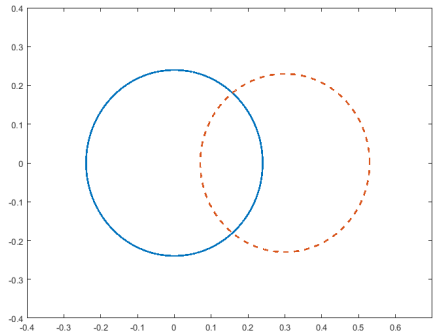

(f) 150 days

Figure 3.9: The spread of the canopy surface area for two competing plants over 6 time points. The growth of the two plants is described by equations (3.33) to (3.36) with the overlap given by equation (3.26). The taller plant (Plant 1) is indicated with a solid line, whereas the shorter plant (Plant 2) is given by a dashed line.

to implement; a disadvantage is that it is not as robust as other methods and can converge to a local minima.

A comparison of the overlap calculated as in equation (3.26) and the approximated overlap calculated as in equation (3.41) can be found in Figure 3.11(a). The parameters σ and λ have been found to be 7.6×10^{-4}m g^{-1} and 34.93g, respectively. The residual norm is a measure of the goodness of fit and in this case is found to

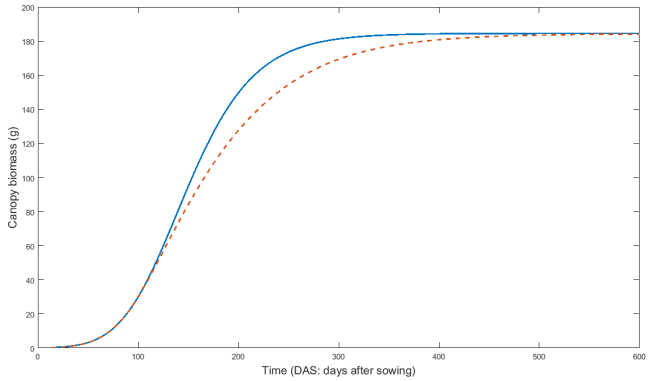

(a) Canopy Biomass

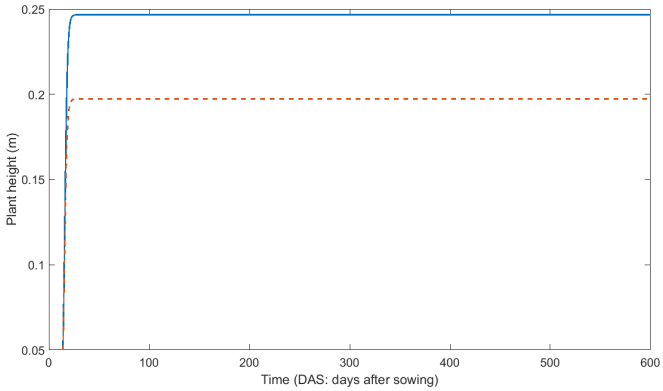

(b) Plant Height

Figure 3.10: (a) The change in canopy biomass of two competing plants, the growth of which is described by equations (3.33) to (3.36). The overlap is calculated analytically as in equation (3.26). (b) The respective height of each plant. The taller plant is indicated with a solid line, whereas the shorter plant has a dashed line. Time is measured in days after sowing, otherwise referred to as DAS.

be 7.1×10^{-4}, where a plot of the residuals can be found in Figure 3.11(b). The goodness of the fit depends on O. Despite this, the residual norm is small enough that we are satisfied with the goodness of fit for the purposes of comparing the full and approximate overlap.

Now that the framework for conducting simulations has been established, we are able to compare the affect that the different types of overlap have on canopy biomass and therefore the validity of our steady-state analysis. Note that the taller plant is entirely unaffected as it does not depend on O and so it is only the shorter plant that we wish to compare. Figure 3.12 shows the evolution of canopy biomass of the

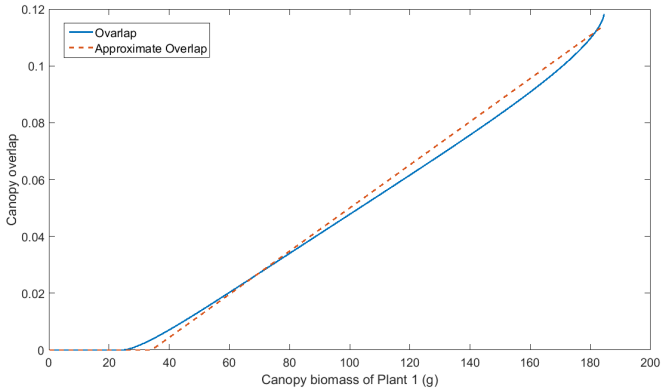

(a) A comparison of the two overlap calculations as functions of the canopy biomass of Plant 2

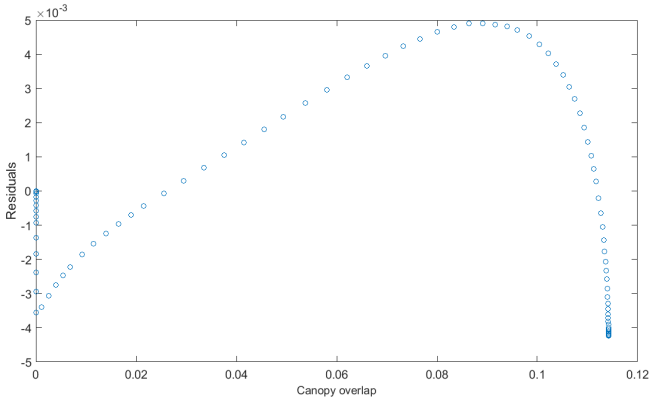

(b) The residuals of the least-squared fit.

Figure 3.11: A examination of the goodness of fit when approximating the analytical overlap as calculated in equation (3.26) with an approximated overlap as given in equation (3.41).

shorter plant for both O_{Approx} and O_{Exact}. Clearly the impact of approximating overlap has not had a significant effect on the model with only a 0.01% change to the canopy biomass of the shorter plant when using the approximate overlap when compared with the exact. Thus the approximation works well.

We now wish to compare the numerical simulations with the steady-state analysis to determine whether the numerical solver being used is appropriate. To do this, it is required that the numerical and analytical simulations are comparable, hence the simplifications made to the model equation so that the steady-state analysis was possible must also be applied to the model equation used for the numerical

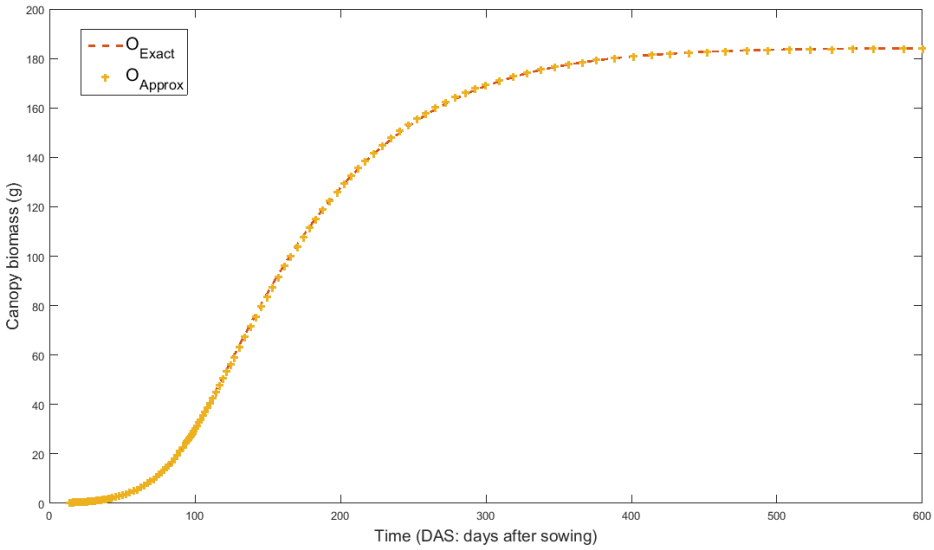

Figure 3.12: The evolution of canopy biomass for the shorter of two competing plants for when overlap is described by O_{Approx} and O_{Exact}.

approximation.

In the steady-state analysis the leaf area index was set to a constant value of 1; this would cause the plants' canopies to have a wider spread and so the planting distance is increased from 0.3m to 0.8m. We use the approximate overlap from equation (3.41) and so once again we must apply a data fitting process to equation (3.41) to find parameters σ and λ since these parameters change for different scenarios. We repeat the process of finding σ and λ using the same non-linear least-squares MATLAB solver as before.

With these new values of $\sigma = 6.1 \times 10^{-3}$m g^{-1} and $\lambda = 70.25$g we conduct a numerical simulation of equations (3.42) and (3.43) using equation (3.41) to calculate the overlap. The numerical solution at 600 days is then compared with the steady-state result given by equation (3.51), where both methods use the parameter values for Uniswa Red found in Table 3.2. The simulation results for the two plant scenario can be found in Figure 3.13.

Table 3.3 compares the analytic values for the canopy biomass values of Plants 1 and 2 with the numerical simulations. It is clear that the numerical simulation and the analytical method produces similar results, with a relative error of $3.64 \times 10^{-5}\%$

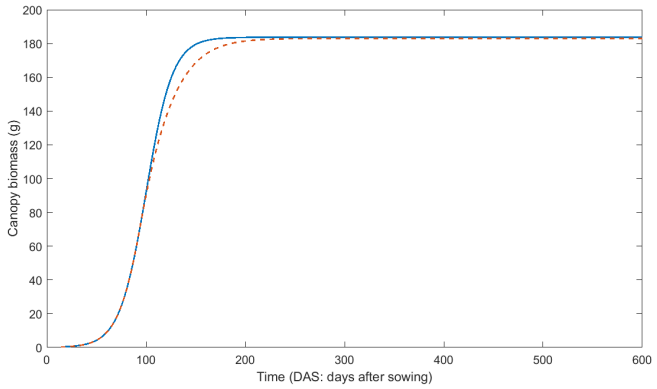

(a)

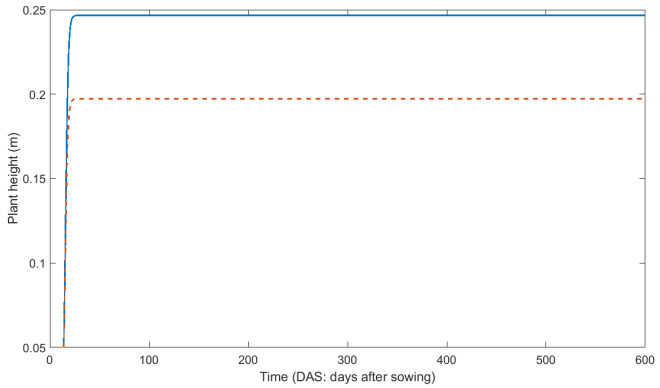

(b)

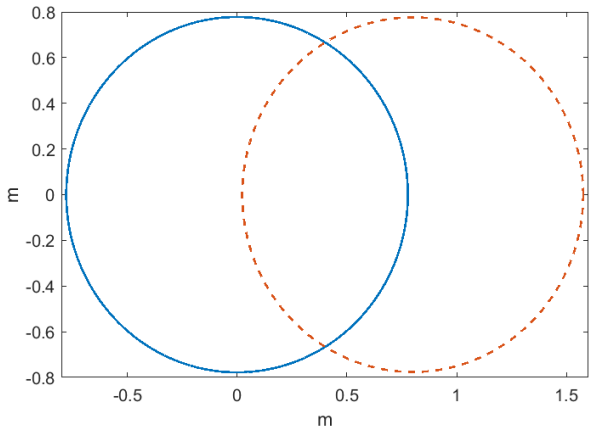

(c)

Figure 3.13: Simulation of the two plant model, where Plant 1 is taller than Plant 2, with a distance between each plant of 80cm. Overlap has been approximated using equation (3.41) and the leaf area index is constant and equal to one. The taller plant is indicated with a solid line, whereas the shorter one by a dashed line. Here, (a) is the simulated canopy biomass of two plants; (b) is the simulated plant height of two plants; and (c) is the birds-eye view of two plants at 150 days.

for Plant 1 and 0.04% for Plant 2. Thus the numerical method used is suitable for future simulations.

Now that this has been established we remove the simplifications applied to the model equations that made the system more amenable to analysis, i.e. leaf area index returns to being a variable which can take a value larger than 1. As such the plant ground cover reduces and so too does the minimum planting distance that allows two plants to interact.

	Canopy Biomass (g)	
	Plant 1	Plant 2
Analytical results	184.7974	184.7974
Numerical results	184.7974	184.7260

Table 3.3: Comparison of simulation and steady-state values given in equation (3.51) at 600 days. The simulation and steady-state values are for two plants, where Plant 1 is taller than Plant 2.

The parameters σ and λ only apply to particular cases since a change in D with no change to plant canopy size would still require a change in O. This has not been accounted for in the approximate expression for O, therefore any change in model parameters such as planting distance, the number of plants, or the carrying capacity would require σ and λ to be recalculated. We therefore conclude that it is not appropriate to replace equation (3.26) with equation (3.41) permanently.

3.5 Refining the model

In the previous sections a two plant model has been formulated and solved both analytically and numerically. We now consider how our results compare to reality and identify flaws in the mathematical model that need refining.

3.5.1 Including the effect of competition in the carrying capacity

Bambara groundnut is assumed to reach plant maturity one hundred and fifty days after sowing. By observing Figure 3.10, it is clear that the affect of competition on Plant 2 at the time of maturity is very small, with approximately 11.30% difference

in canopy biomasses. Kouassi *et al.* [34], discusses the effect that sowing density has on bambara groundnut yield. They found that the difference between plants arranged in a square grid that experience no competition (with a planting distance of 80cm by 80cm) and plants that experience moderate competition (with a planting distance of 40cm by 40cm) is approximately 23%. Although this case is for multiple neighbours at once it causes us to realise that in the case of our two competing plants, we would expect a plant that is shadowed by only one neighbour to be significantly more affected than our current model predicts. As such we now revise the way that competition between plants is described in the model.

Assuming one plant overshadows the other, it would not only reduce the growth rate of its neighbour but also stunt its final canopy size. Thus the carrying capacity of the canopy being shadowed should decrease proportional to the degree of shadowing such that

$$k_{ci}(O_i(t)) = max\left(k_{min}, k_c\left(1 - O_i(t)\right)\right), \tag{3.70}$$

where k_{min} is the carrying capacity of a plant that is fully shadowed, k_c is the carrying capacity without plant-plant competition and O_i is the proportion of area that Plant i has shadowed. If equation (3.70) replaces k_c in equations (3.34) and (3.36) the non-dimensional system of equations becomes

$$\frac{dc_1(\tau)}{d\tau} = \alpha_c\left(1 - exp\left(-\kappa c_1^{(1-B)}(\tau)\right)\right)\left(1 - c_0\frac{c_i(\tau)}{k_{c1}(O_1(\tau))}\right) - d_c c_1(\tau). \tag{3.71}$$

$$\frac{dc_2(\tau)}{d\tau} = \alpha_c\left(1 - exp\left(-\kappa c_2^{(1-B)}(\tau)\right)\right)\left(1 - O_2(h_1, h_2, \tau)\right)\left(1 - c_0\frac{c_2(\tau)}{k_{c2}(O_2(\tau))}\right) - d_c c_2(\tau). \tag{3.72}$$

The description of plant height has not changed and is described by equations (3.37) and (3.38).

The simulation of the model equations (3.71) and (3.72) can be found in Figure 3.14. We choose a distance between plants of 0.4m for this example as this is the planting distance Kouassi *et al.* [34] reported to cause moderate competition. The simulation is run to 150 days as this is the time of maturity. The shorter plant

(Plant 2) is affected by competition, however the taller plant (Plant 1) is not. The difference between the two plant canopies at 150 days is now approximately 21.32%, which is clearly a more significant difference and more in line with that observed experimentally. The change in plant height over time has not changed and is given in Figure 3.13(b).

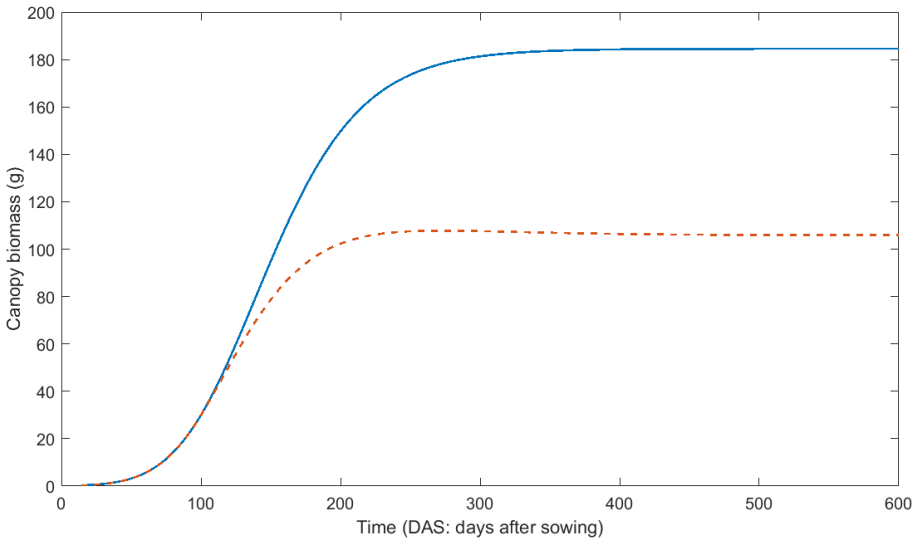

Figure 3.14: Simulation of the two plant model, where Plant 1 is taller than Plant 2 and the distance between plants is 0.4m. Overlap has been calculated using equation (3.26), leaf area index varies over time and canopy carrying capacity varies with overlap. The taller plant is indicated with a solid line, whereas the shorter plant has a dashed line.

3.5.2 Including the effect of temperature into the governing equations

It is well established that temperature has an important impact on canopy development [32]. Greenhouse experiments have been conducted that have allowed the canopy biomass to be recorded for a number of plants for three temperatures. Further details of these experiments can be found in [32]. Figure 3.15 depicts how temperature affects the average canopy biomass over time for three temperature regimes of the experimental data for species Uniswa Red and S19-3. Clearly, a

temperature of 28°C yields the highest canopy biomass, followed by 33°C and then 23°C.

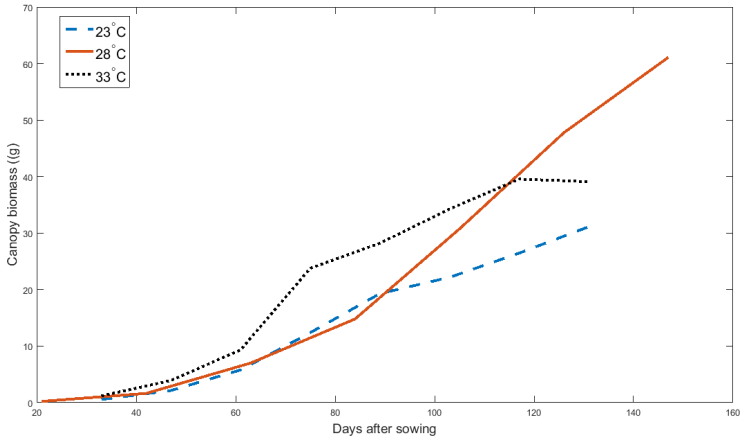

(a)

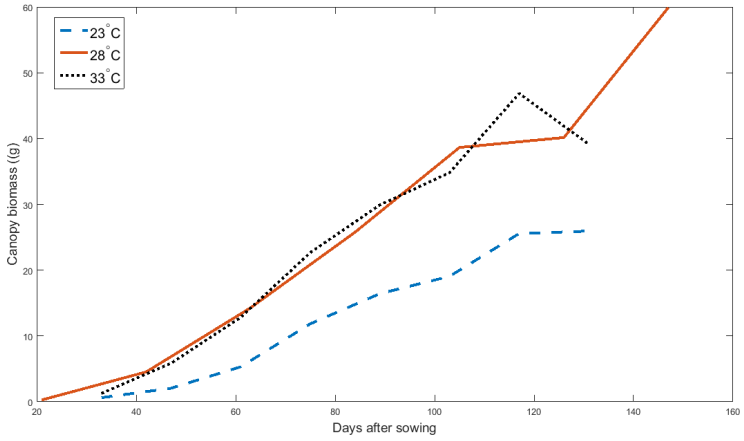

(b)

Figure 3.15: The canopy biomass over time as found in the Tropical Crops Research Unit (TCRU) greenhouse experiments for temperatures of 23°C, 28°C and 33°C for the two species of bambara groundnut: (a) Uniswa Red; and (b) S19-3.

The two-scale mathematical model described by equations (3.71) and (3.72) does not include temperature as a variable. Instead we have indirectly assumed that the incoming radiation R and temperature positively correlate, i.e. varying values of R indicate variations in temperature. This may not always be the case, particularly in controlled greenhouse conditions where a constant temperature is imposed. In this section a method of incorporating temperature into the governing equations is discussed.

In order to incorporate the effect of temperature into the model, a temperature stress is introduced. Let the critical temperature T_{crit} be defined such that it is the minimum temperature required for plant growth. If the ambient temperature falls below T_{crit} then the plant is sufficiently stressed and unable to grow. Similarly, an optimum temperature T_{opt} is defined such that it is the temperature that provides the most favourable conditions for canopy growth. Finally, T_{ceil} is defined to be the upper limit for temperature. Then the temperature stress T_s is calculated as a function of the critical temperature, the optimum temperature, and the actual daily temperature $T(t)$ so that as the daily temperature deviates from the optimum the more stress is put upon the plant. Therefore T_s is a parameter that ranges between 0 and 1 and given by

$$T_s(T) = \begin{cases} 1 - \left|1 - \frac{T(t)-T_{crit}}{T_{opt}-T_{crit}}\right| & \text{if} \quad T_{crit} < T < T_{ceil}, \\ 0 & \text{otherwise.} \end{cases} \tag{3.73}$$

Here a 1 would indicate no stress and 0 would indicate considerable stress. This method is a novel adaptation of the common method of determining the phenological age. To our current knowledge, it has not been used in the form of a temperature stress.

Given incoming radiation is the only environmental factor in our model that is linked to temperature we choose to modify this parameter such that

$$R(t) = R_0(1 - exp(-\kappa\gamma(t))) \left[1 - \left|1 - \frac{T(t) - T_{crit}}{T_{opt} - T_{crit}}\right|\right]. \tag{3.74}$$

For simplicity we have assumed that temperature $T(t)$ remains relatively constant over time and within the range $[T_{crit}, T_{ceil}]$, which is the case for the (TCRU) greenhouse experiments that we compare the model results to.

Substituting equation (3.74) into equations (3.71) and (3.72) gives the modified governing equations

$$\frac{dc_1(\tau)}{d\tau} = \alpha_c \left[1 - \left|1 - \frac{T - T_{crit}}{T_{opt} - T_{crit}}\right|\right] \left(1 - exp\left(-\kappa c_1^{(1-B)}(\tau)\right)\right) \times \left(1 - C_0 \frac{c_1(\tau)}{k_{c1}(O_1(\tau))}\right) - d_c c_1(\tau), \tag{3.75}$$

$$\frac{dc_2(\tau)}{d\tau} = \alpha_c \left[1 - \left|1 - \frac{T - T_{crit}}{T_{opt} - T_{crit}}\right|\right] \left(1 - exp\left(-\kappa c_2^{(1-B)}(\tau)\right)\right) (1 - O_2(h_1, h_2, \tau)) \left(1 - C_0 \frac{c_2(\tau)}{k_{c2}(O_2(\tau))}\right) - d_c c_2(\tau). \tag{3.76}$$

The initial conditions have not changed and are given by

$$c_1(0) = c_{10} \quad \text{and} \quad c_2(0) = c_{20}.$$

Parameter values of T_{crit} and T_{opt} for species Uniswa Red and S19-3 have been taken directly from the thesis of Karunaratne [32] and can be found in Table 3.4.

Parameter	Uniswa Red	S19-3
T_{crit} (°C)	8.5	12
T_{opt} (°C)	28	30
T_{ceil} (°C)	38	45

Table 3.4: The critical and optimum temperatures for Uniswa Red and S19-3 as found in the thesis of Karunaratne [32].

Figure 3.16 shows the simulation of equations (3.75) and (3.83) averaged over the two plants, where Plant 1 is taller than Plant 2 and the critical and optimum temperature for Uniswa Red and S19-3 can be found in Table 3.1. There is a distance of 0.3m between plants and the simulations have been run for three temperatures of 23°C, 28°C, and 33°C. In this case, canopy biomass has been averaged for the two plants in the simulation, the difference between the two plants here is similar to that found in Figure 3.14. As seen in Figure 3.16 the further the temperature is from the optimum, the slower the development in canopy biomass. At 150 days, the point at which the plant reaches maturity, the canopy biomass is less for the non-optimal temperatures. Since the simulation is for two plants we can not compare it with experimental data as the data are for the many plant population.

We later compare our many plant model with experimental data in Section 3.7.5

where we show that the impact temperature has on canopy biomass is well predicted by the model. We can also see from Figure 3.16 that canopy biomasses for temperatures 23°C and 33°C are identical for Uniswa Red. This is because temperatures 23°C and 33°C have the same difference between them and the optimum temperature 28°C, hence their temperature stresses are identical.

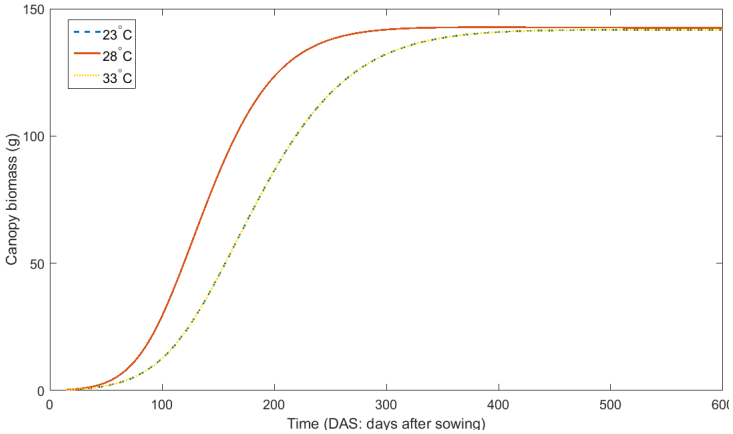

(a) Uniswa Red

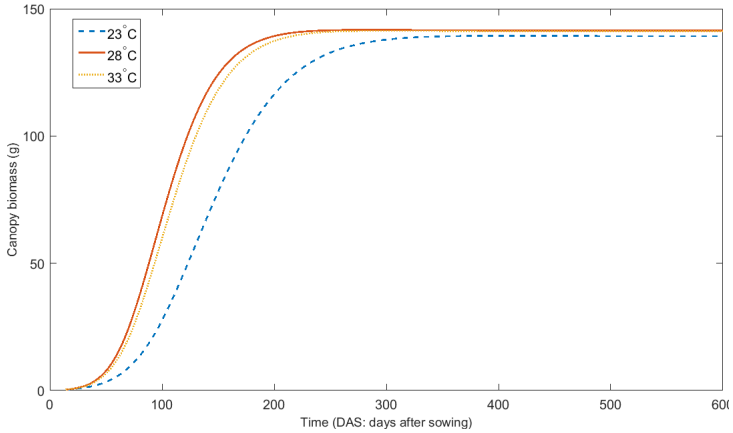

(b) S19-3

Figure 3.16: Incorporating temperature variation: average canopy biomass of two plants described by equations (3.75) and (3.76) for the species Uniswa Red and S19-3, where Plant 1 is taller than Plant 2. The critical and optimum temperature can be found in Table 3.1 for each species. There is a distance of 0.30m between the two plants for all simulations for three temperatures of 23°C, 28°C, and 33°C.

3.5.3 Light penetrating through the canopy

When the canopies of two (or indeed more) plants interact, it is not always the case that one plant canopy grows higher than the other. In fact, with short spreading plants such as bambara groundnut, it is more common for leaves within interacting plant canopies to mingle and cause mutual shading. In addition, it could also be the case that light penetrates through the canopy of the taller plant onto the shorter plant. In this work so far the method for calculating competition is for when one plant is shadowed and the extent of shadowing is equal to the intersection area of the two intersecting circles that represent plant canopies. In this section, the case of mutual shading is introduced as well as the case of light penetrating through the taller canopy.

Consider two plants grown together with a planting distance that allows their respective canopies to interact. It might be the case that the leaves that comprise the canopies intermingle. Thus some leaves of both plants will be shadowed, whilst others are exposed to light. It might also be the case that light can penetrate through a neighbours canopy. Therefore the effect competition has on a plant is no longer $(1 - O_i(t))$ but

$$1 - \omega_i O_i(t), \tag{3.77}$$

where ω_i is a coefficient to be determined that ranges between 0 and 1 depending on the amount of mutual shading, the respective plant heights and the amount of light that can penetrate through the canopy.

There are several cases to now consider. Firstly, consider the case when Plant 1 is definitively taller than Plant 2 but some light is able to penetrate through the canopy of Plant 1. We then have $\omega_1 = 0$ since, as the taller plant, it is not being shadowed, however ω_2 can take any value between 0 and 1 depending on the amount of light that can penetrate through the canopy. Clearly, a value of 1 would be the case that has so far been considered and a value of 0 would indicate no effect by being shadowed. This would cause Plant 2's light interception to be equal to Plant

1.

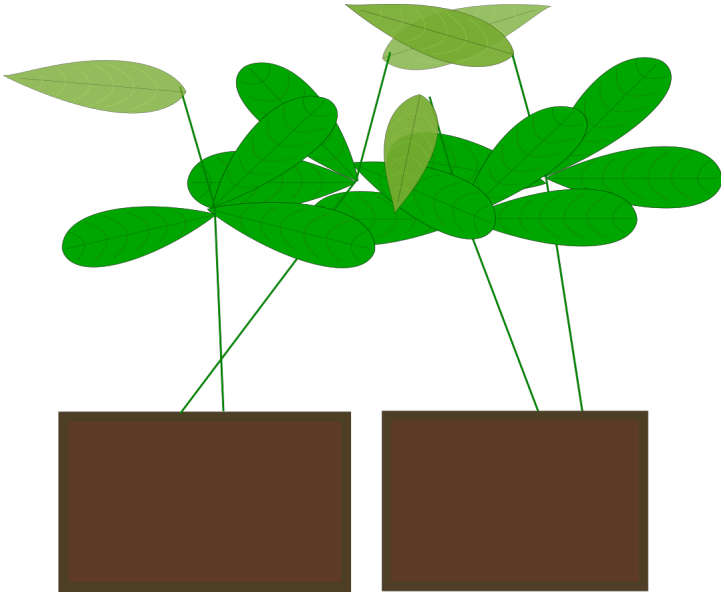

Figure 3.17: Schematic of two competing plant canopies, where both plants are the same height and the leaves intermingle across canopies.

The second case we consider is if both plants grow continuously at the same height and there is mutual canopy border interactions (i.e. intermingling) between their canopies. A schematic of this case can be found in Figure 3.17 where the leaves of two plant canopies intermingle in such a way that it is not immediately clear which leaves belong to which plant, it is clear however that parts of both plants are shadowed by it's neighbour. Here we assume that no light penetrates through either canopy, therefore light blocked from one plant is not blocked from the other so that

$$\omega_1 = 1 - \omega_2. \tag{3.78}$$

If we assume that leaves of two canopies intermingle in such a way that the leaves of the two plants are in equal parts shadowed and exposed, then $\omega_1 = 0.5 = \omega_2$. This would mean that both plants will be affected by the competition, and each plant will be affected exactly half as much as if it was being shadowed by a definitively taller plant. Since both Plant 1 and Plant 2 are now affected by overlap we restate the model equations here with the adjustment that the growth rate of $c_1(t)$ is now

affected by O given by

$$\frac{dc_1(\tau)}{d\tau} = \alpha_c \left[1 - abs\left(1 - \frac{T - T_{crit}}{T_{opt} - T_{crit}}\right)\right]\left(1 - exp\left(-\kappa c_1^{(1-B)}(\tau)\right)\right) \times (1 - \omega_1 O_1(h_1, h_2, \tau))\left(1 - C_0 \frac{c_1(\tau)}{k_{c1}(O_1(\tau))}\right) - d_c c_1(\tau), \quad (3.79)$$

$$\frac{dc_2(\tau)}{d\tau} = \alpha_c \left[1 - abs\left(1 - \frac{T - T_{crit}}{T_{opt} - T_{crit}}\right)\right]\left(1 - exp\left(-\kappa c_2^{(1-B)}(\tau)\right)\right) (1 - \omega_2 O_2(h_1, h_2, \tau))\left(1 - C_0 \frac{c_2(\tau)}{k_{c2}(O_2(\tau))}\right) - d_c c_2(\tau). \quad (3.80)$$

Henceforth, we will assume that $\omega_1 = 0.5 = \omega_2$ and absorb this into O_i.

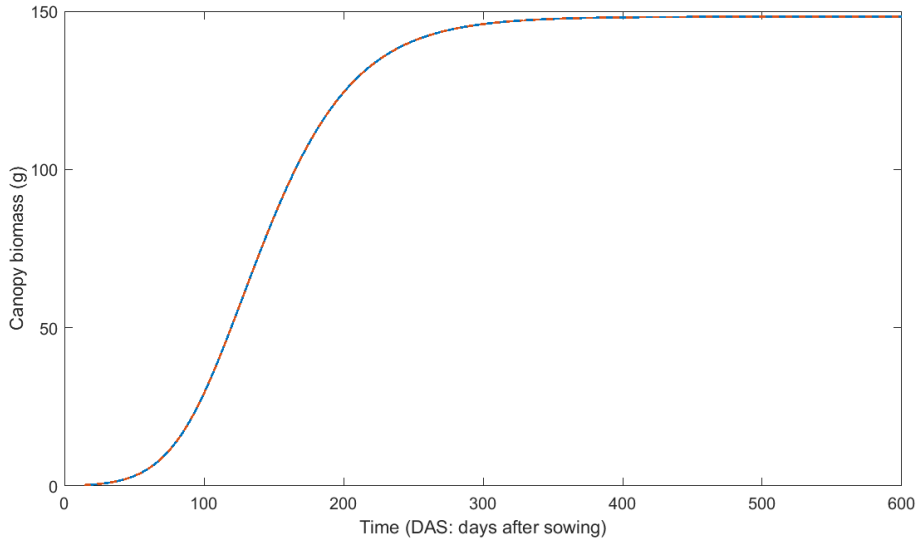

Figure 3.18: Simulation of two plants of the same height, temperature is 28°C and the planting distance is 0.3m. Plant 1 is indicated with a solid line, whereas Plant 2 has a dashed line.

Figure 3.18 shows the canopy biomass over time of two plants of the species Uniswa Red. Plants have the same height with $\omega_1 = 0.5 = \omega_2$, the temperature is 28°C and the planting distance is 0.30m. We only investigate Uniswa Red here, however the results also apply to S19-3. From Figure 3.18, we can see that the canopy biomass over time for the two plants for both species is indistinguishable from each other. This is because each plant is affected by competition in exactly the same way. In the scenario where neither plant experiences competition we would

see both plants behave in the same way, but grow to a larger canopy biomass.

If ω_1 and ω_2 were to change it would no longer be the case that they have the same canopy biomass over time. We investigate the effect ω_1 and ω_2 have on canopy biomass in Figure 3.19. Here $c_1(t)$ and $c_2(t)$ are shown at $t = 150$ days for ω_2 ranging between 0 and 1; the value of ω_1 is determined by ω_2. We choose $t = 150$ days here as this is the time at which the plants would be harvested.

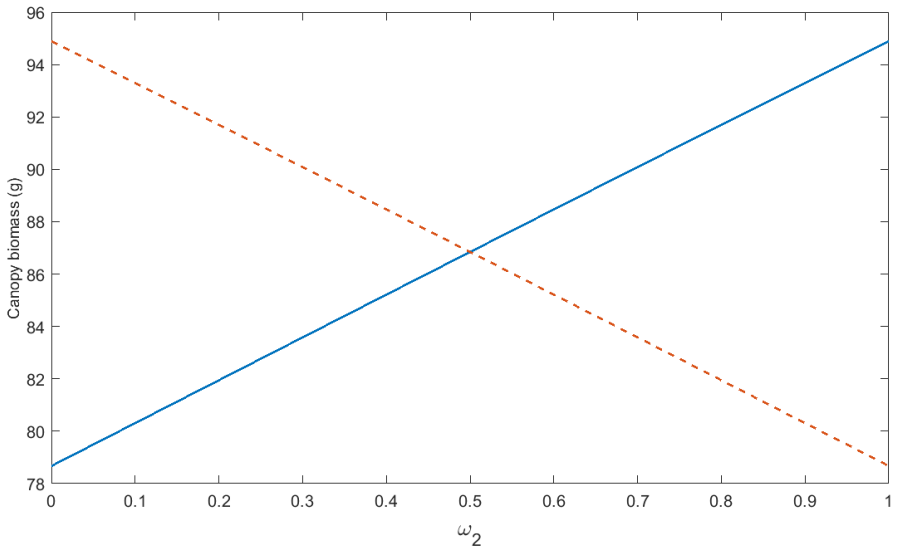

Figure 3.19: Canopy biomass of two interacting plants at 150 days for a range of values of ω_2. Here the temperature is 28°C and the planting distance is 0.3m. Plant 1 is indicated with a solid line, whereas Plant 2 is by a dashed line.

We can see that the canopy biomass is equal for Plants 1 and 2 when $\omega_2 = 0.5$, we also see that as ω_2 increase c_2 decreases and c_1 increases. There is a change of approximately 15g to the biomass of each plant as ω_2 varies. The affect that ω_i has on canopy biomass may become more complex with the addition of more plants.

We now consider the combination of the previous two cases where light can penetrate through the canopy's foliage and also Plant 1 and Plant 2 are of similar heights. It is now not necessarily the case that $\omega_1 = 1 - \omega_2$ as ω_i can now take a whole range of values. We explore this space in Figure 3.20. Here both ω_1 and ω_2 range between 0 and 1 and the canopy biomass of Plant 1 and Plant 2 are recorded in Figures 3.20(a) and 3.20(b), respectively.

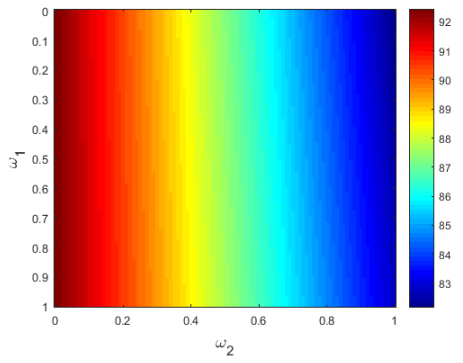

(a) Canopy biomass of Plant 1

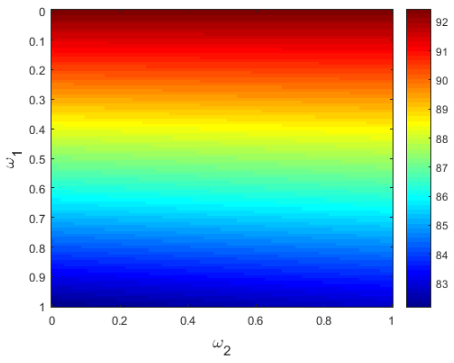

(b) Canopy biomass of Plant 2

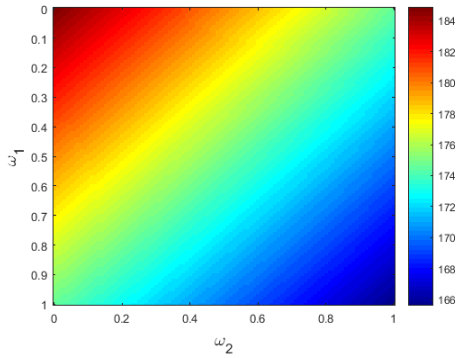

(c) Sum canopy biomass of Plants 1 and 2

Figure 3.20: The canopy biomass of Plants 1 and 2 for a range of values of ω_1 and ω_2. The species is Uniswa Red, the temperature is 28°C, planting distance is 0.3m and both plants are the same height.

Realistically ω_i would be a function of plant height, plant distance and leaf area index. To include this into the model would require experimental data we do not have access to. As such, going forward we will assume that

$$\omega_i = \begin{cases} 1 & \text{if} \quad h_j > h_i, \\ 0.5 & \text{if} \quad h_j = h_i, \\ 0 & \text{if} \quad h_j < h_i, \end{cases} \tag{3.81}$$

where h_j is the height of the neighbouring plant.

3.6 Sensitivity Analysis

It is of interest to learn how robust the model is to variation in parameters. In this section we discuss the results of a local sensitivity analysis applied to the system of equations for two plants described by equations (3.79) and (3.80). The sensitivity analysis is applied to each non-dimensional parameter of the two plant model in turn. These are summarised in Table 3.5 along with their original values for convenience. Parameters are the same for both plants throughout the sensitivity analysis and when variations are applied to parameters they are applied for both plants at the same time. Plants of the species Uniswa Red are arranged at a distance of 30cm and the temperature used for the simulation is $28°C$. Simulations begin at fourteen days, the predicted time of emergence, and are run to one hundred and fifty days, the estimated time of maturity. The original value of each non-dimensional parameter (denoted by x) is both increased and decreased by an order of magnitude of ten, this is done to one parameter at a time. The canopy biomass at one hundred and fifty days is averaged over both plants for each parameter variation. The results are recorded in Table 3.5.

Parameter	Parameter Original Value	Average Canopy Biomass (g)		
	x	$0.1x$	x	$10x$
α_c	0.223	0.77	86.84	151.31
κ	0.6	1.07	86.84	113.53
K_c	1.58×10^{-3}	135.83	86.84	17.68
d_c	6.67×10^{-2}	87.05	86.84	84.80

Table 3.5: Sensitivity analysis of the non-dimensional system given by equations (3.75) and (3.76). The average canopy biomass at 150 days of two plants has been recorded for a tenfold increase and decrease to the non-dimensional parameters denoted here by x. The temperature of the simulations is set to $28°C$ and the species is Uniswa Red. There is a 30cm distance between plants.

The system is particularly sensitive to the non-dimensional growth rate α_c, extinction coefficient κ and carrying capacity K_c. There is more sensitivity to decreases in these parameters than increases. Note that an increase in K_c is equivalent to a decrease in k_{max}. The system is not particularly sensitive to the decay rate d_c.

The effect that variations in plant parameters have on canopy biomass make sense qualitatively. We see that as the growth rate α_c for both plants increases, canopy biomass approaches the carrying capacity k_c faster and thus c is larger at 150 days. Similarly, a decrease in α_c slows biomass growth causing the canopy biomass to be further from the carrying capacity at 150 days. As expected this is the opposite effect to increases and decreases in d_c, where an increase in d_c causes c to be further from it's maximum and a decrease causes c to be larger.

Changes to κ relate to changes in the angle of the leaves. A larger value of κ indicates flatter leaves which are more open to capturing incoming radiation. Thus an increase in κ causes c to increase at 150 days and a decrease in κ causes a decrease in final c.

Since

$$K_c = \frac{c_0}{k_c}$$

an increase in K_c would indicate a decrease in the carrying capacity in relation to the initial condition. As we can see from Table 3.5, this causes c to be significantly lower at plant maturation which is to be expected. Conversely, a decrease in K_c indicates an increase in k_c in relation to the initial condition, which causes c to become larger at plant maturation.

3.7 Multi-plant model

In the previous sections we have focused on two plant canopy interactions, but we now wish to consider scaling our model up to the many plant (population) scale. We initially assume plants are placed in a uniform grid array with a distance between plants in a row of D_r and a distance between plants in a column of D_c. Each plant is indexed from 1 to N with a subscript i where non-dimensional plant height is described such that

$$h_i(\tau) = \frac{h_0(1-d_h)exp((1-d_h)\tau)}{1-d_h-k_{hi}h_0+k_{hi}exp((1-d_h)\tau)h_0}, \tag{3.82}$$

and non-dimensional canopy biomass growth is described such that

$$\begin{aligned}\frac{dc_i(\tau)}{d\tau} &= \alpha_c T_s(T)\left(1 - exp\left(-\kappa c_i^{(1-B)}(\tau)\right)\right)(1 - O_i(h_1, h_2, ...h_N, \tau)) \times \\ &\quad (1 - K_{ci}(\tau)c_i(\tau)) - d_c c_i(\tau). \end{aligned} \tag{3.83}$$

The initial conditions are given by

$$h_i(\tau) = 1 \quad \text{and} \quad c_i(\tau) = 1.$$

Currently parameters for each plant are identical with the only difference between plants being the manner in which it interacts with its neighbours, this is in turn governed by the plants position.

In the multi-plant model there is a chance that several plants will overlap in the same place. The current method of calculating overlap can only be used for two plants, and so can not be applied for when multiple plants overlap at the same point. Therefore, for the multi-plant model to be effective, a new method of calculating overlap needs to be introduced.

Once the multi-plant model has been fine-tuned to include overlap between three or more plants, we investigate how plant height of individual plants affects plant growth. To do this we compare canopy biomass of plants with the same height with that of plants with randomly distributed heights. Following this, the model is then compared to experimental data and a sensitivity analysis is conducted to determine it's robustness.

3.7.1 A numerical approximation of plant canopy interactions

The analytical solution described in Section 3.2.1 works adequately for two overlapping circular plant canopies, however can not be applied to multiple circles that intersect in the same area. First consider the case of three intersecting plants illustrated in Figure 3.21. The proportion of Circle 1's (c_1) area that is shared with Circles 2 and 3 (c_2 and c_3), cannot be found by summing the intersection of Circles

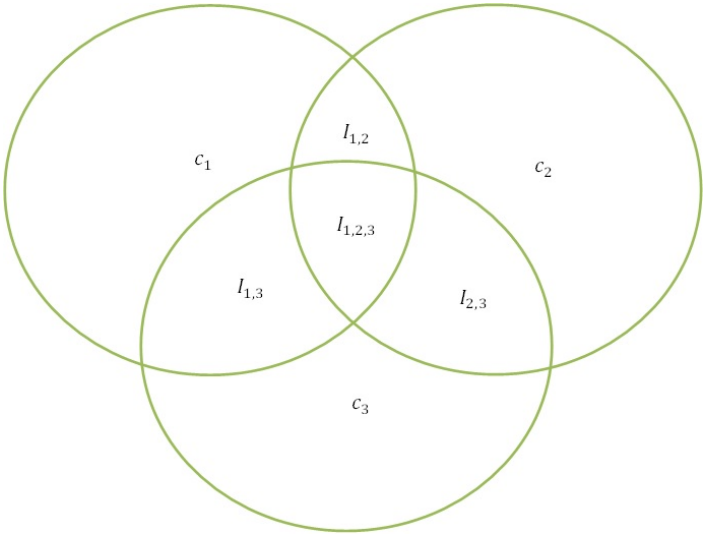

Figure 3.21: Three intersecting circles (c_1, c_2, c_3) that represent three neighbouring plants, where the area's of intersection are labelled as $I_{1,2}, I_{1,3}, I_{2,3}$ and $I_{1,2,3}$.

1 and 2 (I_{12}) and the intersection of Circles 1 and 3 (I_{13}). Instead, it is necessary to find the area that all three circles share (I_{123}). Finding this area analytically is challenging. The difficulty in calculating this area increases with the number of plants. For cases such as these a numerical method for calculating canopy overlap is devised. We introduce such a method in this section and compare the numerical method results to the analytical method described in Section 3.2.1.

We consider the competition one circle, labelled with an i, experiences with neighbouring circles, labelled with k's. Let Circle i be filled with n uniformly allocated points, a distance d apart. Sampling points are arranged in a series of increasing rings within the circle where d is the distance between rings and the distance between points within a ring. Each point, labelled with a j, is allocated an x and y coordinate denoted by x_j and y_j. Each point within circle i can now be tested to determine which circles, other than Circle i, it lies within.

Let the centre point of Circle k have coordinates c_{kx} and c_{ky} and radius r_k. Then a sampling point within Circle i that is also within Circle k holds to the condition that

$$\sqrt{(x_j - c_{kx})^2 + (y_j - c_{ky})^2} < r_k.$$

Then an $n \times N$ array A can be defined such that

$$A_{j,k} = \begin{cases} 1, & \text{if } \sqrt{(x_j - c_{kx})^2 + (y_j - c_{ky})^2} < r_k \\ 0, & \text{otherwise,} \end{cases}$$

where N is the number of neighbouring circles and n is the number of sampling points within Circle i. An element $A_{j,k}$ equals 1 if sampling point j is within Circle k but is otherwise zero. Summing the elements of each row of A gives a column vector B such that

$$B_j = \sum_{k=1}^{N} A_{j,k}.$$

Each element of vector B gives the number of circles that each sampling point j is contained in. All sampling points are contained within at least Circle i and so the minimum value of B_j is 1.

To find the proportion of area Circle i shares with neighbouring circles we must find the number of points that are contained within Circle i only and so we define a $1 \times n$ vector C such that

$$C_j = \begin{cases} 1, & \text{if } B_j = 1 \\ 0, & \text{otherwise.} \end{cases} \tag{3.84}$$

Then the proportion of Circle i that is shared with adjacent Circles j is given by

$$O_i = 1 - \frac{\sum_{j=1}^{n}(C_j)}{n}. \tag{3.85}$$

The arrays A, B and C are calculated for each circle in turn to find O_i, $i \in [1, N]$. Hence O will be a vector of length N.

In order to test this approximation, we consider two intersecting circles as illustrated in Figure 3.2(b). Since O_i is the proportion of Circle i that is intersected, in order to find the actual area of intersection we multiply O_i by the area of Circle i. The area of intersection for Plant 1 is equal to that of Plant 2 and as $O_i = I_i/G(i)$, then $O_1 c_1 = O_2 c_2 = I$, where c_1 and c_2 are the area of Circles 1 and 2 respectively.

The area of intersection has been found using the analytical method, described in Section 3.2.1, and the numerical method, described in this section. The values of both methods are given in Table 3.6 for a range of values for D, r_1, r_2 and n. To better compare the two methods, Table 3.6 also gives the difference between solutions of the two methods as an absolute difference and also a percentage (relative) difference.

Clearly the accuracy of the numerical method depends on the number of sampling points n contained within the circle. There is little improvement between 5000 and 10000 sampling points, however using 10000 sampling points instead of 5000 increases computational time by approximately 24%. When calculating the area of intersection for many plants at multiple time points, this increase to computational time will add up considerably and so using 5000 sampling points is preferable. The error decreases for larger intersection areas but there is no obvious change in error for increased circle sizes. From the results shown in Table 3.6 there is no obvious bias for the method to underestimate or overestimate I. From these results we can judge that this method with 5000 sampling points will give a good approximation of O.

This concludes the numerical method of calculating the area of intersection between two or more circles. We must now consider how this method transfers to measuring the amount of shadowing between plant canopies as there are some subtle differences. Plant canopies are represented using circular discs, however in the method devised for calculating overlap described in this section the intersection area has only been considered in a 2-D space. By doing this we have neglected to consider the heights of the plants. The area we wish to calculate is the proportion of plant canopy that is being shadowed by its neighbours and to do this, the plant heights play a key role in the calculation. An $N \times 1$ vector can be defined such that

$$\omega_{1k} = H_1(h_k - h_i),$$

where h_i is the height of Circle i, h_k is the height of a neighbouring Circle k and H_1

D	r_1	r_2	Analytical I	n	Numerical I	Absolute error	Relative Error (%)
0.25	0.15	0.15	5.63×10^{-3}	1000	5.17×10^{-3}	4.53×10^{-4}	8.05
			5.63×10^{-3}	5000	5.43×10^{-3}	1.97×10^{-4}	3.51
			5.63×10^{-3}	10000	5.64×10^{-3}	1.70×10^{-5}	0.30
		0.3	4.64×10^{-2}	1000	4.55×10^{-2}	9.63×10^{-4}	2.08
			4.64×10^{-2}	5000	4.63×10^{-2}	1.26×10^{-4}	0.27
			4.64×10^{-2}	10000	4.63×10^{-2}	7.56×10^{-5}	0.16
	0.3	0.3	0.1372	1000	0.1372	1.54×10^{-3}	3.32
			0.1372	5000	0.1371	5.76×10^{-4}	0.42
			0.1372	10000	0.1372	2.05×10^{-5}	0.01
0.5	0.3	0.3	0.0225	1000	0.0207	1.81×10^{-3}	8.05
			0.0225	5000	0.0217	7.89×10^{-4}	3.5
			0.0225	10000	0.0226	6.78×10^{-5}	0.30
		0.6	0.1857	1000	0.1819	3.85×10^{-3}	2.07
			0.1857	5000	0.1852	5.03×10^{-4}	0.27
			0.1857	5000	0.1854	3.02×10^{-4}	0.16
	0.6	0.6	0.5488	1000	0.5549	6.17×10^{-3}	1.13
			0.5488	5000	0.5511	2.31×10^{-3}	0.42
			0.5488	10000	0.5789	8.21×10^{-5}	0.015

Table 3.6: A comparison of the numerical and analytical methods of calculating overlap for two interacting circles for a range of planting distances, circle sizes and sampling points. The absolute error is the difference between the value of I for both methods and the relative error is absolute error as a percentage of the analytical solution given in equation (3.26).

is a Heaviside function such that

$$H_1(x) = \begin{cases} 1, & \text{if } x > 0 \\ 0, & \text{otherwise.} \end{cases}$$

Thus

$$\omega_{1k} = \begin{cases} 1, & \text{if Plant } k \text{ is taller than Plant } i, \\ 0, & \text{otherwise.} \end{cases}$$

Here $\omega_{1k} = 1$ indicates that random point i is fully shadowed by the taller plant k, whilst $\omega_{1k} = 0$ means plant i is not shadowed by plant k. Let P_1 be an $N \times 1$ vector such that

$$P_{1j} = \sum_{k=1}^{N} A_{j,k}\omega_{1k},$$

then P_1 will give a list of the sampling points that are overlapped by plants that are strictly taller than plant i. If $P_1 > 1$ then several plants overlap point j. Since we are not currently considering the case of light penetrating the canopy we do not need to concern ourselves with how many plants overlap point j only that some do. Therefore we let

$$C_{2j} = \begin{cases} 1, & \text{if } P_{1j} = 0, \\ 0, & \text{otherwise.} \end{cases} \tag{3.86}$$

The proportion of area that plant i shares with taller plants can then be found as

$$OT_i = 1 - \frac{\sum_{j=1}^{n}(C_{2j})}{n}.$$

For plants of the same height we assume that the leaves of the plant canopies intermingle and that overlap is distributed evenly over the competing canopies as described in Section 3.5.3. Hence each canopy receives half the amount of shadowing within the area of intersection. We define ω_2 such that

$$\omega_{2k} = H_2(h_k - h_i),$$

where H_2 is defined such that

$$H_2(x) = \begin{cases} 0.5, & \text{if } x = 0, \\ 0, & \text{otherwise.} \end{cases}$$

Thus

$$\omega_{2k} = \begin{cases} 0.5, & \text{if Plant } k \text{ is the same height as Plant } i \\ 0 & \text{otherwise.} \end{cases}$$

A value of $\omega_{2k} = 0.5$ indicates that Plant i is competing with a plant of the same height and so the competition is split evenly between both plants. The case of

$\omega_{2k} = 0$ refers to any other scenario. Now let P_2 be an $N \times 1$ vector such that

$$P_{2j} = \sum_{k=1}^{N} A_{j,k}\omega_{2k}.$$

The minimum value that an element of P_2 can take is 0.5 as each point is at least contained within canopy i, which is the same height as itself. When $P_{2j} > 1$ the point j is sharing the space with more than 1 other plant. Since competition is shared evenly among plants sharing a space we must take into account the number of plants point j is contained within. Then the area Plant i shares with plants of the same height is thus found such that

$$OS_i = 1 - \frac{\sum_{j=1}^{n}\left(\frac{0.5}{P_{2j}}\right)}{n}. \tag{3.87}$$

The total proportion of plant canopy that is shadowed can be found such that

$$O_i = OT_i + OS_i. \tag{3.88}$$

Hereafter this will be the method used for calculating the overlap between two or more plant canopies.

3.7.2 Model Summary

This section summarises our first two-scale mathematical model developed to simulate plant growth. The model is described by a system of 2 non-linear differential equations per plant. The equations comprise of one for change in plant height (where the analytical solution is given by equation (3.82)) and another to simulate change in plant canopy mass (given by equation (3.83)). The competition between neighbouring plants is assumed to be in the form of canopy-canopy shadowing and is quantified using the area of intersection of the plant canopies calculated as in Section 3.7.1. Plant competition is dependent on the height of a plant and of it's neighbours. Competition affects the canopy biomass growth rate and carrying capacity.

The model algorithm comprises the following steps for N plants.

1. Input species parameters, temperature and radiation data;.
2. Input initial conditions for plant height h_{i0} and canopy biomass c_{i0}.
3. Calculate leaf area A_i from canopy biomass c_i for each plant.
4. Calculate ground cover G_i from leaf area A_i for each plant.
5. Calculate leaf area index γ_i from leaf area A_i and ground cover G_i.
6. Calculate the inter-plant competition experienced by each plant by evaluating the area of plant canopy that is shadowed O_i using the ground cover G_i of each plant and their respective plant heights h_i and positions as detailed in Section 3.7.1.
7. Calculate the change in height of each plant h_i using equation (3.82).
8. Calculate the change in canopy biomass c_i using equation (3.83).
9. Let $t = t + \delta t$ where δt is the time step chosen by the inbuilt MATLAB ODE solving algorithm ode15s to meet the absolute and relative error tolerances.
10. Repeat steps 3-9 for each plant until $t = T_{end}$.

These steps are summarised in Figure 3.22.

3.7.3 Same height versus different heights

As discussed in Section 3.5.3, two plants of the same height that interact with each other grow to the same size at the same rate, as they both experience competition in the same way. If more plants were to be simulated, this would not necessarily be the case as an increase in the number of plants will affect the dynamics of inter-plant interactions.

Consider nine plants arranged in three rows of three. The centre plant of this arrangement would be in a position to interact with all other plants whereas a plant

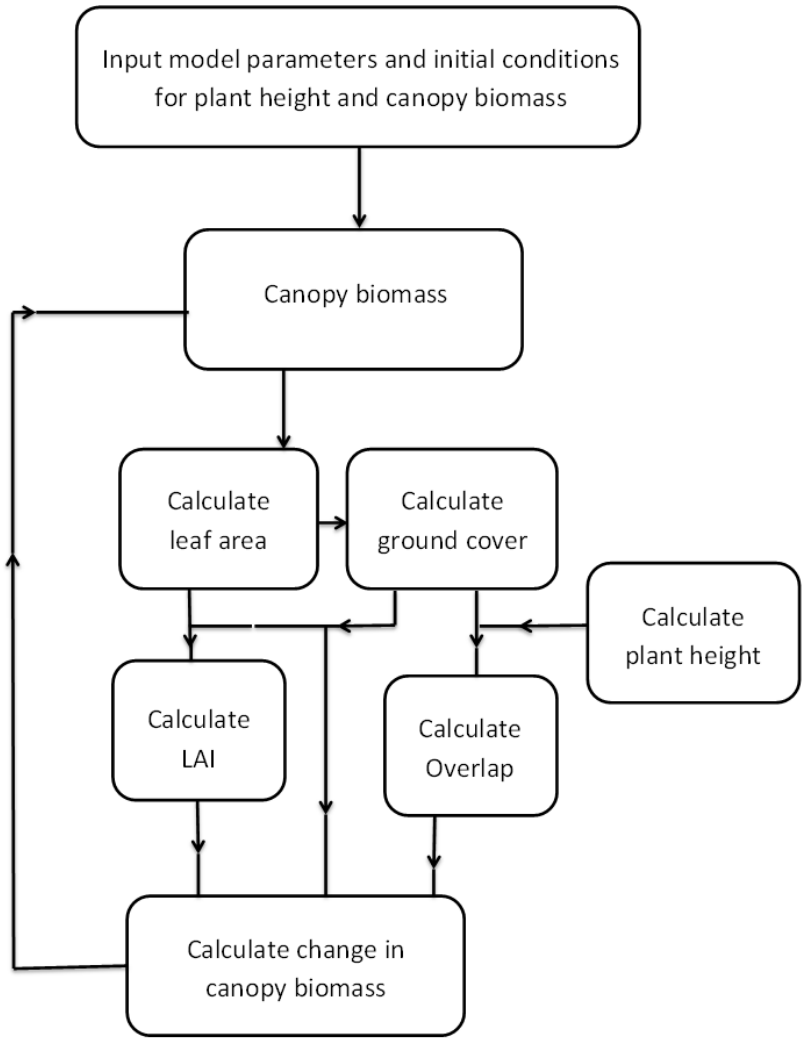

Figure 3.22: Diagram of the multi-plant algorithm for each plant in the population.

placed on the corner of the arrangement would be in a position to interact with three other plants. Thus, even though all plants are the same height and competition is split evenly between interacting canopies, the centre plant will experience more competition than those on the outside. Similarly, plants on the edges will experience more competition than those on the corners, i.e. potentially five other plants.

In order to simulate this, we arrange nine plants in a 3×3 formation where plant heights are described by equation (3.82) and plant canopy biomass is described by equation (3.83). The plant species Uniswa Red is used where plant parameters are the same for all nine plants and can be found in Table 3.1. The temperature

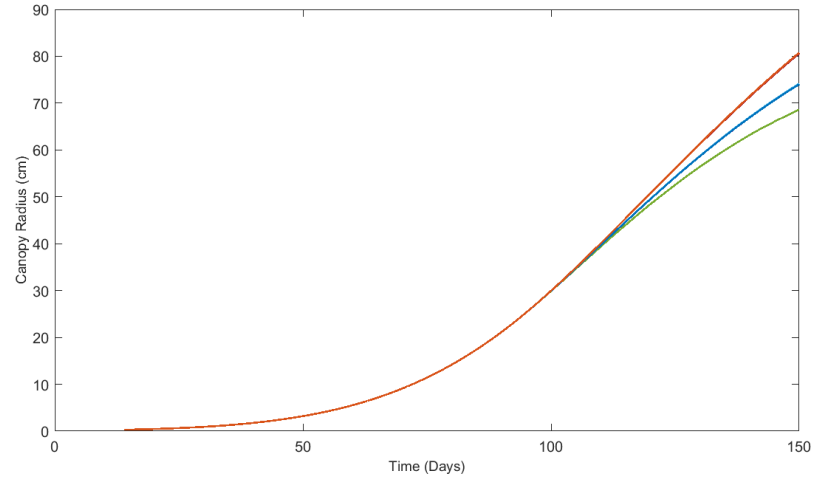

(a)

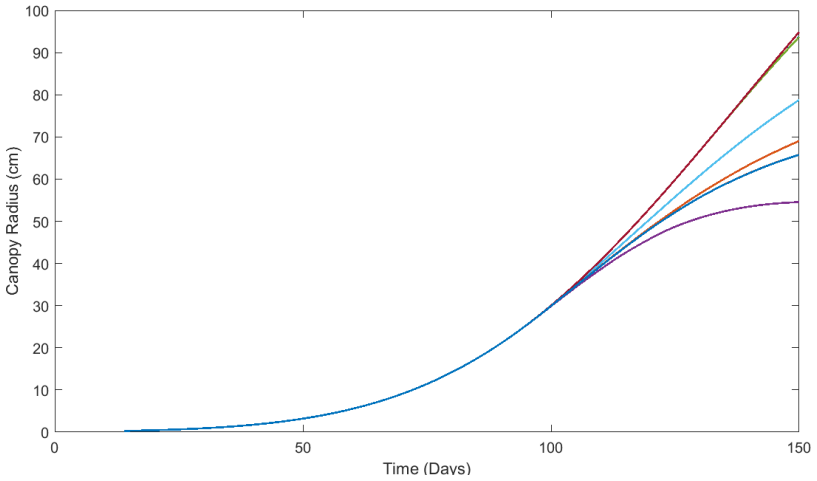

(b)

Figure 3.23: Canopy biomass over time for 9 plants of the species Uniswa Red at a temperature of 28°C and planting distance between rows and columns is 0.30m. (a) plants are the same height and (b) plant height is randomly varied

considered is 28°C. The resulting canopy biomass of each of the nine plants is given in Figure 3.23(a). Here we can see that plants grow uniformly until a point is reached when canopies begin interacting. After this point, the growth rates differ between plants resulting in different canopy biomasses. This clearly illustrates the difference in behaviour of the three groups: centre, middle edge, and corners, since all plants have the same growth parameters, this difference is caused by their position within the plot. In this case, the corner plants have the highest biomass, followed by plants

positioned in the middle of the edges and finally, the centre plant has the lowest canopy biomass.

We now repeat this experiment however we allow the plant height to vary between plants. The variation in height is applied by changing the plant height carrying capacity for each plant. We assume that plant height carrying capacity has a normal distribution with the mean being the original value given in Table 3.1 and with a variance of 10% of the mean. Then a value is randomly selected from this distribution and applied to each plant. The canopy biomass of each of the nine plants can be found in Figure 3.23(b). There are now five groups instead of three, this changes for different random selections of plant height. The reason why plants with all different heights may still have the same canopy biomass is because since heights are randomly generated, there still may be some similarities between plants. In the example shown in Figure 3.23(b), the two tallest plants do not interact with each other and so the tallest plant has the same canopy biomass as the second tallest since neither of them are shadowed by a neighbour. Similarly, the two shortest plants are both on an edge and thus both experiencing shadowing from five other plants.

3.7.4 Sensitivity Analysis

In this section we repeat a local sensitivity analysis on the system of equations described by equation (3.83). The sensitivity analysis is now applied to fifteen plants so that we can see if including more plants increases or decreases the sensitivity of the system. Plants are arranged in three rows of five. Again the distance between rows is 35cm and the distance between plants in a row is set to 20cm, as shown in Figure 3.8. The temperature used for the simulation is $28^{\circ}C$ and the test species being investigated is Uniswa Red. The simulations begin at fourteen days, the predicted time of emergence, and runs to one hundred and fifty days, the estimated time of plant maturity.

Table 3.7 gives a list of the four non-dimensional parameters that are being investigated, with their original values. A tenfold reduction and a tenfold increase is

applied to each of the non-dimensional parameters in turn and the relative change to the canopy biomass at one hundred and fifty days is summed for all fifteen plants. The results are recorded in Tables 3.7.

Parameter	Parameter Original Value	Average Canopy Biomass (g)		
	x	$0.1x$	x	$10x$
α_c	0.223	0.77	62.96	96.57
κ	0.6	1.08	62.96	77.45
K_c	1.58×10^{-3}	89.24	62.96	16.17
d_c	6.67×10^{-2}	63.09	62.96	61.62

Table 3.7: Sensitivity analysis of the non-dimensional system given by equation (3.83). The average canopy biomass at 150 days for fifteen plants has been recorded for a tenfold increase and decrease to the non-dimensional parameters. The temperature of the simulations is set to $28°C$ and the species is Uniswa Red. There is a 20cm distance between plants in a column and a distance of 35cm between columns.

Similar to the sensitivity analysis conducted for two plants, the system is not very sensitive to d_c, however is particularly sensitive to α_c, κ and K_c. There does not appear to be any change in the sensitivity of the model for an increase in plants from 2 to 15, however we find that average c decreases overall. This is due to each plant competing with more plants.

Qualitatively, the results of this sensitivity analysis are the same as in Section 3.6 for two interacting plants.

3.7.5 Comparing the model to experimental data

Having developed the theoretical model, we now validate the model by comparing simulation results to experimental data provided by the Tropical Crops Research Unit (TCRU) greenhouse experiments conducted in 2003 and 2006 [32]. The data consist of two species: Uniswa Red and S19-3, grown at temperatures of 23°C, 28°C, and 33°C. Leaf number, leaf area, leaf mass, stem mass, root mass, pod mass and total biomass have been monitored over sixteen day intervals starting at thirty three days. The distance between plants is constant with 35cm between columns and 20cm between rows. The supply of water is non-limiting, meaning that plant growth is

unaffected by it. A more detailed description of the experimental methodology can be found in [32].

A simulation of 15 plants, where plant parameters are equal, is conducted. Plants are arranged in three columns of five with a distance between columns of 35cm and a distance between rows of 20cm; this has been done to replicate the conditions of the greenhouse experiments; a simulation of the planting arrangement can be found in Figure 3.8. The simulations are repeated for temperatures 23°C, 28°C and 33°C for species Uniswa Red and S19-3 with their respective parameter values described in Table 3.1.

Plant heights in the experiments are unknown to us and are assumed to be the same. This means that instead of one plant definitively overlapping the other, plant canopies intermingle and therefore all plants in the simulation experience competition. We later test this assumption by comparing simulations of canopy biomass, where random variation is applied to plant height with those where plant heights are equal.

Model simulations of leaf area and canopy biomass for Uniswa Red compared to the experimental data are shown in Figures 3.24 to 3.26. The data shown are the average for all fifteen plants for both the simulations and experimental data.

	Canopy biomass (g)				Leaf Area (m^2)			
	Uniswa Red		S19-3		Uniswa Red		S19-3	
Temperature	MAE	N-S	MAE	N-S	MAE	N-S	MAE	N-S
23°C	4.88	0.69	2.80	0.85	410.24	-0.22	471.60	-1.49
28°C	0.60	0.999	2.77	0.96	1091.98	-2.93	1567.43	-8.04
33°C	2.95	0.92	4.54	0.89	388.92	0.80	601.69	0.26

Table 3.8: The mean absolute error (MAE) and the Nash-Sutcliffe value (N-S) for the model's prediction of canopy biomass and leaf area for Uniswa Red and S19-3 when compared to the TCRU experimental data, as shown in Figures 3.24-3.29.

The simulation of canopy biomass gives a reasonable fit to the experimental data for all three temperatures, with the simulated biomass being consistently between the upper and lower bounds of the experimental data for 28°C and 33°C. It is slightly overestimated for 23°C in the early stages of the simulation window. The

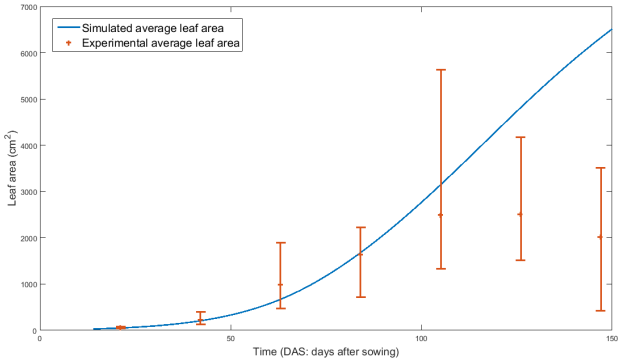

(a)

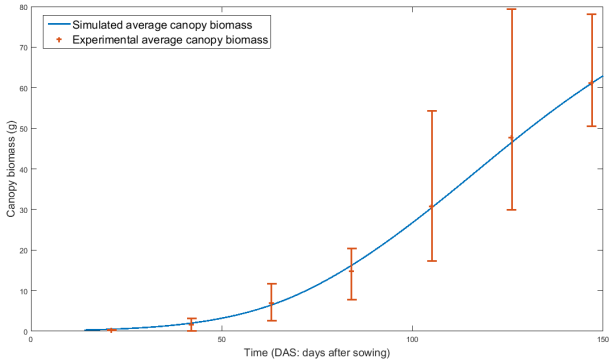

(b)

Figure 3.24: The simulated (a) leaf area and (b) canopy biomass compared with the experimental data for the species Uniswa Red, using the data-fitted case of a temperature of 28°C. The system is described by equations (3.82) to (3.83) and parameter values are given in Table 3.2. Each simulated plant is initiated at day 14, the estimated time of emergence and assumed to have a canopy comprising of one leaf at this point. The simulation data has been averaged over 15 plants grown in a three by five grid, with a distance between rows of 0.2m and a distance between columns of 0.35m (Figure 3.8). Red bars indicate the upper and lower bounds of the experimental data.

mean absolute error (MAE) and the Nash-Sutcliffe efficiency (NSE) value [48] for these simulations are given in Table 3.8. The NSE indicates how well a plot of the observed data versus simulated data fits the 1:1 line; where NSE $\in [-\infty, 1]$ [48]. A value of 1 would indicate a perfect model and a value equal to or less than 0 would indicate that the model is no better at predicting canopy biomass than taking the average of the observed data. By observing Table 3.8 we can see that our model does not simulate the lower temperature of 23° as well as the higher temperatures. Similarly the MAE is larger than that of 28°C and 33°C. The simulation for 28°C

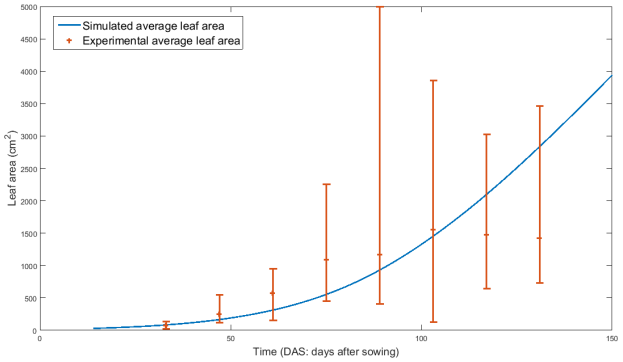

(a)

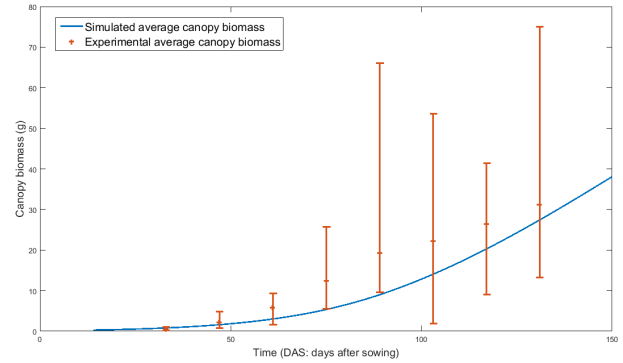

(b)

Figure 3.25: The simulated (a) leaf area and (b) canopy biomass compared with the experimental data for the species Uniswa Red, using the non data-fitted case of a temperature of 23°C. The system is described by equations (3.82) to (3.83) and parameter values are given in Table 3.2. Each simulated plant is initiated at day 14, the estimated time of emergence and assumed to have a canopy comprising of one leaf at this point. The simulation data has been averaged over 15 plants grown in a three by five grid, with a distance between rows of 0.2m and a distance between columns of 0.35m (Figure 3.8). Red bars indicate the upper and lower bounds of the experimental data.

is near perfect, however since this was the data used for the parametrisation this is not surprising.

The simulation of leaf area for Uniswa Red does not fully capture the behaviour of the experimental data. The leaf area is significantly overestimated in the later stages of the simulation window, particularly for 23°C and 28°C. This is corroborated by the particularly high MAE and very low NSE values found in Table 3.8.

Model simulations of the leaf area and canopy biomass for S19-3 compared to the experimental data can be found in Figures 3.27 to 3.29. Similar to Uniswa Red, the

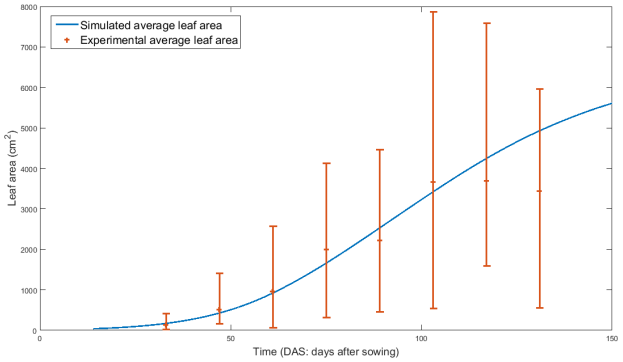

(a)

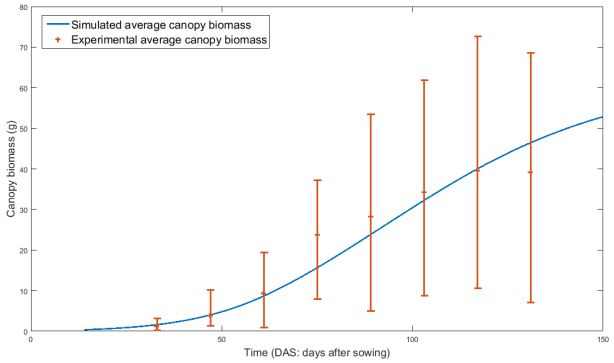

(b)

Figure 3.26: The simulated (a) leaf area and (b) canopy biomass compared with the experimental data for the species Uniswa Red, using the non data-fitted case of a temperature of 33°C. The system is described by equations (3.82) to (3.83) and parameter values are given in Table 3.2. Each simulated plant is initiated at day 14, the estimated time of emergence and assumed to have a canopy comprising of one leaf at this point. The simulation data has been averaged over 15 plants grown in a three by five grid, with a distance between rows of 0.2m and a distance between columns of 0.35m (Figure 3.8). Red bars indicate the upper and lower bounds of the experimental data.

simulation of canopy biomass gives a reasonable fit to the experimental data. The simulation data is within the lower and upper bounds of the experimental data for all three temperatures. The error values given in Table 3.8 show a similar pattern to Uniswa Red in that the NSE value is much closer to 1 for temperatures 28°C and 33°C. Here 23°C is much better simulated for S19-3 compared to Uniswa Red.

The simulation of leaf area for S19-3 does not reproduce the behaviour of the experimental data. As leaf area is calculated empirically as a function of canopy biomass we do not, at this stage, apply a data-fit to this variable. It is being

significantly overestimated at the later stages of the simulation window. This can also be seen in the MAE and NSE values, which are found in Table 3.8.

For both species and all temperature regimes, there is a greater difference in the simulated and experimental leaf area further along in time. This is because of the assumption that all of the canopy biomass is comprised of shoots, and leaves, when in reality the canopy biomass comprises of shoots, leaves, pods and roots. TCRU experimental data tell us that the roots contribute less than 5% to the total biomass, however the pods contribute as much as 60% in the later stages [32]. The current model lacks a means of partitioning out the canopy biomass to the leaves and the pods, therefore the model is overestimating leaf area and hence overestimating the amount of absorbed radiation. For both species, canopy biomass at 23°C is not being well accounted for by the model. This would also indicate that there is some problem with how temperature is being incorporated.

3.8 Chapter summary

The mathematical model developed in this chapter simulates the growth and development of a single plant. The plant architecture is assumed to take the form of a disc representing the layers of leaves on a single stem/trunk. The model is scaled up to the two-plant scale by considering competition between two plants in the form of spatial overlap between the two canopies. This allows competition to be calculated within the model thus avoiding the need to include an empirically calculated density parameter to reduce plant growth. These empirically found parameters are sometimes site specific and are not always transferable across planting sites. Thus by avoiding this we allow for a more robust model.

The two plant model described by equations (3.33) to (3.36) was solved analytically by finding the steady-state values and determining their stability. It was found that the model has one positive real steady-state that the system will tend towards.

The parameterisation of the model was then discussed where parameters have been found directly from literature, empirically from experimental data and using

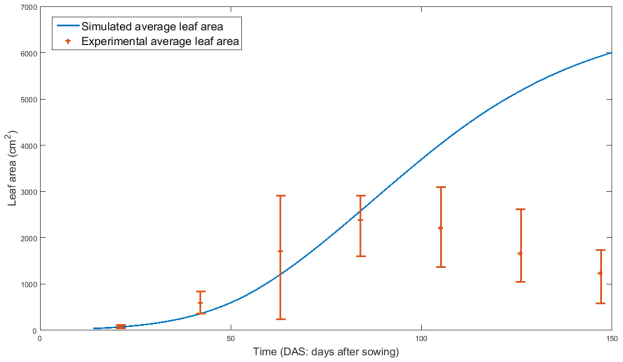

(a)

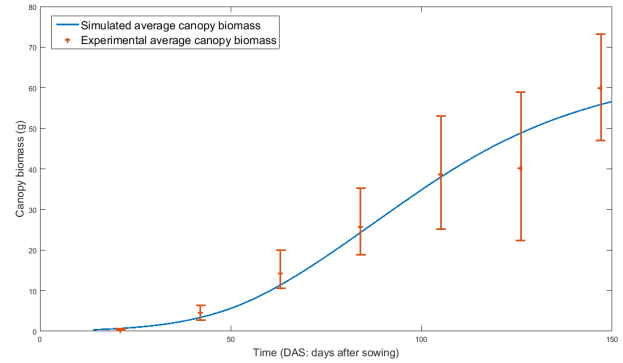

(b)

Figure 3.27: The simulated (a) leaf area and (b) canopy biomass compared with the experimental data for the species S19-3, using the data-fitted case of a temperature of 28°C. The system is described by equations (3.82) to (3.83) and parameter values are given in Table 3.2. Each simulated plant is initiated at day 14, the estimated time of emergence and assumed to have a canopy comprising of one leaf at this point. The simulation data has been averaged over 15 plants grown in a three by five grid, with a distance between rows of 0.2m and a distance between columns of 0.35m (Figure 3.8). Red bars indicate the upper and lower bounds of the experimental data.

data fitting techniques. The mathematical model for two plants was then solved numerically so that the behaviour over time could be observed. Following this, refinements were made to the model so that the simulations better represented the reality. We then scaled the two plant model up to the multi-plant model. This required an adaptation to the method of calculating spatial overlap. A sensitivity analysis applied to both the two-plant and multi-plant model demonstrated that the behaviour of the model was able to describe the plant behaviour qualitatively.

We were then able to replicate the conditions of the experiments for which we

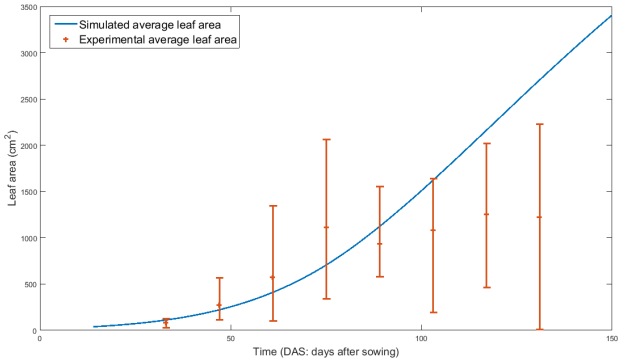

(a)

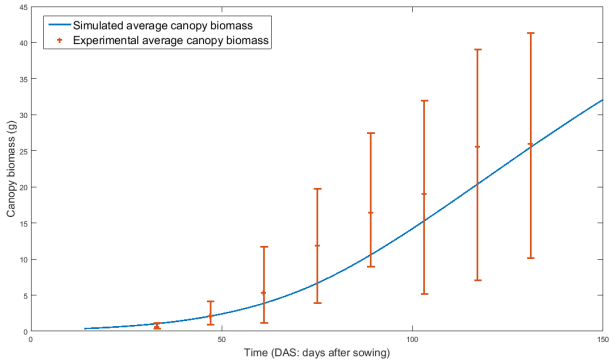

(b)

Figure 3.28: The simulated (a) leaf area and (b) canopy biomass compared with the experimental data for the species S19-3, using the non data-fitted case of a temperature of 23°C. The system is described by equations (3.82) to (3.83) and parameter values are given in Table 3.2. Each simulated plant is initiated at day 14, the estimated time of emergence and assumed to have a canopy comprising of one leaf at this point. The simulation data has been averaged over 15 plants grown in a three by five grid, with a distance between rows of 0.2m and a distance between columns of 0.35m (Figure 3.8). Red bars indicate the upper and lower bounds of the experimental data.

have data, using the mathematical model. This allowed for the simulations results to be compared to the experimental data.

It was found that the model described in this chapter simulates canopy biomass well, however the approximation of leaf area is significantly different to the experimental data. This would indicate that the relationship between leaf area and canopy biomass has not been correctly accounted for. Since ground cover is a function of leaf area, if leaf area is not correctly predicted then we can not trust our predictions of ground cover. The impact of neighbouring plants is incorporated as a function

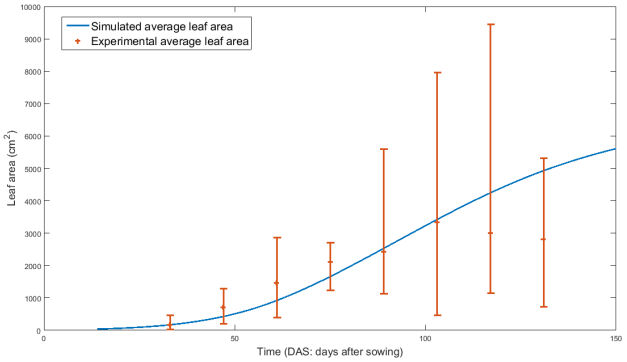

(a)

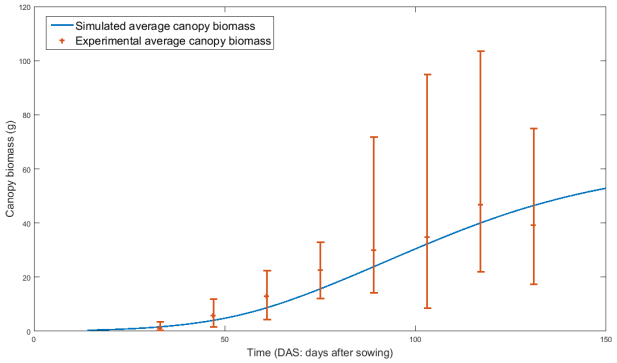

(b)

Figure 3.29: The simulated (a) leaf area and (b) canopy biomass compared with the experimental data for the species S19-3, using the non data-fitted case of a temperature of 33°C. The system is described by equations (3.82) to (3.83) and parameter values are given in Table 3.2. Each simulated plant is initiated at day 14, the estimated time of emergence and assumed to have a canopy comprising of one leaf at this point. The simulation data has been averaged over 15 plants grown in a three by five grid, with a distance between rows of 0.2m and a distance between columns of 0.35m (Figure 3.8). Red bars indicate the upper and lower bounds of the experimental data.

of ground cover and so miscalculating this value has serious knock on effects for simulating the competition between plants.

In addition, the relationship between plant growth and temperature is only loosely accounted for, and it is well known that temperature has a large impact on plant development.

In conclusion, the mathematical model discussed in the chapter provides a good first description of bambara groundnut, with canopy biomass being well described, however the model requires improvement if it is to be used for making recommenda-

tions. In the following chapter we consider model revisions to improve descriptions of the observed growth data for leaf area and thus the relationship between leaf area and canopy biomass.

Chapter 4

Incorporating leaf area

It was found in Chapter 3 that the relationship between leaf area and canopy biomass was not fully captured in the mathematical model since canopy biomass was well described but leaf area was not. We hypothesise that the cause of this was the absence of biomass partitioning to the various components, such as roots and pods. These constituents are often referred to as sinks in the literature. In order to remedy this issue, a non-linear ODE that describes leaf area over time will be formulated and tested in this chapter.

Temperature is a key factor in leaf development. In the previous chapter it was accounted for in the canopy biomass equation using a temperature stress parameter. It can be seen by observing Figures 3.25(a) and 3.28(a) and Table 3.8 that biomass was not well simulated for low temperatures. This would indicate that the effect of temperature on canopy biomass has not been fully accounted for in the model. With the addition of a new governing equation that describes leaf area, temperature will now be more firmly taken into account since the accumulation of leaves is primarily determined by temperature.

The revised mathematical model will be parametrised and tested using data from the literature and the experimental data provided by TCRU greenhouse experiments [32].

4.1 Revised mathematical model

To incorporate a new ODE into the system of equations we refer back to the individual plant model for simplicity. We later scale the model back up to the multi-plant level. In addition to introducing a new ODE, some other adaptations will be made. The similarities and differences between the single plant-scale described in Chapter 3 and the one introduced in this chapter are discussed here.

Our primary motivation in revising our model is that we wish to ensure that leaf area is being correctly accounted for. As ground cover is a function of leaf area, and inter-plant competition is a function of ground cover, if leaf area is not accurately described, neither is the affect competition has on canopy biomass.

Previously, $A(t)$ was calculated as a function of the canopy biomass, however in doing this we made the assumption that leaf area and canopy biomass were linearly related throughout the developmental process. By doing this we neglected to consider the other assimilates that comprise the plant canopy and the various factors that affect the biomass partitioning, e.g. temperature. Before we formulate a new ODE, we first consider the behaviour of leaf accumulation in a plant.

Bambara groundnut is what is known as an indeterminate crop [12] and so leaves are produced over the entire life span of the plant. This is in contrast to determinate plants, which may stop producing leaves when the plant shifts from one developmental stage to another. The leaf development of bambara groundnut is primarily dependent on temperature [38]. So to describe leaf growth, we introduce several temperature-related concepts.

We consider a critical temperature T_{crit} above which the plant will grow and below which it will not. The daily effective temperature $T_D(t)$ is then the average difference between the hourly and critical temperature over the day, subject to the hourly temperature being greater than the critical temperature and below a

maximum temperature T_{ceil}. We then have

$$T_D(t) = \frac{1}{24}\sum_{j=1}^{24}(T_j - T_{crit})$$

where T_j is the average hourly temperature, T_{crit} is the critical temperature required for growth, and j refers to the hour of the day.

Cumulative thermal time $T_C(t)$ is the daily effective temperature integrated over a given period of time so that

$$T_C(t) = \int_0^{\text{DAS}} T_D(t)dt,$$

where DAS are the number of days after sowing [32]. This concept is sometimes referred to as the thermal time or temperature sum. The cumulative thermal time can be thought of as the number of temperature units that are required for plant growth and is measured in units known as 'degree days', thus the daily effective temperature is measured in 'degree days per day'.

During the vegetative phase, the rate of leaf development for bambara groundnut differs over time for different temperatures, however when measured in degree days leaf production is constant for all temperatures [32]. When bambara groundnut passes from the vegetative to flowering and podding stages, leaf production continues but decreases significantly [42].

Data found in the literature indicate that leaf accumulation exhibits Gaussian-like behaviour in relation to cumulative thermal time [32], with a maximum growth rate $a_1(t)$, a time of peak growth $b_1(t)$, and a time window where significant leaf growth occurs, $c_1(t)$. Thus the leaf area growth rate can be described such that

$$\text{Leaf area growth} = L_A a_1(t) exp\left(-\left(\frac{T_C(t) - b_1(t)}{c_1(t)}\right)^2\right), \tag{4.1}$$

where L_A is the leaf area per leaf and $a_1(t)$, $b_1(t)$, and $c_1(t)$ are all species specific parameters [32]. Through preliminary data exploration, it was found that these

parameters best describe leaf development when allowed to depend on the daily effective temperature $T_D(t)$ so that $a_1 = aT_D(t)$, $b_1 = bT_D(t)$ and $c_1 = cT_D(t)$.

Once the plant shifts from the vegetative stage to the flowering and podding phases, the primary sink in energy is no longer leaf development and is instead pod development [42]. This is subject to various stresses put on the plant and it can be seen from the experimental data that one such stress is temperature. For high temperatures, pod growth is decreased but leaf mass continues to increase. What we see in the data is that even though the plant is producing pods, leaf production continues at a higher rate for higher temperatures than for lower temperatures. We apply this in the model by defining a temperature-dependent degradation rate that decreases for high temperatures causing more biomass to be partitioned to the leaves. By doing this, when temperature is high the plant is not diverting as much absorbed energy to podding but instead still partitioning energy to leaf maintenance. Therefore leaf degradation is described by

$$\text{Leaf area degradation} = d_l T_{sl}(T) A(t), \tag{4.2}$$

where

$$T_{sl}(T) = \frac{T_{opt} - T_{crit}}{T(t) - T_{crit}}. \tag{4.3}$$

Thus if the temperature is below the optimum value, leaf area degradation is increased, but decreased for high temperatures. The further temperature moves away from the optimum, the more $T_{sl}(T)$ shifts away from 1.This temperature stress is an adaptation of that found in the work of Karunaratne [32].

Thus leaf area per plant, $A(t)$, over time can be given by

$$\frac{dA(t)}{dt} = L_A a_1(t) exp\left(-\left(\frac{T_C(t) - b_1(t)}{c_1(t)}\right)^2\right) - d_l T_{sl}(T) A(t), \tag{4.4}$$

where T_{sl} is given by equation (4.3) and the initial condition for leaf area is given by

$$A(0) = L_A.$$

Now that $A(t)$ has been formulated we turn our attention to $c(t)$. As before, the growth rate of $c(t)$ is dependent on leaf area index $\gamma(t)$ and ground cover $G(t)$, which in turn are dependent on the leaf area $A(t)$.

Leaf area is no longer a function of canopy biomass and so to find $\gamma(t)$ and $G(t)$ we must substitute the solution of equation (4.4) into equations (3.6) and (3.7), respectively. This allows ground cover to be described as a function of leaf area such that

$$G(t) = G^{(1-B)}(0)A^B(t), \tag{4.5}$$

and leaf area index γ to be described by

$$\gamma(t) = \frac{A(t)}{G^{(1-B)}(0)A^B(t)}. \tag{4.6}$$

Since the initial condition for the ground cover is the area of one fully emerged leaf, the ground cover can be written as

$$G(0) = L_A. \tag{4.7}$$

Then equation (4.6) can then be rewritten so that

$$\gamma(t) = L_A^{(B-1)}A^{(1-B)}(t). \tag{4.8}$$

As canopy biomass growth is dependent upon leaf area and ground cover, which is in turn dependent on leaf area, the effect temperature has on biomass growth is now included within these variables. Thus temperature stress no longer needs to be absorbed into R as shown in equation (3.83), and we instead use the original formula for R given in equation (3.5). It was found during a preliminary investigation that the impact that temperature has on canopy biomass via the leaf area is not strong enough and therefore we impose a temperature stress to the decay rate of canopy biomass. We assume that the further temperature is from the optimum the larger

the decay rate is. Therefore canopy biomass decay rate T_{sc} is described by

$$T_{sc}(t) = \begin{cases} 1 + \omega \left| 1 - \frac{T(t) - T_{crit}}{T_{opt} - T_{crit}} \right|, & \text{if} \quad T_{crit} < T < T_{ceil}, \\ 0 & \text{otherwise.} \end{cases} \tag{4.9}$$

where ω is a species dependent parameter that defines how fast temperature stress deviates from one as temperature moves away from the optimum.

Finally, the way in which plant height is calculated has not changed and is as described by the single plant equation (3.37). Using the substitutions given in equations (4.7) and (4.8), the dimensional mathematical model for an individual plant can be summarised as

$$h(t) = \frac{h_0(\alpha_h - d_h)exp((\alpha_h - d_h)t)}{\alpha_h - d_h - \alpha_h k_h h_0 + \alpha_h k_h exp((\alpha_h - d_h)t)h_0}, \tag{4.10}$$

and

$$\frac{dT_C(t)}{dt} = T_D(t), \tag{4.11}$$

$$\frac{dA(t)}{dt} = L_A a T_D(t) exp\left(- \left(\frac{T_C(t) - bT_D(t)}{cT_D(t)} \right)^2 \right) - d_l T_{sl}(T) A(t), \tag{4.12}$$

$$\frac{dc(t)}{dt} = R_0 c_k L_A^{(1-B)} A^B(t) \left(1 - exp\left(-\kappa L_A^{(B-1)} A^{(1-B)}(t) \right) \right) \left(1 - \frac{c(t)}{k_c} \right) - T_{sc}(T) d_c c(t). \tag{4.13}$$

where

$$T_D(t) = \frac{1}{24} \sum_{j=1}^{24} (T_j - T_{crit})$$

and initial conditions are

$$T_C(0) = \int_0^{14} T_D(t) dt, \quad A(0) = L_A, \quad c(0) = \frac{L_A}{\phi}$$

which are the corresponding values of one fully emerged leaf.

4.1.1 Multi-plant model

In this section we discuss the scaling up of the single plant model, introduced in the previous section, to the many plant (crop) scale. An analysis of the governing equations is conducted and the parametrisation of the model is discussed. Model simulations are then compared to experimental data.

As in Section 3.7 we consider plants arranged in a uniform grid array with distance D_r between plants in rows and a distance D_c between plants in columns. Plants are labelled from 1 to N using a subscript i. Now that we resume the investigation of the multi-plant scale we reintroduce competition into the model equations. As before, competition imposed upon each plant is simulated using the proportion of canopy that is shadowed by neighbouring plants and is approximated using the method described in Section 3.7.1. The affect competition has on the canopy biomass of individual plants is incorporated as in Section 3.7, so that the growth rate and carrying capacity of $c(t)$ is reduced by interactions with taller neighbouring plants. We now also apply the effect of competition to the growth rate of leaf area.

For notational simplicity, we will assume that temperature is constant against time. We do this as the experimental data we are using to parameterise and validate the mathematical model are greenhouse data. As such, the temperature of the experiments is constant against time. Thus, the parameters, a_1, b_1, c_1, d_{sl}, d_{sc} and T_D are now all constant. The governing equations that describe the growth of N plants is then given by

$$\begin{aligned}
\frac{dT_{Ci}(t)}{dt} &= T_{Di}, && (4.14)\\
\frac{dA_i(t)}{dt} &= L_A a_1 \left(1 - O_i(h_1, h_2, ...h_N, t)\right) exp\left(-\left(\frac{T_{Ci}(t) - b_1}{c_1}\right)^2\right) \\
&\quad -d_l T_{sl} A_i(t), && (4.15)\\
\frac{dc_i(t)}{dt} &= R_0 c_k L_A^{(1-B)} A_i^B(t) \left(1 - O_i(h_1, h_2, ...h_N, t)\right) \times \\
&\quad \left(1 - exp\left(-\kappa L_A^{(B-1)} A_i^{(1-B)}(t)\right)\right)\left(1 - \frac{c_i(t)}{k_{ci}(O,t)}\right) \\
&\quad -T_{sc} d_c c_i(t), && (4.16)
\end{aligned}$$

where

$$T_{Di} = T - T_{crit}$$

and height is described by

$$h_i(t) = \frac{h_0(\alpha_h - d_h)exp((\alpha_h - d_h)t)}{\alpha_h - d_h - \alpha_h k_{hi} h_0 + \alpha_h k_{hi} exp((\alpha_h - d_h)t)h_0}. \tag{4.17}$$

The initial conditions of the systems are

$$T_{Ci}(0) = T_{C0}, \qquad A_i(0) = L_A, \qquad c_i(0) = c_0,$$

where T_{C0}, L_A and c_0 are the thermal time, leaf area and canopy biomass at the point of emergence. From equation (4.15) we can see that the leaf area does not depend on canopy biomass, but does depend on the ground cover of each neighbouring plant. The overlap O_i of plant i depends on the height and ground cover of itself and of nearby plants and so equation (4.15) is dependent on plant height given by equation (4.17).

4.1.2 Non-dimensionalisation

We non-dimensionalise equations (4.14) to (4.16) according to

$$T_{Di}(t) = T_{Di0}\hat{T}_{Di}(\tau), \qquad T_{Ci}(t) = \frac{T_{Di0}}{\alpha_h}\hat{T}_{Ci}(\tau), \qquad c_i(t) = c_{i0}\hat{c}_i(\tau),$$

$$A_i(t) = L_A\hat{A}_i(\tau) \qquad \text{and} \qquad t = \frac{\tau}{\alpha_h}$$

where a hat signifies the associated non-dimensional physical variable and τ denotes non-dimensional time. We choose to re-scale $T_{Ci}(t)$ with respect to initial thermal time which is $T_{Di}(0)$, $A_i(t)$ with respect to the initial leaf area, and $c_i(t)$ with respect to the initial mass of the canopy. This is done for each plant separately. Time is rescaled with respect to α_h, the height growth rate. This is assuming that α_h does not vary between plants in the simulations that follow. When this is not the case we non-dimensionalise all equations with respect to α_h of Plant 1, i.e. α_{h1}. Although

not included here, height is rescaled with respect to the height of one fully emerged leaf as in Section 3.3.1. These rescalings lead to

$$\frac{d\hat{T}_{Ci}(\tau)}{d\tau} = \hat{T}_{Di}(t), \tag{4.18}$$

$$\frac{d\hat{A}_i(\tau)}{d\tau} = \bar{\alpha}_L \left(1 - O_i(\hat{h}_1, \hat{h}_2, ...\hat{h}_N, \tau)\right) exp\left(-\left(\frac{\hat{T}_{Ci}(\tau) - \bar{b}}{\bar{c}}\right)^2\right) - \bar{d}_L \hat{A}_i(\tau), \tag{4.19}$$

$$\frac{d\hat{c}_i(\tau)}{d\tau} = \bar{\alpha}_c \hat{A}_i^B(\tau) \left(1 - exp(-\kappa \hat{A}_i^{1-B}(\tau))\right) \left(1 - O_i(\hat{h}_1, \hat{h}_2, ...\hat{h}_N, \tau)\right) \times \left(1 - \bar{K}_{ci}(O_i, \tau)\hat{c}_i(\tau)\right) - \bar{d}_c \hat{c}_i(\tau), \tag{4.20}$$

$$\hat{h}_i(\tau) = \frac{h_0(1 - d_h)exp((1 - d_h)\tau)}{1 - d_h - k_{hi}h_0 + k_{hi}exp((1 - d_h)\tau)h_0}, \tag{4.21}$$

where

$$\bar{K}_h = \frac{h_0}{k_h}, \qquad \bar{d}_h = \frac{d_h}{\alpha_h}, \quad \bar{\alpha}_L = \frac{aT_{Di}}{\alpha_h}, \qquad \bar{\alpha}_c = \frac{R_0 c_k L_A}{c_0 \alpha_h},$$

$$\bar{b} = \alpha_h b, \quad \bar{c} = \alpha_h c, \qquad \bar{d}_L = \frac{d_l T_{sl}}{\alpha_h} \qquad \text{and} \qquad \bar{d}_c = \frac{d_c T_{sc}}{\alpha_h}$$

The initial conditions are

$$\hat{T}_{Ci}(0) = \frac{T_{Ci0}\alpha_h}{T_{Di0}}, \qquad \hat{A}_i(0) = 1, \qquad \hat{G}_i(0) = 1, \qquad \hat{c}_i(0) = 1 \qquad \text{and} \qquad \hat{h}_i(0) = 1.$$

For convenience, hereafter the hats and bars will be dropped.

4.1.3 Mathematical analysis

The system of equations (4.18) to (4.20) are analysed for the general case of N plants. In the case of equations (4.18) to (4.20) we first observe that the newly introduced equation (4.19) is non-autonomous. As such, a steady-state for leaf area would not exist as any solution to $\frac{dA_i(\tau)}{d\tau} = 0$ would depend on τ. Since canopy biomass depends on leaf area, it is now also non-autonomous. Therefore, in order to find a steady-state value we need to examine the behaviour of $\frac{dA_i(\tau)}{d\tau}$ as $\tau \to \infty$. Doing so leads to

$$\lim_{\tau \to \infty} \frac{dA_i(\tau)}{d\tau} = \lim_{\tau \to \infty} (-d_L A_i(\tau)),$$

and thus

$$\lim_{\tau\to\infty} A_i(\tau) = \lim_{\tau\to\infty} e^{-d_L\tau} = 0,$$

providing $d_L > 0$, which it is by definition. From equation (4.20) it can be seen that if $d_c > 0$ then $c_i \to 0$ as $\tau \to \infty$ also, since the growth rate of $c_i(\tau)$ depends on $A_i(\tau)$. Thus our asymptotic system of equations for N plants goes to

$$\lim_{\tau\to\infty} h(\tau) = \frac{(\alpha_h - d_h)}{\alpha_h K_{hi}} \tag{4.22}$$

$$\lim_{\tau\to\infty} A(\tau) = 0 \tag{4.23}$$

$$\lim_{\tau\to\infty} c(\tau) = 0. \tag{4.24}$$

Clearly this is non-physical since it is impossible for a plant without any biomass to have an associated height. However, as the height is only of interest when comparing the heights of neighbouring plants, we are able to satisfy ourselves with the result. As an annual crop, bambara groundnut completes its life cycle within one year and then dies. Thus, by tending to zero exponentially, the long term growth behaviour of leaf area and canopy biomass is being correctly captured by the model equations.

4.1.4 Model summary

This section will give a description of the revised mathematical model devised to simulate canopy biomass. The model is described by a system of 3 non-linear ODEs per plant given by equations (4.18)-(4.20) and also (4.21), which describes plant height. This gives a total of $3 \times N$ ODEs where N is the number of plants in the simulation and an additional N equations that describe the plant height for each of the N plants. The model algorithm is similar to that described in Section 3.7, however leaf area is no longer calculated as a function of canopy biomass and is calculated using equation (4.19).

As before, the competition between neighbouring plants is assumed to be in the form of canopy-canopy shadowing and is quantified by the proportion of canopy that is shadowed by neighbouring plant canopies. The respective plant heights determine

which plants experience competition. Competition affects the leaf area growth rate, canopy biomass growth rate and canopy biomass carrying capacity.

The steps of this model can be summarised as:

1. input landrace and weather parameters;
2. input initial conditions for height, thermal time, leaf area and canopy biomass;
3. calculate ground cover from leaf area;
4. calculate LAI from leaf area and ground cover;
5. calculate plant height using equation (3.82);
6. calculate the inter-plant competition experienced by each plant using the ground cover of each plant, their respective plant heights and positions as detailed in Section 3.7.1;
7. calculate the change in cumulative thermal time, leaf area and canopy biomass using equations (4.18) to (4.20);
8. set $t = t + \delta t$ where δt is a time step chosen by the inbuilt MATLAB ODE solving algorithm ODE15s so that the absolute and relative error tolerances are met; and
9. repeat steps 3-8 until the plant reaches maturity at $t = T_{end}$.

The steps of the algorithm are illustrated in Figure 4.1.

4.2 Numerical simulations

We now investigate the numerical simulation of the system of equations given in equations (4.18) and (4.20). The model equations will relate to N plants that are arranged in a uniform grid like array with a distance between plants in a row of D_r and a distance between plants in a column of D_c. The system is solved numerically as in Chapter 3 using the inbuilt MATLAB programme ode15s, which is an ODE

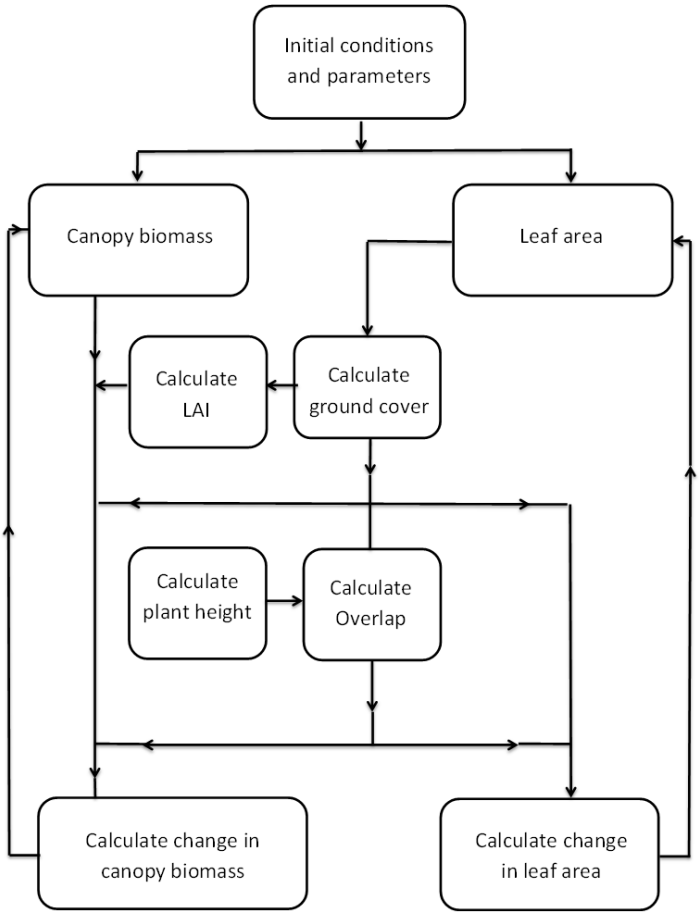

Figure 4.1: Diagram of the multi-plant algorithm for each plant in the population as described by equations (4.18) to (4.20).

solver made suitable for stiff systems. The relative and absolute tolerance have been set to 1×10^{-6} and time steps are determined by the solver to meet these tolerances.

4.2.1 Model parameterisation

The revised mathematical model has now been formulated and new parameters have been introduced. Many of the parameters defined in the previous chapter are relevant here, however the parameter values that were found using the least-squared parameter approximation approach are now redundant and need to be recalculated. The parameterisation of parameters that are newly introduced and those that have changed values are discussed here. A summary of all parameters used in this model for the species' Uniswa Red and S19-3 can be found in Table 4.1.

Parameter	Value	Description	Source
PAR	0.5	Fraction of light that is photosynthetically active	Cornelissen [20]
k_i	16	Total incoming radiation ($MJm^{-2}day^{-1}$)	[41]
α_h	0.75	Height growth rate (day^{-1})	This study
k_h	30*, 25†	Plant height carrying capacity (m)	This study
d_h	0.02	Plant height decay rate (day^{-1})	This study
B	0.74*, 0.84†	Spreading coefficient of the ground cover	Data fitted
T_{opt}	30*, 28†	Optimum temperature (°)C	Karunaratne [32]
T_{crit}	12*, 8.5†	Critical temperature for growth (°)C	Karunaratne [32]
a	0.15*, 0.14†	Maximum growth rate for leaf area $degreedays^{-1}$	Data fitted
b	68.88*, 87.66†	Cumulative thermal time for which maximum growth occurs $degreedays$	Data fitted
c	29.55*, 34.81†	Variance in cumulative thermal time for which leaf growth occurs $degreedays$	Data fitted
d_l	$1.5\times10^{-2*}$, $1.03\times10^{-2\dagger}$	Decay rate for plant leaf area day^{-1}	Data fitted
L_A	$3.9\times10^{-3*}$, $3.0\times10^{-3\dagger}$	Leaf area per leaf (m^2)	TCRU experimental data [32]
c_k	1.97*, 2.15†	Radiation use efficiency gMj^{-1}	Data fitted
e	0.6	Light extinction coefficient	Cornelissen [20], Karunaratne [32]
k_{max}	130.47*, 136.20†	Maximum canopy biomass carrying capacity (g)	TCRU experimental data [32]
d_c	$4.93\times10^{-4*}$, $1\times10^{-2\dagger}$	Canopy biomass decay rate (day^{-1})	Data fitted
h_0	0.05	The initial conditions for plant height (m)	This study
L_0	1	The initial conditions for plant number	This study
c_0	0.24*, 0.19†	The initial conditions for plant canopy (g)	This study

Table 4.1: Table of parameter values and descriptions. For parameters that are species specific, * denotes the species S19-3 and † denotes Uniswa Red.

The parameters α_h, k_h, d_h, T_{opt}, T_{crit}, k_{max}, ϕ, ψ, PAR, e and k_i are all calculated as described in Section 3.4.1.

The leaf area per leaf L_A is a new parameter introduced in this chapter and is found using the experimental data, such that

$$L_{Ai} = \frac{A_i}{L_i},$$

where A_i and L_i are a plants leaf area and leaf number respectively. The Tropical Crops Research Unit (TCRU) provided leaf number data for 28°C [32], which are the same data we used to parameterise the previous model. The data consist of both A_i and L_i for each plant for 28°C for species S19-3 and Uniswa Red over 8 time points. The relationship between leaf number and leaf area for Uniswa Red and S19-3 at all time points can be found in Figure 4.2. There is a clear linear relationship between A_i and L_i and so L_A has been found by averaging the ratio between A_i and L_i for all plants at each time point for which we have data for.

Where parameters could not be found from the literature or empirically from the data, we performed a least squares fit between the relevant TCRU data and the numerical solutions for equations (4.18) to (4.20). This has been done to find the new parameters a, b, c, and d_l and also to find new values for c_k, B and d_c. Plants are arranged in the same way as described in Section 3.4.1. The inbuilt MATLAB function lsqcurvefit is used, which is a nonlinear least-squared solver, that fits the simulation to the experimental data. The fit has been applied to the data set for a temperature of 28°C only, as this is the closest to the optimum temperature for both species Uniswa Red and S19-3.

The parameters are found using the relationships described in Section 4.1.2 and can be found in Table 4.2.

4.2.2 Sensitivity analysis

We now wish to determine how sensitive the model is to variations in specific parameter values. In this section we discusses the results of a local sensitivity analysis

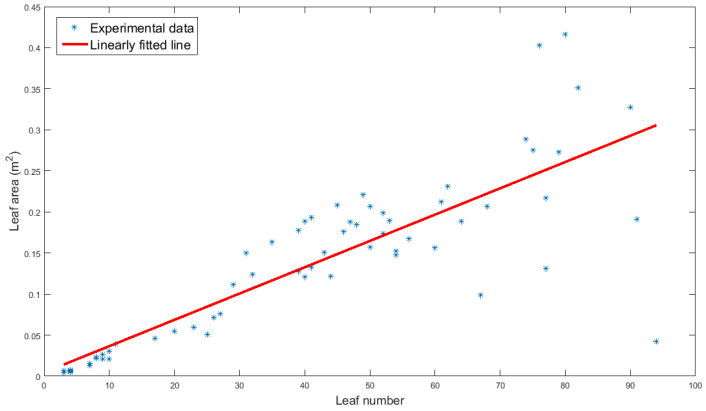

(a) Uniswa Red

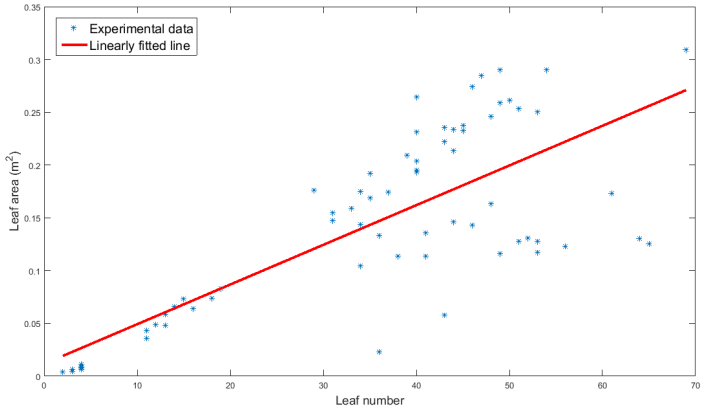

(b) S19-3

Figure 4.2: The relationship between plant leaf number and leaf area in the TCRU experimental data for Uniswa Red in 4.2(a) and S19-3 in 4.2(b).

applied to the model described by the system of equations (4.18) to (4.20). The sensitivity analysis is applied to sixteen plants arranged in a 4×4 grid with a distance of 0.3m between them, the temperature used for the simulation is $28°C$. Simulations begin at fourteen days, the predicted time of emergence, and are run to one hundred and fifty days, the estimated time of maturity. All eight of the non-dimensional parameters are investigated, the original value of each non-dimensional parameter (denoted by x) is both increased and decreased by an order of magnitude of ten. This is done to one parameter at a time for all plants at once. The canopy biomass and leaf area at 150 days (the time of harvest) is averaged over all sixteen plants and found to be 54.96g and 2243.63m^2, respectively. The variations in leaf area and

Non-dimensional parameters	Value
K_h	0.25^*, $0.2^\dagger$
d_h	1.3×10^{-2}
α_L	3.2^*, $3.64^\dagger$
b	51.66^*, $65.745^\dagger$
c	22.1625^*, $26.1075^\dagger$
d_L	0.0225^*, $0.0137^\dagger$
α_c	0.3465^*, $0.3715^\dagger$
κ	0.6
K_c	0.2365^*, $0.1852^\dagger$
d_c	$1.3 \times 10^{-3*}$, $1.3 \times 10^{-3\dagger}$

Table 4.2: Table of non-dimensional parameter values for the leaf area mathematical model. For parameters that are species specific, * denotes the species S19-3 and † denotes Uniswa Red. species specific values are written in the order S19-3, Uniswa Red.

canopy biomass are measured as a percentage difference of the original value and given in Table 4.3.

From Table 4.3 we find that the new system of equations is still very sensitive to changes in parameters. We find that leaf area is not sensitive to the parameters of the canopy biomass equation, but is very sensitive to parameters describing leaf area. In particular we find that leaf area is sensitive to increases in α_L, b, c and d_L.

The value of α_L relates to the maximum growth rate of leaf area, as it increases final leaf area increases. Conversely, as it decreases so too does final leaf area. The relative change to final leaf area is far less than the change undertaken by α_L; this is because of the effect competition has on the model. If competition was removed from the model, we find that a tenfold change to α_L results in a tenfold change to leaf area.

Both an increase and decrease in b causes a decrease in leaf area. Qualitatively, this makes sense as b determines when the window of peak leaf growth occurs. A tenfold increase, causes peak growth to occur close to the time of harvest, which does not give plants time to accrue leaf area. Similarly, a tenfold decrease causes the plant to germinate during peak growth. What this means mathematically is that the entire left side of the Gaussian curve is now excluded, thus discounting a

Parameter	Parameter Original Value	Relative change in			
		Leaf Area (%)		Canopy Biomass (%)	
	x	$0.1x$	$10x$	$0.1x$	$10x$
α_L	3.64	-87.95	543.95	-75.09	4.66
b	65.75	-77.73	-99.67	-22.20	-97.32
c	26.11	-88.23	100.91	-74.60	19.71
d_L	0.01	76.8	-96.73	5.15	-59.05
α_c	0.38	0	0	-85.07	68.92
κ	0.6	0	0	-76.81	22.19
K_c	0.18	0	0	47.28	-83.11
d_c	1.3×10^{-3}	0	0	3.44	-26.49

Table 4.3: Sensitivity analysis of the non-dimensional system given by equations (4.18) and (4.20). The percentage change in leaf area and canopy at 150 days has been recorded for a tenfold increase and decrease to each of the non-dimensional parameters (denoted here by x) in turn. The temperature of the simulations is set to $28°C$, the species is Uniswa Red and the planting distance is 30cm between plants, which are arranged in a 4×4 Uniform Grid.

considerable amount of leaf growth.

The length of time that peak growth occurs is determined by c. As expected, an increase in c would mean that there is a wider time window for peak growth and so leaf area at harvest would be larger. Conversely, a decrease in c means there is less time for the plant to accrue leaves.

Increases to the decay rate d_L means leaves senesce at a faster rate causing the leaf area at harvest to decrease. Conversely, decreases to d_L allows leaf area to increase at harvest.

The impact all four of these parameters have on canopy biomass is more complicated. Up to a point, increases in leaf area causes canopy biomass to have more leaves to absorb sunlight. Subsequently, this causes canopy biomass to reach a larger mass at harvest. The ground cover is also determined by the leaf area; after a certain point ground cover becomes so large that competition within plants, caused by the large ground cover, counteracts the positive effect of increased leaf area.

The parameters α_c, κ, K_c, and d_c have no impact on leaf area but do alter canopy biomass in the same way as described in Section 3.6.

4.2.3 Comparing the model to experimental data

We want to compare the revised mathematical model described by equations (4.18)-(4.20) to the TCRU greenhouse data. In order to replicate the conditions of the greenhouse a simulation of fifteen plants is conducted where plants are arranged in three rows of five with a distance between rows of 35cm and a distance between plants in a row of 20cm. A birds-eye view of the plant layout can be found in Figure 3.8.

As mentioned in Section 3.7.5, plant heights in the experiments are unknown. Previously we assumed that heights were identical for all plants however to test this assumption we now run the simulations twice. Once with plant heights assumed to be equal as in Section 3.7.5, this means that instead of one plant definitively overlapping the other plant canopies intermingle and all plants experience competition. The simulation is then repeated with random variation applied to plant heights. Since plant heights are not equal in this case, some plants experience competition and some do not.

Before we compare the simulations to experimental data we examine the long term behaviour and compare it to the model analysis of Section 4.1.3. Simulations of Uniswa Red and S19-3 for a temperature of 28°C for 3000 days are shown in Figure 4.3 for Uniswa Red. Clearly leaf area and canopy biomass tend to zero as time tends to infinity, thus confirming the analysis of the governing equations conducted in Section 4.1.3. The difference in behaviour over time for the two species is largely caused by the difference in parameters b, c and K_c. Before we compare the simulations to experimental data we examine the long term behaviour and compare it to the model analysis of Section 4.1.3. Simulations of Uniswa Red and S19-3 for a temperature of 28°C for 3000 days are shown in Figure 4.3 for Uniswa Red. Clearly leaf area and canopy biomass tend to zero as time tends to infinity, thus confirming the analysis of the governing equations conducted in Section 4.1.3. The difference in behaviour over time for the two species is largely caused by the difference in parameters b, c and K_c.

We now compare the model to the experimental data. The same TCRU data

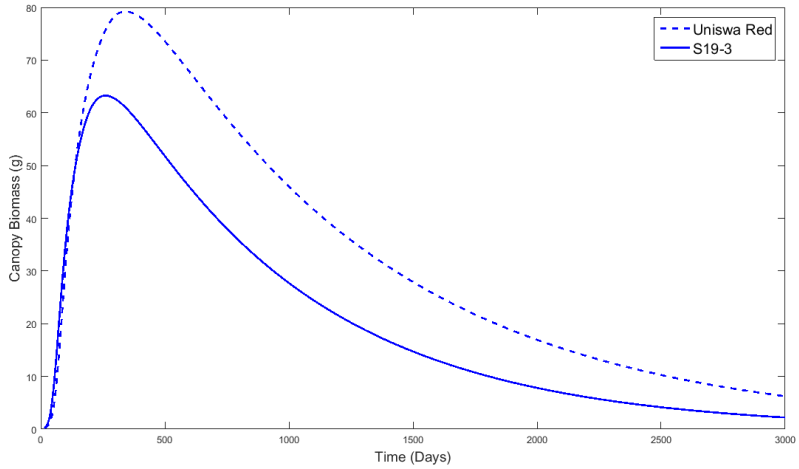

(a) Canopy biomass

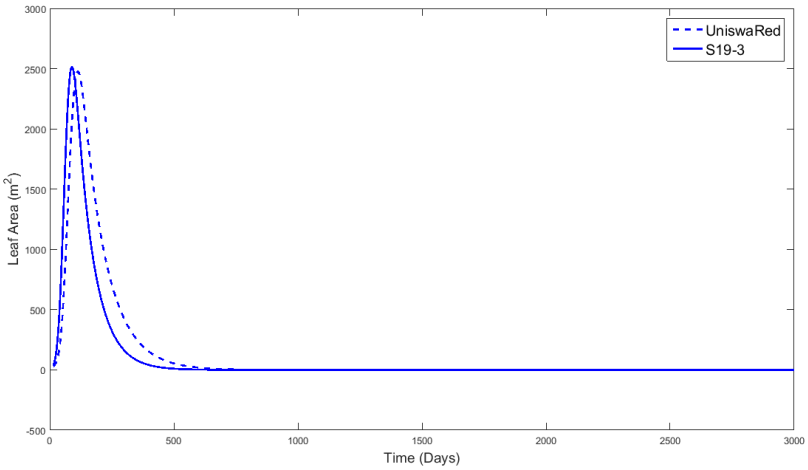

(b) Leaf area

Figure 4.3: The simulated average canopy biomass (a) and leaf area (b) for fifteen plants over 3000 days, of the species Uniswa Red and S19-3 at 28°C. Plants are arranged as in Figure 3.8 with planting distance between rows and columns of 0.35m and 0.2m respectively. All plants are the same height.

set used in Section 3.7.5 is used to validate the model here. The simulation of canopy biomass and leaf area for Uniswa Red is compared to the experimental data in Figures 4.4 to 4.6 respectively. In this case plants have the same height.

It can be seen in Figures 4.4(b), 4.5(b) and 4.6(b) that the simulation data of canopy biomass is within the upper and lower bounds of the experimental data for all time points except one. The mean absolute error and the Nash-Sutcliffe values are given in Table 4.4. Comparing to the error values of the model described in

Table 3.8 in the previous chapter there is some improvement to the simulation of canopy biomass for 23°C and 33°C however canopy biomass for 28°C is slightly impaired. Despite this, all model simulation values lie within an acceptable range of the experimental data.

The leaf area in Figures 4.4(a), 4.5(a) and 4.6(a) is similarly within the upper and lower bounds of the experimental data for all time points except one. There is a clear improvement to simulating leaf area when comparing to Figures 3.24(a), 3.25(a) and 3.26(a), which can also be seen by comparing Tables 3.8 and 4.4.

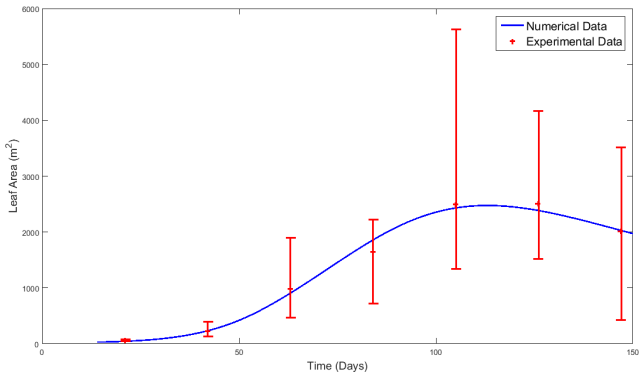

(a)

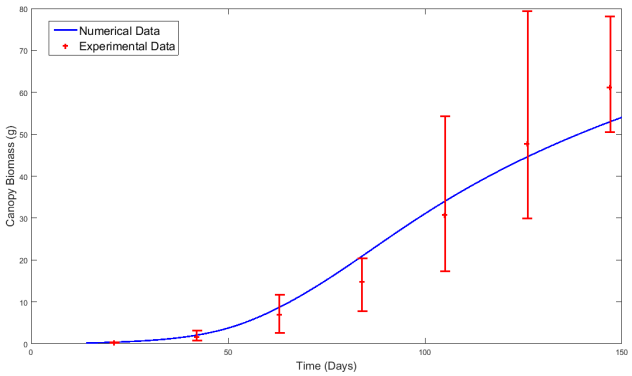

(b)

Figure 4.4: The simulated (a) leaf area and (b) canopy biomass compared with the experimental data for the species Uniswa Red, using the data-fitted case of a temperature of 28°C. The system is described by equations (4.18)- (4.20), where all plant heights are equal and parameters are given in Table 4.1. Each simulated plant is initiated at day 14, the estimated time of emergence and assumed to have a canopy comprising of one leaf at this point. The simulation data have been averaged over 15 plants grown in a five by three grid, the distance between plants in a row is 0.2m and the distance between rows is 0.35m. Red bars indicate the upper and lower bounds of the experimental data.

	Canopy biomass (g)				Leaf Area (m^2)			
	Uniswa Red		S19-3		Uniswa Red		S19-3	
Temperature	MAE	N-S	MAE	N-S	MAE	N-S	MAE	N-S
23°C	2.48	0.87	5.30	0.58	131.48	0.88	331.21	0.26
28°C	3.26	0.96	2.41	0.96	74.85	0.99	63.16	0.99
33°C	2.08	0.95	3.79	0.87	300.43	0.92	509.93	0.72

Table 4.4: The mean absolute error and the Nash-Sutcliffe value for the leaf accumulation model's prediction of canopy biomass and leaf area for Uniswa Red and S19-3 when compared to the TCRU experimental data.

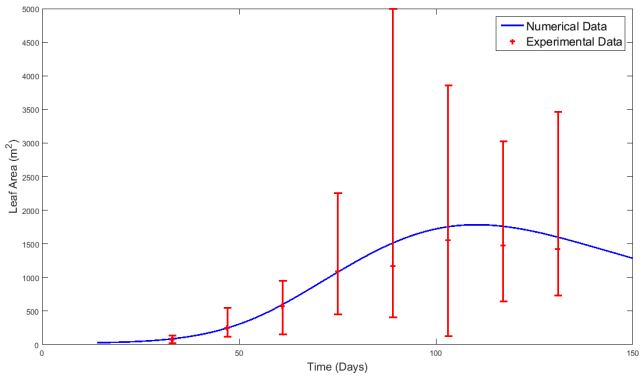

(a)

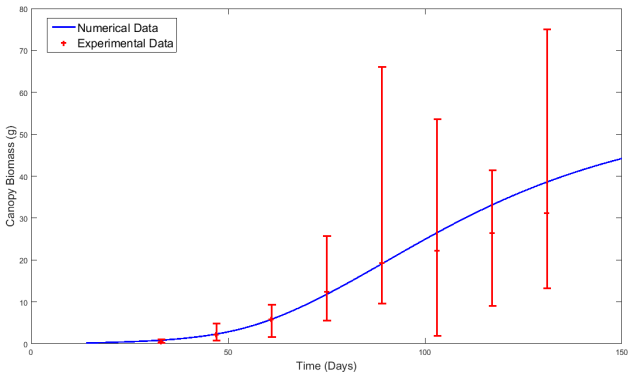

(b)

Figure 4.5: The simulated (a) leaf area and (b) canopy biomass compared with the experimental data for the species Uniswa Red, using the non data-fitted case of a temperature of 23°C. The system is described by equations (4.18)- (4.20), where all plant heights are equal and parameters are given in Table 4.1. Each simulated plant is initiated at day 14, the estimated time of emergence and assumed to have a canopy comprising of one leaf at this point. The simulation data have been averaged over 15 plants grown in a five by three grid, the distance between plants in a row is 0.2m and the distance between rows is 0.35m. Red bars indicate the upper and lower bounds of the experimental data.

We now compare the simulation of canopy biomass and leaf area for S19-3 to

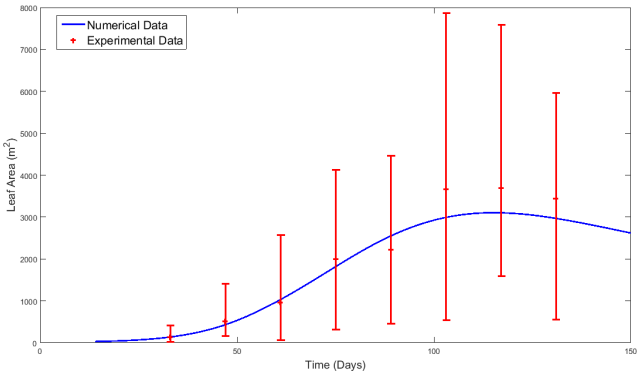

(a)

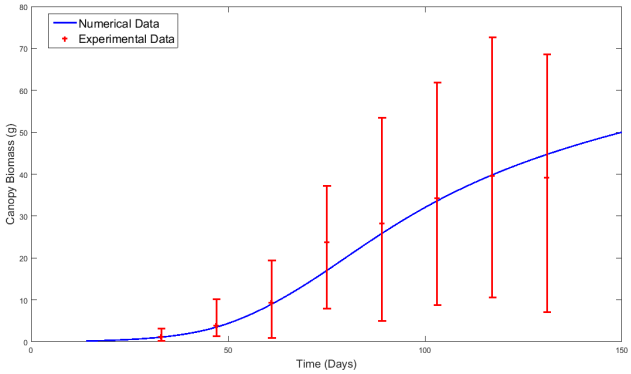

(b)

Figure 4.6: The simulated (a) leaf area and (b) canopy biomass compared with the experimental data for the species Uniswa Red, using the non data-fitted case of a temperature of 33°C. The system is described by equations (4.18)- (4.20), where all plant heights are equal and parameters are given in Table 4.1. Each simulated plant is initiated at day 14, the estimated time of emergence and assumed to have a canopy comprising of one leaf at this point. The simulation data have been averaged over 15 plants grown in a five by three grid, the distance between plants in a row is 0.2m and the distance between rows is 0.35m. Red bars indicate the upper and lower bounds of the experimental data.

the experimental data in Figures 4.7 to 4.9. In this case, canopy biomass of S19-3 is within the upper and lower bounds of the experimental data for all time points in Figures 4.7(b), 4.8(b) and 4.9(b). By comparing the results of this model to those of Figures 3.27(b), 3.27(b) and 3.29(b) we can see little discernible improvement in the predictions for all three temperatures. We can see that canopy biomass for 23°C is now being overestimated instead of underestimated. By observing Table 4.4 we can see that the revised model does not change the predictive power of simulating canopy biomass for temperatures of 28°C and 33°C, however the revised model does

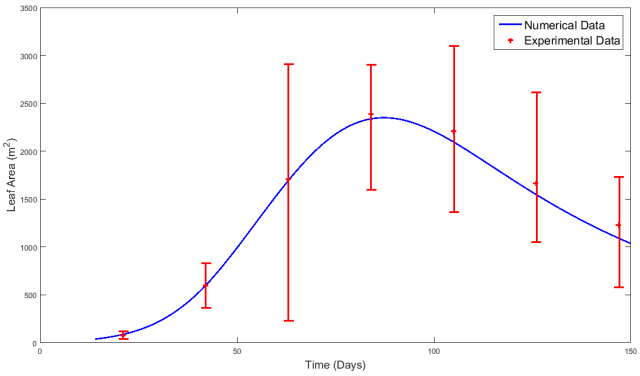

(a)

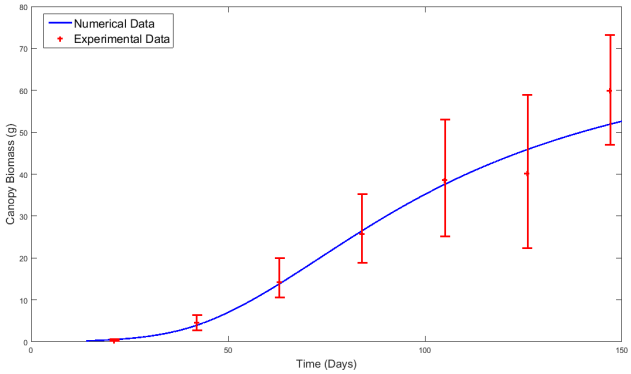

(b)

Figure 4.7: The simulated (a) leaf area and (b) canopy biomass compared with the experimental data for the species S19-3, using the data-fitted case of a temperature of 28°C. The system is described by equations (4.18)- (4.20), where all plant heights are equal and parameters are given in Table 4.1. Each simulated plant is initiated at day 14, the estimated time of emergence and assumed to have a canopy comprising of one leaf at this point. The simulation data have been averaged over 15 plants grown in a five by three grid, the distance between plants in a row is 0.2m and the distance between rows is 0.35m. Red bars indicate the upper and lower bounds of the experimental data.

not give as good a fit to data for 23°C when compared to the previous model.

Similarly to Uniswa Red there has been a significant improvement to simulating leaf area for S19-3 as seen in Figures 4.7(a), 4.8(a) and 4.9(a). The simulation data now follow the behaviour of the leaf area, with results being between the upper and lower bounds of the experimental data for all but two of the data points for the three temperatures. The error values given in Table 4.4 show that leaf area is well simulated for 28°C and 33°C. However, similarly to canopy biomass, 23°C gives a poor fit to the experimental data.

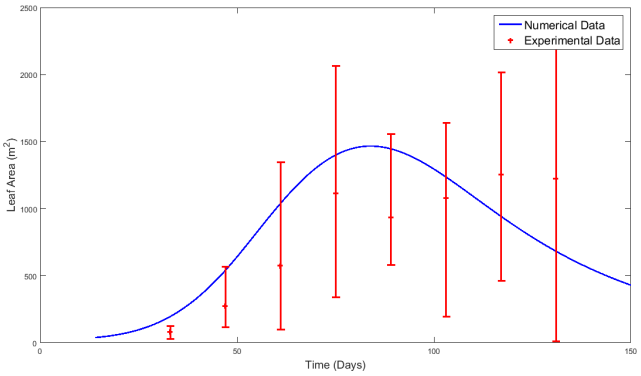

(a)

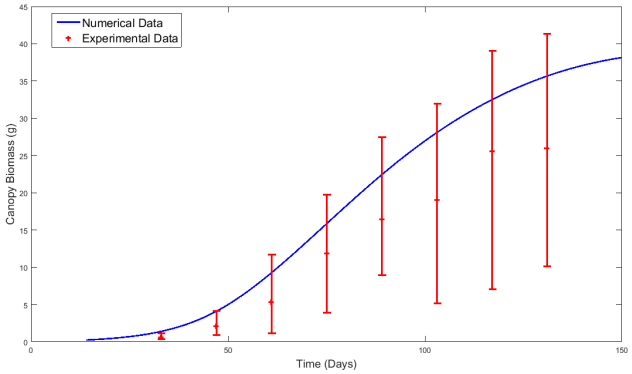

(b)

Figure 4.8: The simulated (a) leaf area and (b) canopy biomass compared with the experimental data for the species S19-3, using the data-fitted case of a temperature of 23°C. The system is described by equations (4.18)- (4.20), where all plant heights are equal and parameters are given in Table 4.1. Each simulated plant is initiated at day 14, the estimated time of emergence and assumed to have a canopy comprising of one leaf at this point. The simulation data have been averaged over 15 plants grown in a five by three grid, the distance between plants in a row is 0.2m and the distance between rows is 0.35m. Red bars indicate the upper and lower bounds of the experimental data.

Thus the leaf accumulation model developed in this chapter is significantly better at simulating leaf area. There is an improvement to simulating 23°C for Uniswa Red but not for S19-3 and so it is difficult to say that we have made the model more able to capture the effects of variation in temperature.

4.2.4 Mathematical model investigation

Now that we are satisfied with the model's ability to describe the behaviour of the experimental data, we can explore its behaviour further. We first investigate

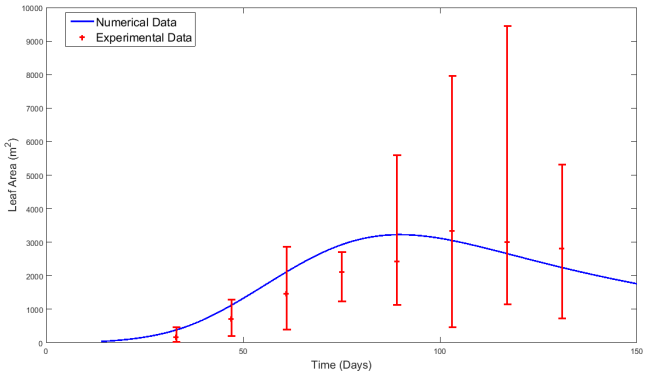

(a)

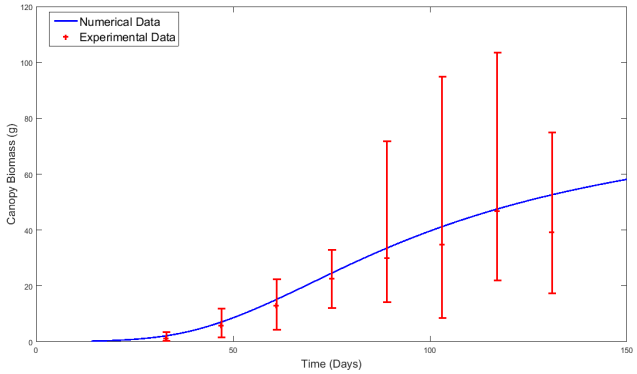

(b)

Figure 4.9: The simulated (a) leaf area and (b) canopy biomass compared with the experimental data for the species S19-3, using the non data-fitted case of a temperature of 33°C. The system is described by equations (4.18)- (4.20), where all plant heights are equal and parameters are given in Table 4.1. Each simulated plant is initiated at day 14, the estimated time of emergence and assumed to have a canopy comprising of one leaf at this point. The simulation data have been averaged over 15 plants grown in a five by three grid, the distance between plants in a row is 0.2m and the distance between rows is 0.35m. Red bars indicate the upper and lower bounds of the experimental data.

the effect variation in simulated leaf area and canopy biomass between the fifteen plants. We simulate the growth of fifteen plants arranged as in Figure 3.8 with a temperature of 28°C and compare it to the experimental data in Figure 4.10. Parameters for all plants are equal and so any difference between plants is incurred by the individual plant position. From Figure 4.10 we can see that plant position has a clear impact on both leaf area and canopy biomass. For leaf area the range of simulation data for the fifteen plants is within the bounds of the experimental data. For canopy biomass however, the data for individual plants are not within the

bounds of the experimental data, although the average of the data set is. Although the canopy biomass of individual plants is not necessarily within the upper and lower bounds of the data, we do see a similar magnitude of variation.

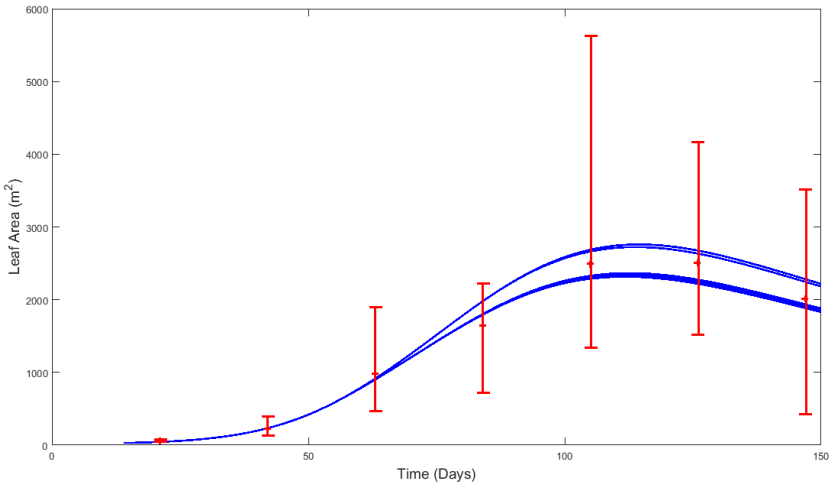

(a)

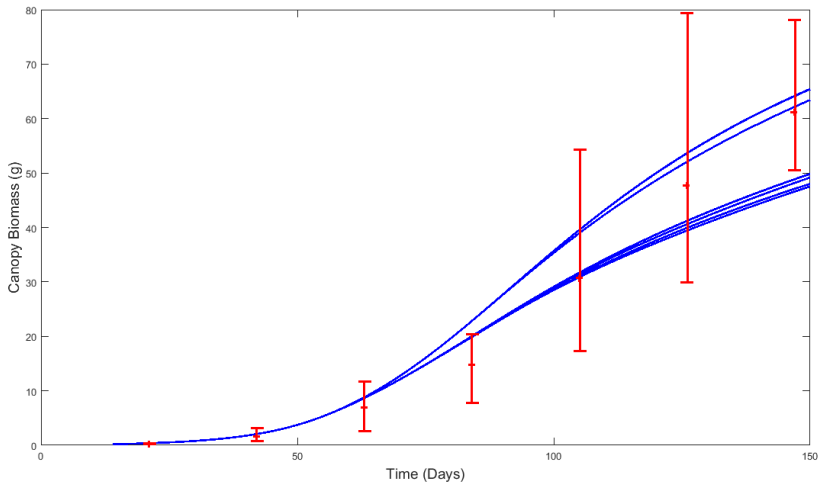

(b)

Figure 4.10: Simulations of fifteen plants of the species Uniswa Red grown at a temperature of 28°C are compared with the experimental data. Here (a) is the leaf area and (b) is the canopy biomass. The system is described by equations (4.18)- (4.20) and parameters are equal between plant and given in Table 4.1. Each simulated plant is initiated at day 14, the estimated time of emergence and assumed to have a canopy comprising of one leaf at this point. Plants are arranged in a five by three grid, the distance between plants in a row is 0.2m and the distance between rows is 0.35m. Red bars indicate the upper and lower bounds of the experimental data.

For a second investigation we now repeat the simulations, however this time

plant heights are randomly varied. In doing so, we can see if randomly varied plant heights improves the models ability to fit to experimental data or hinders it.

Simulations of leaf area and canopy biomass for fifteen plants with randomly varied heights are compared to the experimental data in Figure 4.11. In this case the temperature is 28°C and the species is Uniswa Red. Although we only show an investigation of Uniswa Red here, the results also apply to S19-3. In the same way as described in Section 3.7.3 the variation in height is applied by changing the plant height carrying capacity for each plant. We assume that plant height carrying capacity has a normal distribution with the mean being the original value given in Table 3.1 and with a variance of 10% of the mean. Then a value is randomly selected from this distribution using the inbuilt MATLAB function randn and applied to each plant. The simulation has been run twenty times for different random selections of plant heights from the normal distribution, all twenty simulations are given in Figure 4.11.

By comparing the average leaf area of fifteen plants for twenty different plant height profiles in Figure 4.11(a) with the case of height being equal between plants in Figure 4.4(a) it can be seen that the inclusion of random variation to plant height has little to no effect on the average simulation data. The same result applies to canopy biomass when comparing the results in Figure 4.11(b) with 4.4(b). We do find, however, that although the average behaviour is not strongly affected, the variation between individual plants increases. An example of this is given in Figure 4.12, where the leaf area and canopy biomass of fifteen plants with varying heights is given.

As a final consideration we investigate the range of simulated leaf area and canopy biomass for all fifteen plants when all plant parameters have random values selected from normal distributions. We simulate the growth of fifteen plants arranged as in Figure 3.8 with a temperature of 28°C. All parameters but T_{opt} and T_{crit} have variation applied to them. Each parameter is given a normal distribution with the mean being the original value and the variance being 10% of the original value, a

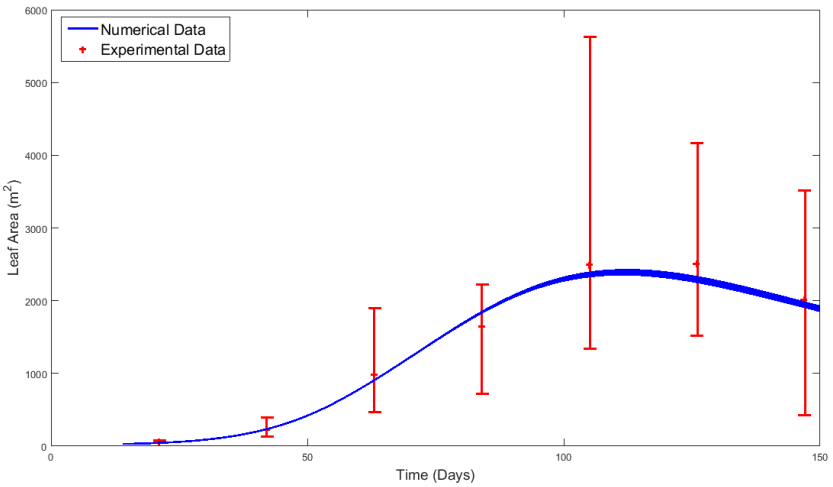

(a)

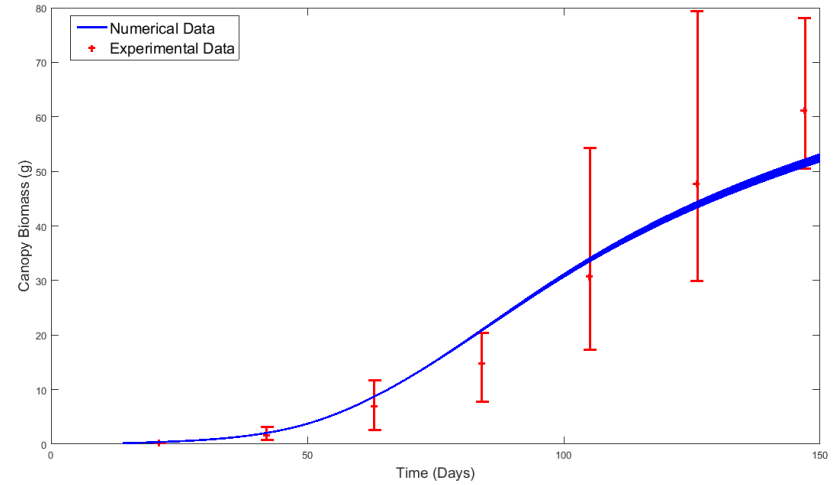

(b)

Figure 4.11: Twenty simulations of the mean (a) leaf area and (b) canopy biomass compared with the experimental data for Uniswa Red. Plant height's are normally distributed with a mean of the original value and a variance of 10% of the original value. Each simulation has a different set of randomly selected values for plant height. The system is described by equations (4.18)- (4.20) where all parameters, except K_h, are equal between plants and given in Table 4.1. Each simulated plant is initiated at day 14, the estimated time of emergence and assumed to have a canopy comprising of one leaf at this point. The simulation data have been averaged over 15 plants grown in a five by three grid, the distance between plants in a row is 0.2m and the distance between rows is 0.35m. Red bars indicate the upper and lower bounds of the experimental data.

value is then randomly selected using the inbuilt MATLAB function randn for each plant. The leaf area and canopy biomass for each of the fifteen plants compared to

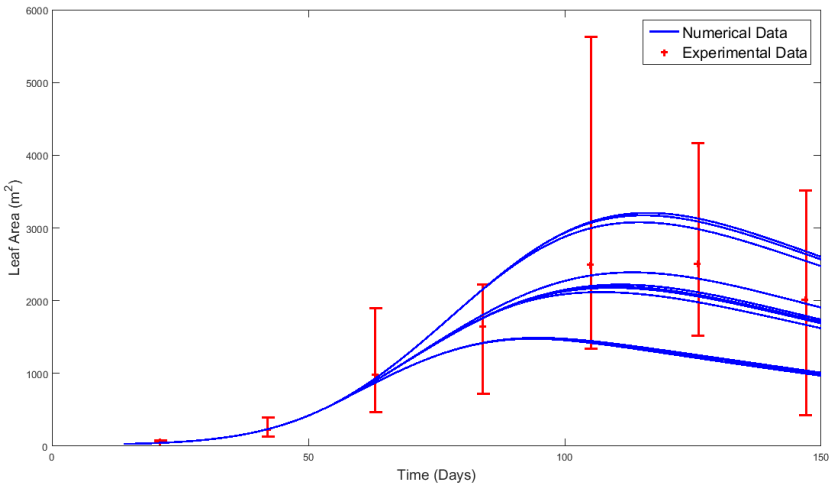

(a)

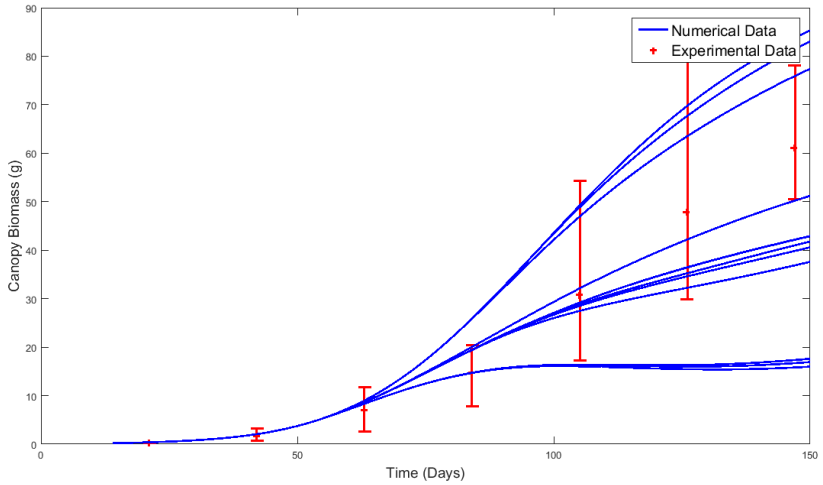

(b)

Figure 4.12: Simulations of fifteen plants of the species Uniswa Red grown at a temperature of 28°C are compared with the experimental data. Here (a) is the leaf area and (b) is the canopy biomass. Plant height's are normally distributed with a mean of the original value and a variance of 10% of the original value. Each simulation has a different set of randomly selected values for plant height. The system is described by equations (4.18)- (4.20) where all parameters, except K_h, are equal between plants and given in Table 4.1. Each simulated plant is initiated at day 14, the estimated time of emergence and assumed to have a canopy comprising of one leaf at this point. Plants are arranged in a five by three grid, the distance between plants in a row is 0.2m and the distance between rows is 0.35m. Red bars indicate the upper and lower bounds of the experimental data.

experimental data is given in Figure 4.13. Here, the variation in individual plant biomass and leaf area is considerably more for randomly varied parameters values

when compared to the case where parameters values are equal among plants. In addition, the range in simulated plants is considerably larger than what was found in the TCRU experimental data.

As we see from comparing Figures 4.12 and 4.13, a large part of the variation between simulated plants is caused by the variation in plant height and that the impact that variation in plant height has on leaf area and canopy biomass is maximised by not allowing light to penetrate though the canopy. Thus some plants (which were taller) were not subjected to any competition and some (which were shorter) were subjected to a lot of competition. Removing variation between plant heights, so that competition is split between two interacting plants, significantly reduces the range in leaf area and canopy biomass between plants even with random variation in all other parameters. Therefore we conclude that assuming that plants have the same height, and therefore imposing competition on all plants in the simulation, causes us to achieve a better fit to experimental data.

We now investigate the average simulated data when all parameters, except those ascertaining to plant height, are randomly varied. For each random value applied to plant parameters there will be a different outcome for leaf area and canopy biomass. Therefore we repeat the simulation 20 times and average the leaf area and canopy biomass for all fifteen plants. The results of the 20 simulations are compared to the experimental data in Figure 4.14. The thickness of the line is the layers that the 20 simulations of leaf area and canopy biomass make. All simulations stay reasonably close to each other and match the behaviour for when there is no random variation in plant parameters found in Figures 4.4(a) and 4.4(b).

4.3 Chapter summary

In this chapter the mathematical model of Chapter 3 has been revised to explicitly account for leaf area accumulation over time. As in Chapter 3 plant height determines which plants experience competition and competition affects the leaf area and canopy biomass. The revised mathematical model was parameterised using a

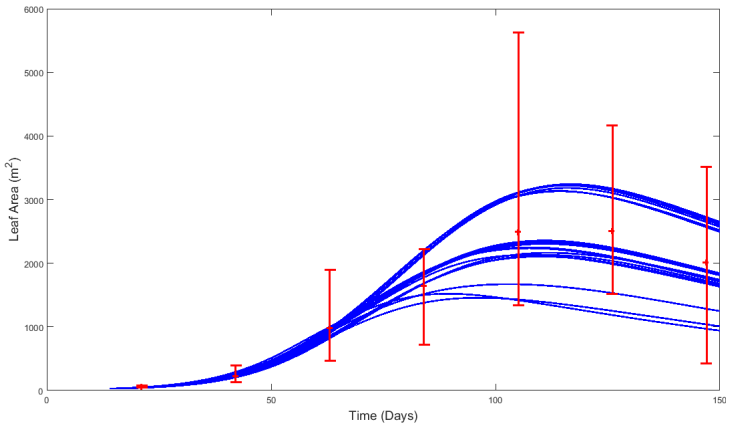

(a)

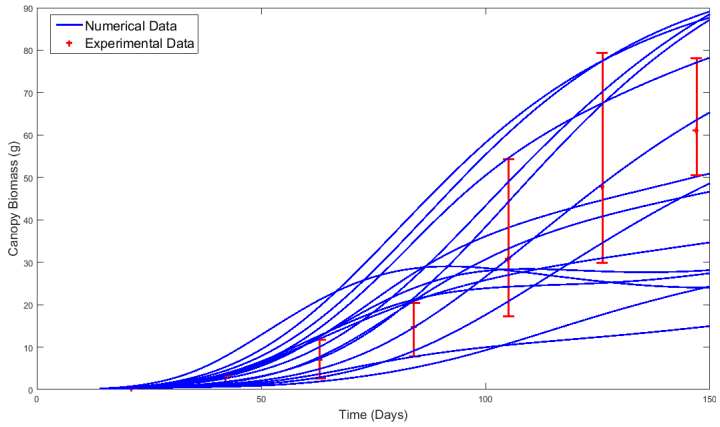

(b)

Figure 4.13: Simulations of fifteen plants of the species Uniswa Red grown at a temperature of 28°C are compared with the experimental data. Here (a) is the leaf area and (b) is the canopy biomass. The system is described by equations (4.18)-(4.20), where each parameter for each plant is randomly varied. All parameter values are normally distributed where the mean is the original parameter value, given in Table 4.1, and the variance is 10% of the original value. Each simulated plant is initiated at day 14, the estimated time of emergence and assumed to have a canopy comprising of one leaf at this point. Plants are arranged in a five by three grid, the distance between plants in a row is 0.2m and the distance between rows is 0.35m. Red bars indicate the upper and lower bounds of the experimental data.

combination of data found in the literature and experimental data collected from the TCRU greenhouses. We then validated the model by comparing simulations of leaf area and canopy biomass to the TCRU greenhouse data.

Contrary to the previous model, leaf area is calculated using two newly introduced ODEs. One for cumulative thermal time and the other for leaf area, which is

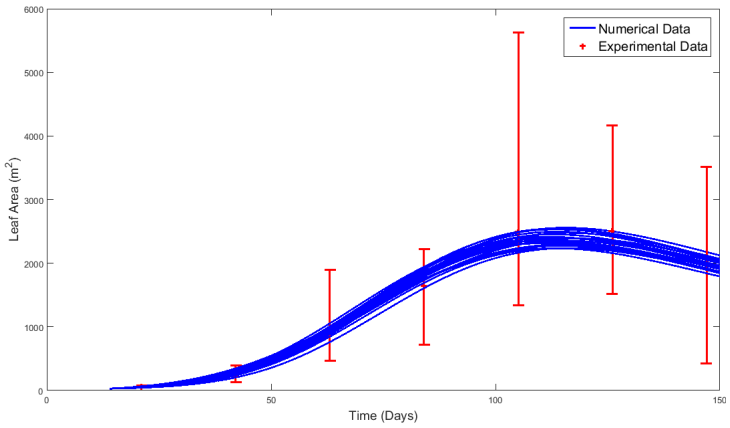

(a) Leaf area

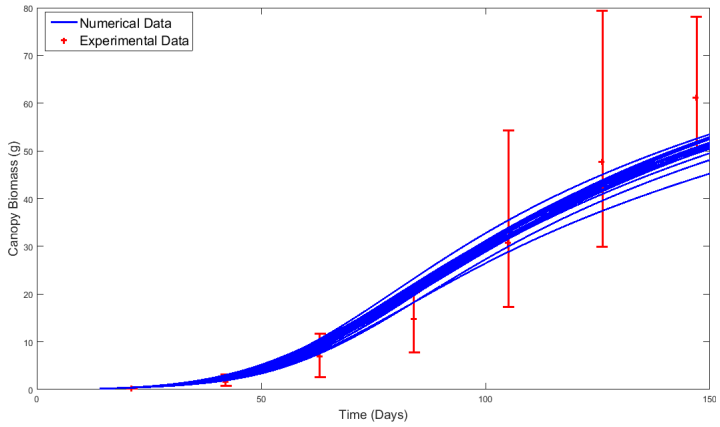

(b) Canopy biomass

Figure 4.14: Twenty simulations of the mean (a) leaf area and (b) canopy biomass compared with the experimental data for Uniswa Red. The system is described by equations (4.18)-(4.20), where each parameter value for each plant is randomly selected from a normal distribution with a mean of the original value, given in Table 4.1, and a variance of 10% of the original value. Each simulation has a different set of randomly selected values for each parameter. Each simulated plant is initiated at day 14, the estimated time of emergence and assumed to have a canopy comprising of one leaf at this point. The simulation data have been averaged over 15 plants grown in a five by three grid, the distance between plants in a row is 0.2m and the distance between rows is 0.35m. Red bars indicate the upper and lower bounds of the experimental data.

a function of cumulative thermal time. In doing this we have explicitly accounted for temperature in the model and achieved a more accurate description of leaf area over time, by allowing leaf area to decrease while canopy biomass continues to increase. By more accurately describing leaf area we gain more confidence in our simulation of canopy biomass, since we are describing its growth in terms of its underlying

processes.

We found in Section 4.2 that this model simulates both canopy biomass and leaf area well for the two bambara groundnut species Uniswa Red and S19-3 for all three temperatures. When comparing this mathematical model to that detailed in Chapter 3 we find that there is a small improvement to the prediction for canopy biomass of Uniswa Red at 23°C and S19-3 at 33°C. The revised mathematical model was marginally worse at predicting canopy biomass for Uniswa Red at 28°C and considerably worse at predicting canopy biomass for S19-3 at 23°C. The simulation of leaf area shows a considerable improvement for leaf area model when compared to the original model for both species and all three temperatures. Although the simulation of leaf area has improved for all data sets, the model still does a poor job at simulating the leaf area of S19-3 at 23°C. Despite this, the simulation of leaf area has been largely improved without incurring a detrimental effect on simulating canopy biomass. The results generally indicate that the new description of leaf area has improved the model data fit.

This mathematical model is a useful tool for predicting canopy biomass and also to optimise yield, since the spatial positioning of plants is included in the model which can be used to explore the most efficient arrangements of plants to optimise growth. By improving the description of underlying processes we have improved the mathematical model's ability to simulate different scenarios. Of the many plant process that are involved in biomass growth, we are particularly interested in those relating to competition for light. As sunlight is absorbed by leaves we have made a considerable effort to accurately describe their growth. Another variable that has a strong impact on competition is the ground cover, a process we have so far only been able to make assumptions for. At this point in the model development we were able to attain experimental data for this variable. This is discussed in more detail in the following chapter.

Chapter 5

Experimental and theoretical investigations of ground cover G

As we do not have data on the size of individual plant canopies, in the development of the models discussed so far we have had to make several assumptions as to the behaviour and size of ground cover. A relationship taken from the literature and described by equation (3.7) has provided a sound preliminary basis that allows our model to fit well to the TCRU greenhouse data [32]. Despite this, as all TCRU greenhouse data sets are for the same planting arrangement, there is a possibility that ground cover, and thus competition, is being miscalculated. This may not be apparent in the simulation results as other approximated parameters could be compensating for the error caused by the incorrectly calculated competition. A primary motivation in the formulation of our model is to investigate the effect that planting layout and canopy shadowing has on crop yield and thus ground cover (or canopy size) is an important component in the model. This issue is problematic because our model may not be able to accurately account for a change in planting arrangement.

As such we are strongly motivated to attain data to either confirm or challenge our assumptions regarding what the individual plant canopy sizes are and if our equation for ground cover G accurately captures the behaviour. Since the conception

of the model we have been able to conduct greenhouse experiments that are designed to provide data on ground cover over time, which we have so far been lacking. We now discuss these experiments in this chapter as well as the impact the results have on the formulation of the mathematical model.

5.1 Canopy experimental data collection

The greenhouse experimental data used to inform the mathematical model give leaf number, leaf area, leaf mass, stem mass, root mass and pod mass over time for a number of plants. However they do so for only one planting arrangement. This amount of data is incredibly useful to a mathematical modeller for parameterisation and model validation. Despite this, one key component is missing, which is integral to the spirit of the model developed in this work. This being the plant size and thus magnitude of inter-canopy competition. Without this we are unable to confirm that competition is being incorporated correctly and therefore cannot investigate how changes in planting density affect yield. With this in mind we decided to conduct our own greenhouse experiments designed to inform the model's ground cover equation.

The newly collected data comprise of the diameter of the plant canopy measured at the longest point every two weeks, the dry canopy biomass per plant at harvest and the dry pod mass per plant at harvest. Due to limitations in available space the experiments were confined to a 2m^2 plot, measuring 1m×2m. The area was split into two plots, where high density and low density experiments were conducted. In the low density experiment the 1m^2 was filled with 9 plants arranged in a 3×3 arrangement with $D_r = 0.4\text{m}$ and $D_c = 0.3\text{m}$. In the high density experiment another 1m^2 was filled with 16 plants arranged in a 4×4 arrangement with $D_r = 0.25\text{m}$ and $D_c = 0.25\text{m}$. This allows the canopy biomass, the pod mass and canopy size to be compared for two different planting densities.

An illustration of the planting arrangement of all plants can be found in Figure 5.1(a). Here the position of plants with respect to each other and the plot borders

can be seen. Plants of the high and low density experiments share a border with a distance of 0.3m between rows. This distance caused some interaction between the two density experiments. In addition to what can be seen in Figure 5.1(a), due to space limitations, this experiment was conducted amongst plants from other experiments and we were unable to prevent interactions with plants external to our own experiments. These interactions came in the form of canopy shadowing, which would have had a detrimental impact on our experiment as plants were experiencing more competition than desired. The largest impact would have been on the high density treatment, as they were positioned closest to plants of other experiments, however all plants, except those placed in the centre of the plot, would have had some interaction with plants external to our experiment.

The experiments were conducted in one climate controlled Future Crops greenhouse in the months June to November of 2016 at the School of Biosciences, Sutton Bonnington Campus, University of Nottingham. The species Uniswa Red was selected with greenhouse temperatures set to 28°C/23°C for day/night. The number of day-light hours per day was controlled by an automatic blackout system and set to a constant day length treatment of 12 hours.

All plants had emerged by 13/14th of June, transplanted on the 23rd of June and harvested on 2nd November. On harvest the number of pods per plant were recorded and separated from the remaining above ground biomass. Above ground biomass was then dried at a temperature of 84°C for 48 hours and pods were dried at a temperature of 37°C for two weeks. Canopy biomass and pod mass were then weighed and recorded.

Since we are strongly limited in the number of plants and space, we are confined to non-destructive data collecting techniques. Every two weeks after transplanting, the plant canopy diameter and plant height were measured. The canopy areas were not strictly circular and so the widest points of each plant were identified and marked and the distance between markers was then measured and recorded for each plant individually. The plant height was measured from the soil to the top of the canopy

crown. Plant height was not uniform across the canopy and so some parts or the plant were taller than other parts. For all plants the highest point was measured. Both methods are non-destructive.

Great care was taken to minimise the impact that measuring had on plant canopies by avoiding manipulating individual leaf positions. It was necessary however, when dealing with competing plants, to touch the plants in order to identify the borders of plant canopies and thus their size. It should be noted that some impact would have been made on the intra-plant competition by the act of measuring the plant canopies.

The average plant radius, with the minimum and maximum values for each plant, in both the high density and low density arrangements can be found in Figure 5.1(b). There is a clear difference in the average canopy radius for the two density treatments, with plants from the lower density having a consistently larger canopy radius.

The average dry canopy biomass and pod mass at harvest for the high and low density arrangements can be found in Table 5.1. There is a clear difference in both average pod mass and canopy biomass at harvest between the two planting densities.

	Canopy Biomass (g)		Pod Mass (g)		Total biomass	
Plants per square metre	Average mass	Standard deviation	Average mass	Standard deviation	Average mass	Standard deviation
9	65.82	15.64	36.71	10.77	102.53	24.06
16	33.46	9.75	20.43	4.60	53.89	13.22

Table 5.1: The average canopy biomass and pod mass for plants of the species Uniswa Red grown at the temperature 28°C for planting densities of 9 plants per square metre and 16 plants per square metre.

The data sets that have been collected are too small, in respect to the number of plants and time points, to be used to parametrise the model, but can be used to comment upon the design of our model so far.

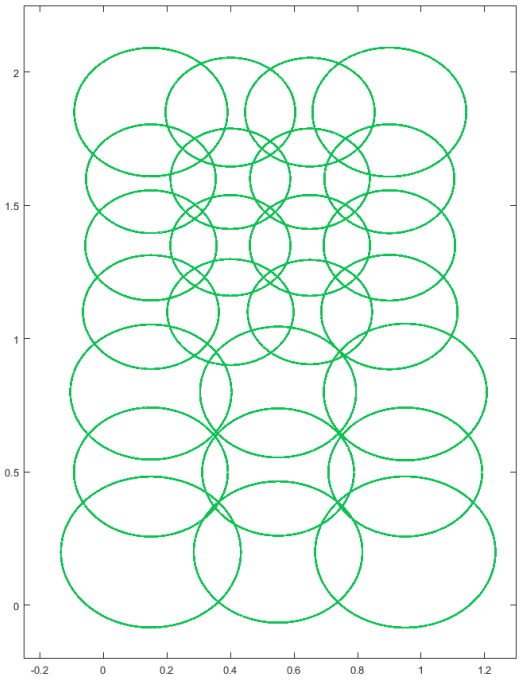

(a)

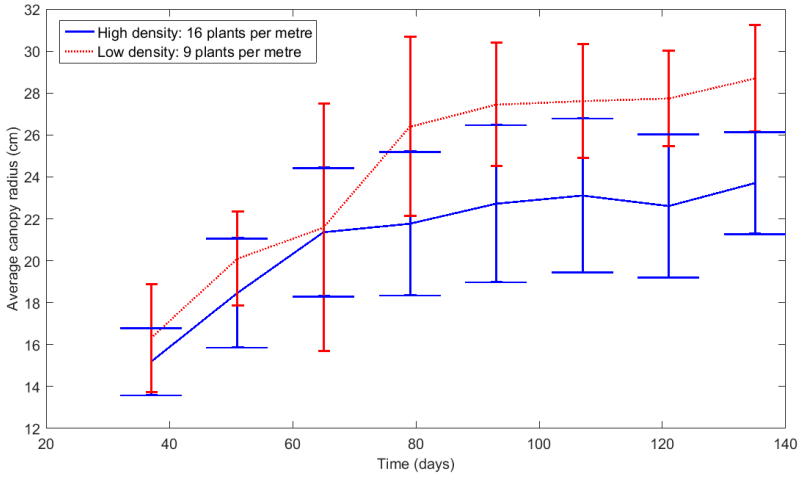

(b)

Figure 5.1: The canopy size and plant arrangement of the greenhouse experiment. Here (a) shows the planting arrangement and (b) shows the average canopy radius for two planting densities, of 9 (low density) and 16 (high density) plants respectively. The maximum and minimum canopy radii is included in (b) for each density treatment over time.

5.2 Estimating ground cover

Now that we have experimental data for ground cover over time, we are able to make a more informed judgement on how ground cover is approximated in the mathematical model. We first compare the simulated ground cover from the model in Chapter 4 with the experimental data and then consider several model refinements to ensure it is appropriately described.

We begin by replicating the experimental set up in our simulations and so using the arrangement illustrated in Figure 5.1(a) we simulate leaf area, canopy biomass and ground cover over time for each plant using equations (4.18) to (4.20). All plants are simulated together and are then divided into the two density treatments of 9 plants per square metre and 16 plants per square metre and the ground cover is averaged over the plants in each treatment. The simulated average ground cover over time for each density treatment with the experimental data can be found in Figure 5.2, with the parameter values as detailed in Table 4.1. Here they are assumed equal for all plants.

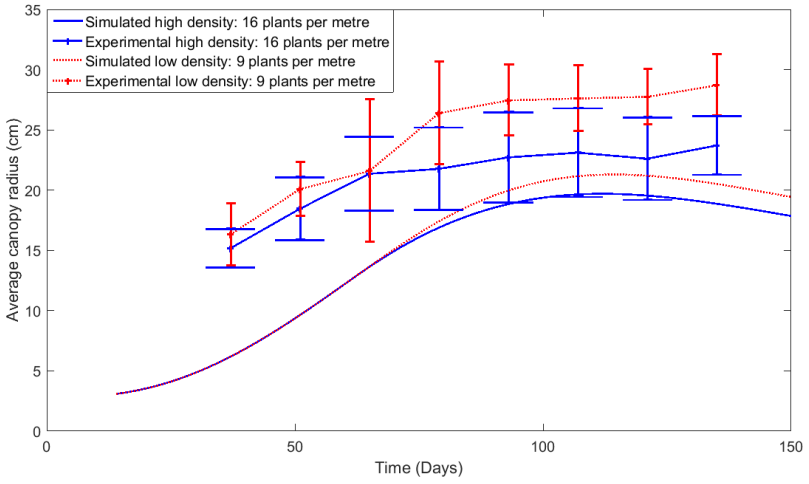

Figure 5.2: The simulated and experimental average canopy radius of density treatments of 9 plants per square metre and 16 plants per square metre. The experimental data used for comparison is that which is described in Section 5.1. The temperature is 28°C and the planting arrangement for both the simulated and experimental plants is given in Figure 5.1(a).

The first thing we notice from Figure 5.2 is that we are underestimating the canopy radius for each scenario. For both the low and high density planting scenarios, simulation results show the average ground cover for all plants in the population to peak at approximately 20cm. The experimental data show the average canopy radius to peak at 22cm and 28cm for the high and low density scenarios, respectively. We can also see that the impact competition has on ground cover is similarly not reflected in the simulation data. Here, the canopy radius for the simulated plants has a relative difference of 8% between each planting density compared to 17.40% for the experimental data. The difference in average ground cover for each density treatment might increase when average ground cover is scaled up to be closer to what we would expect from the experimental data.

With this in mind we now wish to increase the simulated ground cover. This is made possible by increasing the empirical parameter B, but in doing so we incur several side effects on the model. To accommodate for an increase in B we will also need to reparameterise the model.

Previously in our parameterisation process, the parameters a, b, b, d_L, c_k, B, K_c and d_c are found using an inbuilt MATLAB function that applies a least squared fit to simulation data to approximate parameters. The experimental data used to parameterise the model are the full set of data provided by the TCRU greenhouse experiments. We repeat the parameterisation process however, in this case we increase the minimum value of B so that it can not be lower than 0.9; this is the predicted minimum that will allow for the simulated canopy radius to be more comparable to the data collected here.

In order to complete this parameterisation, the experimental set up for the TCRU greenhouse experiments needs to be replicated i.e. fifteen plants arranged in three rows of five with $D_r = 0.2$m and $D_c = 0.35$m. This set up will hereby be referred to as Case 1. We repeat the parameterisation process for Uniswa Red as described in Section 4.2.1. The new values for a, b, c, d_L, c_k, B, K_c and d_c can be found in Table 5.2.

Parameter	Value
α_h	0.75
k_h	20
d_h	0.02
a	0.19
b	96.97
c	39.74
d_L	0.0156
PAR	0.5
k_i	16
c_k	2.35
κ	0.6
k_{max}	125.99
d_c	0.001
ϕ	1.62×10^{-2}
ψ	0.56
B	0.92
h_0	0.05
c_0	0.19

Table 5.2: Table of parameter values for Uniswa Red. These parameter values have been found for when B has a minimum value of 0.9.

With the newly parameterised model we repeat the simulations for Uniswa Red at temperatures of 23°C, 28°C, and 33°C. The simulated average leaf area and canopy biomass for fifteen plants arranged as in Case 1 is compared to the corresponding experimental data in Figures 5.3 to 5.5, respectively. Clearly, increasing B does not alter the simulation of leaf area over time. There is also no discernible change to the simulation of canopy biomass at 23°C and 33°C however, there is a clear impact on the simulations of canopy biomass at 28°C. We find that our revised model for G makes the model-data fit worse for this temperature.

In order to explore the deterioration in the model-data fit for 28°C caused by increasing B, we consider how the simulation of ground cover has changed. To do this we compare the evolution of ground cover over time to the experimental data in Figure 5.1(b). We simulate the growth of plants arranged as in Figure 5.1(a) with a temperature of 28°C and parameters given in Table 5.2. The canopy radius for the two density treatments is averaged over all plants in each density treatment and results are compared to experimental data in Figure 5.6.

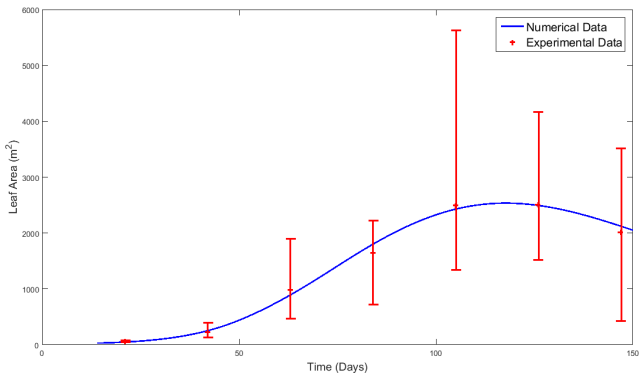

(a)

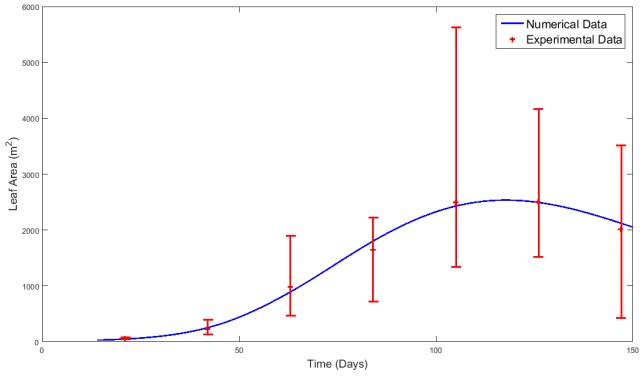

(b)

Figure 5.3: The simulated (a) leaf area and (b) canopy biomass compared with the experimental data for the species Uniswa Red, using the data-fitted case of a temperature of 28°C. All plant parameters for each plant are equal. The system is described by equations (4.18) to (4.20) with the revised parameter values given in Table 5.2. Each simulated plant is initiated at day 14, the estimated time of emergence and assumed to have a canopy comprising of one leaf at this point. The simulation data has been averaged over 15 plants grown in a five by three grid, the distance between plants in a row is 0.2m and the distance between rows is 0.35m. Red bars indicate the upper and lower bounds of the experimental data.

The canopy radius at the later stages of the simulation is now closer to what was observed in the experiments, however the simulated ground cover shows much smaller values at the early stages of growth when compared to the experimental data. We can also see that the change in ground cover for the different planting densities is still not as large for the simulations as what is found in the experimental data, with a difference of approximately 12.5%.

The average simulated canopy biomass for the two density treatments is given in Table 5.3. The difference in average simulated canopy biomass is 43.77% between the

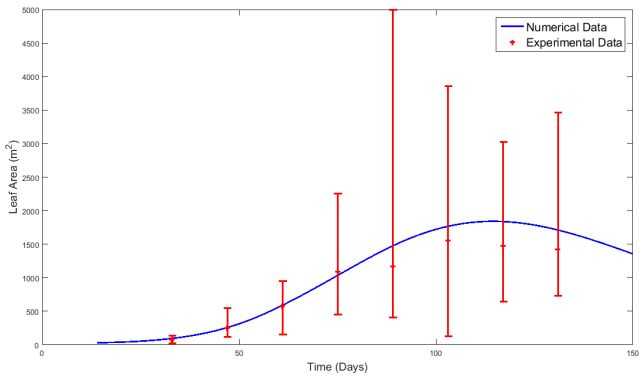

(a)

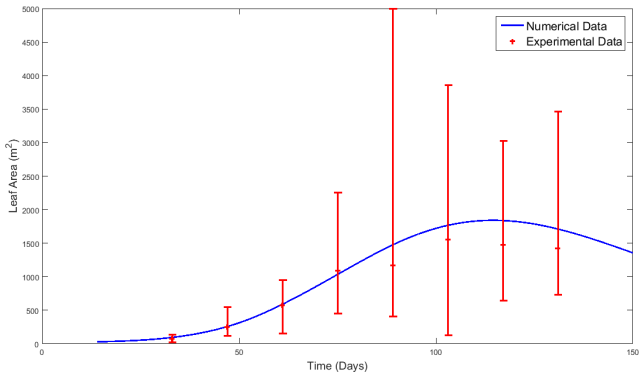

(b)

Figure 5.4: The simulated (a) leaf area and (b) canopy biomass compared with the experimental data for the species Uniswa Red, using the non data-fitted case of a temperature of 23°C. All plant parameters for each plant are equal. The system is described by equations (4.18) to (4.20) with the revised parameter values given in Table 5.2. Each simulated plant is initiated at day 14, the estimated time of emergence and assumed to have a canopy comprising of one leaf at this point. The simulation data has been averaged over 15 plants grown in a five by three grid, the distance between plants in a row is 0.2m and the distance between rows is 0.35m. Red bars indicate the upper and lower bounds of the experimental data.

two density treatments. This is compared to a 90.26% difference between average canopy biomass of the experimental data given in Table 5.1. We must bear in mind however, that the plants in the experiment were subjected to competition imposed by plants external to our experiment. This particularly affected the high density experiment and therefore the difference in canopy biomass between the two treatments.

Since canopy radius is being underestimated in the early stages of growth it is clearly a necessity to not only change B, but to redefine the entire relationship

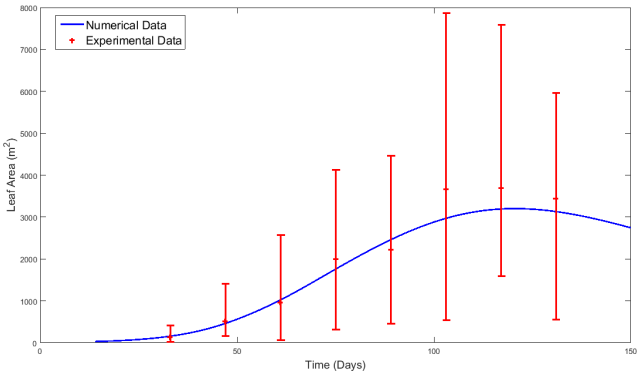

(a)

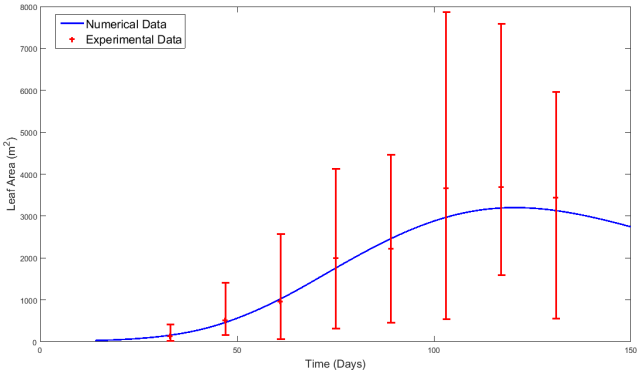

(b)

Figure 5.5: The simulated (a) leaf area and (b) canopy biomass compared with the experimental data for the species Uniswa Red, using the non data-fitted case of a temperature of 33°C. All plant parameters for each plant are equal. The system is described by equations (4.18) to (4.20) with the revised parameter values given in Table 5.2. Each simulated plant is initiated at day 14, the estimated time of emergence and assumed to have a canopy comprising of one leaf at this point. The simulation data has been averaged over 15 plants grown in a five by three grid, the distance between plants in a row is 0.2m and the distance between rows is 0.35m. Red bars indicate the upper and lower bounds of the experimental data.

between leaf area and ground cover.

To develop a new method of simulating ground cover, we first consider why our original method fails. In the early stages, when there is plenty of space for growth, leaves appear randomly leaving large gaps between individual leaves giving a leaf area index of less than one. The original ground cover model assumes no gaps between leaves and that the leaf area index begins at one and increases monotonically as leaf area increases. We now develop a new model that allows a large gap filled area of influence at the initial stages of growth. The gaps within the area of influence fills

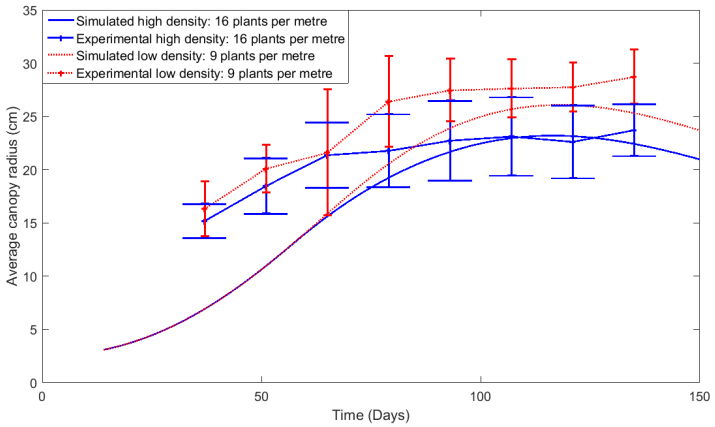

Figure 5.6: The simulated and experimental canopy radius of two density treatments of 9 plants per square metre and 16 plants per square metre. The experimental data used for comparison is that which is described in Section 5.1. The temperature is 28°C and the planting arrangement for both the simulated and experimental plants is given in Figure 5.1(a). The parameter values for this simulation are given in Table 5.2 and ground cover is described by equation (3.7).

	Canopy Biomass (g)	
Plants per square metre	Average mass	Standard deviation
9	66.74	6.97
16	46.42	8.36

Table 5.3: The average simulated canopy biomass for plants of the species Uniswa Red grown at the temperature 28°C for planting densities of 9 plants per square metre and 16 plants per square metre.

over time with newly accumulated leaves. Hence we see large increases in ground cover at the beginning of the simulation with smaller increases in the later stages of growth.

Several models for ground cover have been considered and it has been found that a Gaussian relationship similar to that devised to simulate leaf area best describes the evolution of ground cover. This approach is unique to this work. This relationship allows us to determine when peak growth occurs, how wide the window of peak growth is and the maximum growth rate. It has been decided that the maximum growth rate of the ground cover will be a function of leaf area and the window

of ground cover growth will be affected by overlap, so that as overlap increases the period of peak canopy spreading decreases. We now introduce a dynamical description of ground cover $G_i(t)$ for each plant, such that

$$\frac{dG_i(t)}{dt} = \alpha_g A_i(t) exp\left(-\left(\frac{T_C(t) - b_g}{c_g(1 - O_i(h_1, h_2, ...h_N, t))}\right)^2\right) - d_g G_i(t). \tag{5.1}$$

Here, α_g is the ground cover growth rate, b_g determines the thermal time of peak growth and c_g determines the range of thermal time for which peak growth occurs.

Then the revised system of equations that describe the growth of N plants labelled with a subscript i is described by

$$\begin{aligned}
\frac{dT_{Ci}(t)}{dt} &= T_{Di}(t), && (5.2)\\
\frac{dA_i(t)}{dt} &= L_A a_1 \left(1 - O_i(h_1, h_2, ...h_N, t)\right) exp\left(-\left(\frac{T_{Ci}(t) - b_1}{c_1}\right)^2\right) \\
&\quad -d_l T_{sl} A_i(t), && (5.3)\\
\frac{dG_i(t)}{dt} &= \alpha_g A_i(t) exp\left(-\left(\frac{T_{Ci}(t) - b_g}{c_g(1 - O_i(h_1, h_2, ...h_N, t)}\right)^2\right) \\
&\quad -d_g G_i(t), && (5.4)\\
\frac{dc_i(t)}{dt} &= R_0 c_k G_i(t) \left(1 - O_i((h_1, h_2, ...h_N, t)\right) \left(1 - exp\left(-\kappa \frac{A_i(t)}{G_i(t)}\right)\right) \times \\
&\quad \left(1 - \frac{c_i(t)}{k_{ci}(O_i, t)}\right) - d_c T_{sc} c_i(t). && (5.5)
\end{aligned}$$

Plant height is described by equation (4.17), repeated here for convenience

$$h_i(t) = \frac{h_0(\alpha_h - d_h) exp((\alpha_h - d_h)t)}{\alpha_h - d_h - \alpha_h k_{hi} h_0 + \alpha_h k_{hi} exp((\alpha_h - d_h)t) h_0}. \tag{5.6}$$

The initial conditions of the system are

$$T_{Ci}(0) = T_{Di}(0), \quad A_i(0) = L_A, \quad G_i(0) = L_A, \quad c_i(0) = C_0 \quad \text{and} \quad h_i(0) = h_0.$$

5.3 Non-dimensionalisation

We non-dimensionalise equations (5.2) to (5.5) according to

$$T_{Di}(t) = T_{Di0}\hat{T}_{Di}(\tau), \qquad T_{Ci}(t) = \frac{T_D(0)}{\alpha_h}\hat{T}_{Ci}(\tau), \qquad c_i(t) = c_0\hat{c}_i(\tau),$$

$$G_i(t) = L_A\hat{G}_i(\tau), \qquad A_i(t) = L_A\hat{A}_i(\tau) \qquad \text{and} \qquad t = \frac{\tau}{\alpha_h},$$

where a hat signifies a non-dimensional physical variable and τ denotes non-dimensional time. Then the non-dimensional system of equations if given by

$$\begin{aligned}
\frac{d\hat{T}_{Ci}(\tau)}{d\tau} &= \hat{T}_{Di}(t), && (5.7)\\
\frac{d\hat{A}_i(\tau)}{d\tau} &= \bar{\alpha}_L\left(1 - O_i(\hat{h}_1, \hat{h}_2, ...\hat{h}_N, \tau)\right) exp\left(-\left(\frac{\hat{T}_{Ci}(\tau) - \bar{b}}{\bar{c}}\right)^2\right)\\
&\quad -\bar{d}_L\hat{A}_j(\tau), && (5.8)\\
\frac{d\hat{G}_i(\tau)}{d\tau} &= \bar{\alpha_g}\hat{A}_i(t)exp\left(-\left(\frac{\hat{T}_{Ci}(\tau) - \bar{b}_g}{\bar{c}_g(1 - O_i(\hat{h}_1, \hat{h}_2, ...\hat{h}_N, \tau))}\right)^2\right) - \bar{d}_g\hat{G}_i(t), && (5.9)\\
\frac{d\hat{c}_i(\tau)}{d\tau} &= \bar{\alpha}_c\left(1 - exp(-\kappa\hat{A}_i^{(1-B)}(\tau)\right)\hat{G}_i(\tau)\left(1 - O_i(\hat{h}_1, \hat{h}_2, ...\hat{h}_N, \tau)\right)\\
&\quad \times\left(1 - \bar{K}_{ci}(O_i, \tau)\hat{c}_i(\tau)\right) - \bar{d}_c\hat{c}_i(\tau), && (5.10)
\end{aligned}$$

where

$$\bar{\alpha}_L = \frac{aT_D}{L_A\alpha_h}, \qquad \bar{b} = \alpha_h b, \qquad \bar{c} = \alpha_h c, \qquad \bar{d}_L = \frac{d_l T_{sl}}{\alpha_h},$$

$$\bar{\alpha}_g = \frac{\alpha_g}{\alpha_h}, \qquad \bar{b}_g = \alpha_h b_g, \qquad \bar{c}_g = \alpha_h c_g, \qquad \bar{d}_g = \alpha_h d_g,$$

$$\bar{\alpha}_c = \frac{R_0 c_k L_A}{c_0\alpha_h}, \qquad \text{and} \qquad \bar{d}_c = \frac{d_c T_{sc}}{\alpha_h}.$$

Non-dimensional plant height is described by equation (3.82), which we repeat here for convenience

$$\hat{h}_i(\tau) = \frac{h_0(1 - d_h)exp((1 - d_h)\tau)}{1 - d_h - k_{hi}h_0 + k_{hi}exp((1 - d_h)\tau)h_0}.$$

The initial conditions are

$$\hat{T}_{Ci}(0) = \frac{T_{Ci0}\alpha_h}{T_{Di0}}, \qquad \hat{A}_i(0) = 1, \qquad \hat{G}_i(0) = 1, \qquad \text{and} \qquad \hat{c}_i(0) = 1.$$

For simplicity, hereafter the hats and bars will be dropped.

5.4 Parameterisation

Parameter	Value
α_h	0.75
k_h	30^*, $25^\dagger$
d_h	0.02
T_{opt}	30^*, $28^\dagger$
T_{crit}	12^*, $8.5^\dagger$
a	0.19^*, $0.21^\dagger$
b	67.74^*, $92.0^\dagger$
c	28.78^*, $38.00^\dagger$
d_l	$1.37 \times 10^{-2*}$, $1.6 \times 10^{-2\dagger}$
L_A	$3.9 \times 10^{-3*}$, $3.0 \times 10^{-3\dagger}$
PAR	0.5
k_i	16
c_k	1.87^*, $2.04^\dagger$
κ	0.6
k_{max}	180.66^*, $161^\dagger$
d_c	$1 \times 10^{-3*}$, $5 \times 10^{-4\dagger}$
α_g	53.85^*,$103.33^\dagger$
b_g	17.04^*,$14.00^\dagger$
c_g	21.67^*, $30.00^\dagger$
h_0	0.05
L_0	1
G_0	L_A
c_0	0.24^*, $0.19^\dagger$

Table 5.4: Table of parameter values. For parameters that are species specific, * denotes the species S19-3 and † denotes Uniswa Red. These parameter values have been found for when ground cover is described by equation (5.1).

Once again we must parameterise for the unknown parameters a, b, c, d_L, c_k, B, K_c and d_c, this time for the revised model that includes equation (5.1). In addition to these parameters we must also find the newly introduced parameters α_g, b_g and c_g. All other parameters, that are not listed here, are considered to be the same

as that described in Sections 3.4.1 and 4.2.1. For the leaf area, ground cover and canopy biomass parameters that have been revised we repeat the process described in these sections where a least-squared algorithm is applied to best fit simulation data to the TCRU experimental data. The inbuilt MATLAB function lsqcurvefit is used and the results for Uniswa Red and S19-3 are given in Table 5.4.

5.4.1 Numerical simulation

In this section we compare the revised mathematical model described by equations (5.7) to (5.10) to the experimental data. There are now two sets of data with which to compare, the TCRU experimental data that have been used in Chapters 3 and 4 and also the ground cover data described in this chapter.

Firstly, we repeat the simulation of Figure 5.6 however, in this case ground cover is described by the solution of equation (5.9). The plants are arranged as in Figure 5.1(a) with parameter values given in Table 5.4. Figure 5.7 shows how the simulated average ground cover $G(t)$ for each density treatment changes over time compared to the experimental data.

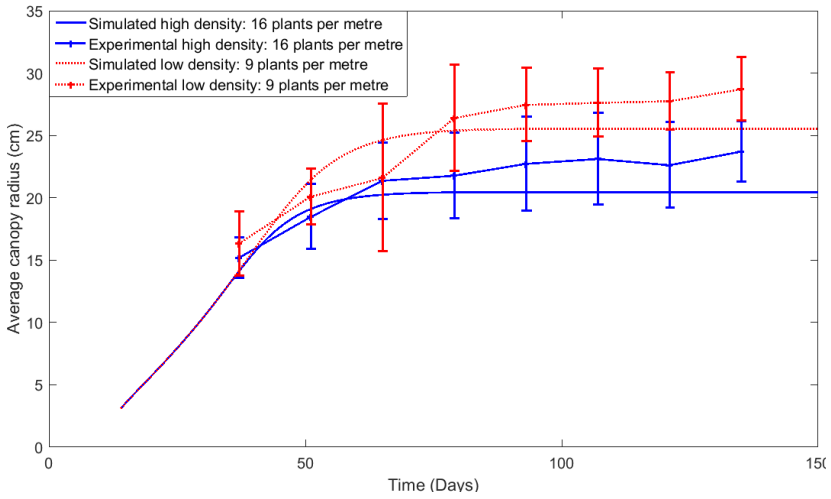

Figure 5.7: The simulated canopy radius of two density treatments of 9 plants per square metre and 16 plants per square metre. Here ground cover is described by equation (5.1), temperature is 28°C and individual plant arrangements with respect to each other and plant borders can be found in Figure 5.1(a). The parameter values for this simulation are given in Table 5.4.

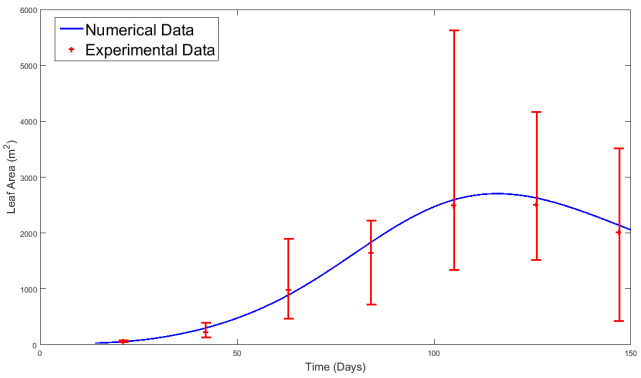

(a)

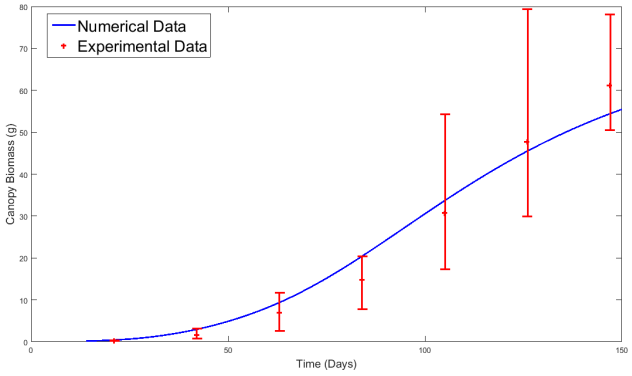

(b)

Figure 5.8: he simulated (a) leaf area and (b) canopy biomass compared with the experimental data for the species Uniswa Red, using the data-fitted case of a temperature of 28°C. All parameters for each plant are equal. The revised system is described by the equations (5.7) to (5.10) with the revised parameter values given in Table 5.4. Each simulated plant is initiated at day 14, the estimated time of emergence and assumed to have a canopy comprising of one leaf at this point. The simulation data have been averaged over 15 plants grown in a five by three grid, the distance between plants in a row is 0.2m and the distance between rows is 0.35m. Red bars indicate the upper and lower bounds of the experimental data.

We can see that ground cover, as described by equation (5.1), gives a larger canopy crown radius at the earlier stages of growth. In addition, there is now a larger difference between the simulated canopy radii of the two density treatments with a relative difference of 17%, which is closer to what was found in the experimental data.

There is a difference of 39.29% between the average simulated canopy biomass of the two density treatments arranged as in Figure 5.1(a). This is a smaller difference than what was found in the experimental data. It is important to note that during

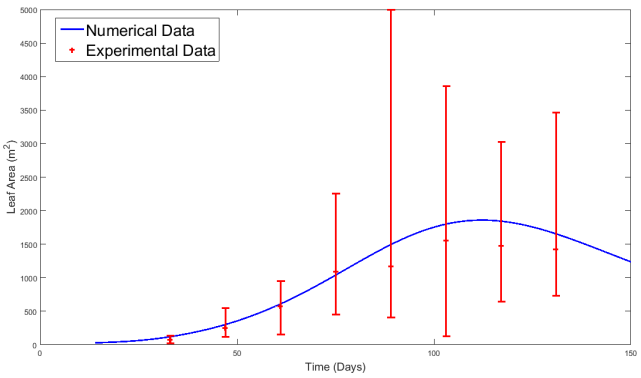

(a)

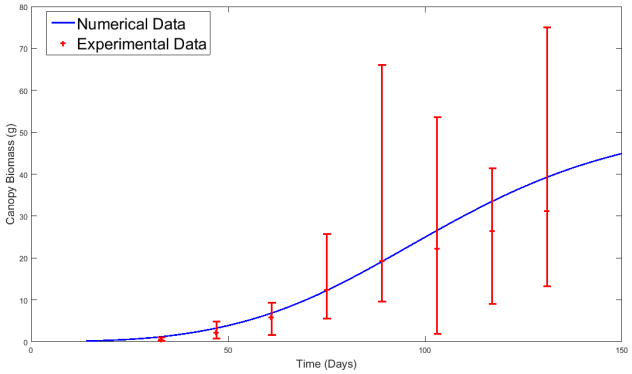

(b)

Figure 5.9: he simulated (a) leaf area and (b) canopy biomass compared with the experimental data for the species Uniswa Red, using the non data-fitted case of a temperature of 23°C. All parameters for each plant are equal. The revised system is described by the equations (5.7) to (5.10) with the revised parameter values given in Table 5.4. Each simulated plant is initiated at day 14, the estimated time of emergence and assumed to have a canopy comprising of one leaf at this point. The simulation data have been averaged over 15 plants grown in a five by three grid, the distance between plants in a row is 0.2m and the distance between rows is 0.35m. Red bars indicate the upper and lower bounds of the experimental data.

the greenhouse experiments it was necessary to share the planting area with other experiments. As such we were unable to prevent competition with plants external to those in the experiment. This would definitely have affected the results of the experiments and also the ratio between canopy biomass for the two density treatments. In addition, the experimental data are for a very small sample size. Therefore, although it was necessary to increase ground cover so that the general behaviour of canopy spread was better represented, it is not in our best interest to adapt the model further to fit this single data set. Despite this, the revised model for ground

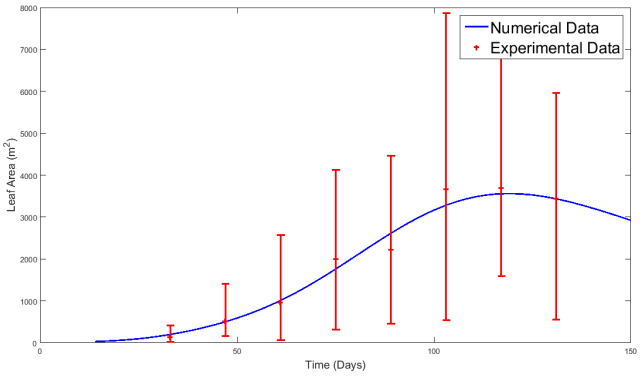

(a)

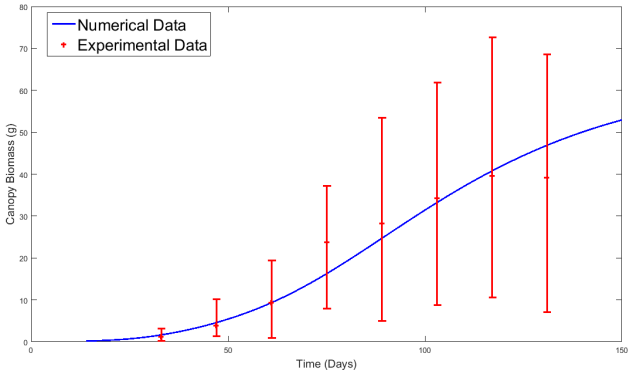

(b)

Figure 5.10: he simulated (a) leaf area and (b) canopy biomass compared with the experimental data for the species Uniswa Red, using the non data-fitted case of a temperature of 33°C. All parameters for each plant are equal. The revised system is described by the equations (5.7) to (5.10) with the revised parameter values given in Table 5.4. Each simulated plant is initiated at day 14, the estimated time of emergence and assumed to have a canopy comprising of one leaf at this point. The simulation data have been averaged over 15 plants grown in a five by three grid, the distance between plants in a row is 0.2m and the distance between rows is 0.35m. Red bars indicate the upper and lower bounds of the experimental data.

cover is demonstrating a stronger ability to simulate the impact of two different planting densities and therefore this is the system that will be used forthwith.

We now compare the refined model to the TCRU greenhouse data set. Plants are arranged as in Case 1 for all three temperatures 23°C, 28°C and 33°C. The average leaf area and canopy biomass for all fifteen plants is given in Figures 5.8 to 5.10 with the corresponding experimental data for Uniswa Red. The parameter values for this simulation are given in Table 5.4.

As seen in Figures 5.8, 5.9 and 5.10, the canopy biomass is well captured by the

revised model and there is little difference in simulated biomass when comparing the error values in Tables 4.4 and 5.5. The same holds for leaf area.

	Canopy biomass (g)				Leaf Area (m^2)			
	Uniswa Red		S19-3		Uniswa Red		S19-3	
Temperature	MAE	N-S	MAE	N-S	MAE	N-S	MAE	N-S
23°C	2.83	0.85	4.57	0.73	168.05	0.84	366.33	0.13
28°C	3.05	0.97	2.67	0.95	101.80	0.99	39.79	0.996
33°C	2.78	0.92	2.95	0.94	160.94	0.97	499.74	0.74

Table 5.5: The mean absolute error and the Nash-Sutcliffe value for the leaf accumulation model's prediction of canopy biomass and leaf area for Uniswa Red and S19-3 when compared to the TCRU experimental data.

The average leaf area and canopy biomass for fifteen plants of the species S19-3 arranged as in Case 1 is shown in Figures 5.11 to 5.13. Similarly to Uniswa Red, there is little discernible difference in simulated leaf area and canopy biomass between the model described in Section 4.1.1 and the one described here.

5.5 Conclusion

The experiments described in this chapter, were conducted by the author during visits to the Crops For the Future greenhouses at the University of Nottingham and have allowed us to modify the mathematical model in such a way that competition for light is now better described.

We found that the previous model for ground cover G given in equation (3.7) and used in Chapters 3 and 4, caused G to be considerably underestimated at the preliminary stages of growth. We also found that the effect that planting density had on canopy spread was not as strong as in the greenhouse experimental data described in this chapter. The difference in simulated ground cover for the two planting densities was 8% compared to 17.4% in the experimental data.

With the addition of a new ODE we were able to better represent the change in ground cover over time. Using the new model for G given in equation (5.9), the difference in simulated ground cover for the two planting densities is now 17%. The canopy spread from the experimental data is not perfectly represented by equation

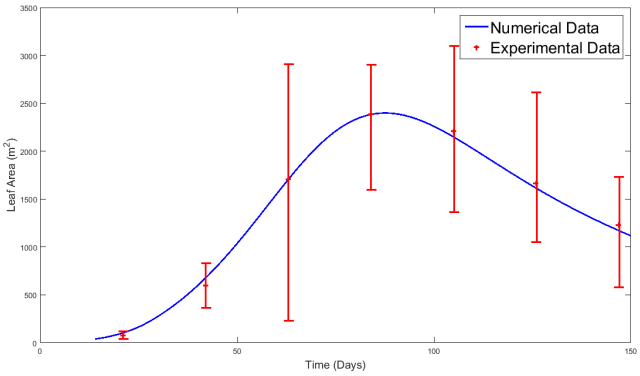

(a)

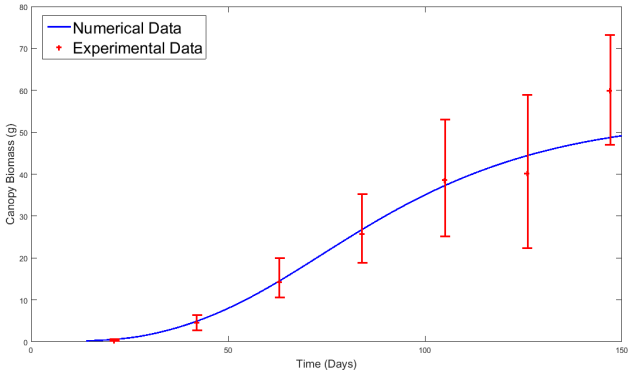

(b)

Figure 5.11: he simulated (a) leaf area and (b) canopy biomass compared with the experimental data for the species S19-3, using the data-fitted case of a temperature of 28°C. All parameters for each plant are equal. The revised system is described by the equations (5.7) to (5.10) with the revised parameter values given in Table 5.4. Each simulated plant is initiated at day 14, the estimated time of emergence and assumed to have a canopy comprising of one leaf at this point. The simulation data have been averaged over 15 plants grown in a five by three grid, the distance between plants in a row is 0.2m and the distance between rows is 0.35m. Red bars indicate the upper and lower bounds of the experimental data.

(5.9) in Figure 5.7. However, since the reliability of the data is questionable, we do not consider it necessary to mimic the results. Instead, we have simply attempted to simulate the qualitative behaviour. Similarly, although our model does not exhibit the same difference in canopy biomass for the two density treatments, we do not attempt to replicate the stronger impact on canopy biomass as we only have one data point.

The change to the way that ground cover is represented has not improved the models ability to simulate the leaf area and canopy biomass of the TCRU greenhouse

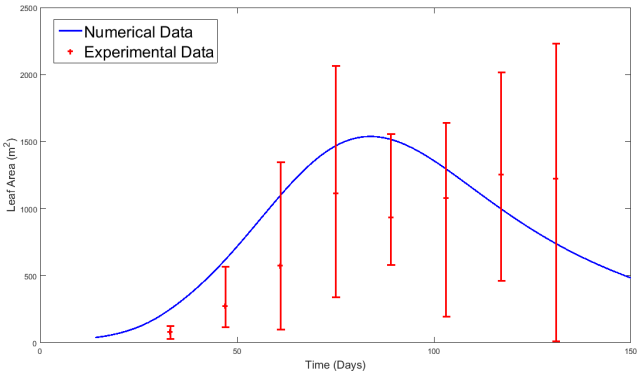

(a)

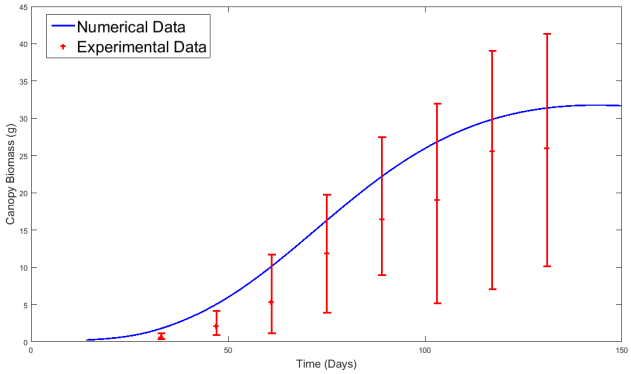

(b)

Figure 5.12: he simulated (a) leaf area and (b) canopy biomass compared with the experimental data for the species S19-3, using the non data-fitted case of a temperature of 23°C. All parameters for each plant are equal. The revised system is described by the equations (5.7) to (5.10) with the revised parameter values given in Table 5.4. Each simulated plant is initiated at day 14, the estimated time of emergence and assumed to have a canopy comprising of one leaf at this point. The simulation data have been averaged over 15 plants grown in a five by three grid, the distance between plants in a row is 0.2m and the distance between rows is 0.35m. Red bars indicate the upper and lower bounds of the experimental data.

data. What it has done is ensure that the impact of plant-plant competition is now more accurately described, thus increasing model robustness. For example, using the previous model for ground cover, we would have assumed that no competition exists when plants are arranged at a distance of 0.5m, as ground cover was being underestimated. We now know that that is not the case. As such, we are no longer limited to mimicking the behaviour of a single data set and are now able to make recommendations for different planting arrangements, which is undertaken in the following chapter.

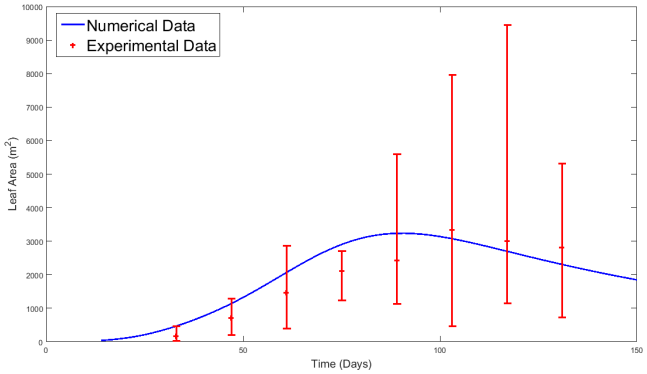

(a)

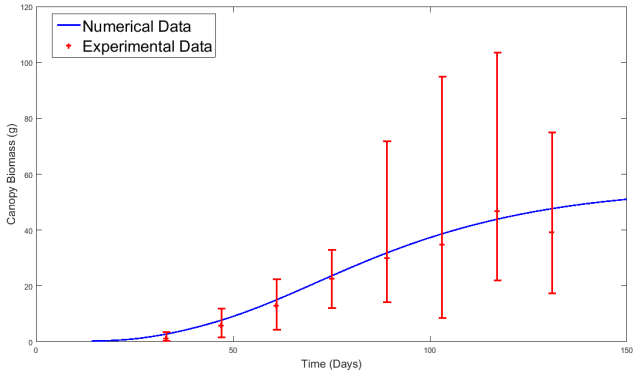

(b)

Figure 5.13: he simulated (a) leaf area and (b) canopy biomass compared with the experimental data for the species S19-3, using the non data-fitted case of a temperature of 33°C. All parameters for each plant are equal. The revised system is described by the equations (5.7) to (5.10) with the revised parameter values given in Table 5.4. Each simulated plant is initiated at day 14, the estimated time of emergence and assumed to have a canopy comprising of one leaf at this point. The simulation data have been averaged over 15 plants grown in a five by three grid, the distance between plants in a row is 0.2m and the distance between rows is 0.35m. Red bars indicate the upper and lower bounds of the experimental data.

Chapter 6

Optimising crop yield: monocrop

In Chapters 3 to 5 a mathematical model of the growth and development of bambara groundnut was formulated, compared to experimental data and revised where needed. It was found that the model was able to predict and describe the change in leaf area and canopy biomass over time to a satisfactory level, thus providing a good forecasting tool for crop yield. The design of the model allows us to investigate the effect individual plant size and position has on the overall population. As such, the model can be used to ask, not only what yield would be expected from a particular planting arrangement, but how might we arrange the plants to maximise crop yield.

In this chapter we define plant layout as the way that plants are set out in a plot; an example would be either regular rows and columns or, in contrast, plants could be placed in rings of increasing diameter around a central point. For these two examples planting distance is either the interval between plant centres along rows and columns or the interval across and within rings. Planting arrangement will then refer to the combination of a specific layout with a particular planting distance.

We begin by investigating the effect different arrangements have on crop yield. We consider a fixed plot area that is filled with N plants. The number of plants is determined by how many will fit into the area with a given planting distance.

Thus, a small planting distance will allow more plants to fit into the area and a large planting distance will allow fewer. We then compare the canopy biomass for different layouts and planting distances. The set up of this investigation allows us to find the pay-off between including more plants and allowing more space per plant in order to maximise total canopy biomass.

The results of the investigation show that the planting distance that gives the largest canopy biomass is that which gives the highest plant density. This is corroborated by our experimental data since, although the average biomass is much lower for the high density treatment, the sum of plant biomass for all plants within a metre squared is higher. For example, in the high density treatment there are 16 plants within 1m^2 with an average biomass of 46.42g giving a total of 742gm^{-2}. In the low density treatment there are 9 plants within 1m^2 with an average biomass of 66.74g giving a total of 600.66gm^{-2}. Within the field, planting distances are approximately 50cm by 30cm, differing between sites, which is not a planting distance that provides the highest planting density. Since the recommendation of our mathematical model is so different to what is done in the field we follow with a discussion of what it is we wish to optimise for. It is found that optimising for canopy biomass is not ideal and it is pod mass which is the desired quantity. We conclude that a means of simulating pod mass is necessary.

Once a means of simulating pod mass has been determined, the effect that layout and planting distance has on pod mass is investigated. An optimisation algorithm is then developed and applied to a number of plants of the same species. This is done for various scenarios, for example different plot sizes, temperatures, and for plant populations with and without random variation between plant parameters. Recommendations made by the optimisation algorithm are then discussed.

We then consider the case where, not only the plot size is fixed, but the number of seeds, and thus the number of plants, is fixed. A new optimising algorithm is developed and the recommendations are analysed and discussed.

6.1 Optimal planting arrangement: canopy biomass

The effect that plant layout and distance have on total canopy biomass is investigated in this section. Five different planting layouts have been chosen and a schematic of each layout can be found in Figure 6.1. The layouts are as follows:

- Figure 6.1(a) is a Uniform Grid, where plants are evenly spaced throughout the plot area.
- Figure 6.1(b) is similar to the Uniform Grid, however here every other row is indented by the amount of excess space between the row ends and the edge of the plot area (Indented grid 1).
- Figure 6.1(c) is another form of indented grid, where every other row is indented by half the planting distance (Indented Grid 2). The difference between this layout and the one shown in Figure 6.1(b) is the extent of the indent. In this layout the amount of indent may cause plants at the end of indented rows to not fit in the plot area and are therefore excluded. In the previous layout, the indentation is such that plants are never excluded.
- Figure 6.1(d) is a Circular layout where plants are arranged in rings with planting distance D between and within each ring.
- Figure 6.1(e) is a Random planting layout.

These five layouts have been chosen as they provide a good range of physically feasible examples.

To demonstrate the effect various planting arrangements have on the total canopy biomass we consider the case of planting in a 1m^2 plot with an initial planting distance of $D = 0.225$m. A planting distance of 0.225m would cause a 0.1m indent in Indented Grid 1 and an indent of 0.1125m for Indented Grid 2. This allows a clear difference between the three grid arrangements. In contrast, a distance of 0.25m would not allow any indentation in Indented Grid 1 and so there would be no

visible difference between the Uniform Grid and Indented Grid 1. For the Random layout, plants are not restricted to a set planting distance and so instead, the number of plants is fixed so that N would be equal to the number of plants in the Uniform Grid Layout with planting distance D. The inbuilt MATLAB function randn is used to generate N random numbers from a uniform distribution for both the horizontal and vertical position of each plant within the plot area.

The species Uniswa Red has been chosen since it is for this species that we have canopy size data. A temperature of 28°C is used as it is the optimum growth temperature for Uniswa Red. We initially set all plant parameters, including plant height parameters, to be equal. This means that any difference in plant growth is incurred by the position in relation to other plants. We later investigate how variation in plant parameters change the optimum planting arrangement. The mathematical model described by equations (5.7) to (5.10) is solved using the inbuilt MATLAB solver ode15s. Time steps are determined by the ODE solver to meet the pre-set relative and absolute tolerances of 1×10^{-6}. The simulations are run to 150 days for each layout illustrated in Figure 6.1 and the total and average canopy biomass for all N plants can be found in Table 6.1.

We see that the Circular Layout gives the highest average biomass per plant, but since the amount of plants that fit within the plot area is significantly fewer when compared to the other layouts, the total crop biomass is less. The Random layout gives the worst average and total canopy biomass. The arrangement that maximises canopy biomass per square metre is Indented Grid 1, followed closely by the Uniform Grid. This is because these layouts have the most plants, whilst making the best use of the available space. This is particularly true for Indented Grid 1 which makes use of the empty space between row ends and the plot boundary. For this layout there is a 2.74g biomass deficit per plant when compared to the Circular Layout, but an extra seven plants. In contrast, the Random layout, which does not make good use of the available space has a 14.14g biomass deficit, so although there are seven more plants than the Circular Layout, it does not make up for the loss of biomass to the

first eighteen plants. In a similar way, the increase in average canopy biomass does not make up for the decrease in N in Indented Grid 2.

	Canopy biomass (g)		
Layout	Average	Total	N
Uniform Grid	48.50	1212.42	25
Indented Grid 1	49.37	1234.17	25
Indented Grid 2	50.07	1101.50	22
Circular	52.81	950.55	18
Random	35.93	898.14	25

Table 6.1: The average and total canopy biomass of N plants within a $1m^2$ plot with a distance between plants of 0.225m.

It is not obvious if the optimum layout for a planting distance of 0.225m will apply to other planting distances. Thus we next investigate how canopy biomass varies for different planting layouts when the distance between plants is allowed to vary. We make the assumption that the supply of plants is unlimited and so the only limitation on N is how many plants can fit within the plot with a distance D between plants. The average and total canopy biomass of N plants within a $1m^2$ plot for planting distances ranging between 0.1m and 1m can be found in Figure 6.2.

From Figure 6.2(a) we see that the circular arrangement gives the highest average canopy biomass for all planting distances D. For large values of D, Uniform Grid, Indented Grid 1, Indented Grid 2, and the Circular Layout all give the same average canopy biomass per plant. This is because the plants are not interacting with each other and so competition is no longer a factor. For the random layout, the number of plants is chosen to match that of the Uniform Grid, Indented Grid 1 and Indented Grid 2, but the plant positions are allocated randomly using a uniform number generator to appoint vertical and horizontal spatial coordinates. This means that when there is no competition between plants for the other four layouts, there still could be for the random layout. This can be seen by observing that for large D, average canopy biomass is constant for all layouts except Random in Figure 6.2(a); here Random layout yields a lower canopy biomass caused by competition.

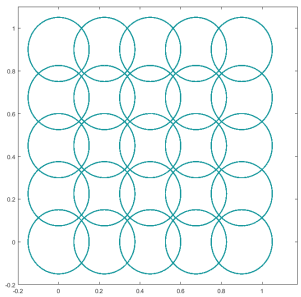

(a) Uniform Grid

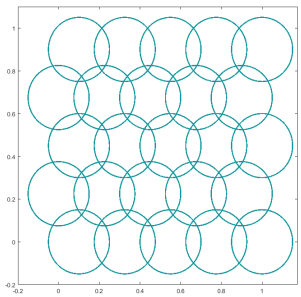

(b) Indented Grid 1

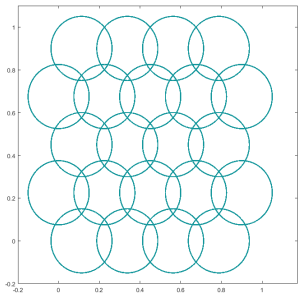

(c) Indented Grid 2

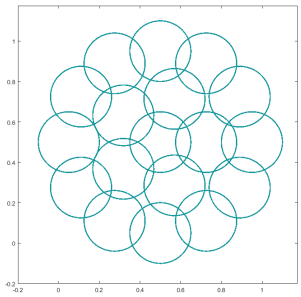

(d) Circular

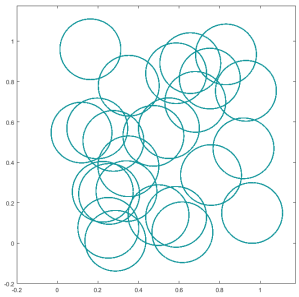

(e) One example of a random layout

Figure 6.1: A birds-eye schematic of five planting layouts in a $1m^2$ plot with planting distance D=0.225m. Here: (a) is a Uniform Grid, where plants are evenly spaced throughout the plot area; (b) is a grid where every other row is indented by the amount of excess space between the row ends and the edge of the plot area (in this case 0.1m); (c) is a grid where every other row is indented by half the planting distance (in this case 0.1125m), this amount of indentation causes one plant of every other row to be excluded from the plot; (d) is a Circular Layout where plants are arranged in rings of increasing diameter around a central plant, with distance D between and within rings; and (e) has plants randomly positioned, the number of plants is fixed so that N would be equal to the number of plants for the Uniform Grid case.

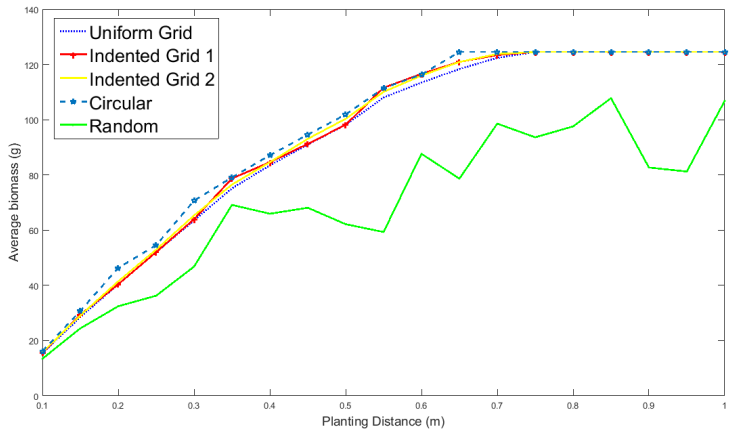

(a) Average individual canopy biomass

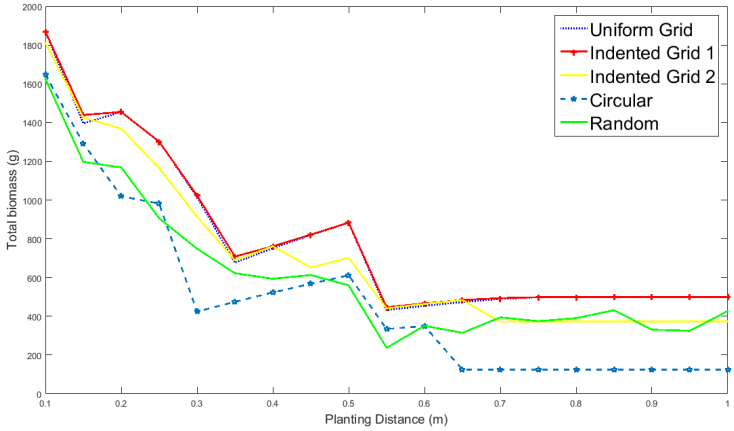

(b) Total Canopy biomass

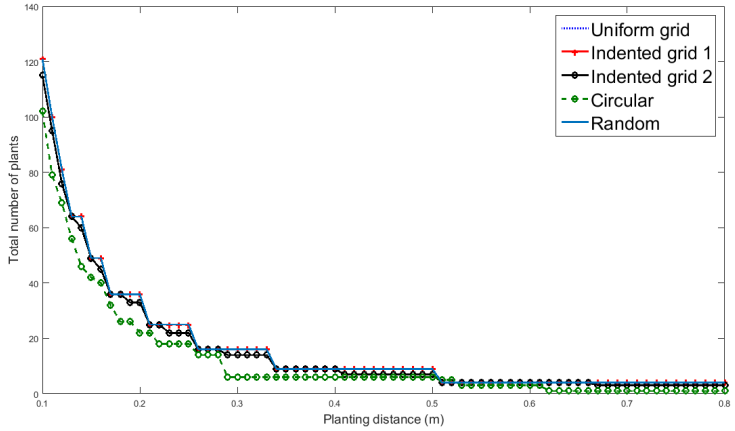

(c) Number of plants

Figure 6.2: A comparison of the average and total canopy biomass for N plants that fill a 1m^2 plot with a range of planting distances D for the five planting layouts shown in Figure 6.1. The temperature is 28°C and the plant species is Uniswa Red described by the system of equations (5.7) to (5.10).

Figure 6.2(b) shows us that the Uniform Grid and Indented Grid 1 layouts give the largest total canopy biomass for all of D, with Indented Grid 1 giving a marginal improvement for some values of D. The Uniform Grid and Indented Grid 1 layouts are equal when planting distance is such that there is no space between the end of rows and the plot edge, thus there is no indentation.

Figure 6.2(c) shows how the number of plants varies with planting distance. It can be seen by comparing Figures 6.2(a) and 6.2(b) that as the average canopy biomass goes up, the total canopy biomass goes down. This is because the number of plants decreases and as it does so the competition between them likewise decreases and so the average canopy biomass increases. With fewer plants in the plot there is a decrease in the total canopy biomass. It can also be seen that a small variation in average individual canopy biomass across layouts causes a large variation in total canopy biomass. The change in scale of variation is partially caused by the different numbers of plants N, but also by the multiplicative nature of summing over the entire plot.

The irregular behaviour of total canopy biomass for increasing D found in Figure 6.2(b) can be explained by the change in N over D as seen in Figure 6.2(c). In Figure 6.2(b) the canopy biomass increases up to a certain point and then suddenly falls; these decreases correspond with decreases in N seen in Figure 6.2(c). The cause of these step changes is a slow increase in the area per plant as D increases until a critical point where a further increase in D means that fewer plants can fit within the space. The decrease in N causes a larger change in biomass than the increase in area per plant.

It can be seen from the simulation results that for all layouts the recommended planting distance which gives the greatest crop yield (here canopy biomass) is that when as many plants as possible were squeezed into the planting area (i.e. $D = 0.1$m). This is contrary to what is typically done in the field, where planting densities are typically within 6 and 29 plants per metre squared [42]. Although this is not a typical field recommendation, experimental data have showm that the optimum

distance for maximising canopy biomass is in fact that which gives the highest plant density [34]. However canopy biomass is not the farmers output of interest, instead it is food yield which is often being optimised for. In the case of bambara groundnut this is the pod mass and so a means of modelling pod mass is now introduced into the model.

6.2 Simulating pod mass

Previously it was assumed that total pod mass is proportional to total canopy biomass at the time of maturation and so by optimising planting arrangement to maximise canopy biomass we were simultaneously maximising pod mass. This is a reasonable assumption for ideal conditions however, when the plant is stressed as a result of inter-plant competition for example, this would no longer be the case. We now wish to develop a more accurate method of simulating pod mass over time so that the effect plant competition has on pod mass can be taken into account.

We therefore introduce a new equation that allows us to calculate pod mass from canopy biomass. To do this we first consider the developmental stages of bambara groundnut and how these relate to pod growth. During the vegetative stage, accumulated energy is used for developing leaf, stem and root mass. During the podding phase however, the production and filling of pods is the primary sink of accumulated energy in optimum conditions. Therefore in order to simulate pod mass, the time at which the plant transitions from vegetative to podding needs to be determined.

There are two main methods for determining when the transition between vegetative and podding phases occurs, one method being a function of thermal time [32] and the other a function of days [11]. In this work we choose to use the number of days as it is more consistent with the TCRU experimental data. We would expect temperature to impact upon the time of podding however, this was not seen in the TCRU experimental data as can be observed in Table 6.2. Therefore we use a fixed number of days after sowing to determine the onset of podding. Improving this part

of the model would come under further work.

	Temperature	Interval of podding commencement (days)
Uniswa Red	23	[61, 75]
	28	[63,84]
	33	[61,75]
S19-3	23	[61,75]
	28	[63,84]
	33	[61,75]

Table 6.2: The range in days for which pod formulation commences in the species Uniswa Red and S19-3 for three temperature regimes of 23°C, 28°C, and 33°C as seen in the TCRU experimental data.

The experimental data for pod mass over time for Uniswa Red and S19-3 for three temperature regimes can be found in Figure 6.3. It can be seen that for Uniswa Red, despite plants producing pods between 61 and 75 days for temperatures of $23°C$ and $33°C$, only a few plants within the samples are producing pods at this time and it is not until 75 and 89 days that we see significant pod development. Thus to be consistent with the experimental data, the time at which podding commences is at 63 and 75 days for S19-3 and Uniswa Red, respectively.

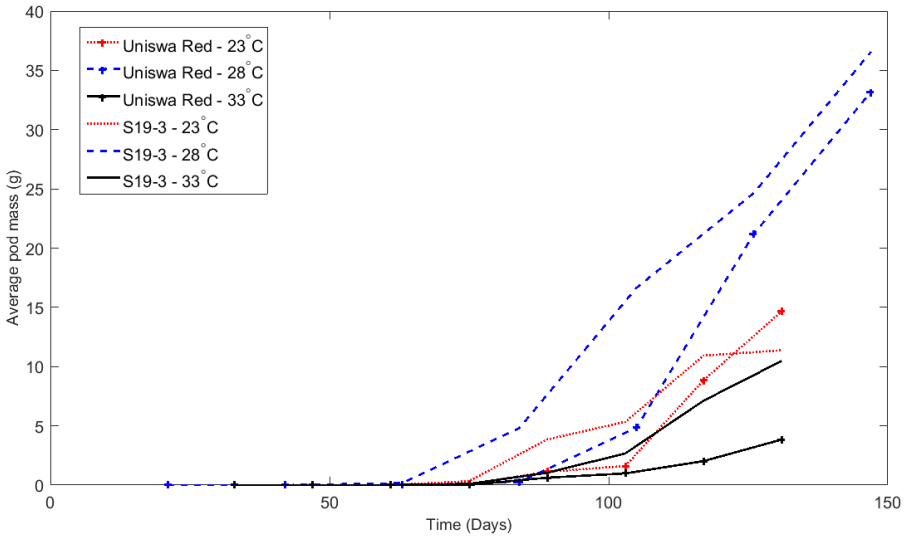

Figure 6.3: Variation in pod mass over time for the three temperature regimes of the TCRU experimental data for species Uniswa Red and S19-3.

Now that the point at which podding occurs has been established a new ODE de-

termining how pod mass varies in time is introduced. Again, we investigated several approaches before settling on the one described in this section. We assume that the increase in pod mass $P_i(t)$ is a proportion of the increase in canopy biomass $c_i(t)$. Hence the growth rate of $P_i(t)$ is controlled by the growth rate of $c_i(t)$. We further assume that as pod mass increases it becomes a stronger sink for absorbed energy and hence acquires a larger proportion of canopy biomass growth as it becomes larger itself. Thus, the change in $P_i(t)$ in time depends on both canopy biomass growth and itself. We finally assume that pod mass can not be larger than the canopy biomass and so $c_i(t)$ will be the carrying capacity for pod mass. Thus we calculate the change in pod mass over time such that

$$\frac{dP_i(t)}{dt} = \alpha_p T_{sp} P_i(t) \frac{dc_i(t)}{dt} \left(1 - \frac{P_i(t)}{c_i(t)}\right) - d_p P_i(t), \tag{6.1}$$

where α_p is a growth rate for pod mass with units g^{-1}, T_{sp} is a temperature stress and d_p is the pod decay rate. The affect that competition has on pod mass is included via $\frac{dc_i(t)}{dt}$. This approach to simulating pod mass is newly introduced in this work.

The temperature stress is only in effect for high temperatures and is a parameter that ranges between 0 and 1 where 1 indicates no stress. Hence T_{sp} is given by

$$T_{sp} = \begin{cases} 1, & T \leq T_{opt}, \\ 1 - \left|1 - \omega \frac{T - T_{crit}}{T_{opt} - T_{crit}}\right| & T_{opt} < T < T_{ceil}, \\ 0 & T \geq T_{ceil}, \end{cases} \tag{6.2}$$

where ω is a species specific parameter to be determined and controls how far temperature stress decreases from 1 as temperature increases from the optimum.

We non-dimensionalise equation (6.1) by rescaling the dimensional variables so that

$$P_i(t) = c_0 \hat{P}_i(t), \quad c_i(t) = c_0 \hat{c}_i(t) \quad \text{and} \quad t = \frac{\tau}{\alpha_h},$$

where a hat signifies a non-dimensional physical variable and τ denotes non-dimensional time. Using these substitutions, equation (6.1) becomes

$$\frac{d\hat{P}_i(\tau)}{d\tau} = \bar{\alpha}_P T_{sp} \hat{P}_i(\tau) \frac{d\hat{c}_i(\tau)}{d\tau} \left(1 - \frac{\hat{P}_i(\tau)}{\hat{c}_i(\tau)}\right) - \bar{d}_p \hat{P}_i(\tau), \tag{6.3}$$

where

$$\bar{\alpha}_P = \alpha_P c_0 \quad \text{and} \quad \bar{d}_P = \frac{d_P}{\alpha_h}.$$

The initial condition for pod mass is $P(0) = P_0$, which for this work is equivalent to 1 pod with a mass of 1g at 75 DAS. For convenience, hereafter the hats and bars will be dropped.

6.2.1 Numerical Simulation

In this section the model equations (5.7) to (5.10) with the addition of (6.3) are solved numerically and the simulated pod mass is compared to experimental data. Before this can be done it is necessary to parameterise equation (6.3) for α_P and d_p. This is done using the inbuilt MATLAB function lsqcurvefit which is a nonlinear least-squared solver. We take a least-squared fit of the TCRU experimental dataset against a model simulation of pod mass for 15 plants described by equation (6.3). Both simulated and experimental plants are arranged as in Figure 3.8 at a temperature of 28°C and it is assumed that all parameters are equal between plants. The parameters devised here are summarised in Table 6.3, all other parameters remain the same as those stated in Table 5.4.

Parameter	Value
α_p	0.22^*, $0.18^\dagger$
α_p	$1 \times 10^{-4*}$, $8 \times 10^{-3\dagger}$

Table 6.3: Table of parameter values and descriptions. For parameters that are species specific, * denotes the species S19-3 and † denotes Uniswa Red. These parameter values have been found for when ground cover is described by equation (5.1).

We can now numerically solve the model equations. There have been no changes made to the equations for cumulative thermal time, leaf area, ground cover and

canopy biomass, which are all described by equations (5.7) to (5.10), as change in pods does not affect the partitioning to other organs. Instead, partitioning to each organ is independent so that changes in parameters, such as specific leaf area, over time do not need to be simulated. The only change is the addition of equation (6.3) to the system. As before we utilise the inbuilt Matlab ODE solver ode15s where the time steps are adapted by the solver's algorithm to meet the pre-set tolerance, which in this case is 1×10^{-6}.

As in previous chapters a simulation of fifteen plants is conducted where plants are arranged in three rows of five with a distance within columns of 35cm and a distance within rows of 20cm (Figure 3.8). This has been done to replicate the conditions of the TCRU greenhouse experiments that have provided us with the experimental data used in the previous two chapters. As before the two species that are simulated are Uniswa Red and S19-3, with their respective parameter values given in Table 5.4 and all plants within the simulations are assumed to have the same height. The simulated pod mass is compared to the experimental data for three temperatures of 23°C, 28°C and 33°C for Uniswa Red and S19-3 in Figures 6.4 and 6.5 respectively. Note that figures 6.4(b) and 6.5(b) are for the simulation data that has been fitted to the experimental. Leaf area and canopy biomass have not changed in our model from those of Figures 5.8 to 5.13 in Chapter 5 and it is not necessary to repeat simulations for these.

The simulations of Uniswa Red and S19-3 show a good fit to the experimental data for all three temperatures, with the average pod mass being within the minimum and maximum of the experimental data for all 8 data points. The mean absolute error and the Nash-Sutcliffe value for both species and all three temperatures can be found in Table 6.4. The mean absolute error is small for all three temperatures and for both species. The Nash-Sutcliffe is similarly within an acceptable distance from 1 indicating that the model is a good representation of the data. Thus we are satisfied with equation (6.3) as being a good representation of the evolution of pod mass in time.

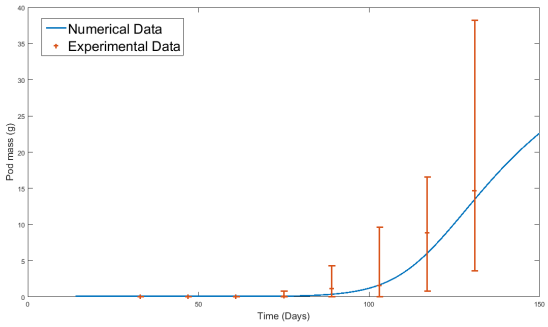

(a)

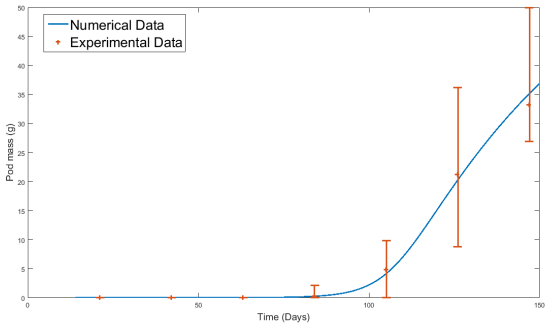

(b)

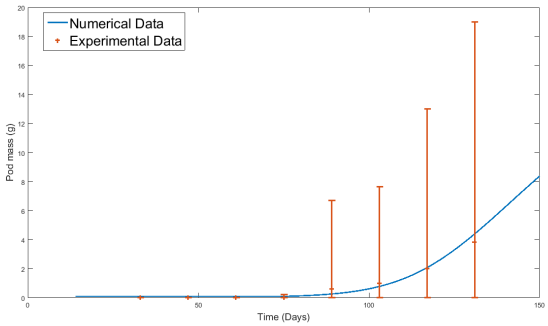

(c)

Figure 6.4: The simulated pod mass compared with the experimental data for the species Uniswa Red, where all parameters for each plant are equal and grown for temperatures of (a) 23°C, (b) 28°C, and (c) 33°C. The system is described by the equations (5.7) to (5.10), with the addition of equation (6.3); the parameter values given in Table 5.4 with additional parameters given in Table 6.3. Here, the data-fitted case is for a temperature of 28°C. Each simulated plant is initiated at day 14, the estimated time of emergence and assumed to have a canopy comprising of one leaf at this point. The simulation data have been averaged over 15 plants grown in a five by three grid, the distance between plants in a row is 0.2m and the distance between rows is 0.35m. Red bars indicate the upper and lower bounds of the experimental data.

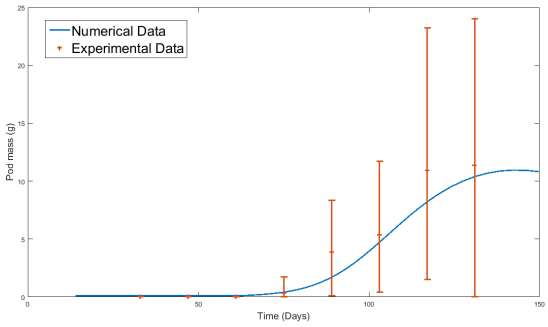

(a)

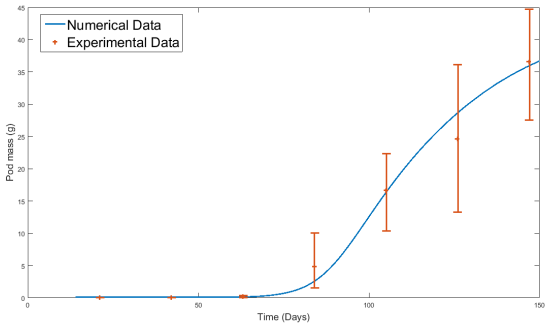

(b)

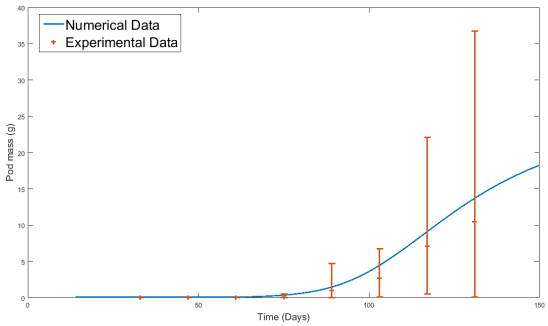

(c)

Figure 6.5: The simulated pod mass compared with the experimental data for the species S19-3, where all parameters for each plant are equal and grown for temperatures of (a) 23°C, (b) 28°C, and (c) 33°C. The system is described by the equations (5.7) to (5.10), with the addition of equation (6.3); the parameter values given in Table 5.4 with additional parameters given in Table 6.3. Here, the data-fitted case is for a temperature of 28°C. Each simulated plant is initiated at day 14, the estimated time of emergence and assumed to have a canopy comprising of one leaf at this point. The simulation data have been averaged over 15 plants grown in a five by three grid, the distance between plants in a row is 0.2m and the distance between rows is 0.35m. Red bars indicate the upper and lower bounds of the experimental data.

	Uniswa Red		S19-3	
Temperature	MAE	N-S	MAE	N-S
23°C	0.65	0.95	0.86	0.92
28°C	0.56	0.995	1.05	0.98
33°C	0.2	0.96	0.84	0.99

Table 6.4: The mean absolute error and the Nash-Sutcliffe value for the prediction of pod mass for Uniswa Red and S19-3 using equation (6.3) when compared to the TCRU experimental data.

6.3 Optimal planting arrangement: pod mass

We repeat the simulation of Section 6.1 for different planting arrangements this time optimising total pod mass.

The average and total pod mass of N plants within a $1m^2$ plot can be found in Figure 6.6 for planting distances between 0.1m and 1m for all five layouts. The number of plants N is determined by how many plants with distance D between them can fit into the $1m^2$ plot.

There are many similarities between the results of this section and those of Section 6.1. Figure 6.6(a) shows the average pod mass per plant for the range of planting distances D. As before, the Circular layout has a slightly higher average pod mass. As D increases so too does the average pod mass. For the Random layout there is much irregularity as D increases, this is due to the randomness of plant positions and so the space is not always best used. For layouts Uniform grid, Indented Grid 1, Indented Grid 2 and the Circular Layout, the average pod mass increases until the point where D is large enough that there is no competition between plants. After this point the average pod mass ceases to increase with further increases to D.

Figure 6.6(b) shows how the total pod mass of all N plants changes with D. The layout that gives the highest pod mass is Indented Grid 1. There are points at which the pod mass for Indented Grid 1 is equal to that of the Uniform Grid layout, these points are when D is such that there is space between row ends and the plot edge and hence no indentation of the plants.

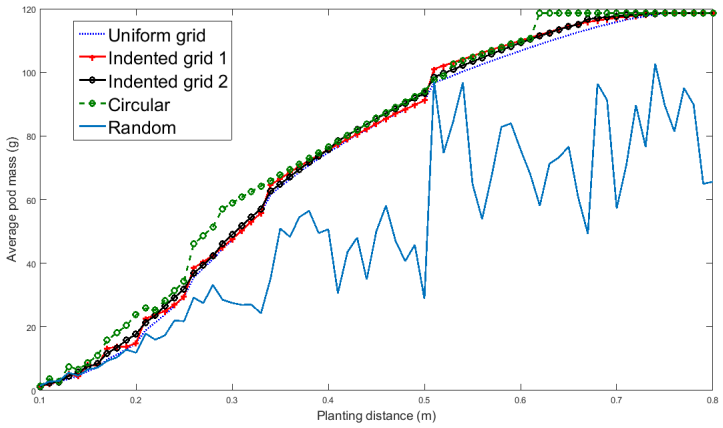

(a) Average pod mass per plant

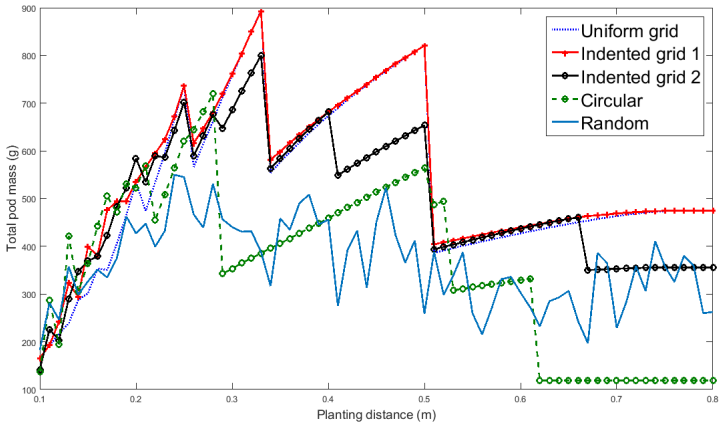

(b) Sum crop pod mass

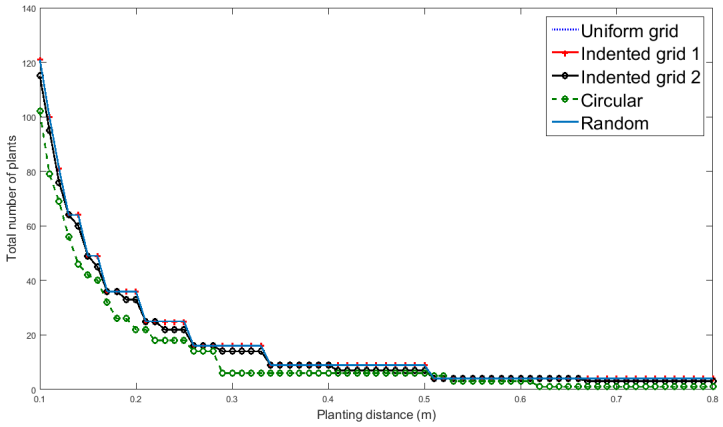

(c) Number of plants

Figure 6.6: A comparison of the average and total pod mass for N plants that fill a 1m^2 plot with a range of planting distances D for the five planting layouts shown in Figure 6.1. The temperature is 28°C and the plant species is Uniswa Red.

As found when investigating the effect planting arrangement has on canopy biomass, total pod mass rises and falls in an irregular pattern. This is because although there is a general downward trend in N as D increases, for small increments in D there is not necessarily a change in N. When D increases, but plant number does not change, there is more space per plant causing an increase in the total pod mass. Eventually D is increased to a critical point whereby the number of plants suddenly decreases and thus there is a sharp drop off of total pod mass. The decreases in total pod mass correspond with the drops in plant number that can be found in Figure 6.6(c).

Contrary to what was found in Figure 6.2, the optimum planting distance that maximises total pod mass is no longer the minimum distance allowed in the system of 0.1m and is now 0.33m. Since the optimum planting distance is no longer that which gives the highest planting density we can no longer intuitively determine D for different layouts, plot sizes and plant size. Therefore a new way of finding the optimum D must be devised for various scenarios and plant characteristics.

6.4 An optimisation algorithm for homogeneous crops

We introduce here an optimisation algorithm which maximises total crop yield (pod mass) by optimising planting distance for the different planting layouts discussed so far.

In order to allow for different planting distances between rows and columns we define D_r as the distance between plants in a row and D_c as the distance between plants in a column. We then set a fixed plot size $\hat{P} \times \hat{P}$ and a minimum distance D_{min} which is the smallest feasible spacing between plants and a maximum distance D_{max} which is the smallest value for which plants no longer interact.

The algorithm begins by letting $D_c = D_{max}$ and defining a set of values to be substituted for D_r denoted by $\mathbf{D}_r$. Thus rows of plants do not interact with each other but plants within rows might. Here, $\mathbf{D}_r$ spans between D_{min} and D_{max} with increments of 10cm to give an initial sampling space.

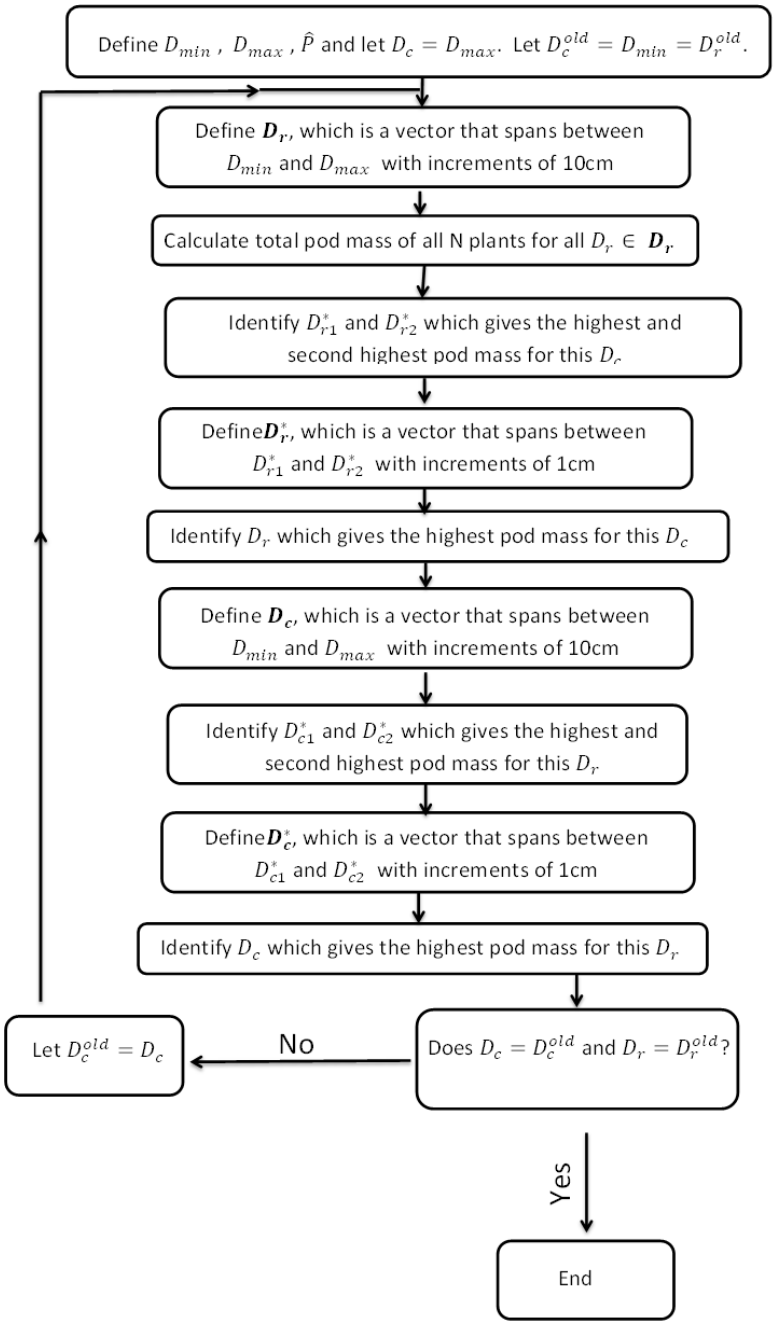

Figure 6.7: Diagram of the optimisation algorithm for finding D_r and D_c that maximises total pod mass of a homogeneous field of crops.

To complete the forward optimisation of D_r, the pod mass is simulated for $D_c = D_{max}$ and for all $D_r \in \mathbf{D}_r$. The total pod mass at 150 days is summed for all N plants within the plot area and compared for all $D_r \in \mathbf{D}_r$. The highest

and second highest total pod mass are identified and, with them, the associated elements of $\mathbf{D}_r$ labelled D^*_{r1} and D^*_{r2} respectively. The aim of this is to narrow in on the optimum planting distance space that gives the maximum pod mass. Having confined the range of planting distances we now test the yield for a finer resolution of planting distances.

We define a new set of values, denoted by $\mathbf{D}^*_r$, that span between D^*_{r1} and D^*_{r2} with increments of 1cm. This has been chosen as it is unlikely that a higher level of sensitivity could be achieved in a physical environment. The total pod mass at 150 days is summed for all N plants within the plot area and compared for all $D_r \in \mathbf{D}^*_r$. We then identify the highest pod mass and its associated element of $\mathbf{D}^*_r$, which is labelled D^*_r.

Once the optimum distance between plants in a row is found, we set $D_r = D^*_r$ and repeat the process for D_c to find the optimum distance between plants in a column. We then start the algorithm from the beginning, however, instead of letting $D_c = D_{max}$ as before, we begin the algorithm with $D_c = D^*_c$ and find new values for D^*_r and D^*_c. This process is repeated until the new values of D^*_r and D^*_c are the same as those from the previous iteration. These steps are summarised in Figure 6.7.

It is possible in this algorithm for the optimum recommendations to approach a local maximum and not the global maximum. This can be avoided by taking a finer resolution in the initial sampling space, i.e $\mathbf{D}_r$. In doing this however, we incur a significant time increase. It is important for us to ensure that the optimisation algorithm is accessible in a reasonable amount of time and so we wish to minimise algorithm running times where possible. Further investigation, described in more detail in Section 6.4.1, has shown us that when the algorithm gives a local maximum, instead of the global, the difference in total pod mass is less than 2% between the two. Since this is well within model error it has been decided to not increase the resolution of the sampling space.

Plot Size	Temperature	Layout	D_r	D_c	Total pod mass	N
1	23°C	Uniform Grid	0.5	0.5	666	9
	28°C	Indented Grid 1	0.33	0.33	897.3	16
	33°C	Uniform Grid	0.5	0.5	704.1	9
1.5	23°C	Uniform Grid	0.5	0.37	1196	20
	28°C	Uniform Grid	0.37	0.3	1616.3	30
	33°C	Uniform Grid	0.5	0.5	1200	16
2	23°C	Uniform Grid	0.4	0.5	1873.6	30
	28°C	Uniform Grid	0.4	0.33	2555.4	42
	33°C	Uniform Grid	0.5	0.5	1823.9	25
2.5	23°C	Uniform Grid	0.5	0.41	2649.1	42
	28°C	Indented Grid 1	0.31	0.41	3670.4	63
	33°C	Uniform Grid	0.5	0.5	2578.3	36
3	23°C	Indented Grid 1	0.41	0.5	3589.1	56
	28°C	Uniform Grid	0.3	0.42	5050.7	88
	33°C	Uniform Grid	0.5	0.5	3462.7	49
3.5	23°C	Indented Grid 1	0.43	0.43	4682.4	81
	28°C	Uniform Grid	0.35	0.35	6628.6	121
	33°C	Uniform Grid	0.5	0.5	4477.1	64
4	23°C	Uniform Grid	0.4	0.5	6032.7	99
	28°C	Indented Grid 1	0.33	0.4	8348	143
	33°C	Indented Grid 2	0.4	0.57	5690.4	88
4.5	23°C	Indented Grid 1	0.4	0.45	7500.8	132
	28°C	Uniform Grid	0.25	0.45	10702.5	209
	33°C	Uniform Grid	0.5	0.45	6900.3	110

Table 6.5: The optimum layout, column and row distance that gives maximum pod mass for temperatures of 23°C, 28°C and 33°C and species Uniswa Red.

6.4.1 Results

The algorithm described in Section 6.4 is applied to Uniswa Red for temperatures of 23°C, 28°C and 33°C for plot sizes ranging between 1m^2 and 4.5m^2. To simplify this process there is no variation between plant parameters, i.e. all plants are identical. The optimal layout, row and column distances for varying plot sizes are stated in Table 6.5. For this optimisation process we only consider the layouts Uniform Grid, Indented Grid 1 and Indented Grid 2 as these produced consistently higher total pod yield than the Circular and Random Layouts.

The recommendations for optimising planting distance and layout vary dependant on plot size and temperature. It can be seen that the optimal layout and planting distance changes as plot size changes, indicating that the results are not

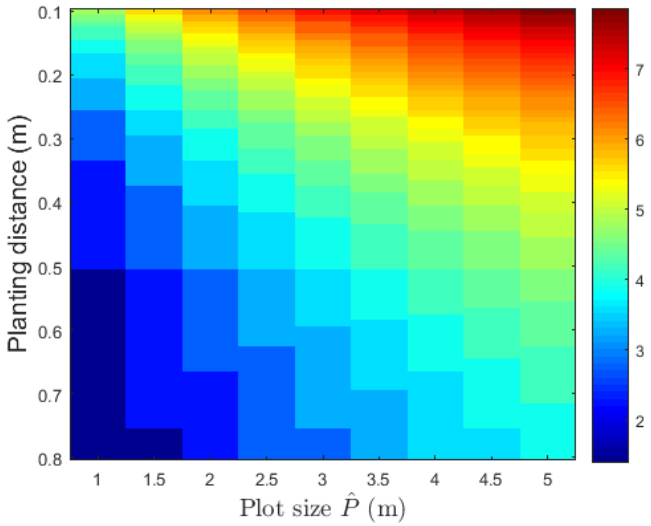

(a) Plant number

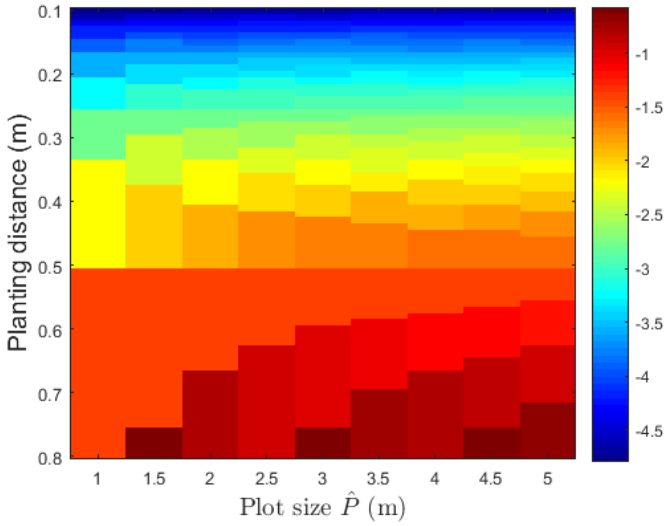

(b) Average area per plant

Figure 6.8: The plant number and average area per plant for a range of planting distances and plot sizes for the Uniform Grid layout. Note here, the average area per plant is shown on a logarithmic scale.

scalable. The reason for this is that the optimisation algorithm is attempting to find the balance between the number of plants and the space per plant. This balance shifts as plot size increases because the number of plants that can fit within the plot changes.

We find that the recommended arrangement varies between Uniform Grid and

Indented Grid 1. Further investigation shows that in all cases, the optimum distance is such that a further increase of 0.01m to D_r or D_c would cause a drop in N. Sometimes this planting distance would cause space to be left between the end of the rows and the plot edge, leaving room for every other row to be indented. If this is the case then Indented Grid 1 is recommended. If we were to increase planting refinement further so that minimum distance is less than 1cm we would reduce the occurrences of Indented Grid 1 being the optimum arrangement.

In general the recommendation for temperatures of 23°C and 33°C is to plant with a lower density than when compared to the recommendation for 28°C. This would imply that the combination of temperature and competition stresses is particularly detrimental to plant growth and hence not linear.

To make sense of the recommendations we explore how the number of plants and the space per plant changes in relation to each other. We calculate the number of plants and the average space per plant for a range of planting distances and plot sizes. We use a uniform grid and explore $D_r = D_c$ ranging between 0.1m to 0.8m with increments of 0.01m. The number of plants and the average area per plant for a range of plot sizes and planting distances are shown in Figure 6.8.

It can be seen that the number of plants within the plot increases monotonically with plot size and decreases with increased planting distance. What can be seen is a 'step' effect such that as planting distance increases there is no change in the number of plants until a critical point at which there is a sudden change in N. This is the cause of the 'block-like' effect in Figure 6.8(a). For larger values of D there is more robustness in regards to changes in N with further increases to D. For example, for $\hat{P} = 1$m and $D = 0.1$m, there are 121 plants in the plot. An increase of 0.01m to D would cause N to reduce to 100. This is compared to when D=0.51m giving 4 plants in the plot. The number of plants will not change until D increases to more than 1m at which point there will only be 1 plant in the plot area.

The average area per plant increases monotonically with increased planting distance in the same 'step' pattern found with the number of plants in Figure 6.6(c).

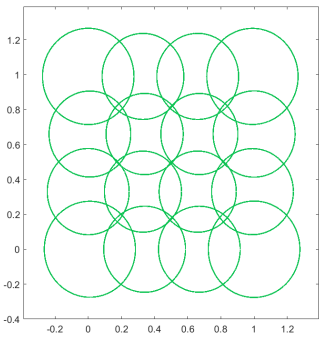

(a) $\hat{P} = 1\text{m}$ ($\frac{\hat{P}^2}{N} = 0.0625\text{m}^2$).

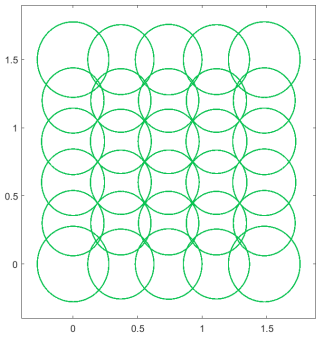

(b) $\hat{P} = 1.5\text{m}$ ($\frac{\hat{P}^2}{N} = 0.075\text{m}^2$).

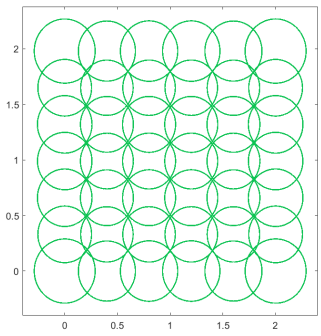

(c) $\hat{P} = 2\text{m}$, ($\frac{\hat{P}^2}{N} = 0.095\text{m}^2$).

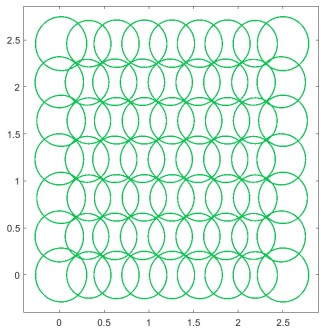

(d) $\hat{P} = 2.5$, ($\frac{\hat{P}^2}{N} = 0.099\text{m}^2$).

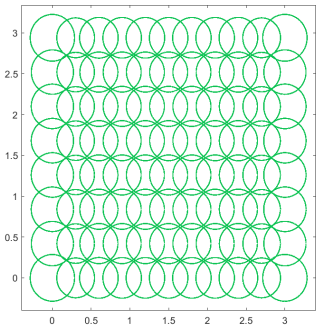

(e) $\hat{P} = 3\text{m}$, ($\frac{\hat{P}^2}{N} = 0.102\text{m}^2$).

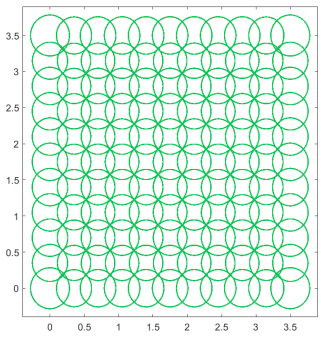

(f) $\hat{P} = 3.5\text{m}$, ($\frac{\hat{P}^2}{N} = 0.101\text{m}^2$).

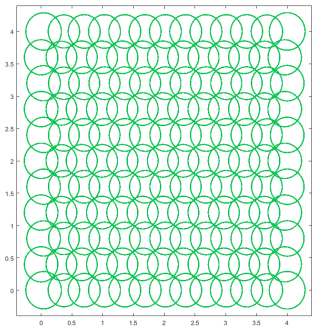

(g) $\hat{P} = 4\text{m}$, ($\frac{\hat{P}^2}{N} = 0.1119\text{m}^2$).

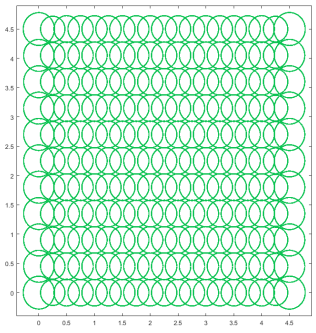

(h) $\hat{P} = 4.5\text{m}$, ($\frac{\hat{P}^2}{N} = 0.0969\text{m}^2$).

Figure 6.9: The above plant view of the optimum arrangement of Uniswa Red grown at 28°C as detailed in Table 6.5. The canopy arrangements are shown at 150 days. Here, $\frac{\hat{P}^2}{N}$ is plot size over the number of plants which gives the average area per plant.

Conversely, the average area per plant does not show monotonic behaviour with regards to plot size. What we see is a staggered effect where average space per plant shows a general non-monotonically increasing trend. The cause of this is that for

fixed D, there may be wasted space for a particular plot size, for example when $D = 0.8$m and $\hat{P} = 1$m there are 4 plants within the plot size with 0.2m of empty space at the end of rows and columns, this gives 0.25m^2 per plant. Increasing $\hat{P}$ to 1.5m will not allow more plants into the space, giving 0.56m per plant. A further increase to $\hat{P} = 2$m will allow an extra row and column of plants to fit within the plot. This gives 9 plants with 0.4m of empty space at the end of each column and row and 0.44m^2 per plant.

There is a clear shift in behaviour at a planting distance of 0.51m; for this planting distance the number of plants increases uniformly for increases of 0.5m to $\hat{P}$. This can be seen by the constant average area per plant for planting distance of 0.51m in Figure 6.8(a). This only happens when $\hat{P}$ increases by 0.5m increments.

To further investigate the recommendations we take a closer look at each optimum planting arrangement for Uniswa Red grown at a temperature of 28°C for the different plot sizes discussed in Table 6.5. We first examine what the recommendations are; a bird's-eye view of the simulation for optimum arrangements for each plot size can be found in Figure 6.9.

From Figure 6.9 we can see that the recommended layout changes between Uniform Grid and Indented Grid 1, with a general trend for increasing indent for increased plot size. As mentioned previously, D_r is always such that a further increase of 0.01m would cause a decrease in N. As the plot size increases, this generally causes that particular value of D_r to give a larger indentation.

The average area per plant for each recommendation has a general upward trend as plot size increases. This would imply that as plot size increases, more plants can fit into the plot area and so including another row or column of plants may not be as beneficial as increasing the pod mass of all N plants. Conversely, for small plot sizes, another row or column may have a significant impact.

The total pod mass of all N plants for the full range of planting distances for a plot size of $\hat{P} = 2.5$m is recorded and given in Figure 6.10. Plants are arranged in Indented Grid 1. What can be seen is that for both plot sizes the total pod

mass varies considerably over the range of D_r and D_c. We see the same 'step' effect described previously where pod mass increases until a peak point at which any further increase to D_r or D_c causes a drop in N and therefore a sudden drop in pod mass. These peaks occur at multiple points in the sample space for both plot sizes and the magnitude of some of the peaks are relatively similar. One such example of this can be found for $\hat{P} = 2.5$m in Figure 6.10(a), when for D_r =0.41m and D_c =0.25m the pod yield is 3722.8g, which gives the highest yield with 77 plants. Similarly when $D_r = 0.31$m and D_c =0.41m there is a pod yield of 3672.8g for 63 plants, this is 1.34% less than the highest yield however for 22.22% decrease in N. What causes one peak to be larger than the other is the fine balance between plant number and pod mass per plant, hence even a small change in the environment can cause the highest pod mass peak to switch. The result of this is that the optimum arrangement changes drastically, however pod yield may only be improved by a few grams.

Figure 6.10(a) gives the total pod mass of all N plants for the full range of planting distances for a plot size of $\hat{P} = 2.5$m where plants are arranged in Indented Grid 1. We can compare this to the Uniform Grid in Figure 6.10(b). There is a clear difference in the symmetry of between Uniform Grid and Indented Grid 1. This is caused by the shifted rows for some of values of D_r in Indented Grid 1. Thus we would not expect the same pod mass when we switch D_r and D_c.

This approach to finding the maximum pod mass for a given arrangement is exhaustive and has a considerably longer running time than our optimisation algorithm. Although not shown here, we applied this exhaustive technique to several of the scenario's given in Table 6.5. It was found that in all cases we tested, the difference in pod mass between the given local maximum and the global was less than 2%. This is well within the model error. We also found, that by increasing the sampling point resolution, we were able to find the global maximum.

In Figure 6.9, we find that generally the average area per plant decreases between $\hat{P} = 4$m and $\hat{P} = 4.5$m. As a further investigation we consider each of these

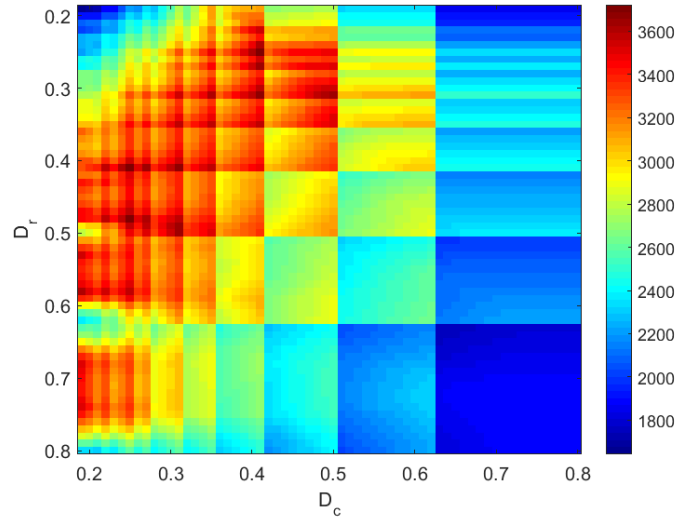

(a)

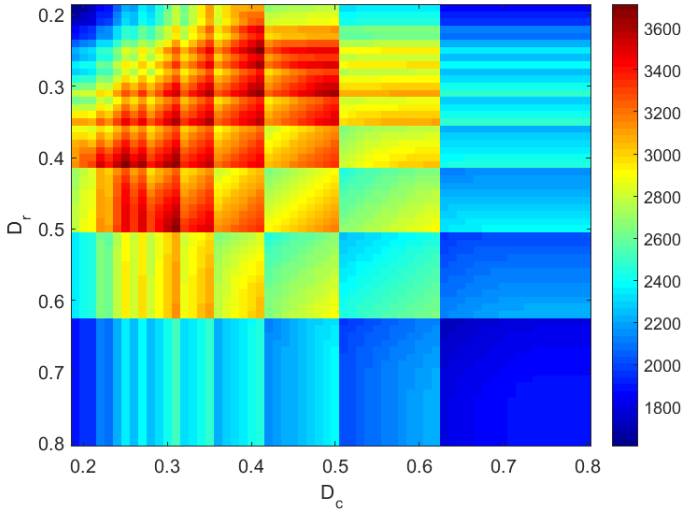

(b)

Figure 6.10: The total pod yield for for a range of values of D_r and D_c in a plot sizes of 2.5m×2.5m in both an Indented Grid 1 (a) and a Uniform Grid (b).

plot sizes against the other's optimal recommended arrangement. We do this to highlight how the recommendation for one plot size does not necessarily suit another, which demonstrates that the system is not scalable. An above plant view of both plot sizes with their respective recommended arrangements can be found in Figure 6.11 along with an above plant view of each plot size with the other's recommended arrangement. For a plot size of 4m×4m we can compare the recommended arrangement in Figures 6.11(a) with the recommended arrangement of 4.5m×4.5m

in Figure 6.11(b). For a plot size of 4.5m×4.5m we can compare the recommended arrangement for 4m×4m in Figure 6.11(c) with the recommended arrangement for 4.5m×4.5m in Figure 6.11(d). For simplicity we will refer to these as (a), (b), (c) and (d), respectively as these correspond with the figures for which each scenario can be observed.

To summarise, (a) and (b) have a plot size of $\hat{P} = 4$m, whereas (c) and (d) have a plot size of $\hat{P} = 4.5$m. (a) and (c) are arranged in Indented Grid 1 with $D_r = 0.33$ and $D_c = 0.4$, whereas (b) and (d) are arranged in a Uniform Grid with with $D_r = 0.25$ and $D_c = 0.45$.

As seen in (c) in Figure 6.11(c) if we use the recommendations for $\hat{P} = 4$m when $\hat{P} = 4.5$m then there will be 168 plants in the plot area, which is a 17.5% increase to N compared to (a). This is a much smaller percentage increase in N when comparing to how N changes between cases (a) and (d). The average pod mass for (c) is 57.81g which is slightly lower than 58.38g for (a), this shows that the mean pod mass changes with plot size even when layout, D_r and D_c stay the same. The reason for this is that there is a lower proportion of plants on the border of the plot for (c) and so more plants are experiencing competition from all sides. The average pod mass for (d) is 51.21g for 209 plants, this is 6.6g less than what is found in (c). Clearly for an increase of 46.15% to N it is more efficient to continue planting at the higher density with a loss of 11% to the average biomass. This is an example of how the balance between the number of plants and the average area per plant changes with $\hat{P}$. In this case, an addition of 41 plants with an average of 51.21g average pod mass per plant will give an extra 2099.6g of yield. However increasing the yield of 168 plants by 6.6g gives a total increase to yield of 1108.8g.

6.4.2 Including random variation between plants

So far in this chapter, plant parameters have been the same for all plants. We have previously considered how random variation affects the canopy biomass over time and found that there was minimal impact for a variation of 10%. We would now like

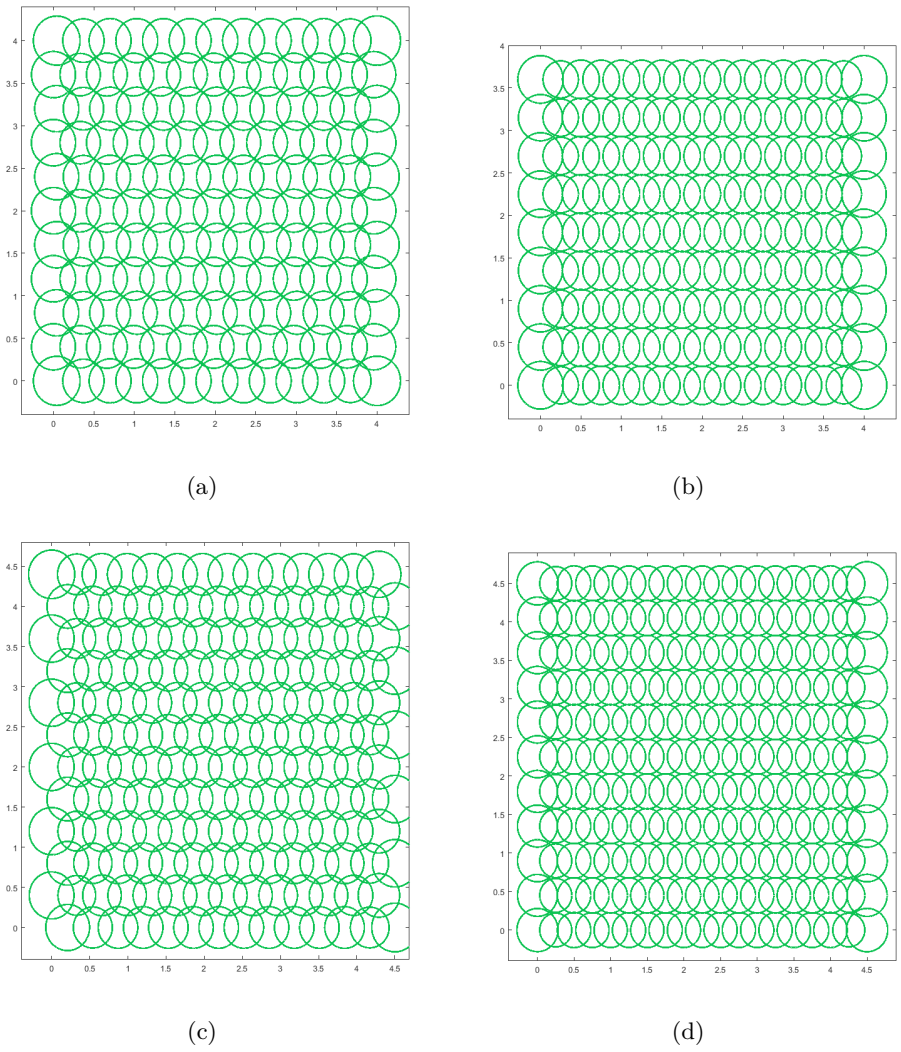

(a) (b)

(c) (d)

Figure 6.11: An above plant view of the optimum distance and layout of plants for plot sizes of 4m×4m and 4.5m×4.5m and also an above plant view of same plot sizes, but with the others optimum distances and layout. The species is Uniswa Red and the temperature is set to 28°C. Here, (a) is the recommendations for a 4m×4m plot in a 4m×4m plot size; (b) is the recommendations for a 4.5m×4.5m plot in a 4m×4m plot size; (c) is the recommendations for a 4m×4m plot in a 4.5m×4.5m plot size; and (d) is the recommendations for 4.5m×4.5m plot in a 4.5m×4.5m plot size.

to confirm this result by investigating how random variation between plants would affect the algorithm's recommendations. In this section all parameters of Uniswa Red have been randomly selected from a normal distribution where the mean is the original value found in Table 5.4 and the variance is 10% of the original value. The algorithm described in Section 6.4 is now applied for Uniswa Red for a temperature

of 28°C and for all plots sizes. The results can be found in Table 6.6.

The recommendations for plants with randomly varied parameters show similar behaviour to what was found in Section 6.4.1 in that recommendations change for different plot sizes and temperatures. We find that, when random variation is applied to plant parameters, it is generally recommended to plant with a larger planting distance. The difference in planting distances between Tables 6.6 and 6.8 decreases as plot size increases. This is because with the increased number of plants the average behaviour of all N randomly varied plants becomes closer to the plant behaviour when there is no random variation.

Plot Size	Temperature	Layout	D_r	D_c	Pod mass	N
1	23°C	Indented Grid 1	0.33	0.5	591.2	12
	28°C	Indented Grid 1	0.33	0.5	821.1	12
	33°C	Uniform Grid	0.33	0.5	603.9	12
1.5	23°C	Uniform Grid	0.5	0.5	1016.7	16
	28°C	Uniform Grid	0.3	0.37	1357.2	30
	33°C	Uniform Grid	0.5	0.5	1039	16
2	23°C	Uniform Grid	0.4	0.4	1570.6	36
	28°C	Uniform Grid	0.4	0.4	2194.9	36
	33°C	Uniform Grid	0.5	0.6	1403.9	20
2.5	23°C	Uniform Grid	0.5	0.5	2222	36
	28°C	Indented Grid 2	0.45	0.35	2967.4	48
	33°C	Uniform Grid	0.5	0.5	2108.7	36
3	23°C	Uniform Grid	0.5	0.5	2998.4	49
	28°C	Uniform Grid	0.3	0.42	3957.5	88
	33°C	Uniform Grid	0.6	0.6	2748.5	36
3.5	23°C	Uniform Grid	0.5	0.5	3894.1	64
	28°C	Uniform Grid	0.35	0.43	5322.8	99
	33°C	Uniform Grid	0.5	0.5	3478.7	64
4	23°C	Uniform Grid	0.4	0.44	5029.8	110
	28°C	Uniform Grid	0.4	0.44	6818.3	110
	33°C	Uniform Grid	0.5	0.44	4423.3	90
4.5	23°C	Uniform Grid	0.45	0.45	6238.8	121
	28°C	Uniform Grid	0.4	0.45	8077.7	132
	33°C	Uniform Grid	0.45	0.5	5531.7	110

Table 6.6: The optimum layout, column and row distance that gives maximum pod mass for Uniswa Red at a temperature of 28°C. All parameters except those describing plant height are taken from a normal distribution where the average is the original value and the variance is 10% of the base.

6.5 Optimising for a limited number of plants

In the optimisation algorithm described in Section 6.4 it was assumed that an unlimited number of plants was available. Thus there are enough plants to fill a plot for any given D_r and D_c. It may be that, in addition to the plot size being limited, the number of available plants is also finite. In this section, we ask ourselves what is the best way to fill a limited space with a predetermined fixed number of plants.

Although this is a simple enough question, in practice the problem is challenging. There are many possible arrangements for N plants in a $\hat{P}\text{m}\times\hat{P}\text{m}$ area and so in order to optimise, an iterative process that identifies all arrangements needs to be developed. There are infinite possible arrangements and so we set limitations on the iterative process to ensure that only physically practical ones are recommended.

Firstly, it is assumed that plants are arranged systematically such that the distance between, and within, rows is constant throughout the plot area. We limit the potential layouts to Uniform Grid, Indented Grid 1 and Indented Grid 2. The investigation has been limited to these layouts as it has been demonstrated that the Circular and Random Layouts are very inefficient when compared to these three.

The algorithm begins by determining the distance between plants if all N plants were planted in a single row. This arrangement is clearly not the best one as it leaves a lot of wasted space in the plot area, but it provides a starting point from which to work. In a plot size of $\hat{P}\text{m}\times\hat{P}\text{m}$ the within row planting distance is given by

$$D_r = \hat{P}/(N-1).$$

We then let D_r increase in set increments of 0.01m so that plants no longer fit into the row and are pushed onto a different row. The size of the increments are limited to the sensitivity achievable in practice (e.g. farmers planting in the field). The number of rows, nr, is recorded for each increment of D_r and the distance between rows is calculated such that

$$D_c = \frac{\hat{P}}{nr-1}.$$

Clearly if $nr = 1$ then $D_c = \infty$; this still allows one row to exist. An illustration of this method can be found in Figure 6.12 for 15 plants and a range of D_r values. The values that D_r takes are not limited to those found in Figure 6.12, in the algorithm D_r would take all values between $\frac{\hat{P}}{N-1}$ and 1 with an increment of 0.01m labelled $\mathbf{D}_r$. We have selected only 8 values so that the behaviour of the algorithm can be observed.

Figure 6.12 shows that the algorithm is testing layouts of plants that will clearly be inefficient when maximising pod mass. Despite this, we do not want to exclude possible layouts without confirming their efficiency.

For $\hat{P} = 1$ and $N = 15$, the total pod mass for all plants for values of D_r ranging between 0.1m and 1m with increments of 0.01m can be found in Figure 6.13 for the layouts Uniform Grid, Indented Grid 1 and Indented Grid 2. From these results we can see that the pod mass rises and falls as D_r increases for all three layouts. For each layout, total pod mass initially rises as D_r increases because plants within columns are being spread more evenly horizontally. There is then a critical point where a further increase to D_r causes one less column to fit within the space and hence the plants that have been pushed out of the plot are added to the remaining columns. This leaves an inefficient arrangement where plants are squeezed into columns and columns are unnecessarily close together. Then the process repeats itself as the columns shift away from each other, making better use of the horizontal space and so increasing total pod mass as D_r increases.

For the Uniform Grid, once $D_r > 0.5$m there is no further increase to pod mass. This is because at this point, plants are arranged in two columns where there is no competition between columns. As D_r increases the two columns continue to move further apart until a critical point at which plants are now arranged in a single vertical column. For the Indented Grid 1, when $D_r > 0.5$m the plants are similarly arranged in two columns, however in this case every other row is indented and so there appears to be four columns. In this case there is competition between columns, and hence we see pod mass rise and fall as D_r increases past 0.5m as the spacing

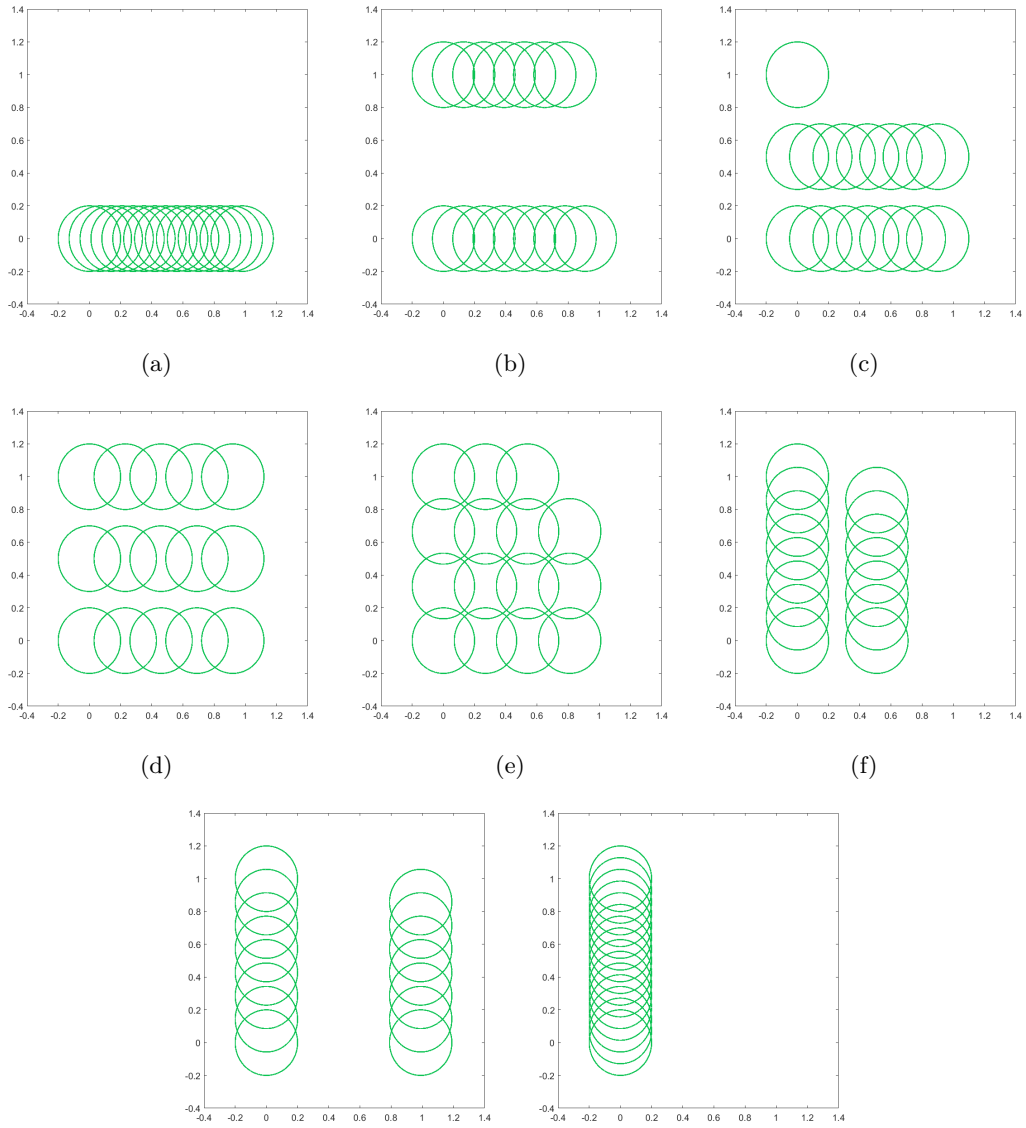

Figure 6.12: An above plant view of the planting arrangement for eight values of D_r in the optimisation algorithm for a limited number of plants. The number of plants is 15 and the plot size 1m×1m. Here, (a) is for $D_r = 0.07$m; (b) is for $D_r = 0.13$m; (c) is for $D_r = 0.15$m; (d) is for $D_r = 0.23$m; (e) is for $D_r = 0.27$m, (f) is for $D_r = 0.51$m; (g) is for $D_r = 0.99$m and (h) is for $D_r = 1.01$m.

between the four columns changes, this is contrary to what was found to the Uniform Grid. The indent is equal to the space between the last plant in a non-indented row and the edge of the plot and so when $D_r > 0.5$m and $\hat{P} = 1$m the size of the indent decreases as D_r increases. At $D_r = 0.51$m the indent is equal to 0.49m and so the

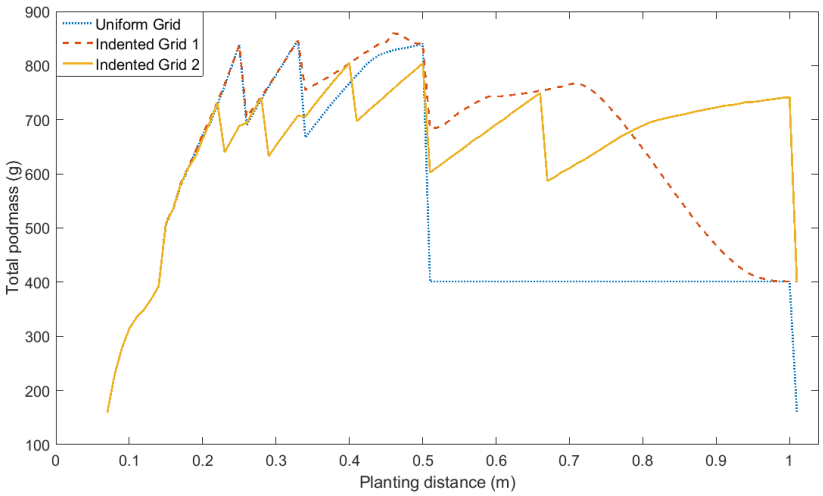

Figure 6.13: The total pod mass of 15 plants in a 1m×1m plot for a range of planting distances D_r and for the three planting layouts of Uniform Grid, Indented Grid 1 and Indented Grid 2.

four columns are positioned on $D_r = [0 \quad 0.49 \quad 0.51 \quad 1]$m, respectively. Clearly in this case, two columns experience large inter-column competition. As D_r increases past this point the four columns become more evenly spaced until $D_r = 0.74$m, at which point the four columns are positioned such that $D_r = [0 \quad 0.36 \quad 0.74 \quad 1]$m when columns are the most evenly spread out and pod mass peaks. After this two columns bunch together and we see pod mass fall. Eventually D_r hits a critical point when plants are arranged in a single column, at this point for Indented Grid 1 every other plant is indented by the length of the plot size and so plants appear to be in two columns.

For Indented Grid 2, when $\hat{P} = 1$m and $D_r > 0.5$m, plants are arranged in two columns with every other row indented by half the planting distance. Thus in this case, columns including the indented columns are evenly spaced for all D_r and so we see more uniform behaviour as D_r increases. Hence we see pod mass rise and fall as columns become further apart until the number of columns decrease. We see some irregularity in the behaviour of pod mass as it rises with increased D_r. The cause of this is that D_r has become such an amount that $0.5D_r$ causes a plant of every other row to be excluded from that row and added to another column.

Thus the algorithm consists of finding pod mass for all $D_r \in \mathbf{D}_r$. The largest total pod mass is identified and with it the associated value of D_r and D_c. This is done for the Uniform Grid, Indented Grid 1 and Indented Grid 2. It is not clear how the number of plants and the plot size affects the optimum recommendations. Therefore, we run the algorithm for a range of N and $\hat{P}$ values with the results recorded in Table 6.6. The test species Uniswa Red is used, grown at a temperature of 28°C.

$\hat{P}$	N	Layout	D_r	D_c	Total pod mass (g)
1m×1m	10	Indented Grid 2	0.5	0.33	776.15
	15	Indented Grid 1	0.46	0.25	859.87
	20	Uniform Grid	0.25	0.33	845.18
	25	Uniform Grid	0.33	0.17	748.67
1.5m×1.5m	30	Uniform Grid	0.37	0.3	1610.83
	35	Uniform Grid	0.25	0.38	1585.23
	40	Uniform Grid	0.37	0.21	1503.36
	45	Indented Grid 1	0.37	0.19	1423.3
2m×2m	50	Indented Grid 1	0.47	0.22	2482.06
	55	Indented Grid 1	0.47	0.2	2440.50
	60	Uniform Grid	0.4	0.22	2521.03
	65	Uniform Grid	0.4	0.2	2365.81
2.5m×2.5m	70	Uniform Grid	0.41	0.27	3711.01
	75	Uniform Grid	0.25	0.42	3670.29
	80	Indented Grid 2	0.83	0.11	3594.39
	85	Indented Grid 1	0.41	0.21	3530.34
3m×3m	90	Indented Grid 1	0.48	0.25	4999.13
	95	Indented Grid 1	0.27	0.43	5087.06
	100	Indented Grid 2	0.25	0.43	5070.06
	105	Indented Grid 1	0.48	0.21	4996.72
3.5m×3.5m	110	Indented Grid 1	0.38	0.35	6448.89
	115	Indented Grid 1	0.29	0.44	6602.08
	120	Indented Grid 1	0.48	0.25	6559.67
	125	Indented Grid 1	0.26	0.44	6671.62
4m×4m	130	Indented Grid 1	0.33	0.44	8272.40
	135	Uniform Grid	0.5	0.29	8323.74
	140	Indented Grid 1	0.44	0.31	8430.99
	145	Indented Grid 1	0.89	0.14	8396.64

Table 6.7: The optimum layout, column and row distance that gives maximum total pod mass for Uniswa Red at 28°C for each plot size.

From Table 6.7 we see that for all plot sizes, planting distance decreases as N increases which is to be expected. Similarly for all plot sizes, it is not necessarily

better to squeeze more plants into the area. This is something that we would expect from the results of Section 6.4.

There are several similarities in recommendations when compared to Section 6.4. We find that it is generally better to plant with D_r not equal to D_c and we also find that the recommended layout changes for different N and for different plot sizes. Further investigation shows that in almost all cases the recommended D_r and D_c will give a number of plants in a row and a column that, when multiplied together give N exactly. Thus all the rows are filled as in Figure 6.12(d), avoiding inefficient arrangements as shown in Figure 6.12(c). Sometimes, the factors that give the number of plants in a row and column, respectively, have a value D_r that allows for room to be available between the end of rows and the plot edge. In these cases Indented Grid 1 is the optimum layout, otherwise the Uniform Grid is recommended. For Indented Grid 2, there are values of D_r that cause plants at the end of every other row to be shifted outside of the plot area. These plants are added onto other columns in the plot area making another row. In doing this there are more pairs of factors that give the number of plants in a row and the number of plants in a column, that make viable optimal arrangements. For example, consider $N = 10$ and $\hat{P} = 1$m, for a Uniform Grid and Indented Grid 1 plants must either be arranged in one row of ten, or two rows of five or take the inefficient form of Figure 6.12(c). For Indented Grid 2 however, plants can also be arranged in two rows of two and two rows of three thus making it a more efficient arrangement.

The algorithm works by testing each layout in turn; further investigation shows that the maximum total pod mass for each planting layout can vary by as much 11% or as little as 1.55% depending on N or $\hat{P}$. This is reminiscent of the delicate balance described in the previous section whereby a small change in plant layout plot size can cause a large change in the recommended arrangement, but not necessarily a great gain in pod mass. However, in the case of an 11% improvement to total pod mass, seeking the optimum layout for a particular N and $\hat{P}$ would make a significant difference.

6.6 Chapter summary

In this chapter we investigated how the layout of a homogeneous crop of bambara groundnut effects the total canopy biomass and pod mass of all plants. Two forward optimisation algorithms were introduced that made recommendations as to how to arrange plants in order to maximise yield. One algorithm considered the scenario of limited area and unlimited availability of plants while the other considered the scenario where both the area and the number of available plants is limited.

It was found that to maximise canopy biomass the optimum layout was Indented Grid 1 that shifts every other row by the distance between the end of rows and the edge of the plot. It was further found that the planting distance that maximises canopy biomass is the smallest allowed. Since this find contradicts what we know from planting bambara groundnut in the field, it was decided that optimising canopy biomass was not ideal and so instead we decided that optimising pod yield would be preferable.

Thus the model was extended to include the change in pod mass over time. It was found that a small adaptation to the model allowed us to capture the behaviour of pod mass over time for the greenhouse experiments for Uniswa Red and S19-3, for all three temperatures 23°C, 28°C and 33°C. Using this adaptation we were then able to optimise planting distance and layout in order to maximise pod yield for a range of conditions.

For pod mass we found that the optimum layout varied for different planting distances. The optimum planting distance is no longer the smallest feasible and so a forward optimisation algorithm was used so that the optimum planting distance could be found. The algorithm was applied to a range of plot sizes, temperatures and for limited and unlimited N.

Both optimisation algorithms worked well and gave sensible recommendations. It was found that recommended arrangements are not scalable in plot size, as a change in plot size affects the pay off between adding more plants and increasing the space

per plant. It was further found that temperature affected planting recommendations so that a lower planting density is recommended for high and low temperatures compared to the optimum temperature of 28°C.

This concludes optimising the planting layout for the case of a monocrop. In the following chapter, we extend this process in order to optimise the planting layout for intercropping bambara groundnut with one other plant species.

Chapter 7

Optimising crop yield: intercropping

The multi-scale mathematical model developed in this work has so far been used to optimise the planting distance and layout of a single species of crop. As mentioned in Chapter 1, the test species is bambara groundnut, and plants with both uniform and randomly distributed parameters have been investigated. In traditional farming systems bambara groundnut is intercropped with at least one other plant species. With this in mind we are particularly interested in being able to simulate and make recommendations for such cases. In this chapter, we take the optimisation algorithms of Chapter 6 one step further and investigate the growth of different species of plants grown together in the same plot. Following a preliminary investigation, we develop another optimisation algorithm, this time optimising the arrangement of two species of plants in a single piece of land.

We do not have experimental data for the growth and development of other species of plants, which would be necessary to parameterise the mathematical model. Therefore we can not investigate intercropping with a specific species. Instead we simulate intercropping with several fictional species with particular genetic traits that contrast with bambara groundnut, for example plant height, canopy spread and canopy biomass.

In the same way as in Chapter 6, we define plant layout as the way that plants are set out in a plot. In this chapter, we introduce plant pattern, which is defined as the positioning of different species of plants in relation to each other. An example of this would be species alternating over rows or columns. The planting arrangement is the combination of a specific layout, pattern and planting distance.

A key question we must ask ourselves at this point is 'What are we trying to optimise when intercropping'? Initial investigations using the mathematical model detailed here found that in order to maximise for total yield (of both species) the optimum arrangement of two species is to fill the plot with the species that produces the highest pod mass. In the literature, there is much debate about the role that diversity has on productivity [46]. Even if a mixed-species cropping system does not maximise crop yield the advantages of inter-cropping go beyond maximising yield. They include, but are not limited to, the reduction in risk of a total crop failure due to unpredictable weather conditions [46]. Therefore in order to optimise arrangement we must consider more than what gives the highest yield.

Once we have developed an optimisation algorithm, we proceed to investigate several other scenarios to which the model could be applied. These include the optimisation of the sowing date of one species in relation to the other and also the arrangement of an annual crop (bambara groundnut) in relation to a perennial crop (oil palm).

7.1 Secondary plant species

To investigate intercropping we require a secondary species of crop to plant with bambara groundnut. We now introduce the fictional species of plants that will be used to investigate mixed-species cropping systems. We will consider four species labelled, Species 1, Species 2, Species 3 and Species 4. Each of these species will be intercropped with Uniswa Red in turn. To avoid confusion the Primary Species will refer to bambara groundnut and the Secondary Species will refer to one of Species 1-4 depending on which one is being considered at the time.

All four of the fictional species of plants have parameter values equal to Uniswa Red except for three key parameters, k_h, α_g, and k_c. These parameters relate to plant height, canopy spread and the maximum canopy biomass. From the sensitivity analysis in Section 4.2.2 it is clear that these are not the only parameters that have an impact on plant growth, however including all parameters would be excessive. These particular parameters have been chosen as they have the biggest effect on plant physiology with regards to three key characteristics; plant height, canopy biomass and canopy spread.

Table 7.1 details the differences in parameter values for the four Secondary Species that will be tested against Uniswa Red. Unless specified otherwise, all other parameter values are the same as in Table 5.4. In all cases a factor of two is used to scale the original parameter value so that if a parameter of the fictional species is larger than Uniswa Red it is twice as large, if it is smaller it is half the size. A factor of two has been chosen as it allows for a significant difference, while remaining within the scope of what is physically possible. These four variations have been chosen to give an overall view of how differences in certain parameters will affect both the overall growth and how plants interact.

Qualitatively, the four plants given in Table 7.1 can be described as follows: Species 1 is shorter, has a smaller canopy spread and thus lower ground cover and also grows to a much smaller mass making it lower yielding when compared to Uniswa Red. Species 2 is taller than Uniswa Red, but also narrower and lower yielding. Species 3 is shorter and has a lower yield compared to Uniswa Red, but it's canopy is wider spreading, giving it a larger ground cover. Finally, Species 4 is shorter, has a narrower canopy and grows to a much larger mass than Uniswa Red, making it higher yielding. These plants, although fictional would be suitable representation of other legumes or spreading annual plants.

The growth of these four test species are compared to Uniswa Red in Figure 7.1. Here the average leaf area, canopy biomass and pod mass of 16 plants arranged in a Uniform Grid with a planting distance $D_r = 0.3 = D_c$ are compared for Uniswa

Species 1	Species 2	Species 3	Species 4
$k_{hS} < k_{hP}$	$k_{h1S} > k_{hP}$	$k_{hS} < k_{hP}$	$k_{hS} < k_{hP}$
$\alpha_{gS} < \alpha_{gP}$	$\alpha_{gS} < \alpha_{gP}$	$\alpha_{gS} > \alpha_{gP}$	$\alpha_{gS} < \alpha_{gP}$
$k_{cS} < k_{cP}$	$k_{cS} < k_{cP}$	$k_{cS} < k_{cP}$	$k_{cS} > k_{cP}$

Table 7.1: Summary of the four scenarios of parameter values that we are investigating the optimum planting conditions for. Here a subscript P refers to the Primary Species Uniswa Red and a subscript S refers to the Secondary Species.

Red and each of Species 1-4. The temperature is 28°C and the plot size is 1m×1m.

By observing the results of Figure 7.1 we can see how the changes in parameters affects the evolution of leaf area, canopy biomass and pod mass through time. The leaf area against time is given in Figure 7.1(a) for the five species. Species 1, 2 and 4 have the same leaf area, this is because all of these species have the same canopy spread value, α_g, which is smaller than for the other two species. Since α_g is smaller for Species 1, 2 and 4 when compared to Uniswa Red and Species 3, the ground cover is less and so there is less competition applied to the 16 plants in the simulation. Conversely, Species 3 has a larger value of α_g causing it to have a larger ground cover and thus more competition within the 16 plants compared to the other four species. Clearly, of the parameters, only α_g has an impact on leaf area and this is via the inter-plant competition.

The mean canopy biomass against time is given in Figure 7.1(b). If planting distance was increased the larger ground cover would become an advantage. The only difference between Species 1 and 2 is the height and since plant height does not affect canopy biomass in a homogeneous planting arrangement we find that canopy biomass over time is the same for Species 1 and 2. Species 4 has the largest canopy biomass, which may have been predicted by it having a larger canopy biomass carrying capacity. Species 3 has the smallest canopy biomass for all time. The cause of this is that, in addition to k_c being smaller for Species 3 compared to Uniswa Red and Species 4, α_g for Species 3 is the largest of all five species. Thus, ground cover is larger and hence there is an increased amount of competition between plants of this species. Therefore, even though k_c is the same for Species 1,2 and 3, the canopy biomass is smaller for Species 3 compared to the other two. Species 1 and 2 initially

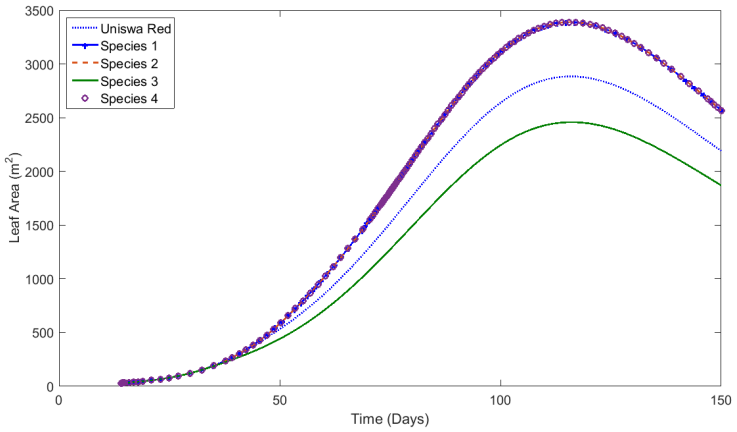

(a)

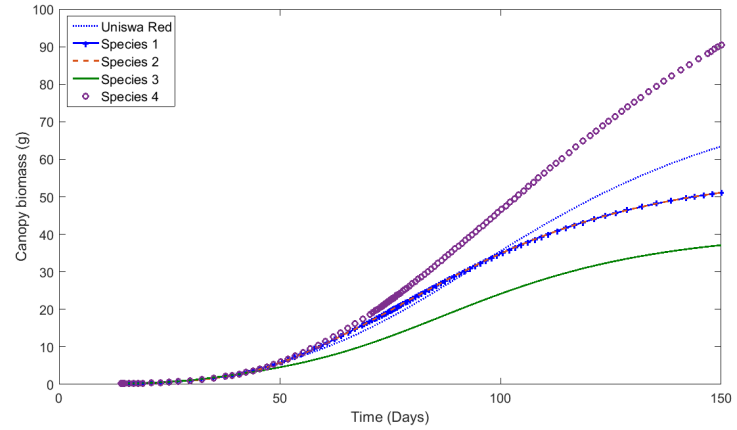

(b)

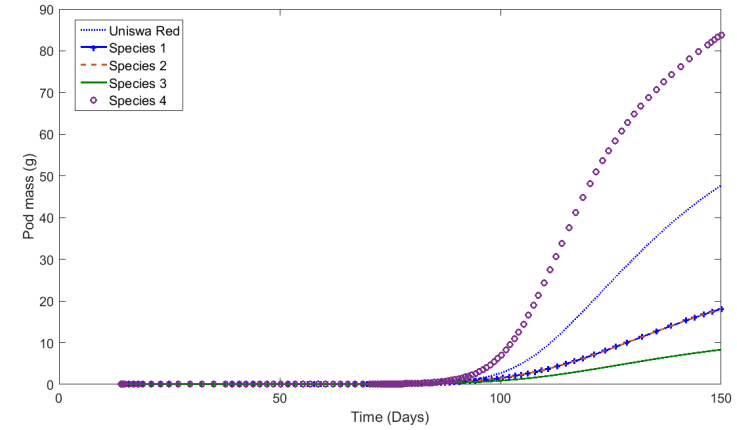

(c)

Figure 7.1: A comparison of the growth of Uniswa Red and four fictional species of plants with the differences in parameters detailed in Table 7.1. Here, (a) shows the average leaf area per plant, (b) shows the average canopy biomass per plant and (c) shows the average pod mass per plant.

have a larger canopy biomass than Uniswa Red, but at approximately 90 days the canopy biomass of Uniswa Red overtakes both of them. This is because Species 1 and 2 have less inter-plant competition when compared to Uniswa Red caused by the smaller α_g. Despite this, since Uniswa Red has a larger carrying capacity, it's canopy biomass increases to larger than that of Species 1 and 2.

The pod mass against time for the five species is given in Figure 7.1(c). The results show a similar behaviour to canopy biomass in regards to the behaviour of the five species in relation to each other. This is because pod mass is a function of canopy biomass.

Although Species 1 and 2 show the exact same growth behaviour for leaf area, canopy biomass and pod mass, Species 2 is taller than Uniswa Red and Species 1 is shorter. Thus their behaviour when intercropped with Uniswa Red will be different and this will be further investigated in the following section.

7.2 Arrangements of two species

Now that the features and comparitive behaviour of the Secondary Species' of plants to intercrop with Uniswa Red have been introduced, we determine what arrangements of two species we will consider. There are an impractically large number of arrangements that two species can be placed within a plot area and so it is necessary to impose some limitations. We initially limit the number of planting patterns to the three illustrated in Figure 7.2. Here the three patterns can be summarised as alternate rows, alternate plants and alternate blocks. These patterns have been chosen as they are three simple, feasible examples that can give some insight into the affect of different arrangements. Once we have investigated these preliminary examples we will go on to consider more intercropping patterns in order to develop an optimisation algorithm. The affect of these patterns will change for different layouts and so we will investigate each of these patterns for the Uniform Grid, Indented Grid 1 and Indented Grid 2 described in Chapter 6. We do not consider the Circular and Random Layouts as, in the previous chapter, these were shown to be

particularly inefficient.

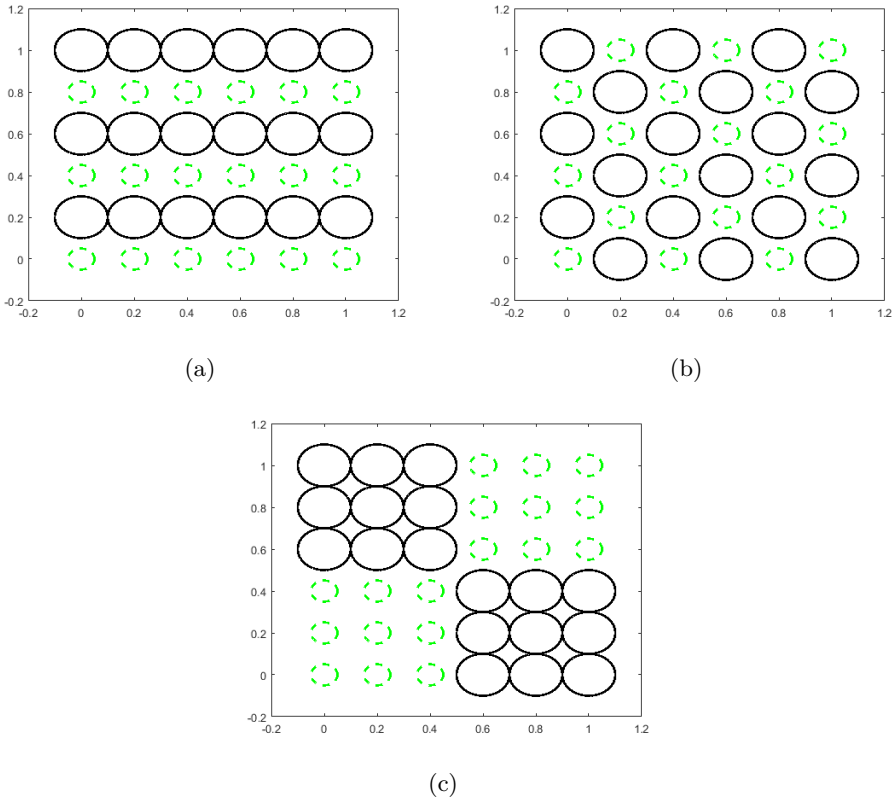

Figure 7.2: A schematic of three potential arrangements of two species. Here (a) shows Pattern 1 which is alternate rows, (b) shows Pattern 2, which is plants alternate over rows and columns and (c) show Pattern 3, which is an alternate block pattern. Species 1 is indicated with a dashed green line and Species 2 with a solid black line.

We repeat a simulation of Uniswa Red as a monocrop, but we now also include Uniswa Red intercropped with each of Species 1, 2, 3, and 4. When simulating Uniswa Red as a monocrop we divide plants into two groups (Group 1 and Group 2). Group 1 are plants with positions of the Primary Species, whereas Group 2 has the positions of the Secondary Species. Whilst this seems like repetition of the previous chapter, in that chapter we considered yield as a whole, but now we consider it in terms of subgroups. We do this to gain some insight into what effect the spatial positioning of one group in relation to the other has on the yield of each subgroup before introducing different species. This is done for all three layouts shown in Figures 6.1(a), 6.1(b) and 6.1(c) and for all patterns shown in Figure 7.2. This

gives a total of 45 simulations to compare. The plot size is 1m×1m, temperature is 28°C and the planting distance is 0.3m. The total pod mass of the Primary and Secondary Species and also of all N plants together is given in Tables 7.2 to 7.6.

Plant pairing		Uniform grid			Indented Grid 1			Indented Grid 2		
		Pattern 1	Pattern 2	Pattern 3	Pattern 1	Pattern 2	Pattern 3	Pattern 1	Pattern 2	Pattern 3
Uniswa Red_1	Pod Mass	**429.65**	**429.65**	429.61	430.35	390.28	**437.61**	307.48	**451.07**	389.42
	N_1	8	8	8	8	8	8	6	8	7
Uniswa Red_2	Pod Mass	429.63	429.62	**429.67**	430.32	**470.39**	423.07	**462.56**	318.97	380.62
	N_2	8	8	8	8	8	8	8	6	7
Total	Pod Mass	**859.28**	**859.28**	**859.28**	**860.68**	**860.68**	**860.68**	**770.04**	**770.04**	**770.04**
	N	16	16	16	16	16	16	14	14	14

Table 7.2: Summary of pod mass and plant number for species Uniswa Red divided into Groups 1 and 2 and grown together in Patterns 1, 2, and 3 for layouts Uniform Grid, Indented Grid 1 and Indented Grid 2. Maxima is given in bold.

Plant pairing		Uniform grid			Indented Grid 1			Indented Grid 2		
		Pattern 1	Pattern 2	Pattern 3	Pattern 1	Pattern 2	Pattern 3	Pattern 1	Pattern 2	Pattern 3
Uniswa Red	Pod Mass	597.47	**676.38**	526.93	597.53	**651.66**	539.76	459.2	**638.06**	496.92
	N_1	8	8	8	8	8	8	6	8	7
Species 1	Pod Mass	42.33	1.3	**148.89**	41.1	3.58	**141.99**	37.76	4.2	**106.41**
	N_2	8	8	8	8	8	8	8	6	7
Total	Pod Mass	639.79	**677.68**	675.82	638.63	655.24	**681.75**	496.96	**642.27**	603.33
	N	16	16	16	16	16	16	14	14	14

Table 7.3: Summary of pod mass and plant number for species Uniswa Red and Species 1 grown together in Patterns 1, 2, and 3 and for layouts Uniform Grid, Indented Grid 1 and Indented Grid 2. Maxima is given in bold.

Plant pairing		Uniform grid			Indented Grid 1			Indented Grid 2		
		Pattern 1	Pattern 2	Pattern 3	Pattern 1	Pattern 2	Pattern 3	Pattern 1	Pattern 2	Pattern 3
Uniswa Red	Pod Mass	204.1	41.09	**300.38**	194.46	20.18	**307.23**	139.74	157.04	**260.36**
	N_1	8	8	8	8	8	8	6	8	7
Species 2	Pod Mass	370.04	**463.94**	329.61	**370.24**	479.7	326.4	**370.12**	336.97	297
	N_2	8	8	8	8	8	8	8	6	7
Total	Pod Mass	574.14	505.04	**629.99**	564.69	499.88	**633.64**	509.86	494	**557.35**
	N	16	16	16	16	16	16	14	14	14

Table 7.4: Summary of pod mass and plant number for species Uniswa Red and species 2 grown together in Patterns 1, 2, and 3 and for layouts Uniform Grid, Indented Grid 1 and Indented Grid 2. Maxima is given in bold.

Plant pairing		Uniform grid			Indented Grid 1			Indented Grid 2		
		Pattern 1	Pattern 2	Pattern 3	Pattern 1	Pattern 2	Pattern 3	Pattern 1	Pattern 2	Pattern 3
Uniswa Red	Pod Mass	597.51	**676.35**	526.93	597.54	**651.65**	539.84	459.27	**638.06**	496.93
	N_1	8	8	8	8	8	8	6	8	7
Species 3	Pod Mass	10.42	1.95	**80.11**	12.46	7	**88.79**	19.82	6.76	**56.46**
	N_2	8	8	8	8	8	8	8	6	7
Total	Pod Mass	607.93	**678.3**	607.04	610	**658.64**	628.63	479.09	**644.81**	553.38
	N	16	16	16	16	16	16	14	14	14

Table 7.5: Summary of pod mass and plant number for species Uniswa Red and Species 3 grown together in Patterns 1, 2, and 3 and for layouts Uniform Grid, Indented Grid 1 and Indented Grid 2. Maxima is given in bold.

Plant pairing		Uniform grid			Indented Grid 1			Indented Grid 2		
		Pattern 1	Pattern 2	Pattern 3	Pattern 1	Pattern 2	Pattern 3	Pattern 1	Pattern 2	Pattern 3
Uniswa Red	Pod Mass	597.53	**676.36**	526.93	597.53	**651.61**	539.8	459.21	**638.06**	496.9
	N_1	8	8	8	8	8	8	6	8	7
Species 4	Pod Mass	224.42	3.31	**465.95**	227.56	19.86	**447.19**	212.25	29.38	**349.31**
	N_2	8	8	8	8	8	8	8	6	7
Total	Pod Mass	821.94	679.67	**992.88**	825.1	671.47	**986.99**	671.46	667.44	**846.21**
	N	16	16	16	16	16	16	14	14	14

Table 7.6: Summary of pod mass and plant number for species Uniswa Red and Species 4 grown together in Patterns 1, 2, and 3 and for layouts Uniform Grid, Indented Grid 1 and Indented Grid 2. Maxima is given in bold.

In Table 7.2 Uniswa Red is monocropped, with the total 16 plants split into two groups labelled with a subscript 1 or 2; each group has the same number of plants in it. There is a different total pod mass for the three layouts which is a result we would expect from our findings in Chapter 6. The sum of pod mass for Group 1 and Group 2 is the same for all three patterns, which is what we would expect as all plants are the same species. What we might not expect is that there is a different total pod mass for the two groups across patterns. For example, in Indented Grid 1 with Pattern 2 there is a lower total pod mass for Group 1 when compared to Group 2. A schematic of this arrangement can be found in Figure 7.3, where we can see that due to the nature of the indentation, plants on every other row extend past the other plants. As a cause of the alternating pattern this position is always taken by a member of Group 2 and so four members of Group 2 are exposed to less competition than the other plants. As such, Group 2 has a higher total pod mass for the same number of plants. It is clear from this, that even before we start mixing species there is already an impact on pod mass caused by the planting pattern of two species.

From Tables 7.2 to 7.6 we find that there is no consensus as to which is the most efficient layout or pattern, which is consistent with the behaviour we found in Chapter 6. Instead we find that the recommended arrangement changes for which species is being investigated. The intercropping arrangement that yielded the highest overall pod mass is when Uniswa Red and Species 4 are arranged using Pattern 3 in a Uniform Grid as seen in Table 7.6. Species 4 has a higher canopy biomass carrying capacity than the other species and therefore grows to a larger mass which then gives a larger pod mass. Thus the intercropping of the two highest yielding species results in the highest yield which is to be expected. Since plants of Species 4 are shorter than Uniswa Red, the most effective pattern is to minimise the higher yielding plants' interactions with the taller plants. This can also be seen when Uniswa Red and Species 2 are planted together. Species 2 is taller, but Uniswa Red is higher yielding and therefore the best arrangement is also the block pattern as this

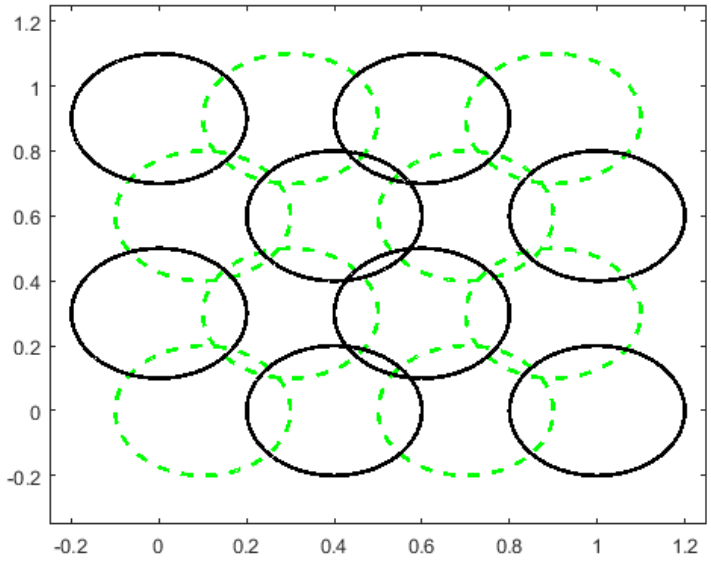

Figure 7.3: Schematic illustrating how two groups are arranged in relation to each other for Indented Grid 1 and Pattern 2. Species 1 is indicated with a dashed green line and Species 2 with a solid black line.

minimises interactions between species. When Uniswa Red is monocropped, there is a higher overall pod mass than when intercropped with a taller plant. Although not shown in the tables, this is also the case when Species 4 is monocropped.

When Uniswa Red is intercropped with shorter plants that also have smaller carrying capacities (i.e. Species 1 and Species 3), the best arrangement is to minimise the interaction between Uniswa Red plants. (This can be seen in Tables 7.3 and 7.5 by observing that Pattern 2 (diagonal rows) gives the highest total pod mass for all N plants.) This is for all layouts with the one exception of intercropping with Species 1 with Indented Grid 1 given in Table 7.3. Here, Pattern 3 (alterating blocks) gives the highest overall pod mass for all N plants. When plants are arranged as with the layout Indented Grid 1, Pattern 3 gives the lowest pod mass for Uniswa Red but the largest for Species 1. Note that this is also the case for intercropping Uniswa Red with Species 3 in Table 7.5. The difference between intercropping with Species 1 and 3 is that for Species 1 the decrease to pod mass from Pattern 2 to Pattern 3 for Uniswa Red is small when compared to the increase to Species 1. For Species

3 however, as this species is wider spreading, when arranged in the block pattern there is more competition across Species 3 plants and so the increase to total pod mass is reduced when switching from Pattern 2 to 3.

This demonstrates the fine balance between recommended planting arrangement for intercropping with different species. From Tables 7.2 to 7.6 there is no specific behaviour that we can extrapolate to other scenarios and so in order to make recommendations for a number of scenarios an optimisation algorithm must be developed.

7.3 Optimisation Algorithm

Having gained some preliminary insight into the behaviour of intercropping two species of plants, we now develop an algorithm that will provide the optimum arrangement in order to maximise the pod mass of both species. It has been found that in all cases that have been investigated so far the optimum arrangement is solely planting the highest yielding species. As previously stated, the reason we might wish to intercrop is not necessarily to maximise pod mass as intercropping provides many other benefits. With that in mind, one of the limitations we impose on the algorithm is that intercropping patterns will be set by the user. This way, we ensure that all of the patterns that are considered are practical intercropping recommendations i.e. realistically achievable in the field.

In a similar fashion to Chapter 6, we consider a forward optimisation algorithm that loops through all of the potential layouts and patterns. Thus for a particular plot size, intercropping pattern and layout, the optimum distance that maximises pod mass is found in the same way as discussed in Section 6.4. We do this for all patterns and for each layout and compare the pod mass for each case to find the optimum arrangement. This is done for a plot size of $\hat{P} = 3$m and a temperature of 28°C. We repeat this for Uniswa Red paired with each of the four fictional plant species described in Section 7.1.

We have increased the number of planting patterns to obtain a more thorough range of recommendations. As we want to investigate a multitude of scenarios we

must include in our model a way to easily input patterns. We allow the planting array of the two species that are to be simulated to be described by a repeatable pattern that the model user inputs. For example, arrangements given in Figure 7.2 are given by scaling up

$$\text{Pattern 1} = \begin{bmatrix} 1 \\ 2 \end{bmatrix}, \quad \text{Pattern 2} = \begin{bmatrix} 1 & 2 \\ 2 & 1 \end{bmatrix} \quad \text{and} \quad \text{Pattern 3} = \begin{bmatrix} 1 & 1 & 1 & 2 & 2 & 2 \\ 1 & 1 & 1 & 2 & 2 & 2 \\ 1 & 1 & 1 & 2 & 2 & 2 \\ 2 & 2 & 2 & 1 & 1 & 1 \\ 2 & 2 & 2 & 1 & 1 & 1 \\ 2 & 2 & 2 & 1 & 1 & 1 \end{bmatrix}.$$

Here 1 indicates the Primary Species (Uniswa Red) and 2 the Secondary (one of Species 1-4). Then we see that scaling the pattern

$$\begin{bmatrix} 1 \\ 2 \end{bmatrix}$$

up to a 4×4 planting array leads to

$$\begin{bmatrix} 1 & 1 & 1 & 1 \\ 2 & 2 & 2 & 2 \\ 1 & 1 & 1 & 1 \\ 2 & 2 & 2 & 2 \end{bmatrix}.$$

This can continue for however many plants we wish to consider.

In the optimisation algorithm of this section we consider seven planting patterns,

which are given by

$$\text{Pattern 1} = \begin{bmatrix} 1 \\ 2 \end{bmatrix}, \quad \text{Pattern 2} = \begin{bmatrix} 1 & 2 \\ 2 & 1 \end{bmatrix}, \quad \text{Pattern 3} = \begin{bmatrix} 1 & 1 & 1 & 2 & 2 & 2 \\ 1 & 1 & 1 & 2 & 2 & 2 \\ 1 & 1 & 1 & 2 & 2 & 2 \\ 2 & 2 & 2 & 1 & 1 & 1 \\ 2 & 2 & 2 & 1 & 1 & 1 \\ 2 & 2 & 2 & 1 & 1 & 1 \end{bmatrix},$$

$$\text{Pattern 4} = \begin{bmatrix} 1 & 2 \end{bmatrix}, \quad \text{Pattern 5} = \begin{bmatrix} 2 & 1 \\ 1 & 2 \end{bmatrix}, \quad \text{Pattern 6} = \begin{bmatrix} 1 \\ 1 \\ 2 \end{bmatrix},$$

$$\text{and} \quad \text{Pattern 7} = \begin{bmatrix} 2 \\ 2 \\ 1 \end{bmatrix}.$$

The result the optimisation process gave was a planting distance that caused the shorter, lower yielding plants to be unable to grow. This gave us a homogeneous array of plants instead of the desired intercropping system. Although this is not what we wanted from our algorithm it does give us some confidence in that the algorithm is working the way that it should. The results of Section 7.2 told us that a homogeneous field of crops, filled with the highest yielding species, is actually what would give the highest yield. Despite this, since the benefits of intercropping go beyond increasing the yield, we only wish to consider intercropping scenarios. Therefore it is necessary to make a further adaptation to the optimisation algorithm so that only recommendations that allow both species to grow together will be considered.

If we impose the condition that if the mean pod mass of the Primary or Secondary Species is less than a user imposed threshold, then the yield is equal to zero as this

is a non-viable recommendation. Thus yield is given by

$$\text{Yield}_{(1,2)} = \begin{cases} \sum_{i=1}^{N_{(1,2)}} P_{(1,2)i}(t_{end}) & \text{if} \quad \bar{P}_{1,2)}(t_{end}) < P_{f(1,2)}, \\ 0 & \text{otherwise,} \end{cases} \tag{7.1}$$

where P_f is the imposed fresh-hold for minimum mean pod mass.

For this optimisation process we allow $P_f = 0.25 \times k_{max}$, which is slightly less than the minimum mean pod mass that was given by each of the recommendations given in Section 6.4.1. The results of the optimisation process with this adaptation is given in Table 7.7 for plant pairings of Uniswa Red with each of Species 1-4. We do not consider multiple plot sizes and temperatures in this section as the results of doing so are not different from Chapter 6; we find that planting recommendations are not scalable for increasing plot sizes and that planting distances are larger for non-optimum temperatures.

These results clearly show that the recommended arrangement changes for different plant pairings. One element of the recommendations that is consistent for all patterns and species is that any further increase to the recommended values for D_r or D_c in Table 7.7 would cause a decrease in N. Thus in all cases, the algorithm is giving recommendations that are making full use of the planting area in a way that we would expect from the algorithm in Section 6.4.

We find that the species pairing of Uniswa Red and Species 4 gives the highest overall yield, which is not surprising as Species 4 is highest yielding. The species pairing of Uniswa Red and Species 3 gives the lowest yield, again this is not surprising as Species 3 is wider spreading and thus requires a higher planting distance and therefore a smaller N. This corroborates the results found in Tables 7.2 to 7.6.

From Table 7.7, we find that Pattern 6 is the recommendation for intercropping Uniswa Red with Species 1, 2 and 3. Pattern 6 maximises the number of plants of the Primary Species (Uniswa Red), which is the higher yielding plant. In fact, what we find is that for each of these species the order of highest to lowest pod mass corresponds with the order of highest to lowest N_1.

Pattern	Secondary Species	D_r	D_c	Pod mass	Layout	N	N_1	N_2
1	1	0.33	0.5	3778	Indented Grid 1	70	40	30
	2	0.33	0.5	3832.7	Indented Grid 1	70	40	30
	3	0.42	0.75	2469.9	Indented Grid 1	40	24	16
	4	0.3	0.5	6055	Uniform Grid	77	44	33
2	1	0.6	0.42	3126.7	Indented Grid 2	44	24	20
	2	0.5	0.5	3578.8	Uniform Grid	49	25	24
	3	0.75	0.75	1902.5	Uniform Grid	25	13	12
	4	0.65	0.2	6432	Indented Grid 1	80	40	40
3	1	0.5	0.5	3197.3	Uniform Grid	70	36	34
	2	0.37	0.5	3618	Indented Grid 1	63	32	31
	3	0.75	0.6	2088.2	Uniform Grid	30	16	14
	4	0.42	0.42	5656.2	Indented Grid 1	64	32	32
4	1	0.5	0.33	3793.1	Uniform Grid	70	40	30
	2	0.5	0.33	3847.5	Uniform Grid	70	40	30
	3	0.75	0.42	2473.2	Uniform Grid	40	24	16
	4	0.5	0.3	6069.9	Uniform Grid	77	44	33
5	1	0.6	0.42	2963.7	Indented Grid 2	44	20	24
	2	0.5	0.5	3526	Uniform Grid	49	24	25
	3	0.75	0.75	1849	Uniform Grid	25	12	13
	4	0.65	0.2	6433.2	Indented Grid 1	80	40	40
6	1	0.3	0.5	4168.7	Uniform Grid	77	55	22
	2	0.3	0.42	4208.4	Indented Grid 2	84	63	21
	3	0.46	0.75	2792.5	Indented Grid 2	35	28	7
	4	0.3	0.5	5708.7	Uniform Grid	77	55	22
7	1	0.5	0.6	2982.4	Uniform Grid	42	14	28
	2	0.5	0.5	3162.2	Uniform Grid	49	14	35
	3	0.46	0.75	1338.1	Indented Grid 2	35	7	28
	4	0.3	0.42	7202.9	Indented Grid 2	84	21	63

Table 7.7: The optimum layout, column and row distance that gives maximum pod mass for Uniswa Red arranged with a Secondary Species. The temperature is 28°C and the plot size $\hat{P} = 3$m.

Species 4 produces more pods than Uniswa Red and so when these two plants are arranged together, Pattern 7 is the recommendation as it maximises the number of Species 4. Contrary to the recommendations for the other three plants, the order of highest to lowest pod mass does not corresponds with the order of highest to lowest N_2. The reason for this is not entirely intuitive as we might expect the results to be similar to that of the species pairing of Uniswa Red and Species 2. For both cases we have a taller plant intercropped with a shorter, higher yielding plant; the

difference between these cases is the ground cover of the taller plant. For Uniswa Red and Species 2, the taller plant is narrower, whereas for Uniswa Red and Species 4, the taller plant is wider.

From Table 7.7 we find that in general $N_1 \geq N_2$. The only scenarios where this is not the case is for Patterns 5 and 7. The cause of this is the selection of planting patterns we are looking at; in all patterns except Patterns 5 and 7 the first plant is the Primary species Uniswa Red. This means that it is a row or column of the Secondary species that is likely to be excluded.

We can see some symmetry in the recommended planting distances for some of the patterns. For all species pairings, the recommendations of D_r and D_c for Pattern 1 is the reverse of Pattern 4. This makes sense as alternating rows and columns are symmetric. Similarly, the recommendations for Pattern 2 are the same as that as for Pattern 5, which is something we would expect from the algorithm. Despite the recommendations being the same, they do not necessarily produce the same amount of pod mass, for example there is a 5.2% change in pod mass between Patterns 2 and 5 even though D_r and D_c stay the same. This is a consequence of two reasons: Firstly, there may be some difference in plant number of each species between the two patterns and secondly, a consequence of model error incurred by the approximation of overlap. An example of model error coming into play can be seen by comparing Patterns 1 and 4, here the recommendations for D_r and D_c are symmetric but total yield changes by 0.4%.

For this optimisation process, as the algorithm initially chose D_r and D_c to be small enough to prevent the growth of the shorter, lower yielding species, it was necessary to input a minimum mean pod mass for each species so that the algorithm would not recommend a homogeneous array of plants. There are however, many ways in which we can restrict the algorithm. For example, we may wish to impose a minimum number of a species instead or a particular ratio of one species to the other. Further to this, it may no longer be necessary to impose any restrictions if more plant growth process were incorporated into the model (e.g. soil nutrients or

water limited growth). There are clearly a limitless number of scenarios to which we can apply our model. The investigation we have done here, although only explores a small set of circumstances, does give us some confidence that the recommendations are at least sensible.

7.4 Investigation of sowing date

So far, in regards to optimising conditions to maximise pod yield, we have only considered the best arrangement of plants. There are however, many applications for an individual-based modelling approach, in particular the time of planting for each species can be very important [50, 54]. In some circumstances, a delay in sowing can cause a reduction in the final yield as it may cause the plants to be growing out of the desired season. However, given certain conditions, for example an insufficient level of soil moisture at the desired time of planting, it can sometimes be beneficial to delay planting [54]. Identifying the optimum time of sowing for a monocrop can have a significant impact on yield and even more so when intercropping, as each species may have slightly different optimum conditions for sowing. When planting two species together it is not necessary to plant them at the same time and instead delaying the planting date of the two species could be beneficial. This is already an established practice and the amount of delay between planting the Primary and Secondary Species can vary [49]. In our model, we only take into account competition for light and we assume that weather conditions are constant over time. However, our model can still be applied to the investigation of optimum sowing date with regards to minimising competition for light at critical points in plant growth.

We now consider how delaying the sowing date of the Secondary Species can impact upon the total yield of both species. Of course, when two species are planted together they not only compete for light but also nutrients and water. These all have an impact on the optimum sowing date, however simulating the response of plant growth to these resources is beyond the scope of our work. Therefore we limit our investigation to optimising sowing date in terms of minimising inter-species

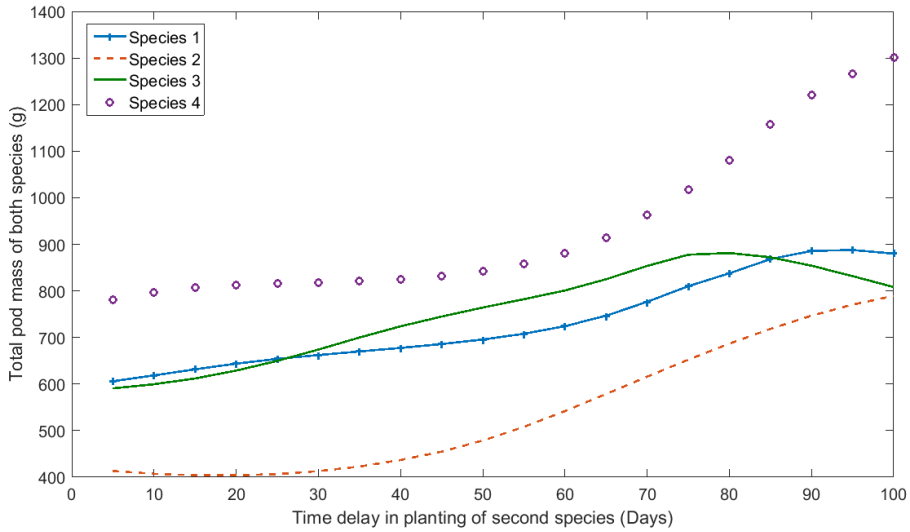

Figure 7.4: The total canopy biomass of 16 plants planting according to Pattern 1 in Figure 7.2(a). Here, 8 plants are of the species Uniswa Red and the other 8 are one of Species 1-4. The sowing of the second species is delayed in relation to the first by the number of days shown on the x-axis. Planting distance is 0.3m, temperature is 28°C, different species are arranged in alternating rows and for a plot size of $\hat{P} = 1$m.

shadowing at critical times of growth.

As a preliminary investigation we consider two species arranged in alternating rows as in Figure 7.2(a). We set the distance between rows and columns to be 0.3m, the temperature to be 28°C and the plot size to $\hat{P} = 1$m. We then simulate the growth of all N plants with varying amounts of delay between sowing dates. We consider increments of five days to the delay in planting, up to a maximum of 100 days. In the field, this magnitude of delay could cause the growth of the Secondary Species to occur out of the desired growing season and therefore weather conditions will not be optimal. We still consider this magnitude, however, to observe the impact in terms of competition for light. These simulations are for Uniswa Red intercropped with each of the fictional species of plant labelled Species 1-4. The results of the investigation are shown in Figure 7.4.

In agreement with the results found in Tables 7.2 to 7.6, intercropping with Species 4 gives the highest total pod mass. This is because the carrying capacity,

and therefore the final yield, is much higher for Species 4. Similarly, Species 2 gives the lowest pod yield for all planting scenarios, this is also something we found in Tables 7.2 to 7.6. Species 2 is taller than Uniswa Red, but has a lower carrying capacity. This means that the yield of Uniswa Red is reduced and Species 2 does not compensate for this loss.

Total pod yield increases for larger sowing delays when Uniswa Red is intercropped with Species 1, 2 and 4. This is because, at the time of podding, competition between species is reduced with increased planting delay. This can be seen more clearly by observing Figure 7.5, here an above plant view of the plant canopies of Unsiwa Red and Species 1 growing together can be seen for 50 day intervals, where the time of sowing for Species 1 is delayed by 75 days.

In Figure 7.5(b) we can see the canopy spread of both species 100 days after Uniswa Red has been planted and 25 days after the sowing of Species 1. Here we can see the wide spread of Uniswa Red, which is causing a lot of shadowing to the shorter Species 1. At 150 days after the initial sowing, shown in Figure 7.5(b), Uniswa Red has been harvested and Species 1 now has room to grow. Larger delays would mean that there is more time for the second species to grow without increased competition incurred by Uniswa Red. Although Figure 7.5 only describes the case where Uniswa Red is intercropped with Species 1, these results also hold for Species 4.

We find that, when intercropping Uniswa Red with Species 2 and 3, total pod yield does not increase monotonically with sowing delay. For Species 2 we find that a sowing delay of between 5 and 35 days has a negative impact on the final yield. Here, Species 2 is unaffected by Uniswa Red as it is the taller species and so a decrease in final yield is caused by decreases in the yield of Uniswa Red. We find that shadowing Uniswa Red in the initial stages of growth causes its ground cover to decrease, thus by delaying the sowing of the Secondary Species we allow the ground cover of Uniswa Red to be larger than it otherwise would be. Increases in ground cover does mean there is a larger canopy surface area to absorb radiation but it

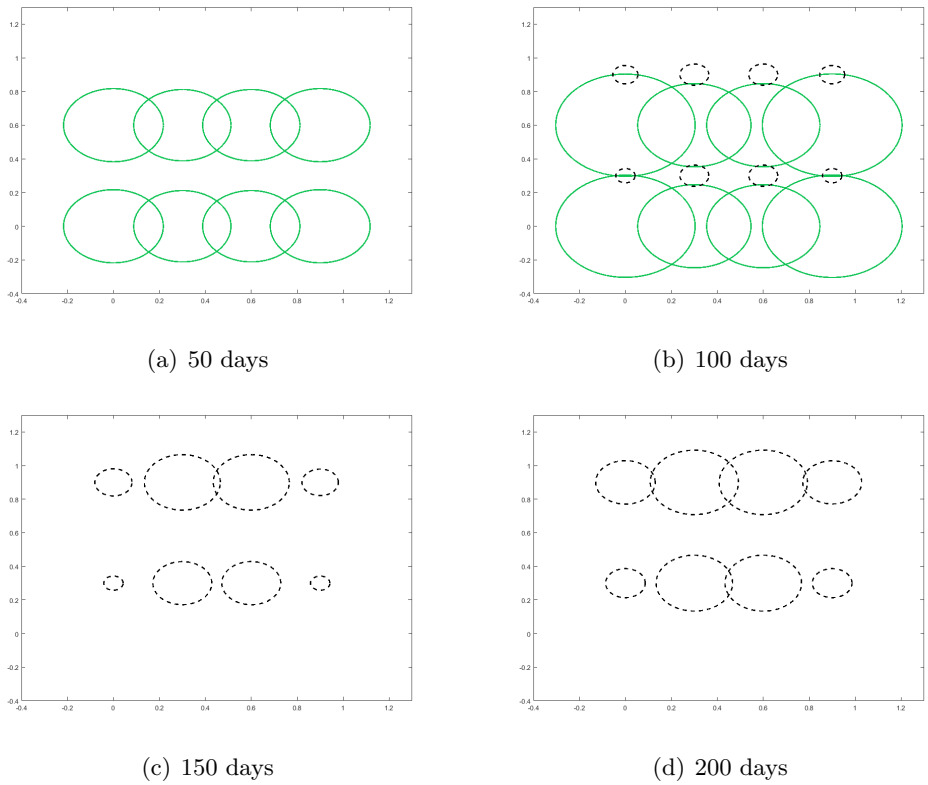

(a) 50 days

(b) 100 days

(c) 150 days

(d) 200 days

Figure 7.5: An above plant view of Uniswa Red (solid lines) and Species 1 (dashed lines) at fifty day intervals. Uniswa Red is sown at $t = 0$ days and Species 1 is sown at $t = 75$ days. Both are harvested 150 days after sowing.

comes at the cost of increased competition, particularly when the taller species is introduced after a delay. We find that the gain in absorbed radiation, caused by a larger ground cover, does not counteract the impact competition has in the later stages of growth.

In the case of intercropping Uniswa Red with Species 3 we find that increases to sowing date past 75 days causes a decrease in total pod yield. It is important to note that since Uniswa Red is taller than Species 3, it is unaffected by the sowing delay. It is only Species 3 that is affected by its sowing delay. Like all species in our simulations, Species 3 has a much wider spreading canopy when it is unaffected by competition. Conversely, if it is shadowed by a taller plant in the initial stages of growth the final ground cover is decreased. This means that, when the taller plants are removed, there is less competition between the remaining plants than there

otherwise would be. Conversely, no shadowing at the initial stages of growth causes the average plant ground cover of Species 3 to increase, causing more competition between plants at a critical point in pod production. Clearly a delay of 75 days causes the optimum amount of shadowing at the early stages of growth.

These results indicate that a delay in planting the shorter plant is beneficial, however only up to a certain critical point. This point may vary depending on planting distance and species. It is important to ask what all this means in terms of recommendations in the field. The maximum amount of sowing delay shown in Figure 7.4 is beyond what may actually be recommended in the field due to weather constraints, however we have shown that, when possible, there is a benefit in delaying the sowing of the shorter species. The amount of delay would depend on the length of the growing season. This is for the case when the two species are arranged in alternating rows. For a different pattern we may have different results. For example, the results for when plants are arranged as in Figure 7.2(b) are given in Figure 7.6.

In this case, plants of each species are entirely surrounded by the plants of the other species. For Species 1, 2 and 3, Uniswa Red is unaffected by the Secondary Species as it is taller. When intercropping with these species with this planting distance, the plant canopies of the Secondary Species are completely shadowed by Uniswa Red in the initial period of growth, where peak spreading occurs. Thus it is not until much larger delays in sowing do we see any change in total pod yield. For Species 2, which is taller than Uniswa Red, we see a consistent increase in yield with increased sowing delay. This is because, although it shadows Uniswa Red, it has a smaller spreading canopy and so the extent of shadowing is not as large when compared to Uniswa Red planted with Species 1, 2 and 3.

Clearly, the effect that a delay in sowing has on final yield is very different for Pattern 2, when compared to Pattern 1. This is a further demonstration of the delicate balance when optimising for yield.

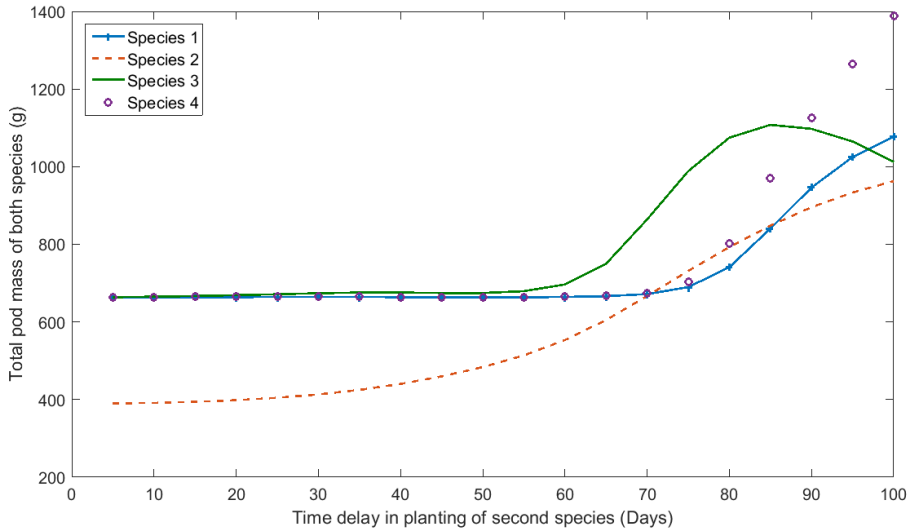

Figure 7.6: The total canopy biomass of 16 plants where 8 plants are of the species Uniswa Red and the other 8 are one of Species 1-4. The sowing of the second species is delayed in relation to the first by a number of days given in the x-axis. Planting distance is 0.3m, temperature is 28°C, different species are arranged in alternating rows and columns and plot size is $\hat{P} = 1$m.

7.5 Real world application: Intercropping Uniswa Red with oil palm

Up to this point, the investigation of intercropping has been limited to the planting of annual plants with similar growth behaviours to Uniswa Red. We now consider optimising plant arrangement when this is not the case. In particular, we consider intercropping Uniswa Red with a perennial crop such as oil palm. Before we do this however, it is necessary to formulate our model to simulate the growth and development of oil palm. As such, in this section we discuss the model adjustments that are required to be able to do this. In doing so we have made reasonable assumptions, however the model formulation has not been as rigorous as it was for bambara groundnut as the work in this section is solely exploratory.

The harvested product of oil palm are fruit bunches from which crude palm oil and palm kernel oil can be extracted. In the past 100 years, oil palm has become

one of the worlds most important vegetable oils, contributing as much as 36% of the worlds total vegetable oil production. It is typically grown at a density of 120-150 palms per hectare, where they have been reared in polybags for 6-12 months until they are transplanted to the field. Once transplanted, there is little opportunity for repositioning or replacing plants with undesirable characteristics [58].

The first fruits can be harvested at 2.5 years, which is considerably earlier than full canopy closure. The canopy of oil palm reaches it's maximum size at 10 years and has an economic life span of 25 years [33]. Since it spends 15 years at full canopy size, the optimal planting density must be considered for the mature canopy size as it is very impractical to change planting density within the growth cycle. A full size canopy radius of oil palm is approximately 6m [33]. As such there is a great deal of space left between trees so that yield is not heavily impaired by competition. In order to make use of the space, the gaps between trees can be filled with other crops, such as bambara ground, so that space is not wasted.

Kraalingen *et al.* [33] discusses a mathematical model that simulates the growth and yield of oil palm. Vegetative biomass over time is described using a dynamical model, from which plant leaf area is calculated, much in the same way as described in Chapter 3. Interactions between tree crowns is described in a similar way as what is described in Section 3.7.1. The canopy crown is represented with a horizontal disc; however, in the case of oil palm it can not be assumed the leaves are uniformly distributed over the canopy. Instead it was necessary to include a gradient from the central stem to the canopy edge. This model was able to describe leaf area index, plant biomass and yield well in the first seven years, however after this there was a considerable difference between simulation and experimental data. The cause of this was leaf pruning done in the field which was not accounted for in the mathematical model.

7.5.1 Formulating the mathematical model for oil palm

In order to intercrop oil palm with bambara groundnut it is necessary to formulate our mathematical model so that its behaviour is captured. Our motivation in doing this is to make recommendations about planting bambara groundnut around an oil crop. We assume that bambara groundnut does not impact upon the growth of oil palm and so its behaviour will not be altered by the presence of bambara groundnut. It is not necessary to simulate the canopy biomass and yield of oil palm as we are only interested in variables that will impact upon the growth and development of bambara groundnut. In addition, reparameterising the model to predict the yield of oil palm is beyond the scope of this work as we do not have access to data.

The growth behaviour of oil palm can be captured with a few changes in parameter values, namely, α_h, k_h, a, b, c, d_l, a_g, b_g, c_g and d_g. As we have no data to fit the model to, we choose parameters using a 'best guess' approximation which allows us to simulate the average behaviour of a population of oil palm plants as detailed in the literature.

As a perennial, oil palm does not complete its life cycle in one year. At a point in its life the leaf accumulation will equal the leaf decay and the leaf number will remain approximately constant over time. This can be also be observed in the simulations of bambara groundnut, however the time for which this occurs is short compared to oil palm. If a change is made to the tree during it's growth, i.e. pruning, we would expect the leaf number to initially decrease and then regrow over time. This phenomenon is not currently included in the mathematical model developed in this work because a Gaussian function for leaf area accumulation only allows for one single peak in leaf growth. To include the impact of pruning and regrowth of leaves in the mathematical model we add an oscillating function in equation (5.8). The result of this is that the leaf number will reduce and then regrow over time. The oscillating function d_{prune} takes the form of a sin wave where the frequency is set to

once every three years so that

$$d_{prune} = d^*_{prune} sin\left(\frac{2\pi t}{3 \times 365}\right)$$

where d^*_{prune} is a constant indicating the pruning magnitude. We chose once every three years using a trial and error approach as this frequency caused us to best replicate the data given in the work of Kraalingen *et al.* [33].

Thus the system of equations that describe the growth of oil palm is given by

$$\begin{aligned}
\frac{dT_{Ci}(t)}{dt} &= T_{Di}(t), && (7.2)\\
\frac{dG_i(t)}{dt} &= \alpha_g A_i(t) exp\left(-\left(\frac{T_{Ci}(t) - b_g}{c_g(1 - O_i(h_1, h_2, ...h_N, t)}\right)^2\right) \\
&\quad -d_g G_i(t), && (7.3)\\
\frac{dA_i(\tau)}{d\tau} &= a_1\left(1 - O_i(h_1, h_2, ...h_N, t)\right) exp\left(-\left(\frac{T_{Ci}(t) - b_1}{c_1}\right)^2\right) \\
&\quad -d_{prune} sin\left(\frac{2\pi\tau}{3 \times 365}\right) - d_l T_{sl} A_i(t), && (7.4)\\
& && (7.5)
\end{aligned}$$

Plant height is described by equation (4.17), repeated here for convenience

$$h_i(t) = \frac{h_0(\alpha_h - d_h)exp((\alpha_h - d_h)t)}{\alpha_h - d_h - \alpha_h k_{hi} h_0 + \alpha_h k_{hi} exp((\alpha_h - d_h)t)h_0}. \qquad (7.6)$$

We non-dimensionalise equations (7.2) to (7.4) according to

$$T_{Di}(t) = T_{Di0}\hat{T}_{Di}(\tau), \qquad T_{Ci}(t) = \frac{T_D(0)}{\alpha_h}\hat{T}_{Ci}(\tau)$$

$$G_i(t) = L_A\hat{G}_i(\tau), \qquad A_i(t) = L_A\hat{A}_i(\tau) \qquad \text{and} \qquad t = \frac{\tau}{\alpha_h}$$

which yields

$$\frac{d\hat{T}_{Ci}(\tau)}{d\tau} = \hat{T}_{Di}(t), \tag{7.7}$$

$$\frac{d\hat{A}_i(\tau)}{d\tau} = \bar{\alpha}_L\left(1 - O_i(h_1, h_2, ...h_N, \tau)\right) exp\left(-\left(\frac{\hat{T}_{Ci}(\tau) - \bar{b}}{\bar{c}}\right)^2\right) - \bar{d}_{prune} sin\left(\frac{2\pi\tau}{3 \times 365}\right) - \bar{d}_L\hat{A}_i(\tau), \tag{7.8}$$

$$\frac{d\hat{G}_i(\tau)}{d\tau} = \bar{\alpha_g}\hat{L}_i(t) exp\left(-\left(\frac{\hat{T}_{Ci}(\tau) - \bar{b}_g}{\bar{c}_g(1 - O_i(h_1, h_2, ...h_N, \tau))}\right)^2\right), \tag{7.9}$$

$$\tag{7.10}$$

where

$$\bar{\alpha}_L = \frac{aT_{Di}}{L_A\alpha_h}, \qquad \bar{b} = \alpha_h b, \qquad \bar{c} = \alpha_h c, \qquad \bar{d}_{prune} = \frac{d_{prune}}{L_A\alpha_h}, \qquad \bar{d}_L = \frac{d_l T_{sl}}{\alpha_h},$$

$$\bar{\alpha}_g = \frac{\alpha_g}{\alpha_h}, \qquad \bar{b}_g = \alpha_h b_g, \qquad \bar{c}_g = \alpha_h c_g, \qquad \bar{d}_g = \alpha_h d_g,$$

The non-dimensional parameter values for oil palm can be found in Table 7.8. These have been found using trial and error until the growth behaviour matches that found in the work of Kraalingen *et al.* [33].

Parameter	Value
$\bar{\alpha}_L$	0.052
$\bar{b}$	1095
$\bar{c}$	547.5
$\bar{d}_{pruce}$	0.01
$\bar{d}_L$	1.3×10^{-4}
$\bar{\alpha}_g$	5.3×10^{-4}
$\bar{b}_g$	365
$\bar{c}_g$	1095

Table 7.8: Table of non-dimensional parameter values for oil palm.

Since we have no experimental data with which to compare the simulation, we refer the reader to the work of Kraalingen *et al.* [33] for comparison (which were the data used to intuitively parameterise the model). To replicate the field experiments described in this work, we arrange 144 trees in a 12 by 12 uniform grid with a planting

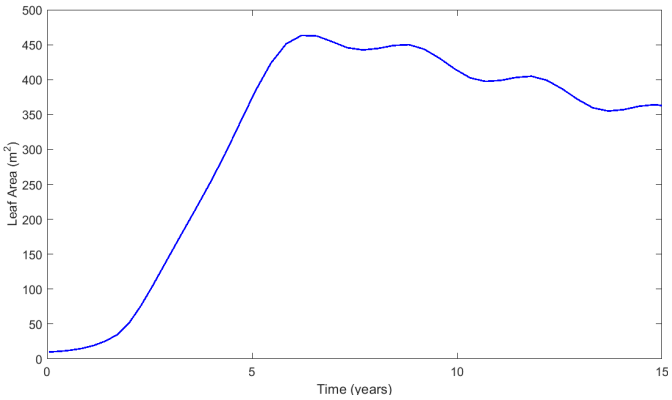

(a)

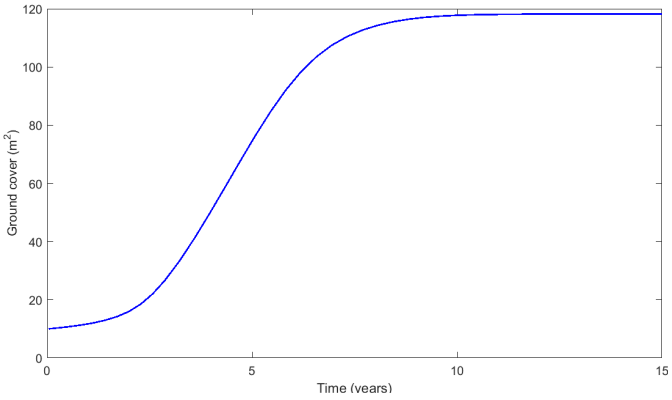

(b)

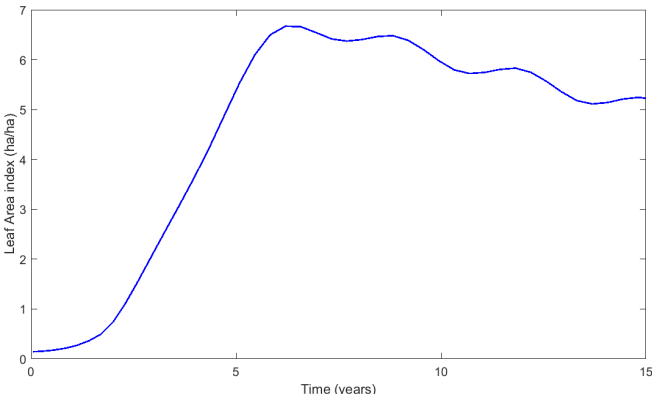

(c)

Figure 7.7: The growth behaviour of 144 oil palm trees in a 12 by 12 uniform grid with a planting distance of 9m. The mathematical model is described by equations (7.7)-(7.9) where growth begins at six months, the supposed time of transplanting, and is run to fifteen years. Here (a) is the average leaf area per tree, (b) is the average ground cover per plant and (c) is the leaf area index for the total population of trees.

distance of 9m. The mathematical model described by equations (7.7)-(7.9) is then solved numerically using the inbuilt MATLAB function ode15s. The simulation begins at six months, the supposed time of transplanting, and is run to fifteen years. The average leaf area, ground cover and leaf area index per plant is given in Figure 7.7. Here the leaf area index for all plants is calculated such that

$$\text{Leaf area index} = \frac{\text{Sum leaf area of all plants}}{\text{Area of field}},$$

where the field is one hectare in area.

By comparing Figure 7.7 to the work of Kraalingen *et al.* [33] we find we are simulating the general behaviour well and if given adequate data, we feel confident that we could parameterise the model for this species.

7.5.2 Calculating competition caused by the canopy of oil palm

Now that we have formulated the model for oil palm, we would like to make some adjustments to the way that the taller plant (oil palm) impacts upon the shorter plant (bambara groundnut). We now consider some revisions to the model. Firstly, for this investigation we allow some light to penetrate through the canopy of oil palm to the ground below and secondly, we allow the leaf area density of oil palm to vary across the plant canopy.

Since we assume that the canopy of oil palm does not completely block sunlight from reaching the ground, some of the light penetrates through the canopy. Then plants arranged below the canopy will still be able to absorb some sunlight, albeit much less than if they were not shadowed. Then the effect of competition previously given by

$$1 - O_i(h_1, h_2, ...h_N, \tau),$$

is now given by

$$1 - \omega_i O_i(h_1, h_2, ...h_N, \tau)$$

where $\omega_i < 1$ for a plant that is shadowed by a taller plant.

Since we do not have data to parameterise ω_i, we assume that amount of light that is blocked by the taller canopy is a function of the local leaf area index ϕ_i. Then ω_i is described by

$$\omega_i = \frac{\phi_i}{\boldsymbol{\phi}},$$

where $\boldsymbol{\phi}$ is the minimum leaf area index that blocks all sunlight.

As described by Kraalingen *et al.* [33] there is a density gradient in the tree canopy, where the leaves are denser closer to the stem. This is contrary to how we have modelled for Uniswa Red where leaves are assumed to be uniformly distributed. Therefore, for oil palm, more light will penetrate through the canopy around the edge of the tree crown than closer to the trunk. The way that this is incorporated into the model will now be discussed.

We adopt the method described by Kraalingen *et al.* [33] where the canopy is split into two rings, an outer and inner ring. The area of ground that the inner ring and outer ring covers is given by G_I and G_O, respectively. This is illustrated in Figure 7.8, and by doing this we drastically reduce the complexity of the density gradient. The total leaf area A_i is split over each ring so that half of A is contained within each ring. As the outer ring has a larger area, the leaf area density is lower there. Then a local leaf area index for the inner and outer rings can be calculated such that

$$\phi_{Ii} = \frac{0.5 \times A_i(t)}{G_{Ii}(t)}$$

and

$$\phi_{Oi} = \frac{0.5 \times A_i(t)}{G_{Oi}(t)},$$

respectively.

The way that this would impact upon plants below the oil palm canopy is that ω_i would change when being shadowed by an inner or outer ring.

Consider two plants, one of which is an oil palm and labelled with a j, and the other a bambara groundnut labelled with an i.

To calculate how much light is stopped from reaching Plant i, by a taller canopy

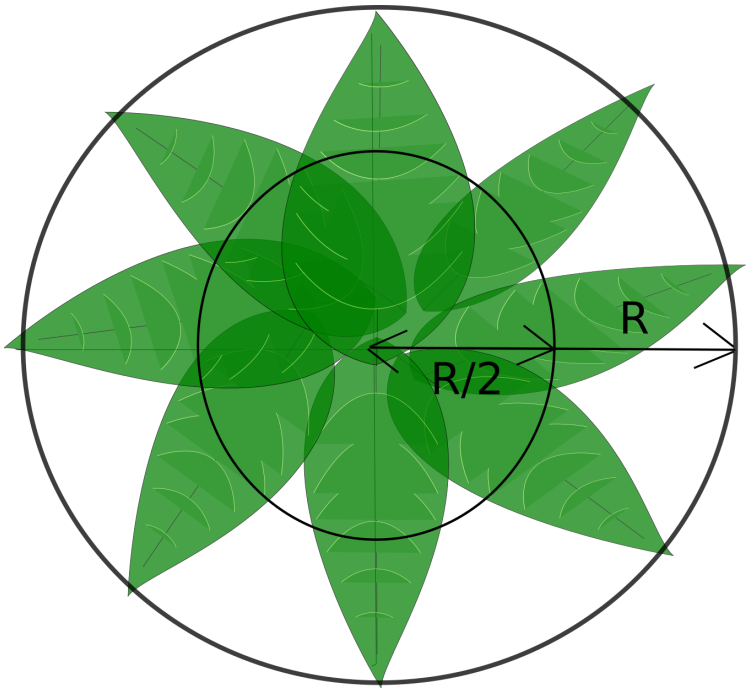

Figure 7.8: Schematic of an above plant view of oil palm. The canopy ground cover has been split into an inner and outer ring, where the radius of the inner ring is half of the outer ring. It is assumed that half of the total plant leaf area is contained in the inner ring and half in the outer.

we must calculate overlap imposed upon bambara groundnut O_i twice, once for the part of Plant i that is shadowed by the inner ring O_{Ii} and again for the outer ring O_{Oi}. Then the growth of the shorter Plant i, which is shadowed by the taller oil palm, is reduced by a magnitude of

$$1 - \omega_{Ii} O_{Ii}(h_1, h_2, ...h_N, t) - \omega_{Oi} O_{Oi}(h_1, h_2, ...h_N, t)$$

where ω_{Ii} is the amount of light blocked by the inner ring and ω_{Oi} the amount of light blocked by the outer ring. The values of ω_{Ii} and ω_{Oi} would be different for each plant depending on the value of A_i. Including this into the model would require a great deal of complexity and so instead we allow ω_I and ω_O to take values that have been averaged over the entire field.

The way that bambara groundnut interacts with plants of the same species is the same as that described in Section 3.5.3 so that $\omega_{Oi} = 0.5 = \omega_{Ii}$.

Thus the revised dimensional system of equations for bambara groundnut is given by

$$\frac{dTC_i(t)}{dt} = TD_i(t), \tag{7.11}$$

$$\frac{dG_i(t)}{dt} = \alpha_g A_i(t) \times exp\left(-\left(\frac{T_c(t) - b_g}{c_g(1 - \omega_I O_{Ii}(h_1, h_2, ...h_N, t) - \omega_O O_{Oi}(h_1, h_2, ...h_N, t) - O_i(h_1, h_2, ...h_N, t)}\right)^2\right) - d_g G_i(t), \tag{7.12}$$

$$\frac{dA_i(t)}{d\tau} = a_1 \left(1 - \omega_I O_{Ii}(h_1, h_2, ...h_N, t) - \omega_O O_{Oi}(h_1, h_2, ...h_N, t) - O_i(h_1, h_2, ...h_N, t)\right) \times exp\left(-\left(\frac{TC(t) - b_1}{c_1}\right)^2\right) - d_l T_{sl} A_i(t), \tag{7.13}$$

$$\frac{dc_i(t)}{d\tau} = R_0 c_k G_i(t) \left(1 - \omega_I O_{Ii}(h_1, h_2, ...h_N, t) - \omega_O O_{Oi}(h_1, h_2, ...h_N, t) - O_i((h_1, h_2, ...h_N, t))\right) \times \left(1 - exp\left(-\kappa \frac{A_i(t)}{G_i(t)}\right)\right)\left(1 - \frac{c_i(t)}{k_{ci}(O, t)}\right) - d_c T_{sc} c_i(t), \tag{7.14}$$

$$\frac{dP_i(t)}{dt} = \alpha_P T_{sp} P_i(t) \frac{dc_i(t)}{dt}\left(1 - \frac{P_i(t)}{c_i(t)}\right) - d_p P_i(t). \tag{7.15}$$

Plant height is described by equation (4.17), repeated here for convenience

$$h_i(t) = \frac{h_0(\alpha_h - d_h)exp((\alpha_h - d_h)t)}{\alpha_h - d_h - \alpha_h k_{hi} h_0 + \alpha_h k_{hi} exp((\alpha_h - d_h)t)h_0}. \tag{7.16}$$

This system is then non-dimensionalised in the same way as described in Section 5.3 for equations (7.11)-(7.14) and Section 6.2 for equation (7.15).

7.5.3 Optimising arrangement of bambara groundnut and oil palm

In this section, we investigate the optimum planting arrangement of oil palm and bambara groundnut using the model for oil palm described by equations (7.2) to (7.4) and the model for bambara groundnut given by equations (7.11) to (7.16).

For this optimisation process, we assume that the positions of oil palm trees are fixed and we refine our investigation to the placement of bambara groundnut around oil palm. We then have five planting distances to consider, the row and column distance between oil palm trees (D_{pr} and D_{pc}), the row and column distance between bambara groundnut (D_r and D_c) and the distance between oil palm plants and bambara groundnut D_{pb}. We define $D_{pr} = 9\text{m} = D_{pc}$ and then find D_r, D_c and D_{pb} using the algorithm described for a homogeneous field of crops in Section 6.4.

The only change that has been made to the algorithm is finding the optimal value of the additional planting distance D_{pb}.

We consider a field with size $\hat{P} = 9\text{m}$. With $D_{pr} = 9\text{m} = D_{pc}$ this will give 4 oil palm trees. We assume a temperature of 28°C and restrict our investigation to finding the optimum planting distance for a uniform arrangement. The simulation begins at 6 months, as this is the supposed time of transplantation. Bambera groundnut is not planted around the oil palm trees until the open of the following year. As the palm trees grow the optimum planting distance may change and so we run the algorithm over 16 years where at the beginning of every year bambara groundnut is sown and then harvested 150 days later.

On an initial run through of the algorithm, it was found that the recommended values of D_{pb} were the minimum values that were allowed by the algorithm. What this means is that the algorithm is recommending we position plants in areas that they are unable to grow and so pod mass does not exceed the initial condition P_0. This is because there is no consequence in the simulation for a plant that does not grow and therefore the final yield is only benefited by the addition of the extra plants that do not exceed P_0. To avoid this, we impose a minimum pod mass for each plant, whereby if plants do not grow past this value the arrangement is considered unviable. We choose this value to be 10g, however this would be a user defined parameter which takes into the account both the financial and time cost of growing and harvesting each plant. This is different to what we did in Section 7.3, where a minimum average pod mass was imposed. The reason we have changed how we restrict the algorithm is that there are now more scenarios for individual plants. In this case, we have bambara groundnut plants that are interacting with each other and only some of which will be interacting with oil palm. We find that although some plants may be unable to grow, these are few enough so that the average pod mass does not go below the threshold. Despite this, having plants that are unable to grow is not a viable recommendation and hence we choose a minimum pod mass for each plant. The results of the optimisation algorithm are given in Table 7.9.

Year	D_r	D_c	D_{pb}	N_2	Pod mass (g)
1	-	-	-	-	-
2	0.25	0.42	2	678	32992.6
3	0.25	0.42	2.5	601	29073.1
4	0.31	0.35	3	491	23914.2
5	0.25	0.41	3.6	389	18831.9
6	0.27	0.44	4.6	103	5895.2
7	-	-	-	-	-
8	-	-	-	-	-
9	-	-	-	-	-
10	-	-	-	-	-
11	-	-	-	-	-
12	-	-	-	-	-
13	-	-	-	-	-
14	-	-	-	-	-
15	-	-	-	-	-

Table 7.9: The optimum planting distance for intercropping Uniswa Red and oil palm for sixteen years of oil palm growth. The distances are for between Uniswa Red and also for between oil palm and Uniswa Red. A $-$ means that at this point the minimum bamara groundnut pod mass did not exceed 10g for any planting distance.

From Table 7.9 we see that recommendations for D_r, D_c and D_{pb} for planting bambara groundnut change over the growth years of oil palm. To make sense of this an above plant view of the recommended planting arrangement of both oil palm and bambara groundnut for years 2-5 of oil palm growth can be found in Figure 7.9. The above plant view is taken 150 days after bambara groundnut is sown.

From Figure 7.9 we can clearly see that D_{pb} changes with the size of oil palm canopy, so that plants are placed just on the edge of the oil palm's canopy. From this we can see that even though we are letting light penetrate through the canopy, it is not enough for bambara groundnut plants to grow.

As the recommendations for D_{pb} increases over the years, the unoccupied area that can be used for bambara groundnut is decreasing. This causes changes to the recommendations for D_r and D_c, which is what we would expect from Section 6.4.1.

After 7 years of oil palm growth, there is no longer any space for Uniswa Red to be planted between them. If more light was able to penetrate through the plant canopy this might not be the case.

7.6 Chapter summary

In this chapter we investigated how the arrangement of two species of crop in one planting area affected the final yield. We were able to apply the mathematical model to several scenarios: the growth of two annual crop species, the impact of different sowing dates of crop species and finally, the growth of bambara groundnut interspersed with oil palm.

To do this four fictional annual crops were introduced and investigated. Each plant had similar growth characteristics to bambara groundnut, however, each was different in regards to the three key growth parameters of plant height, ground cover and canopy biomass. In addition to these fictional plant species we simulated the growth of oil palm. By doing so we were able to demonstrate the robustness of the mathematical model in terms of simulating other plant species and found that we were successfully able to describe the canopy development of oil palm.

Two algorithms were developed in this chapter. One for two annual species of crops, and another for oil palm and bambara groundnut. Both algorithms worked well and gave sensible recommendations, however both required constraints to be imposed so that only viable planting distances were proposed.

We found that the recommendations are dependant on a range of factors for each scenario. We have also found that the algorithm is adaptable to a very large number of planting scenarios and in order to make recommendations in a reasonable time, we need to impose certain constraints on the optimisation algorithm.

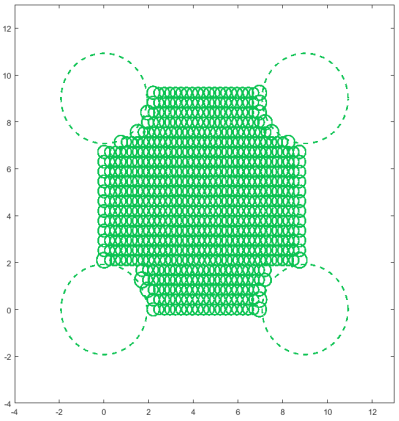

(a) Year 2 (D_r=0.25m, D_c=0.42m, D_{pb}=2m and N_2=678)

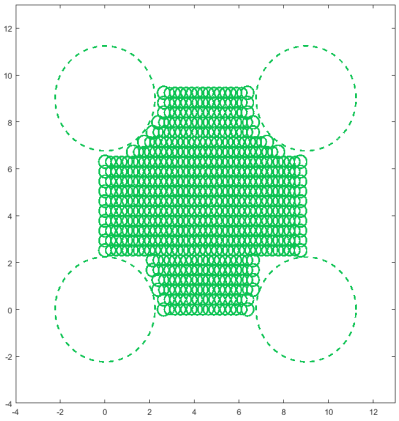

(b) Year 3 (D_r=0.25m, D_c=0.42m, D_{pb}=2.5m and N_2=601)

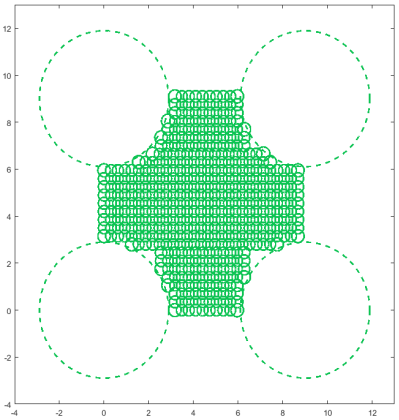

(c) Year 4 (D_r=0.31m, D_c=0.35m, D_{pb}=3m and N_2=491)

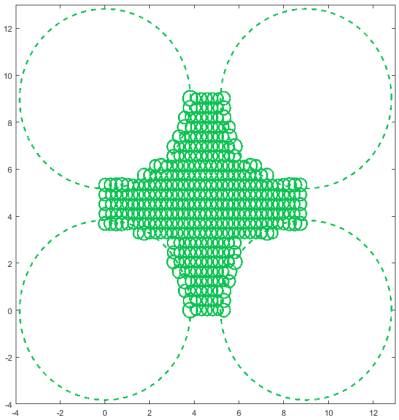

(d) Year 5(D_r=0.25m, D_c=0.41m, D_{pb}=3.6m and N_2=389)

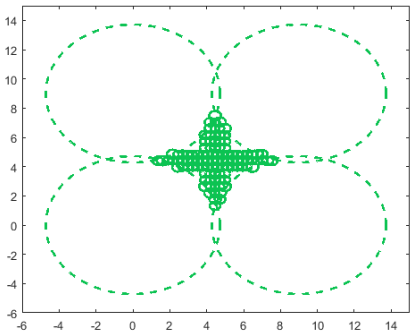

(e) Year 6 (D_r=0.27m, D_c=0.44m, D_{pb}=4.6m and N_2=103)

Figure 7.9: An above plant view of the recommended arrangement at of intercropping Uniswa Red and Oil Palm for 6 years of oil palm growth. Uniswa Red is sown at the beginning of the growth year and harvested 150 days later. Oil palm canopies are indicated with a dashed line and bambara groundnut with a solid line.

Chapter 8

Conclusions

This thesis has been focused on the optimisation of planting arrangement to maximise crop yield. A key motivation in the formulation of these optimisation techniques was to not only make recommendations for a monocropped field, but to also propose arrangements for an intercropping environment. In order to do this, a mathematical model was developed that incorporated the spatial positioning of individual plants, with the ability to include variation between plants.

In the process of developing this model, we began with the simplest description of plant growth. We then went through several iterations of comparing the simulation results to experimental data and then making model revisions to include any necessary additional details. The end result was a system of ODEs that described the cumulative thermal time, leaf area, ground cover, canopy biomass and pod mass of individual plants, which are all found to be essential in accurately describing the competition of plants in a field.

In this final chapter, a brief overview of the work described in this thesis is given. We finish with a summary of the major findings of this PhD and a discussion of recommended further work.

8.1 Thesis summary

In Chapter 1, we introduced the project and the role it plays within the larger project of CFF's BAMyield group. Here, we defined some key terminology and also described the growth behaviour of the test species, bambara groundnut.

In Chapter 2, a review of the literature surrounding mathematical modelling of crops was provided. A summary of the basic modelling approaches was given in addition to a more detailed discussion of simulating the many-plant level in terms of individual plants. We also discussed other mathematical models that describe the growth and development of bambara groundnut, paying particular attention to growth in terms of plant biomass rather than phenological age.

Chapter 3 introduced the first mathematical model derived from first principles that was formulated to describe the growth of bambara groundnut. A basic plant physiology of a disc raised above the ground on a core stem was adopted. The model required the spatial positioning of individual plants so that plant interactions could be measured in terms of the spatial overlap of the circles that represented plant canopies. The model comprised of one ODE for each plant describing canopy biomass. Equations were coupled between plants via an overlap term. This overlap term was dependent on the size of the respective plant canopies, their heights and also their proximity to one another. To our knowledge, this numerical approach of measuring plant competition is novel. This initial model was able to fit the experimental data for canopy biomass well, however was not able to do so for leaf area. It was stipulated in the chapter that, to develop a robust mathematical model that can be applied to a multitude of scenarios, we would want to describe the development of canopy biomass with regards to the underlying processes more accurately. Canopy biomass growth is a function of absorbed sunlight, and absorbed sunlight is a function of leaf area. Simulating the growth of canopy biomass well, but the growth of leaf area poorly would indicate that we are not accurately describing the connection between biomass and leaf area.

Chapter 4 introduced the importance of adequately describing leaf area dynamics in the model and consequently two ODEs were added to the model. In doing this, the model provided a better fit to the leaf area data. There are many areas in which we can investigate the model's behaviour, but in this chapter we limited our exploration into the investigation of variability in growth of individual plants and also the impact that imposed variation in plant parameters has on crop yield.

Chapter 5 addressed the question as to whether ground cover was accurately represented in the model. Since plant-plant competition is directly dependent on canopy size, any inaccuracy in describing ground cover would result in an inaccuracy in describing competition. Thus we were strongly motivated to attain experimental data detailing this variable. Data attained from glasshouse experiments, specifically designed for this work, subsequently showed us that we were underestimating the magnitude and range of ground cover over time. As such, we revised the method of describing ground cover in this chapter. We found that, with a relatively simple revision, we were able to better account for ground cover.

By Chapter 6 we had finished the formulation of the model and began building a novel framework for optimising the arrangement of plants to maximise crop yield. We found that it was necessary to simulate pod mass in order to make reliable recommendations. As such, a discussion of the addition of a final ODE for pod mass was given. We then designed two algorithms for optimising pod mass, one for a fixed plot size and unlimited number of available plants and another for a fixed plot size and a limited number of plants. The results of the optimisation algorithms were then thoroughly analysed to ensure that sensible recommendations were being made. Having gained confidence in the optimisation algorithms we went on to explore how random variation in parameters of individual plants within a monocrop affects optimum planting arrangements and final yield.

Finally, in Chapter 7 an investigation of bambara groundnut in an intercropping environment was conducted. It was necessary to introduce four fictional species of plants here, so that numerical experiments of a heterogenous field of crops could

be undertaken. These crops shared all characteristics with bambara groundnut except for three key physiological features which are plant height, canopy spread and canopy biomass. Several elements of optimisation were explored in this chapter, the optimisation of planting distance, layout, planting pattern and also sowing date. In addition to this, we considered the placement of bambara groundnut around oil palm trees over 15 years of growth. To do this it was necessary to formulate the model for oil palm. Since we lacked experimental data for oil palm, we were not able to formulate the model as rigorously as we did for bambara groundnut. Despite this we found that we were able to capture the general behaviour of oil palm demonstrating the robustness of our mathematical model. The results of this particular optimisation algorithm demonstrated a lot of potential in the planting of bambara groundnut around trees, a practice that is not yet common in the field.

8.2 Conclusions

From the work in this thesis we have been able to draw several conclusions about optimising crop growth. The key findings are discussed in this section.

Firstly, we found that when simulating the competition between a homogeneous array of plants, it is important that all plants are affected by competition. This was applied in our model by stipulating that all plants have the same height and thus share competition equally across interacting plant canopies. If this is not done we find that the total variation in simulated biomass data (and also pod yield) is much larger than what is seen in the experimental data. This is particularly relevant when simulating bambara groundnut as experimental observations have shown that plants do not definitively shadow their neighbours and instead their leaves intermingle so that parts of each plant are shadowed. By allowing competition to be shared across canopies, we allow our model to account for this phenomenon without adding any unnecessary complexity to the geometry of the simulated plant canopy.

The adopted method of simulating the plants physiology, although simple, was found to be effective. We were not only able to achieve a good fit to data for

bambara groundnut, but also to describe the growth of oil palm. These two species are very different in physiology and so to be able to account for both demonstrates a considerable robustness of the model. This method also allows the mathematical model to be applied to a wide range of scenarios that require optimisation.

Regarding optimisation, we found that it was important to consider the output of interest, in this case pod mass. Although doing this required an additional layer of detail in the model, not doing so would give misleading recommendations. This highlights a compromise that was important throughout the formulation of a mathematical model, including enough detail so that key factors were described, but not causing the mathematical model to become unnecessarily complicated.

One of the key findings of our optimisation algorithm was that recommendations were very scenario specific. We found that both temperature and plot size had an impact on the best way to arrange individual plants when monocropping. The recommendations became more varied when considering a Secondary Species of plant. In the case of intercropping, our optimisation algorithms revealed a considerable potential in the placement of bambara groundnut around oil palm, particularly in the early years of oil palm growth. We also found that with regards to competition for light, a delay in the sowing of the Secondary Species is beneficial in maximising yield. The amount of delay would depend on the species and the growth season to which it is adapted. In general we found that layouts; Uniform Grid and Indented Grid 1 were recommended, both of which were considerably better at maximising pod mass when compared to the Circular and Random layout.

The mathematical model we developed here is adaptable to a multitude of scenarios, only some of which were discussed in this thesis. The search space is so large that it was necessary to impose limitations on the algorithms so that recommendations could be made in good time. The way this was done was to only examine a subset of possible scenarios. In the real world a particular scenario we would wish to optimise would really depend on a farmers requirements, which can be as varied as the recommendations our algorithms give.

8.3 Further work

In this work, the mathematical model that has been developed is only able to simulate light limited growth. It is found that although bambara groundnut grows well with minimal rainfall, its growth is affected [36]. Thus, in a water limited environment our model might not reliably predict the crop yield. Further to this, there is little quantifiable information on the additive effects of limited water and planting density on crop yield. Water limited growth models operate by dividing the total depth of the soil into layers. The change in soil moisture of each layer is a function of vertical drainage, soil evaporation and root uptake. The root uptake is then a function of the plants genetic traits and the soil moisture [20, 30, 32]. As with light limiting growth models, plants are treated as a single entity. In such a model, the layers of soil span the entire plot and thus ignore the variation in soil moisture across the field. These variations can be a cause of environmental factors, e.g. a slope in the plot, or caused by variability in the water uptake of individual plants. Including this aspect of competition into the optimisation algorithm would provide a more robust tool, particularly when optimising growth in the semi-arid regions that bambara groundnut is indigenous to.

Further to this, a thorough investigation into the effect of variable temperature in addition to the inclusion of a water limited module would allow us to apply the mathematical model to field data. This would be an extension of the greenhouse trials we have conducted so far.

As in all aspects of mathematical modelling, we are ever driven by a desire for experimental data. As outlined in the Introduction, a key principle of the work undertaken here is that it can be easily applied to other species and in keeping with this we attempted to accurately simulate the growth of oil palm with promising results. Attaining experimental data for other plant species would allow us to inform the mathematical model so that the framework developed here can be utilised in describing their growth and development. In doing so we could further confirm the

models robustness and also provide more accurate recommendations for intercropping scenarios. Similarly, further experimental data for bambara groundnut with various planting arrangements would help us build further confidence in our model.

Above all else, the primary motivation in this work is to make recommendations to farmers that will help maximise crop yield. For this to be achievable, we must be able to tailor the optimisation algorithm to each farmers personal needs. The framework of the mathematical model is already in place, however making it more accessible to the people who can make use of the information is integral. As such, the development of an application (app) with an accessible user interface so that individuals can gain personal insight into what impact planting arrangements can have on yield would be invaluable. To make such an app feasible, it would be necessary to provide as many general and plant specific parameters in order to minimise the input of said farmer. In the model so far, plant parameters are provided for two species of bambara groundnut, all that would need to be provided then, are parameters for the predicted weather conditions.

Bibliography

[1] Aggarwal, P. K., (1994) Uncertainties in crop, soil and weather inputs used in growth models: implications for simulated outputs and their applications. *Agricultural Systems*, 48, 361−384.

[2] Aggarwal, P. K., Kalra, N, Singh, A. K., & Sinha, S. K. (1994) Analyzing the limitations set by climatic factors, genotype, water and nitrogen availability on productivity of wheat: I. The model documentation, parameterisation and validation. *Field Crop Research*, 38, 73-91.

[3] Aggarwal, P. K., Kalra, N. (1994) Analyzing the limitations set by climatic factors, genotype, water and nitrogen availability on productivity of wheat: II Climatically potential yield and management strategies. *Field Crop Research*, 38, 93-103.

[4] Aliyu, S., Massawe, F., and Mayes, S., (2015) Beyond landraces: developing improved germplasm resources for underutilized species - a case for Bambara groundnut. *Biotechnology and Genetic Engineering Reviews* 30(2), 127-141.

[5] Alm, D. M., Pike, D. R., Hesketh, J. D., and Stoller, E. W. (1988) Leaf area development in some crop and weed species. *Biotronics: Environment Control and Environmental Biology* 17 29-39.

[6] Alshareef, I. (2010) The effect of temperature and drought stress on Bambara Groundnut (*Vigna subterranea* (L.) Verdc) landraces. Ph.D. Thesis. University of Nottingham, U.K.

[7] Azam-Ali, S. N., Sesay, A., Karikari, K. S., Massawe, F. J., Aguilar-Manjarrez, J., Bannayan, M., and Hampson, K. J., (2001) Assessing The Potential of an Underutiized Crop - A Case Study Using Bambara Groundnut. *Journal of Exploratory Agriculture* 37:433-472.

[8] Bauer, S., Berger, U., Hildenbrandt, H., & Grimm, V. (2002) Cyclic dynamics in simulated plant populations. *Proc. R. Soc. London Ser. B-Biol. Sci* 269: 2443-2450.

[9] Bella, I. E., (1971) A new competition model for individual trees. *Forest Science* 17: 364-372.

[10] Bernsten, A., Hauggard-Nielsen, H., Olesen, J. E., Petersen, B. M. Jensen & E. S., Thomsen, A. (2004) Modelling dry matter production and resource use in intercrops of pea and barley. *Field Crops Research* 88: 69-83.

[11] Brink, M., Sibuga, K. P., Tarimo, A. J. P. & Ramolemana, G. M. (1999) Quantifying photothermal influence on reproductive development in bambara groundnut (*Vigna subterranea*): models and their validation. *Field Crop Research* Res. 66, 114.

[12] Brink, M., (1999) Development, growth and dry matter partitioning in bambara groundnut (*Vigna subterranea*) as influenced by photoperiod and shading. *Journal of Agricultural Science* 133, 159-166.

[13] CFF. [online] Available at: `http://http://www.cffresearch.org/Updates-@-Growing_Bambara_Groundnut_in_Malaysia` [Accessed 02 June 2017]

[14] Collinson, S. T., Azam-Ali, S. N., Chavula, K. m., and Hodson, D. A. (1996) Growth, development and yield of bambara groundnut (*Vigna subterranea*) in response to soil moisture. *Journal of Agricultural Science*; 126, 307-318.

[15] de Wit, C. T., (1965) Photosynthesis of leaf canopies. *Agriculture Research Reports* Center for Agriculture Publication and Documentation. 663, 57.

[16] Esnal, A. R., Lopez-Fernandez, M. L., (2010) Modelling leaf development in Oxalis latifolia. *Spanish Journal of Agricultural Research*; 1695-971-X.

[17] Graf, B., Gutierrez, A., P., Rakotobe, O., Zahner, P., Delucchi, V., A (1989) Simulation Model for the Dynamics of Rice Growth and Development: Part II - The Competition with Weeds for Nitrogen and Light. *Agricultural Systems* 32: 367-392.

[18] Granier, C., Massonnet, C., Turc, O., Muller, B., Chenu,. K and Tardieu, F. (2002). Individual leaf development in *Arabidopsis thaliana*: a stable thermal-time-based programme. *Annals of Botany* 89: 595-604.

[19] Cournede, P.H., Mathieu, A., Houllier, F., Barthelemy, D. and De Reffye, P. (2008). Computing competition for light in the GREENLAB model of plant growth: A contribution to the study of the effects of density on resource acquisition and architectural development. *Annals of Botany*. 101:12071219.

[20] Cornelissen, R. L. E. J. (2005). Modelling variation in the physiology of bambara groundnut. Ph.D. Thesis. Cranfield University at Silsoe: U.K.

[21] Fourcaud, T., Zhang, X., Stokes, A., Lambers, H., Korner, C., (2008) Plant Growth Modelling and Applications: The Increasing Importance of Plant Architecture in Growth Models. *Annals of Botany*. 101(8): 1053-1063.

[22] Garcia-Barrios, L., Mayer-Foulkes, D., Franco, M., Urquijo-Vasquez, G., and Franco-Perez, J. (2001) Development and validation of a spatially explicit individual-based mixed crop growth model. *Bulletin of Mathematical Biology* 63:507-526

[23] Gou, F., van Ittersum, M. K., and van Werf, W., (2016) Simulating potential growth in a relay-strip intercropping system: Model description, calibration and testing. *Field Crops Research* 200:122-142

[24] Godin, C., (1999) Representing and encoding plant architecture: A review. *Annals of Forest Science* 57: 413-438.

[25] Godin, C., Caraglio, Y., (1997) A multiscale model of plant topological structures. *Journal of theoretical biology.* 191, 1-46.

[26] Goudriaan, J. & H.H. Van Laar (1994): Modelling potential crop growth processes. *Kluwer Academic Publishers, Dordrecht*, 1.

[27] Gramig, G., and Stoltenberg, D., (2007) Leaf appearance base temperature and phyllochron for common grass and broadleaf weed species. *Week Technology* 21:249-254.

[28] Hammer, G. L., Kropff, M. j., Sinclair, T. R., and Porter, J. R., (2002) Future contributions of crop modelling - from heuristics and supporting decision making to understanding genetic regulation and aiding crop improvement. *European Journal of Agronomy* 18(1-2):15-31

[29] Heuvelink, E. (1996) Tomato growth and yield: quantitative analysis and synthesis. Ph.D. Thesis. Wageningen University, Netherlands.

[30] Jones, J. W., Hoogenboom, G., Porter, C. H., Boote, K. J., Batchelor, W. D., Hunt, L. A., Wilkins, P. W., Singh, U., Gijsman, A. J., and Ritchie, J. T. (2003) The DSSAT cropping system model. *European Journal of Agronomy* 18: 235-265

[31] Karunaratne, A. S. Azam-Ali, S. N. and Crout, M.J. (2011). Bamgro: A simple model to simulate the response of bambara groundnut to abiotic stress. *Experimental Agriculture*, volume 47, pp. 489-507, Cambridge University Press doi:10.1017/S0014479711000093

[32] Karunaratne, A. S. (2009). Modelling the response of bambara groundnut (*Vigna subterranea (L.) Verdc*) for abiotic stress. Ph.D. Thesis. University of Nottingham. U.K.

[33] Kraalingen, D. W. G., Breure, C. J., and Spitters, C. J. T., (1988) Simulation of oil palm growth and yield. *Agricultural and Forest Meteorology* 46:227-244

[34] Kouassi, N. J., Zoro, I. A. (2009). Effect of sowing density and seeded type in yield and yield components in Bambara Groundnut (*Vigna Subterranea*) in woodland savannas of Cote D'Ivoire. *Experimental Agriculture* volume 46 (1), pp. 99-110.

[35] Li, T., Feng, Y., Li,. X., (2009) Predicting crop growth under different cropping and fertilizing management practices. *Agricultural and Forest Meteorology* 149: 985-998

[36] Linnemann, A. R., and Azam-Ali, S., (1993) Bambara Groundnut (Vigna subterranea). In *Underutilized Crops: Pulses and Vegetables*, 13-57 (Ed. J. T. Williams). London: Chapman and Hall.

[37] Mabhaudhi, T., Modi, A., and Beletse, Y., (2014) Parameterisation and evaluation of the FAO-AquaCrop model for a South African taro (*Colocasia esculenta L. Schott*) landrace, *Agricultural and Forest Meteorology*, 193-193 132-139.

[38] Massawe, F., J., Azam-Ali, S., N., and Roberts, J., A., (2003) The Impact of Temperature on Leaf Appearance in Bambara Groundnut Landraces. (*Crop Science*) Vol 43:1375-1379.

[39] Mayes, S., Massawe, F. J., Alderson, P. G., Roberts, J. A., Azam-Ali, S. N., and Hermann, M., (2011) The potential for underutilized crops to improve security of food production. *Journal of Experimental Botany* doi:10.1093/jxb/err396

[40] Marcelis, L. F. M., Heuvelink, E., Goudriaan, J., (1998) Modelling biomass production and yield of horticultual crops: a review. *Scientia Horticulture* 74 pp 83-111

[41] Met office. [online] Available at: http://www.metoffice.gov.uk/renewables/solar [Accessed 28 June 2016]

[42] Mkandawire, C., (2007) Review of Bambara Groundnut (*Vigna subterranea* (L.) Verdc.) Production in Sub-Sahara Africa. *MedWell Agricultural Journal* 2(4): 464-470.

[43] Murray, J.D., (2002) Mathematical Biology I: An Introduction. (Springer, Berlin).

[44] Ma, Y.T., Wubs, A. M., Mathieu, A., Heuvelink, E., Zhu, J, Y., Hu, B. G., Cournede, P. H., and de Reffye, P. (2010) Simulation of fruit-set and trophic competition and optimization of yield advantages in six *Capsicum* cultivars using functional-structural plant modelling. *Annals of Botany* 107(5): 793803.

[45] Mabhaudhi, T., Modi, A., (2013) Growth, phenological and yield responses of a bambara groundnut (Vigna subterranea (L.) Verdc.) landrace to imposed water stress under field conditions. *South African Journal of Plant Soil* 30(2): 69-79

[46] Malezoeux, E., Crozat, Y., Dupraz,. C., Laurans, M., Makowski, D., Ozier-Lafontaine, H., Rapidel, B., de Tourdonnet, S., Valantin-Morison, M. (2008) Mixing plant species in cropping systems: concepts, tools and models. A review. *Agronomy for sustainable development* 29: 43-62.

[47] Monteith, J. L., Gregory, P. J., Marshall, B., Ong, C. K., Saffell, R. A., and Squire, G. R. (1980) Physical measurements in crop physiology in growth and gas exchange. *Experimental Agriculture* 17 : 113-126.

[48] Nash, J. E., and Sutcliffe, J. V., (1970) River flow forcasting through conceptiual models: Part I-A discussion of principles. *Journal of Hydrology* 10:282-290.

[49] Ntare, B. R., Williams, J. H. (1991) Response of Cowpea cultivars to planting pattern and date of sowing in intercrops with pearl millet in Niger. *Experimental Agriculture* 28:41-48.

[50] Ozer, H., (2003) Sowing date and nitrogen rate effects on growth, yield and yield components of two summer rapeseed cultivars. *European Journal of Agronomy* 19(3):453463.

[51] Patricia, O. D., Yeboah, S.,Addy, S.N.T., Amponsah, S. and Owusu Danquah, E. (2012). Crop Modelling: A tool for agricultural research-A review. *Journal of Agricultural Research and Development* Vol. 2(1): 001-006

[52] Prusinkiewicz P. (2004) Modelling plant growth and development. *Current Opinion in Plant Biology* 79-83.

[53] Schneider, M., Law, R., Illian, J. B. (2006) Quantification of neighbourhood-dependent plant growth by Bayesian hierarchical modelling. *Journal of Ecology* 94, 310-321.

[54] Soler, C. M. T., Sentelhas, P. C., and Hoogenboom, G., (2007) Application of the CSM-CERES-Maize model for planting date evaluation and yield forecasting for maize grown off-season in a subtropical environment. *European Journal of Agronomy* 27(2-4):165-177.

[55] Summerfield, R. J., Roberts, E. H., Ellis, R. H., and Lawn, R. J. (1991) Towards the reliable prediction of time to flowering in six annual crops. I. The development of simple models for fluctuating field environments. *Experimental Agriculture* 27: 11-31.

[56] Watanabe, T., Hanan, J., Room, P., Hasegawa, T., Nakagawa, H., Takahashi, W. (2005) Rice morphogenesis and plant architecture: measurement, specification and and the reconstruction of structural development by 3D architectural modelling. *Annals of Botany* 95:1131-1143.

[57] Williams, J. T., and Haq, N. (2002) Global research on underutilized crops. An assessment of current activities and proposals for enhanced cooperation. Southampton, UK: ICUC.

[58] Woittiez, L. S., van Wijk, M. T., Slingerland, M., van Noordwijk, M., and Giller, K., (2017) Yield gaps in oil palm: A quantitative review of contributing factors. *European Journal of Agronomy* 83:57-77.

[59] Yin, X. Van Laar, H.H. (2005) Crop system dynamics. (Wageningen Academic Publishers, Wageningen) 1-6.

[60] Yan, H., Kang, M., Reffye, P., and Dingkuhn, M., (2004) A dynamic, architectural plant model simulating resource-dependent growth *Annals of Botany* 93: 591-602.